Isolation, Characterisation and Biosynthetic Precursors of Natural Products from Myxobacteria

Dissertation zur Erlangung des Grades des Doktors der Naturwissenschaften (Dr.rer.nat) der Naturwissenschaftlichen-Technischen Fakultät III Chemie, Pharmazie, Bio- und Werkstoffwissenschaften der Universität des Saarlandes

von

Wiebke Zander

Saarbrücken

2011

Tag des Kolloquiums:	10.05.2011
Dekan:	Prof. Dr. Wilhelm F. Maier
Berichterstatter:	Prof. Dr. Rolf Müller
	Prof. Dr. Uli Kazmaier
Vorsitz:	Prof. Dr. Johann Jauch
Akad. Mitarbeiter:	Dr. Josef Zapp

Liste der Publikationen

Teile dieser Arbeit wurden vorab mit der Genehmigung der Naturwissenschaftlichen-Technischen Fakultät III, vertreten durch den Mentor Prof. Dr. Rolf Müller, in folgenden Beiträgen veröffentlicht oder sind in Vorbereitung zur Veröffentlichung:

Publikationen:

W. Zander, **K. Gerth, K. I. Mohr, W. Kessler, R. Jansen, R. Müller (2011).** Roimatacene, an Antibiotic against Gram-negative Bacteria Isolated from *Cystobacter ferrugineus* Cb G35 (Myxobacteria). *Chem. Eur. J.* (im Druck)

W. Zander, K. I. Mohr, K. Gerth, R. Jansen, R. Müller (2011). *p*-Hydroxyacetophenone Amides from *Cystobacter ferrugineus*, strain Cb G35. (Manuskript ist eingereicht.)

W. Zander, H. Irschik, H. Augustiniak, M. Herrmann, R. Jansen, H. Steinmetz, K. Gerth, W. Kessler, M. Kalesse, G. Höfle, R. Müller (2011). Sulfangolids, Macrolide Sulfate Esters from *Sorangium cellulosum*. (Manuskript wird in Kürze eingereicht.)

Tagungsbeiträge:

W. Zander, K. I. Mohr, K. Gerth, R. Jansen, R. Müller (September 2010). Three Different Types of Secondary Metabolites from *Cystobacter* Cb G35 (Myxobacteria). International VAAM-Workshop: "*Biology of bacteria producing natural products*", Tübingen, Germany. (Posterpresentation)

Danksagung

Mein besonderer Dank gilt meinem Doktorvater Prof. Dr. Rolf Müller, der mir die Möglichkeit gab, meine Studien zu diesem interessanten Themengebiet in Zusammenarbeit mit seiner Arbeitsgruppe am Helmholtz Zentrum für Infektionsforschung in Braunschweig und seiner Arbeitsgruppe an der Universität des Saarlandes in Saarbrücken anfertigen zu können. Zudem gilt mein Dank Prof. Dr. Uli Kazmaier für die Übernahme meines Koreferates und seine motivierende Unterstützung zu Beginn meiner Promotion mit den Worten: „Sie schaffen das schon“.

Für die Übernahme meiner Betreuung am Helmholtz Zentrum für Infektionsforschung in Braunschweig habe ich mich besonders bei Rolf Jansen zu bedanken. Er begleitete mich mit einem großartigen Engagement und einer Empathie für die Naturstoffforschung über die Zeit meiner Promotion, die mich immer wieder mitgerissen hat. "Vielen Dank für den Einblick in Deine spannenden Arbeiten und die vielen Stunden, in denen wir gemeinsam diskutiert haben und ich an Deiner Erfahrung partizipieren konnte."

Nicht zu vergessen, die weiteren Chemiker, die mich mit Rat und Tat durch meine Doktorandenzeit begleitet haben Heinrich Steinmetz und Victor Wray. Gemeinsam haben wir zu jedem Problem immer mindestens einen Lösungsansatz finden können.

Danke an die routinierten Hände der Chemie Silke Reinecke, Aileen Teichmann und meiner „langjährigen“ Laborkollegin Kerstin Schober für die wunderbare Zeit. Auch den Wegbegleitern Patrick Okanya und den Auszubildenden Hendrik Tauscher danke ich an dieser Stelle.

Aus dem Fachbereich der Biologie danke ich ganz besonders Herrn K. Gerth für die hervorragende Wahl des *Cystobacter ferrugineus* Projektes und die gute Betreuung während meiner Doktorarbeit. Des Weiteren gilt mein Dank, Frau K. I. Mohr für die Übernahme dieses Projektes und Herrn H. Irschik für die Bereitstellung der Stämme im Sulfangolid Projekt, sowie weiterführenden Unterweisungen zu den Arbeiten im Biologielabor, und die langen interessanten Gespräche.

Den helfenden Händen der Biologie Diana Telkemeyer, Claudia Körner, Birte Trunkwalter, Klaus Conrad und Christiane Mollenschott danke ich für ihren Einsatz, nicht zu letzt bei meiner eigenen Fortbildung im Bereich der Mikrobiologie.

Der Fermenter-Crew Burkhard Ebert, Andrew Perreth, Axel Schulz, Reinhard Sterlinski und Wolfgang Kessler gilt mein Dank für die hervorragende Zusammenarbeit. Mein Respekt gilt Eurer Erfahrung mit "den großen, alten Kesseln"!

Christel Kakoschke und Beate Jaschok-Kentner danke ich für das Messen unzähliger NMR Spektren und die netten erfrischenden Kaffeerunden.

"Allen zusammen noch einmal ein ganz herzliches Dankeschön für das sehr gute und produktive Arbeitsklima am Helmholtz Zentrum für Infektionsforschung und Eure wunderbare Unterstützung."

Der Arbeitsgruppe von Prof. Dr. Rolf Müller im Saarland sage ich vielen Dank dafür, dass sie mir den Mut gegeben haben, mich auf dieses Experiment einzulassen. Die Besuche zu Progress Berichten im Saarland und Eure Arbeitsbesuche in Braunschweig, sowie sämtliche Kneipenbesuche haben mir immer sehr viel Spaß gemacht!

Meiner Familie lasse ich einen herzlichen Dank dafür zukommen, dass sie mir in den ganzen Jahren zur Seite stand und alle Höhen und Tiefen während des Studiums und der Doktorandenzeit mit mir durchgestanden haben und meinen Zweifeln keinen allzu großen Raum ließ. "Ich konnte mir Eurer Unterstützung immer sicher sein." Ein Dankeschön geht auch an meine Patentante U. Rinas, die mir die Naturwissenschaften schon früh im Leben näher gebracht hat.

Mein abschließender Dank gilt den Menschen, die mir in dieser intensiven Zeit des Lernens und Forschens dazu verhalfen, die Sicht auf andere Dinge im Leben nicht zu verlieren. Für ein wenig Abwechslung während des gemeinsamen Studiums bedanke ich mich bei Stefanie Böhm, Robert Lehmann und Inga Degenhardt, sowie meiner Nachbarin Kirsten Deppner und meiner Schwimmkollegin Kristin Schake. Außerdem danke ich natürlich Alexander Neumann für die schönen gemeinsamen Jahre und noch viel schöneren Urlaube.

Zusammenfassung

Myxobakterien sind außergewöhnliche Bodenbakterien und vielseitige Produzenten von zahlreichen biologisch aktiven Naturstoffen. Ziel dieser Arbeit war die Charakterisierung von neuen Sekundärstoffen dieser gleitenden Bakterien.

Im Rahmen dieser Arbeit wurde das Sauerstoff- und Licht- empfindlichen Roimatacene (**26**) aus dem Rohextrakt von *Cystobacter ferrugineus* Stamm Cb G35 auf Grund einer Aktivitäts-basierten Isolierung identifiziert. Die milde Isolierungsstrategie beinhaltete neben weiteren Stabilisierungstechniken die Zugabe des Radikalfängers 4-Ethoxyphenol. Die relative Konfiguration von **26** wurde mit Hilfe von Rychonovsky´s Acetonid Methode sowie 1D und 2D NMR Studien in Kombination mit Molekulardesign hergeleitet. Anschließend wurde die absolute Konfiguration mit der Mosher Methode bestimmt. Der Stamm Cb G35 produzierte zusätzlich sechs *p*-Hydroxyacteophenon Amide **34a-f**. Die biologischen Vorstufen von Roimatacene (**26**) und *p*-Hydroxyacetophenon *iso*-Butanamid (**34a**) wurden durch Fütterungsexperimente mit den D, ^{13}C und ^{15}N-Isotopenmarkierten Vorstufen ermittelt.

Die Strukturen der myxobakteriellen Sulfangolide **25a-d** wurden mit Hilfe ihrer NMR Daten verifiziert. Durch detaillierte NMR Analysen und dem Vergleich der modellierten 13R^* und 13S^* Diastereomere von Sulfangolid C (**25c**) wurde die relative Konfiguration als all-*trans* 13R^*,14S^*,15R^*,16R^*,17S^*,19S^*,20R^*,26R^*,27R^* hergeleitet. Zusätzlich wurden die biosynthetischen Vorstufen von **25c** durch Fütterungsexperimente bestimmt.

Abstract

Myxobacteria are an extraordinary group of soil bacteria and versatile producers of numerous biologically active natural products. The aim of the thesis was the characterisation of novel secondary metabolites from these gliding bacteria.

An activity guided isolation procedure for the oxygen- and light-sensitive roimatacene (**26**) from the crude extract of *Cytsobacter ferrugineus* strain Cb G35 was developed. The mild isolation strategy included among other stabilization techniques the addition of the free radical scavenger 4-ethoxyphenol. The relative configuration of **26** was establishing by applying Rychonovsky´s acetonide method combined with 1D and 2D NMR studies and molecular modelling. The absolute configuration of **26** was assigned by Mosher´s method. In addition, strain Cb G35 was found to produce a family of six *p*-hydroxyacetophenone amides **34a-f**. The biosynthetic precursors of roimatacene (**26**) and *p*-hydroxyacetophenone *iso*-butanamide (**34a**) were studied by feeding experiments with D-, ^{13}C- and ^{15}N-labelled precursors.

The structures of the myxobacterial sulfangolids **25a-d** were verified from their NMR data. The relative configuration of sulfangolid C (**25c**) was derived by detailed NMR analyses and comparison of the modelled 13R^* and 13S^* diastereomeres of **25c** to finally establish the relative all-*trans* 13R^*,14S^*,15R^*,16R^*,17S^*,19S^*,20R^*,26R^*,27R^* configuration. The biosynthetic precursors of **25c** were studied by feeding experiments.

Table of Content

List of Abbreviations

Å	angstrom
ACN	acetonitrile
$[\alpha]_D^{RT}$	specific optical rotation at RT and 589 nm
APT	attached proton test
B.C.	Before Christ
c	concentration [g/100 mL]
calc.	calculated
°C	degree Celsius
$CaCl_2 \times 2\ H_2O$	calcium chloride dihydrate
CD	circular dichroism
$CDCl_3$	deutero chloroform
CD_3OD	deutero methanol
CoA	Coenzym A
COSY	correlation spectroscopy
DCM	dichloromethane
δ_C	^{13}C chemical shift
$[D_6]$DMSO	deutero DMSO
DEPT	distortionless enhancement by polarization transfer
δ_H	^{1}H chemical shift
DMAP	4-(dimethylamino)-pyridine
DMSO	dimethylsulfoxide
DNA	deoxyribonucleic acid
E. coli	*Escherichia coli*
ELISA	enzyme-linked immunosorbent assays
ESI	electrospray ionisation
ESI-TOF-MS	electrospray ionisation- time of flight- mass spectrometry
Et_3N	triethylamine
Et_2O	diethyl ether
Eu	europium
FDA	US Food and Drug Administration
FR	flow rate
g	gram

GBF	Gesellschaft für Biotechnologische Forschung
GC	gas chromatography
h	hour
H_2	hydrogen gas
HCl	hydrochloric acid
HEPES	(4-(2-hydroxyethyl)-1-piperazineethanesulfonic acid
HETLOC	hetero half-filtered TOCSY
HMBC	heteronuclear multiple-bond correlation
HMQC	heteronuclear multiple quantum coherence
H_2O	water
HPLC	high-performance liquid chromatography
HRESIMS	high-resolution electronspray ionisation mass spectrum
HRMS	high resolution mass spectrometry
H_2SO_4	sulphuric acid
HSQC	heteronuclear single quantum coherence
HTS	high-throughput-screening
Hz	hertz
HZI	Helmholtz Centre for Infection Research
IC_{50}	half maximal inhibitory concentration
ir	incorporation rate
IR spectrum	infrared spectrum
J	coupling constant
KBr	potassium bromide
kg	kilogram
KNO_3	potassium nitrate
KOH	potassium hydroxide
KR	ketoreductase
L	liter
LC-MS	liquid chromatography-coupled mass spectrometry
LC-NMR	liquid chromatography coupled NMR
LC-SPE-NMR/MS	liquid chromatography coupled solid-phase extraction and NMR/MS
m	multiplicity
M	molar
MeOH	methanol

mg	milligram
$MgSO_4 \times 7\ H_2O$	magnesium sulfate heptahydrate
Mbp	mega base pair
MHz	mega hertz
MIC	minimum inhibitory concentration
min	minute
mL	milliliter
MM	molecular mechanics
mp	melting point
MPLC	medium-performance liquid chromatography
MRSA	methicillin-resistant *Staphylococcus aureus*
MS (DCI)	direct chemical ionisation mass spectrometry
MTPA	methoxy(trifluoro-methyl)phenylacetyl
M. xanthus	*Myxococcus xanthus*
mM	milli molar
nM	nano molar
m/z	mass-to-charge ratio
NaAc	sodium acetate
NaCl	sodium chloride
Na-Fe-EDTA	sodium iron ethylenediaminetetraacetate
N_2-gas	nitrogen gas
NH_4Ac	ammonia acetate
$NaHCO_3$	ammonia bicarbonate
nm	nanometer
NMR spectroscopy	nuclear magnetic resonance spectroscopy
nOe	nuclear Overhauser enhancement
NOESY	nuclear Overhauser enhancement spectroscopy
obsd.	observed
ORD	optical rotatory dispersion
Pd/C	palladium/carbon
PKS	polyketide synthase
ppm	parts per million
PPTS	pyridine-*p*-toluenesulfonic acid
Pr	praseodymium

PS-HMBC	phase sensitive HMBC
QM method	quantum mechanical method
R_f	retention factor
R&D	Research & Development
RNA	ribonucleic acid
RND efflux pump	resistance-nodulation-cell division efflux pump
RNAP	RNA polymerase
ROESY	rotating frame Overhauser enhancement spectroscopy
RP-chromatography	reversed phase chromatography
rpm	revolutions per minute
R_t	retention time
RT	room temperature
$Ru(PPh_3)_3Cl$	tris(triphenylphosphine)rhodium (I) chloride
SAM	S-adenosyl-L-methionine
SAR	structure-activity relationship
S. aureus	*Staphylococcus aureus*
sp.	species
TEA	triethylamine
TLC	thin-layer chromatography
TOCSY	total correlation spectroscopy
u	unified atomic mass unit
UDB	universal NMR database
UV/Vis spectrum	ultraviolet-visible spectrum
VRE	vancomycin-resistant enterococci sp.
Yb	ytterbium
µg/ µm/ µL	microgram / micrometer / microlitre
φ	torsion angle
λ_{max}	wavelength of the most intense UV/Vis absorption
ε	molar extinction coefficient

1 Introduction

1.1 The Role of Natural Products in Drug Discovery

Human medicine has been revolutionized by the application of natural products, which have assisted to double the life expectancy from 40 years to more than 77 years in the 20th century.[1]

1.1.1 Natural Products as a Source for Drug Development

The influence of natural products in medicine is enormous. By 2002 over 60% of the approved drugs were derived from natural products as a drug themselves, derivative or as lead structure.[2] The power of Nature is already known for centuries. As one example, Hippocrates described the use of willow tree bark extracts against fever and pain in the 5th century B.C..[3] However it is just 200 years ago that morphine was isolated from opium introducing purified drugs from plants in drug application.[1] It was as late as the 1870s that microorganisms were recognized for their therapeutic potential, and it took until 1929, when Alexander Flemming published his observation that *Penicillium notatum* inhibited the growth of *Staphylococcus aureus*. Ten years later the first stable penicillin was described and started the industrial production of penicillin during the Second World War. The antibacterial use of penicillin in human and animal medicine initiated the golden age of antibiotics, and different classes of the "wonder drug" were identified until the 1980s.[4] All antibiotics are classified according to their structural relations and targets. The commercial antibiotic classes include the most important β-lactams, quinolones, tetracyclines, macrolides, aminoglycosides, ansamycins, glycopeptides and polypeptides.[5] A number of examples of the antibiotic classes are presented in Figure 1. The golden age of antibiotics lead to the assumption that infectious diseases were no longer life threatening. But today resistances among microbes from hospital and community-acquired pathogens are continuously rising and infectious diseases have become the third major cause of death in developed nations again.[6,7] *S. aureus* isolates resistant to penicillin G were already found in the 1940s and today virtually all *S. aureus* isolates are resistant to β-lactam antibiotics.[8] The number of "superbugs" resistant to nearly all antibiotics has increased enormously among hospital and also community-acquired pathogens in the last years. Abesides *S. aureus* isolates resistant to methicillin and glycopeptides, the vancomycin and multidrug resistant enterococci sp. and multidrug resistant Gram-negative bacteria as e.g. *Pseudomonas aeruginosa* are the new threats in infectious diseases with high mortality rates.[7]

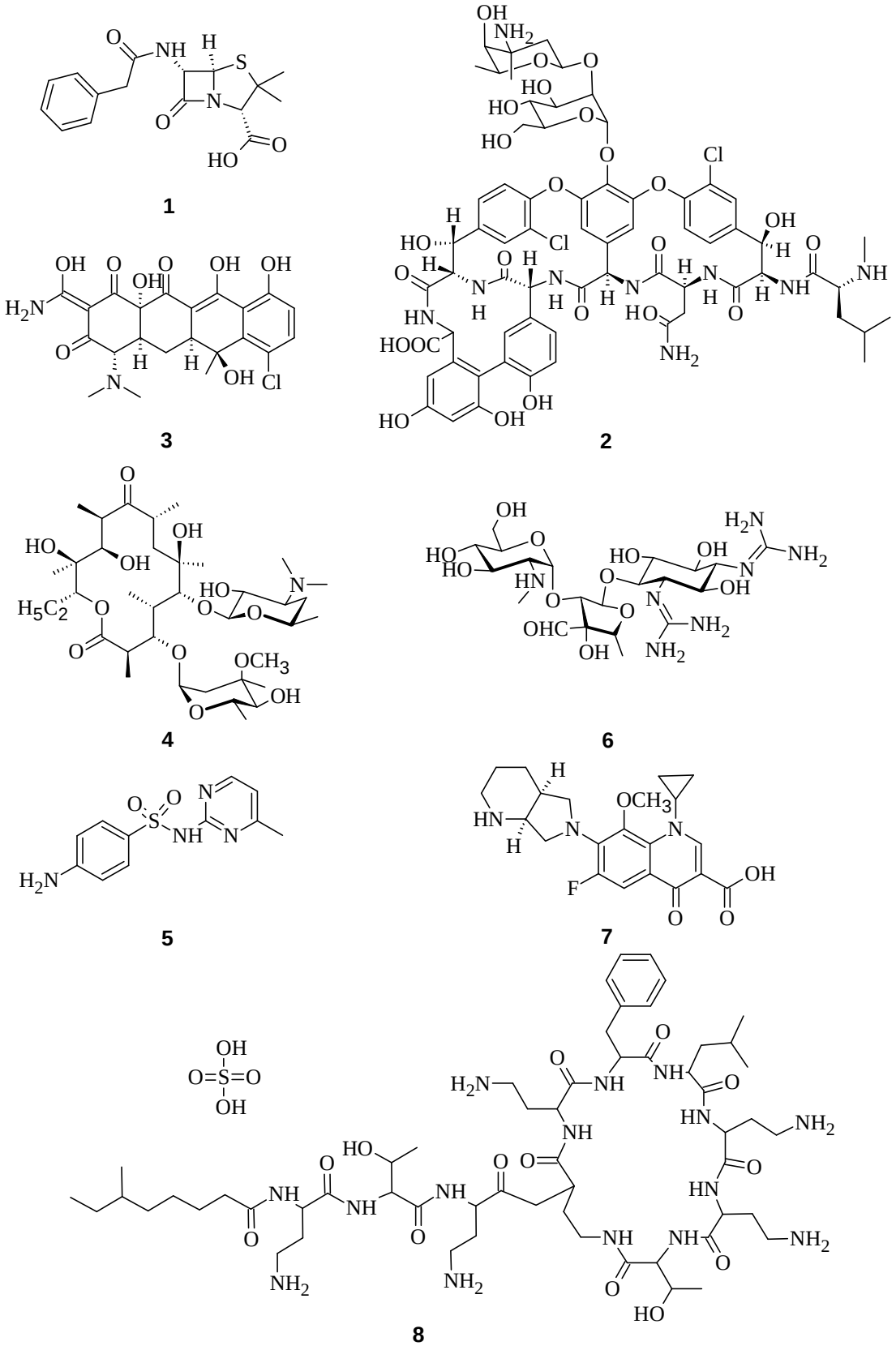

Figure 1. Examples of different antibiotic classes (class and targets are given in parentheses): penicillin G (**1**, β-lactame; transpeptidase cell wall); vanosamin (**2**, glycopeptide, cell wall); chlortetracycline (**3**, tretracycline, 30S-ribosome); erythromycin A (**4**, macrolide, 50S-ribosome); sulfamerazin (**5** , sulfonamide, nucleic acid synthesis); streptomycin (**6**, aminoglycoside, 30S ribosome); moxifloxacin (**7**, quinolone, gyrase inhibitor); polymyxin B (**8**, polypeptides, cell membrane).

1.1.2 Drug Development

New drugs and cellular targets are urgently needed to fight multidrug-resistant pathogens like MRSA, VRE and *Pseudomonas aeruginosa*.[9] The combination of combinatorial chemistry and high-throughput-screening (HTS) has failed to meet these demands over the last 25 years.[10] Due to the high development cost and fast development of resistances, large pharmaceutical companies have abandoned their antibiotic research programs leaving this field to biotechnology companies and universities.[11]

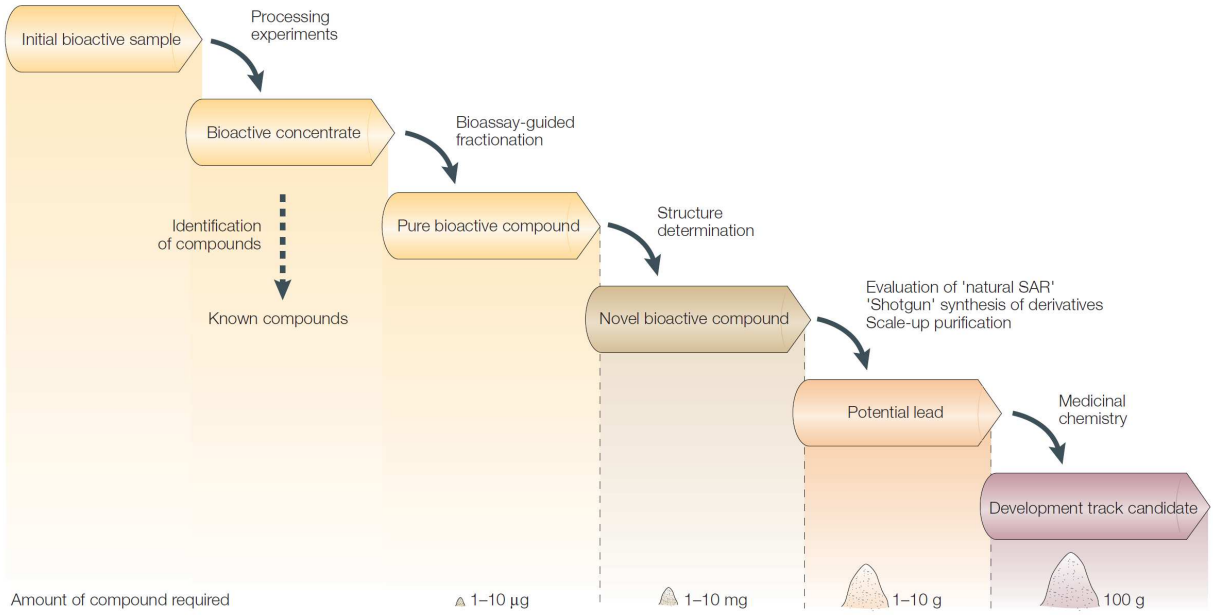

Figure 2. Chemical processes involved in natural product discovery: Starting from a biologically active sample, avoiding replication, purification and characterization of the active natural product, carrying out structure-activity relationship (SAR) studies to finally develop a lead compound.[12]

The combination of synthetic libraries and HTS enabled a fast screening of numerous compounds, which were easily available through chemical synthesis. The low "hit rate" of purely synthetic libraries of < 0.001% induced the screening of privileged libraries, which are based on biological active drugs.[13-15] Although purified natural products can be applied in HTS, the purification costs of complex extracts resulting from fermentation of microorganism or other natural sources are extremely high. The identification of an active secondary metabolite from a complex fermentation mixture and the effort associated with isolation and identification are challenging. Known antibiotics, as for example streptomycin, can mask other biological activities in crude extracts and it occurs in 1% of soil actinomycetes.[1] Separation techniques like high-performance liquid chromatography (HPLC) can reduce the complexity of crude extracts before applying biological assays. The combination of HPLC and high-resolution mass spectrometry can avoid replication of known secondary metabolites.

The biological test systems differ from whole-cell screenings, for example conducted with MRSA strains as well as hypersensitive mutants for the identification of selective protein-inhibitors,[16,17] as well as target specific biochemical assays, like enzyme-linked immunosorbent assays (ELISA) for kinases activity.[18] Natural products are complex structures with a high number of oxygen-containing substituent and stereocentres.[19] For these reasons, an unambiguous identification is time consuming and larger amounts of material are essential (Figure 2). Therefore, the supply has to be secured in order to successfully accomplish the verification and development of a drug candidate through medicinal chemistry.[12]

In order to provide the necessary amount of metabolite, different microbiological techniques that include feeding strategies, mutagenesis and up-scale fermentation are necessary. For example, optimized producer strains are capable of synthesizing 1.8 g/L of penicillin, which reduced the costs from 11.000 $/kg penicillin in 1945 to 4.5 $/kg 50 years later.[4] After 40 years of "brute force" genetics to improve production, combinatorial biology with genome-based strain reconstruction and heterologous expression are the new tools to increase the biotechnological out-put of "biological engineers".[4]

Today a large number of biologically active natural products are known, but only one out of 10,000-150,000 compounds is of medical use. One out of 3,600 active candidates from pharmaceutical screenings is developed further, and only three functional antibiotics were found in a screening of 400,000 microorganisms over 10 years. Five out of 5,000 compounds approached clinical trials, while only one was approved by the FDA.[5]

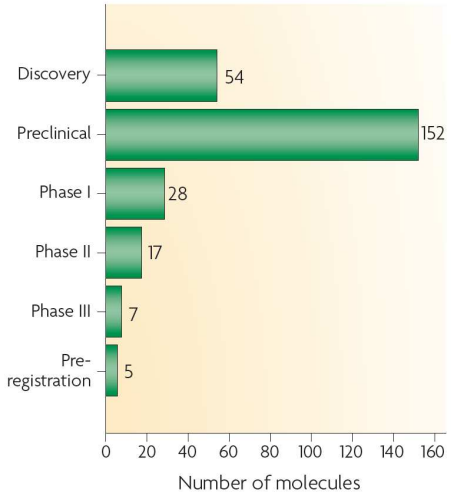

Figure 3. Current status of antibiotic R&D activity at each development stage (source IMS Health 2009).[20]

Figure 3 presents the current status of the development of new antibiotics. In 2009 there were 152 candidates in preclinical testing, but such a low number as 52 candidates were in clinical phase I/II and III. The five candidates in pre-registration are ceftobiprole (new class of cephalosporin, Basilea Pharmaceutica), dalbavancin (glycopeptide, Pfizer), iclaprim (dihydroholate reductase inhibitor, Arpida) and oritavancin (glycopeptide, the Medicines Company). Some of these were especially designed against resistant pathogens and the majority is targeting MRSA.[20]

1.2 Myxobacteria: a Promising Source for Secondary Metabolites

"Myxobacteria are a rich source of novel structural ideas."[21]

1.2.1 The Social Life of Myxobacteria

Myxobacteria belong to the Gram-negative bacteria allocated at the delta branch of the Proteobacteria. They have rod-shaped vegetative cells about 4-12 μm long and 0.7–1.2 μm wide. Myxobacteria were first recognized by their extraordinary and sophisticated social life: they live in swarm colonies, which move by gliding over surfaces (Figure 4a).[22] They have a remarkable intercellular communication system for swarming in colonies and forming myxospores upon starving conditions.[23] The formation of fruiting bodies guarantees the start of a new life cycle as a swarm rather as an individual cell. The fruiting bodies can have simple shapes of soft slime balls like *Myxococcus fulvus* (Figure 4b) or complex structures as the trees of the *Chondromyces crocatus* (Figure 4c), which consists of a brown slime stalk and bright yellow sporangioles. Fruiting bodies come usually in bright colours of yellow, orange, red, brown, or black and measure 20-1000 μm.

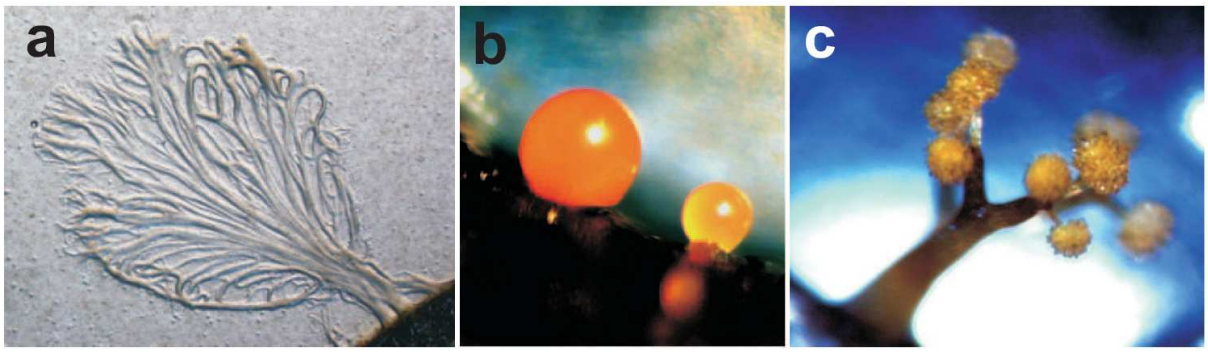

Figure 4. (a) Swarming colony of *Sorangium cellulosum* from cellulose paper on agar, fruiting bodies of (b) *Myxococcus fulvus* and (c) *Chondromyces crocatus* (pictures by K. Gerth, HZI).

Living in large colonies is indispensable for myxobacteria. They are commonly known as soil bacteria, even though some halo-tolerant myxobacteria were isolated from the marine environment of the Pacific.[24,25] The environment, from which the majority of myxobacteria were isolated, is rich in organic matter providing sufficient nutrition of soil, rotting plant material or dung of various animals as well as other microorganisms.[26] Myxobacteria are specialized in degrading biomacromolecules, like cellulose or other bacteria and fungi, using extracellular enzymes.

These environmental niches are not only rich regarding nutrition, but also accommodate numerous microbial inhabitants. For this reasons myxobacteria are not only interesting organisms for studying their remarkable life style, but are also a rich source for structurally novel secondary metabolites with new modes-of-action that are excreted from their biochemical defence systems in order to protect themselves against other predators such as bacteria or fungi.[21,27,28]

1.2.2 Secondary Metabolites from Myxobacteria

During a screening of 1700 *Sorangium cellulosum* strains about 90% of the extracts were found to be biological active. Some secondary metabolite families were frequently found during this screening, like icumazole (**9**) (unpublished data R. Jansen, H. Irschik, HZI), and spirangien (**10**),[29] while others are relatively rare, e.g. jerangolid (**11**)[30] was synthesised by only 4 producer strains (Figure 5).[31] The immense biological activity and high diversity of secondary metabolites from myxobacteria is presumably due to their microorganism-rich habitat. In the three decades of myxobacterial research approximately 7500 strains have been isolated at the Gesellschaft für Biotechnologische Forschung (GBF, today Helmholtz Centre for Infection Research, HZI) and about 100 distinct core structures (about 67 have been published) and about 500 derivatives have been isolated.[28]

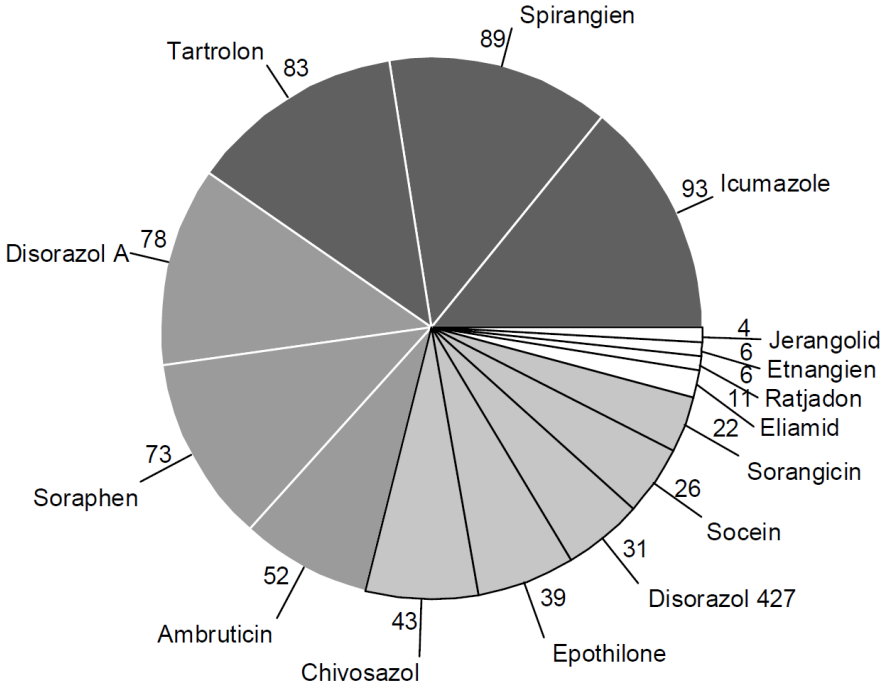

Figure 5. Frequency of selected secondary metabolite families in the screening of 1700 strains of the genus *Sorangium cellulosum*.[31]

At the time of their publication 40% of these secondary metabolites had a completely new structural carbon skeleton, while others were still new but contained structural elements previously known from other microorganism as *Streptomyces* or marine microorganism (sponges, tunicates and mollusks).[21] Myxobacterial secondary metabolites not only possess a high structural diversity, as the few examples in Figure 6 show, but exhibit remarkable new modes-of-action.[28] The soraphen family (**12**) for example was found to inhibit the growth of yeasts and molds (MIC 0.03-4 µg/mL) by selectively targeting fungal acetyl-CoA carboxylase.[32] Field trials with soraphen against numerous plant pathogenic fungi were carried out in cooperation with Ciba-Geigy, although its teratogenic activity prevented a commercial application as antifungal agent.[31]

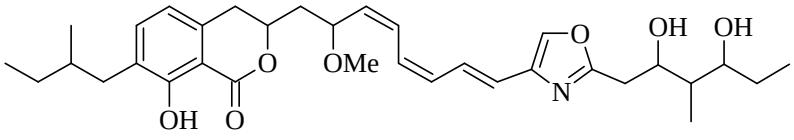

9

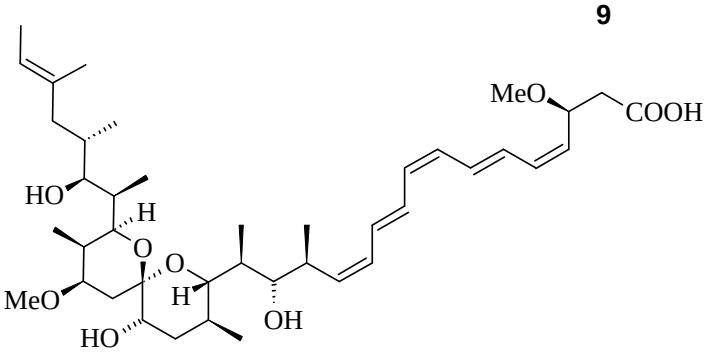

10

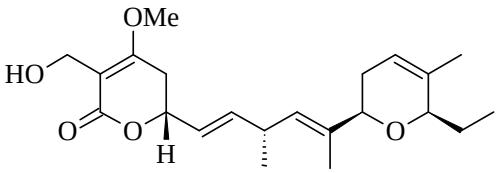

11

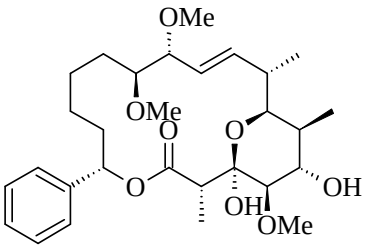

12

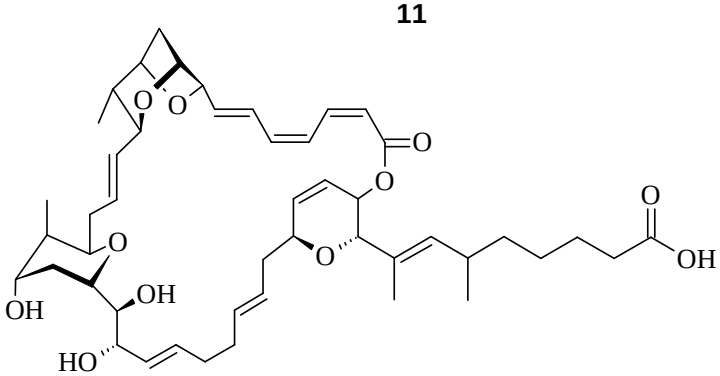

13

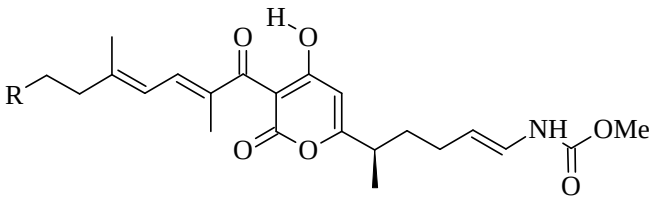

14 R = Me

15 R = CH(OH)C(CH$_3$)=CHCH$_2$CH=CHCH$_3$

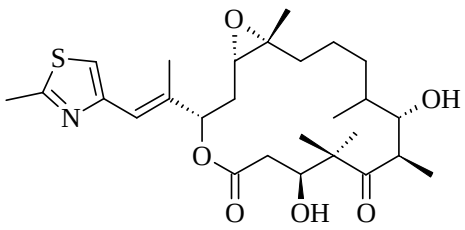

16

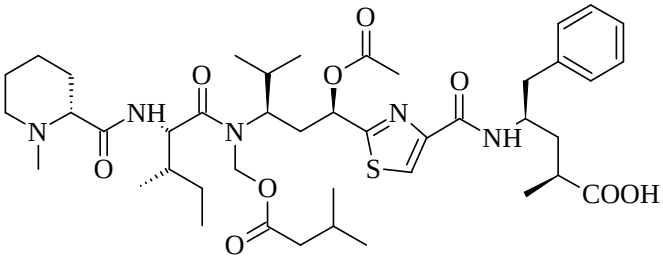

17

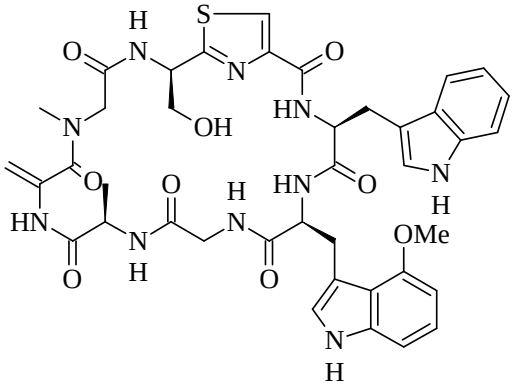

18

Figure 6. Examples of the structural diversity of myxobacterial secondary metabolites: icumazole A (**9**), spirangien A (**10**), jerangolid A (**11**), soraphen A$_{1\alpha}$ (**12**), sorangicin A (**13**), myxopyronin A (**14**), corallopyronin A (**15**), epothilon B (**16**), tubulysin (**17**), agyrin F (**18**).

Other antimicrobial metabolites proved to be active against known targets, but established a new mode-of-action: the myxobacterial antibiotic myxopyronin (**14**)[33] and corallopyronin(**15**)[34,35] bind to bacterial RNA polymerase (RNAP) as do the rifamycins[36] and sorangicins (**13**),[37,38] but show a different mode-of-action. Figure 7 shows the mode-of-action of myxopyronin (**15**) at the switch region of RNAP, which inhibits the opening of the clamp needed for DNA transcription.[39]

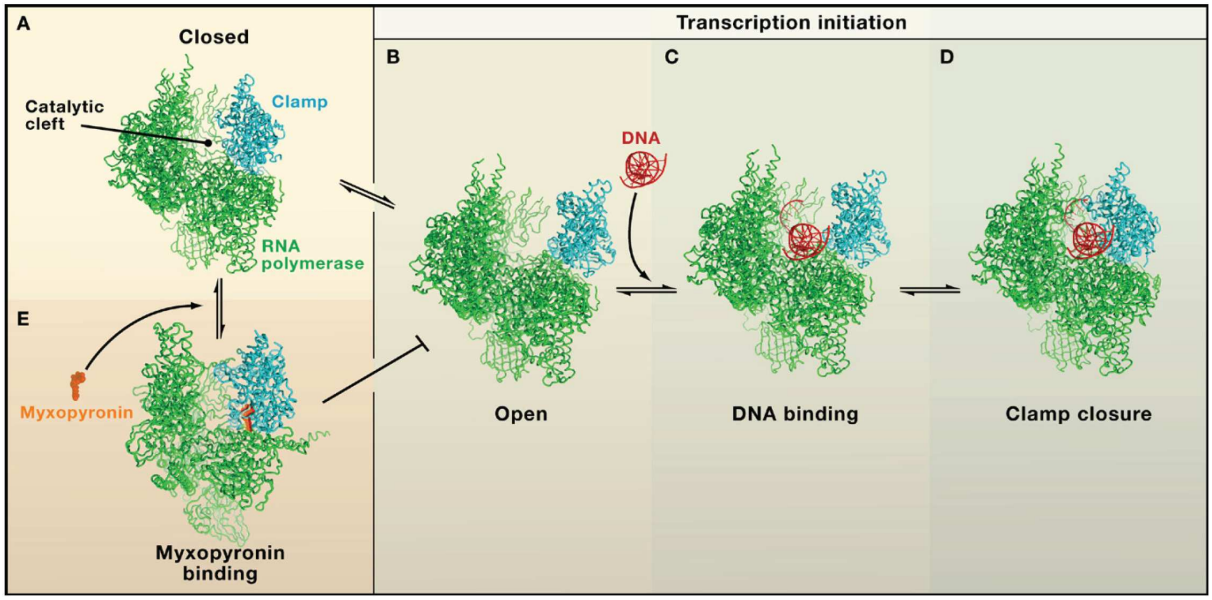

Figure 7. Initiation of RNA polymerase (RNAP) transcription: the RNAP can open (B) and close (A) by a 30° rotation of the clamp domain (cyan) at the switch region. The clamp is open (B) in order for DNA to bind to the catalytic cleft (C), before the clamp is closed (D) and transcription is promoted. Myxopyronin binds in the switch region and inhibits opening the clamp (E).[40]

Astonishingly, 10% of myxobacterial metabolites specifically interact with the cytoskeleton of eukaryotes.[21] Epothilon (**16**) was found to stabilize microtubule formation in eukaryotic cells. Consequently a semi-synthetic azaepothilon B was developed by Bristol-Myers Squibb (Ixempra®) and is used currently as an antineoplastic agent against Paclitaxel-resistant tumours.[41-43] In contrast to the microtubule stabilization of epothilon (**16**), the highly affective antimitotic peptide tubulysin (**17**) dissolved microtubules (IC_{50} of 0.01-10 nM).[44] Further investigation of the tubulysin family revealed 23 natural metabolites as well as the initial enzyme-free derivative pre-tubulysin.[45,46] Various synthetic approaches lead to optimized tubulysin–folate conjugates specifically targeting folate-receptor enriched tumours with especially good *in vivo* activity and favourable toxicity profile as drug candidates.[47-49] An additional myxobacterial compound for therapeutically application against intestinal cancer is the proteasome inhibitor (protein p27) argyrin (**18**) which is currently under investigation.[50]

The last three decades of research have demonstrated that myxobacteria are a rich source of potent natural products. The number of myxobacteria-derived secondary metabolites established these microorganisms as multiproducers comparable with the Cyanobacteria, Actinomycetales (~ 8000 compounds), Bacilli (1400 compounds) and Pseudomonads (400 compounds). Genome analyses of myxobacteria indicate that the isolated 100 core structures just scratch the surface of the true potential of these bacteria.[51] With 13.0 Mbp the genome of *Sorangium cellulosum* So ce56 is the largest bacterial genome known.[53] The genome of the model strain DK1622 from *Myxococcus xanthus* assigns more than 8.5% to natural product synthesis.[54] A study comparing the metabolic profiles by liquid chromatography coupled mass spectrometry (LC-MS) analysis of 98 *M. xanthus* strains collected worldwide insinuated the numbers of non-ubiquitous compounds per strain ranged from 6 to 24 metabolites.[55]

1.3 Structure Elucidation of Natural Products

"Indeed, structural miss-assignments clearly provide opportunities for synthetic chemists to make discoveries through total synthesis, and certainly show that there is still adventure to be had in the process of structure assignment."[56]

1.3.1 Structure Elucidation of Natural Products by 1D and 2D NMR Spectroscopy

Nuclear magnetic resonance (NMR) spectroscopy is the most important method for structure elucidation of natural products combined with high resolution mass (HRMS) spectrometry. Improvement of hardware and development of multi-pulse sequences for NMR techniques (discussed below) in the last years has made NMR spectroscopy a powerful tool in structure elucidation of unknown complex natural products. The ultimate tool for molecular structure determination will remain X-ray crystallography, but suitable monocrystals of X-ray quality are rare in natural products research.[57] NMR technology has been dramatically improved over the last decade through the use of superconducting cryogenic probeheads, superconducting cryogenic high-field magnets (1000 MHz) and smaller sample volumes (30 µL) to enhance sensitivity.[58] The new NMR hardware enabled liquid chromatography coupled NMR (LC-NMR) analysis for fast dereplication in high-throughput-screenings (HTS). This approach has recently been further improved by Bruker Biospin, who have developed a post column-solid-phase-extraction unit (LC-SPE-NMR/MS) coupled HPLC/NMR/MS system in order to reduce costs and accumulate the metabolite on cartridge systems allowing smaller NMR sample volumes (30 µL).[59] Figure 8 shows the amount of natural product which was required

for complete structure analysis in the year 1995 up to the year 2009 to give an impression of the practical advances in analytical technology.[60]

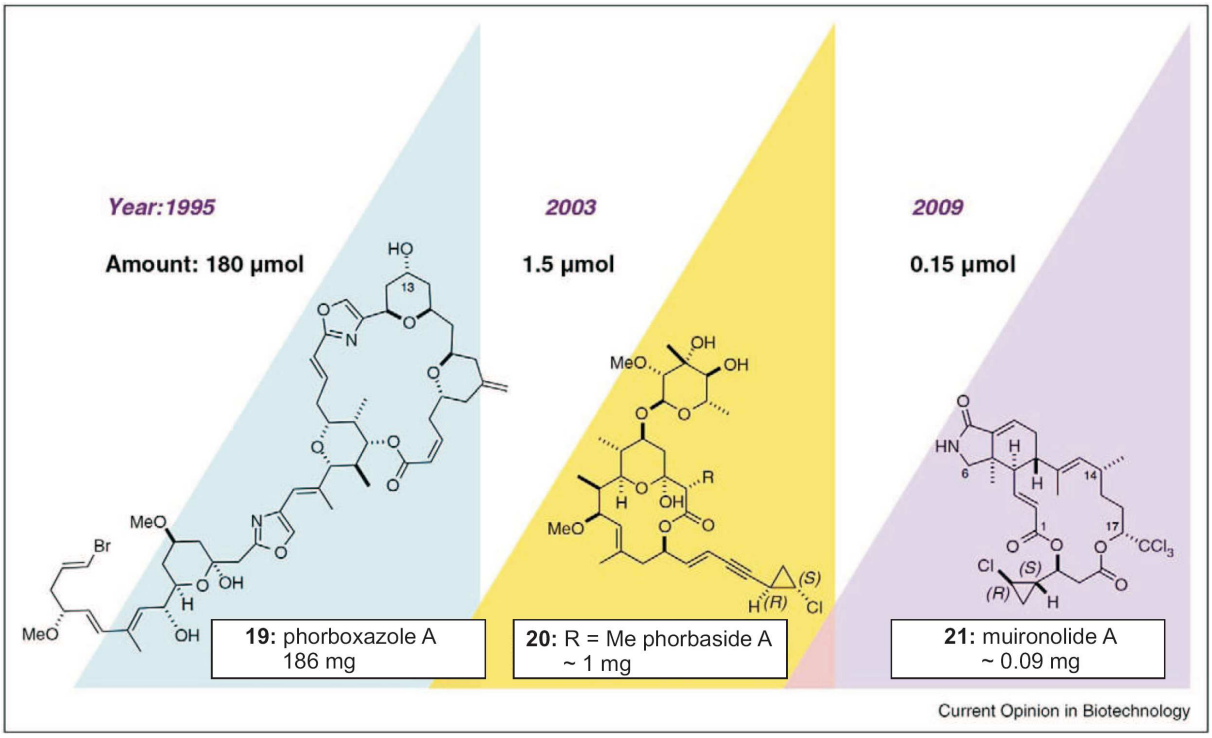

Figure 8. Decrease in the required amount of three generations of marine natural products for complete structure elucidation due to the continuous improvement in analytical technology.[60]

Practical structure elucidation begins with the molecular formula predicted by HRMS. Subsequently verification of the proposed molecular formula is based on 1D ^{1}H and ^{13}C NMR experiments, as well as on the calculated degree of unsaturation* and on information about functional groups obtained from IR- and UV/Vis spectra. The skeleton of an unknown compound can be further explored with 2D NMR experiments. The first step is to uniquely identify each proton directly bound to carbons by using heteronuclear HMQC (heteronuclear multiple quantum coherence) or the phase sensitive HSQC (heteronuclear single quantum coherence) experiments. HSQC provides information about carbon multiplicity, which can also be gained by 1D NMR experiments like APT or DEPT (see Table 1). The homonuclear $^{1}H,^{1}H$ COSY (correlation spectroscopy) experiment identifies structural fragments by through-bond coupling of geminal, vicinal and long-range protons. A TOCSY (total correlation spectroscopy) experiment is helpful for the analysis of polysaccharides or peptides by revealing proton correlations within one spin-system. After the assignment of structural fragments, the overall skeletal connectivity is established through a HMBC (heteronuclear multiple-bond correlation) experiment, revealing correlations through intervening

* Degree of unsaturation = $a + 1 - \frac{1}{2}(b - d)$; $C_aH_bO_cN_d$

heteroatoms and quaternary carbons linking the structural fragments to an overall connectivity of a compound.[57,61] All NMR experiments mentioned are tabulated in Table 1 which provides basic information about the experiments.[62]

Table 1: Overview of the basic NMR experiments used for structure elucidation.[62]

Abbreviation	Experiment	Purpose	Comment	Enhanced Experiments
APT	attached proton test	1D inverse technique for ^{13}C multiplicity	includes signals for quaternary carbons	DEPTQ
DEPT	distortionless enhancement by polarization transfer	1D inverse technique for ^{13}C multiplicity	standard	diverse
HMQC	heteronuclear multiple quantum coherence	2D inverse H,C correlation	decoupled ^{13}C NMR spectrum	diverse, better HSQC
HSQC	heteronuclear single quantum coherence	2D inverse H,C correlation	phase-sensitive gradient-selected version	gs-HSQC, E-HSQC
COSY	correlation spectroscopy	2D spin coupling nucleus	most important 2D NMR experiment: possible nucleus ^{1}H, ^{19}F, ^{31}P	Long-Range COSY, COSY-45, E.COSY
TOCSY	total correlation spectroscopy	2D correlations of protons in one spin-system	also called HOHAHA, used for peptides and oligosaccharides	gs-TOCSY, gs-SELTOCSY,
HMBC	heteronuclear multiple bond correlation	2D long-range H,C correlation	^{2}J(C,H) and ^{3}J(C,H) coupling	gs-HMBC, ACCORD-HMBC
NOESY	nuclear Overhauser enhancement spectroscopy	2D dipolar cross-relaxation of nuclei in close spatial relationship	assignment of peptide conformation and tertiary structure of proteins	gs-NOESY, (3D): HN-NOESY-HSQC, HC-NOESY-HSQC
ROESY	rotating frame Overhauser enhancement spectroscopy	2D dipolar cross-relaxation of nuclei in close spatial relationship	also called CAMELSPIN, shorter time compared to NOESY, also applied for molar mass of 1000- 3000	
HETLOC	heteronuclear long range coupling	2D determination long-range C,H spin coupling constants	low sensitivity, overlapping signals and coupling constants of the same spin system, enhanced versions	PS-HMBC, J-HMBC, HSQC-TOCSY, HSQMBC

1.3.2 Assignment of the Relative Configuration of Natural Products

The biological behaviour of compounds is strongly affected, not only by the connectivity and diversity of functional groups, but also by their spatial arrangement. Disclosing the relative and absolute configuration is therefore necessary to fully understand their chemical behaviour and biological interaction.[63]

NMR techniques play an important role providing geometric information of organic compounds. The 2D NMR experiments NOESY (nuclear Overhauser enhancement spectroscopy) and ROESY (rotating frame Overhauser enhancement spectroscopy) provide information about the dipolar cross-relaxation of protons with close spatial relationships. The cross peak intensities in these spectra are inversely proportional to the sixth power of the

distance separating the interacting protons and are therefore used in the assignment of relative configurations.[64] Another phenomenon in NMR spectroscopy is the scalar coupling of nuclei. The direct correlation of dihedral angles of protons corresponding to their vicinal $^{3}J_{H,H}$ coupling constant was first described by Karplus and became a very essential tool for conformation analysis.[65] This method has been further developed for heteronuclear coupling constants $^{2,3}J_{C,H}$ and different substituent patterns. Murata´s method is a *J*-based configuration analysis comparing experimental and predicted $^{3}J_{H,H}$ and $^{2,3}J_{C,H}$ values of possible rotamers of (1,2) or (1,3) acyclic carbon chains.[66] The $^{2,3}J_{C,H}$ values are measured using 2D HETLOC (hetero half-filtered TOCSY) or PS-HMBC (phase sensitive HMBC) NMR pulse-sequences. Another approach is the comparison of carbon and proton chemical shifts of an unknown configuration with model compounds of defined stereochemistry.[67] A compound library is realized in the universal NMR database (UDB).[68,69] Larger molecules with diverse stereocentres like natural products can be divided into fragments for comparison with suitable known compounds in the database, as shown in the example of oasomycin in Figure 9.[68]

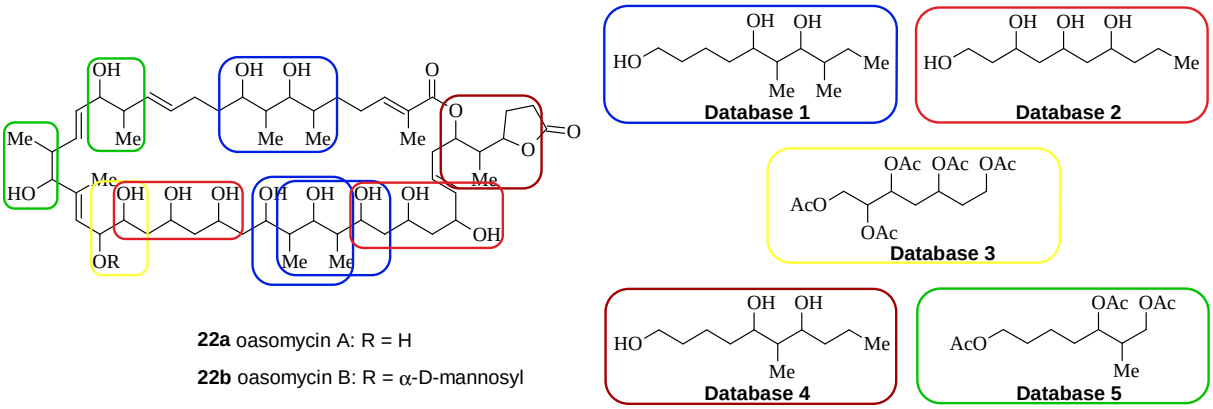

Figure 9. Example of an UDB approach for the natural product oasomycin and suitable fragments for the library search.[68]

In the last decade computational developments in quantum mechanical (QM) methods have progressed into fast empirical methods for calculating NMR parameters useful for the configuration assignment of natural products. Here the conformational search and geometry optimization of all significant conformers of each stereoisomer are carried out by empirical methods such as molecular mechanics (MM) or on the semiempirical level (PM3) followed by a QM method for final optimization.[70] The ^{13}C and ^{1}H NMR chemical shifts are calculated for each stereoisomer and compared with the experimental data. In addition, the resulting geometries can be compared with calculated coupling constants analoguously to Murata's method and nOe interactions.[71]

The relative configuration of 1,3-diols can also be established by the synthetic approach of Rychonovsky´s acetonide method.[72] For this method a six-membered acetonide is synthesized from the 1,3-diol. A *syn*-1,3-diol furnishes a chair conformation of the six-membered acetonide, which is indicated by distinct chemical shifts, like δ_C < 100 ppm for the quaternary carbon *C*Me$_2$, δ_C of 20.0 ppm for the axial methyl group and δ_C of 30.0 ppm for the one in the equatorial position. An *anti*-configuration of the 1,3-diol leads to a twisted-boat conformation with a characteristic *C*Me$_2$ δ_C value > 100 ppm and an average δ_C value for both methyl groups at about 25.0 ppm. The two conformation and the resulting characteristic chemical shifts are shown in Figure 10.[72] The relative structure of the natural products dermostatins A and B were assigned by synthesising multiple acetonides simultaneously and subsequently analysing their positions and their chemical shift with 2D NMR spectroscopy.[73]

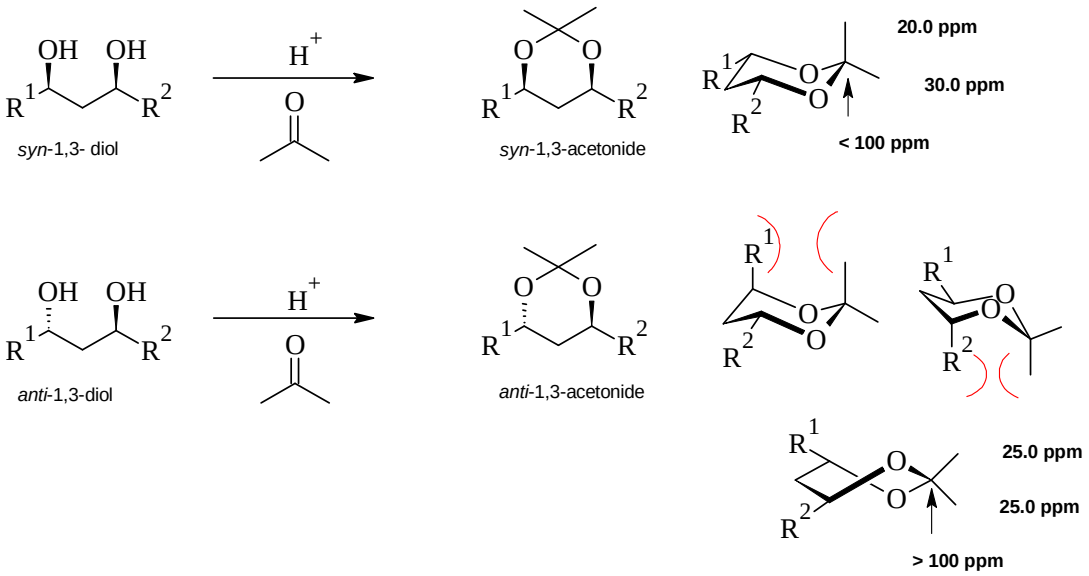

Figure 10. The chair and the twisted-boat configuration of the six-membered acetonides derived from either *syn*-1,3-diols or *anti*-1,3-diols, with the resulting characteristic δ_C shift for Rychonovsky`s acetonide method.[72]

1.3.3 Assignment of the Absolute Configuration of Natural Products

Good quality monocrystals of a compound would be required for an assignment of the absolute stereochemistry by X-ray crystallography. Unfortunately they are rarely produced for small natural products. Another common approach is the degradation of natural products by chemical synthesis using for example ozonolysis, hydrolysis or olefin metathesis. The degradation products can be compared to their corresponding enantiomeres by chiral HPLC or GC (gas chromatography), as commonly used for amino acid analysis of peptides after hydrolyses.[74,75] Chiro-optical methods are instrumental approaches that include optical rotatory dispersion (ORD) and circular dichroism (CD). The differential absorption of chiral molecules of either the specific optical rotation in ORD or the absorption bands in CD are used to compare synthetic material to the original natural product for determination of the absolute stereochemistry.[76,77] The universal NMR database (UDB) uses chiral NMR solvents to generate a chiral environment for the enantiomers. This causes small chemical shift differences allowing discrimination of the enantiomers, which are subsequently compared with the NMR data of the natural product or degradation products.[78-80] A larger chemical shift difference is produced by covalent binding of a chiral reagent producing diastereomers. Lanthanide shift reagents such as chiral complexes of europium (Eu), ytterbium (Yb) and praseodymium (Pr) are used to determine enantiomeric purity.[81] Mosher´s method is most widely used to explore the absolute stereochemistry of alcohol and amine moieties by using methoxy(trifluoro-methyl)phenylacetyl (MTPA) acids or derivatives.[82,83] For this method the compound is derivatized with both enantiomers of the MTPA acids to give diastereomers. The ligand of the MTPA ester shields or deshields the proton NMR signal of the neighbouring protons next to the MTPA ester as is shown in Figure 11. The shift difference $\Delta\delta^{SR}$ of the neighbouring protons in the two distereomers is calculated by subtracting the chemical shift δ_H of the (*R*)-MTPA ester derivative from the chemical shift δ_H of the (*S*)-MTPA ester derivative. The resulting $\Delta\delta^{SR}$ values (+/-) of the neighbouring protons are interpreted to give the configurational assignment based on the chiral centre of the auxiliary (Figure 11 c and d).[84]

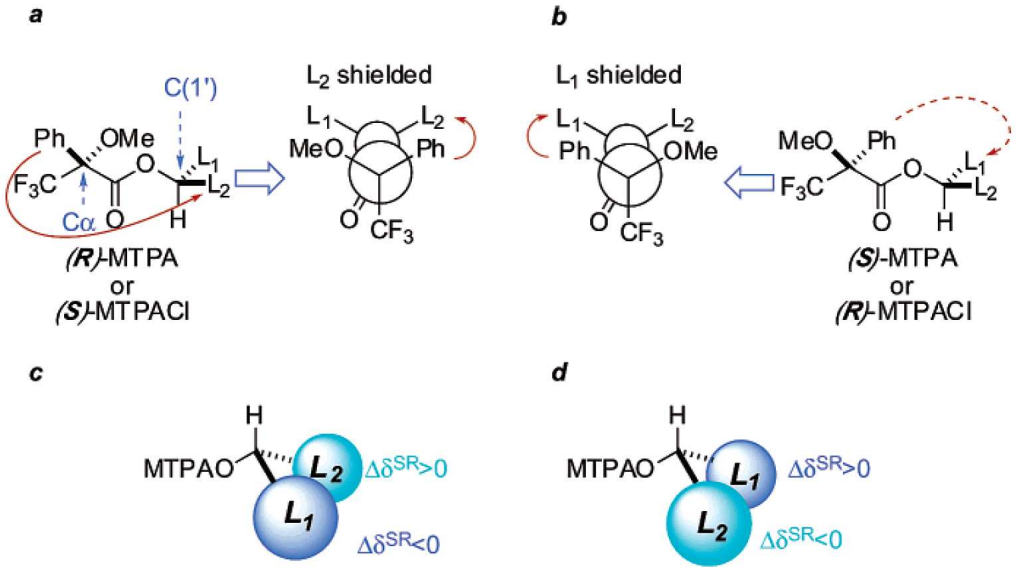

Figure 11. Mosher model of the (*R*)-MTPA ester (a) and (*S*)-MTPA ester (b) of an alcohol and the interpretation of the observed $\Delta\delta^{SR}$ values of protons for both possible configurations (c and d).[84]

Research of Reid et al. and Caffrey et al. on stereospecific ketoreductases (KR) enabled a complementary genetic approach to assign the absolute configuration of ketoreductase-derived hydroxyl-bearing stereogenic centres.[85,86] The stereochemical determination of the complex myxobacterial polyketide etnangien (**35**) for example was established by a combination of high-field NMR studies, molecular modelling, synthetic derivatization and by biosynthetic studies.[87]

The improvement of NMR and CD instrumentation permitted the absolute structure elucidation of muironolide A (**21**) (see Chapter 1.3.1, Figure 8) with only 90 µg of material. The absolute stereochemistry was assigned by using microcryoprobe NMR spectroscopy, high resolution mass spectrometry, circular dichroism (CD), and synthesis.[88]

The first results of a structural elucidation of a natural product using atomic-resolution scanning probe microscopy for structural determination have been published recently, suggesting a novel tool for structure elucidation of organic natural products.[89]

1.3.4 Structure Elucidation of Natural Products by Total Synthesis

The final step in the structure elucidation of natural products is the verification of a proposed structure by checking all the data for consistency and by comparison of similar natural products with common biosynthetic origins. However, the stereoselective total synthesis remains the final proof. A review by Nicolaou and Snyder investigated 300 revised structures between January 1990 and April 2004 through all classes of natural products.[56] The progress

in spectroscopic skills has made structure elucidation of unknown compounds a routine task, but does not rule out all pitfalls.

An exciting discussion of structure elucidation is the case of maitotoxin (**23**), the largest polyether from marine organism and a highly active biotoxin.[90,91] The gross structure of maitotoxin was described in 1993 by Yasumoto et al.[92] and the relative structure by Kishi et al.,[93] contemporaneously with the absolute stereochemistry by Tachibana et al. in 1996.[94,95] Biosynthetic studies of polyethers by Gallimore and Spencer suggested an opposite configuration of two stereocentres connecting the polyether rings J and K (marked red in Figure 12).[96] Nicolaou et al. applied computational chemistry to support the original published structure[97] and finally proved the molecular architecture by synthesis of the GHIJKLMNO ring system of maitotoxin 2008.[98] A total synthesis of the largest natural polyether known has not been accomplished as yet.

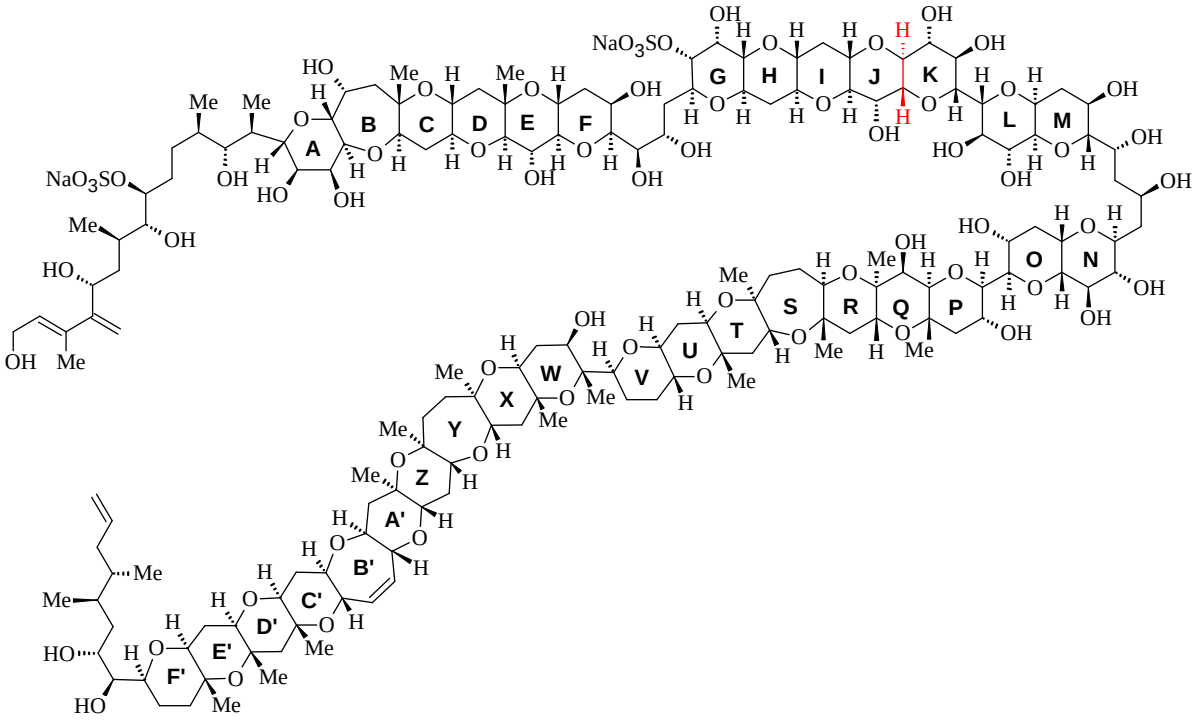

23

Figure 12. The structure of the largest polyether isolated so far, maitotoxin (**23**). The stereocentres questioned by Gallimore and Spencer at the connection of the J and K ether ring system are highlighted in red.

This is one of many examples in which the final proof of stereochemistry will be clarified by total or partial synthesis. Total synthesis can also provide confirmation if the proposed structure correlates with the assigned biological activity.[99]

1.4 Outline of this Work

Since myxobacteria have proved to be very versatile producers of biologically active secondary metabolites, the aim of the present thesis was to identify novel natural products from this extraordinary group of gliding bacteria. This thesis comprises the process of the isolation of a biologically active metabolite from a complex crude extract, as well as the structure elucidation not only the planar structures, but also the determination of the relative and absolute configuration of the complex compounds by applying chemical derivatization techniques, and detailed 1D and 2D NMR studies combined with molecular modelling.

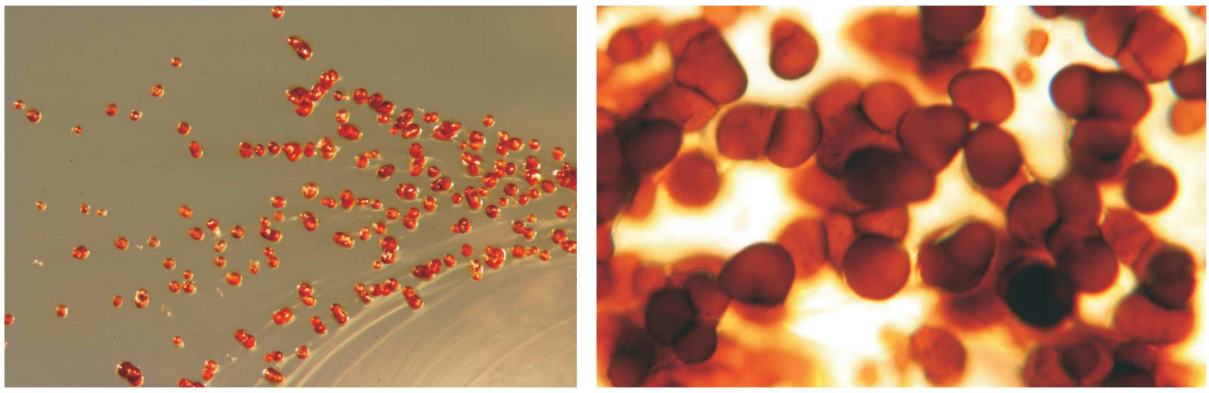

Figure 13. Fruiting bodies of the *Cystobacter ferrugineus* strain Cb G35 on agar plates (pictures by K. Gerth).

The *Cystobacter ferrungineus* strain Cb G35 was isolated from a soil sample by Klaus Gerth at the Helmholtz Centre for Infection Research (HZI). The crude extract of this strain was found to inhibit growth of *Staphylococcus aureus*, *Nocardia flava*, *Escherichia coli*, *Mucor hiemalis*, and *Rhodotorula glutinis* in an antimicrobial screening of myxobacteria. The strain was found to produce myxalamide C (**24c**), which is responsible for the *Nocardia flava*, *Mucor hiemalis*, and *Rhodotorula glutinis* growth inhibition by the crude extract.[100] Four homologues metabolites of the myxalamide family (Figure 14) were previously described from *Myxococcus xanthus* Mx x12,[101,102] and were further reported from the gene cluster analysis of *Stigmatella aurantiaca* Sg a15.[103] The aim of this work was to identify the unknown secondary metabolites synthesized by this strain and to subsequently elucidate their structures. Of special interest was the compound responsible for the *Escherichia coli* inhibition, due to the low number of effective antibiotics against Gram-negative bacteria.

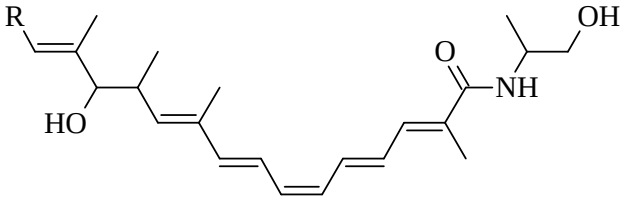

24

myxalamide A (**24a**)	R = 1-methylpropyl
myxalamide B (**24b**)	R = *iso*-propyl
myxalamide C (**24c**)	R = ethyl
myxalamide D (**24d**)	R = methyl

Figure 14. The myxalamide family described from *Myxococcus xanthus* and *Stigmatella aurantiaca*.

This thesis presents the developed isolation procedure of the light- and oxygen-sensitive polyunsaturated carboxylic acid roimatacene (**26**). The absolute stereochemistry of roimatacene (**26**) was derived by 1D and 2D NMR spectroscopy, derivatization to acetonides and Mosher´s esters as well as by molecular modelling. In addition, six novel *p*-hydroxyacetophenone amides (**34a-f**) were isolated from the crude extract of strain Cb G35 and their structures were elucidated. The biosynthetic precursors of **26** and **34a** were studied by feeding experiments and are presented in the course of this thesis.

Another project involved the family of sulfangolids (**25a-d**). Sulfangolid A (**25a**) and B (**25b**) were first reported in the annual report of the GBF 1996.[104] Further the sulfangolids were mentioned in numerous review articles as frequently found metabolites from the genus *Sorangium cellulosum*.[21,31,51,105] In the past the four myxobacterial sulfangolids **25a-d** were isolated from different strains of *Sorangium cellulosum* and the planar structures presented in Figure 15 were postulated in the research groups of Prof. Dr. H. Reichenbach and Prof. Dr. G. Höfle, but unfortunately not described exhibiting the required data (unpublished data H. Augustiniak, M. Herrmann, R. Jansen, H. Steinmetz, K. Gerth, H. Irschik, H. Reichenbach, W. Kessler, G. Höfle at HZI, former GBF). During my diploma thesis I concentrated on the isolation and further structure elucidation of sulfangolids A (**25a**) and C (**25c**). Subsequently to the isolation, complete sets of NMR data of **25a** and **25c** were measured and analysed. In my diploma thesis I presented a first proposal of the relative configuration of sulfangolid C (**25c**), subsequently I continued to verify the proposed relative configuration of **25c** by molecular modelling studies and extensive comparison of the NMR data. In addition, the biosynthetic precursors of sulfangolid C (**25c**) were studied by feeding experiments as a basis for further genetic studies. Further I verified all proposed structures of sulfangolids **25a-d** from their NMR data and summarized the combined detailed data (Manuscript is to be submitted).

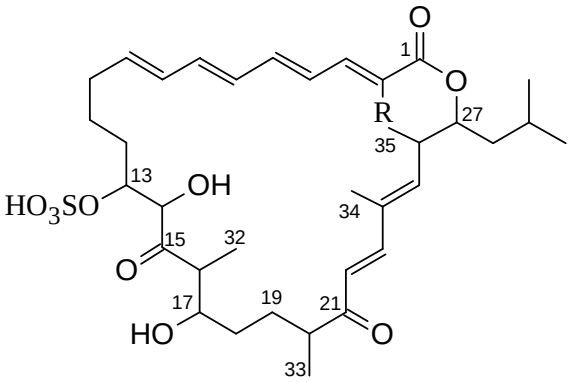

sulfangolid A (**25a**) R = H

sulfangolid B (**25b**) R = OMe

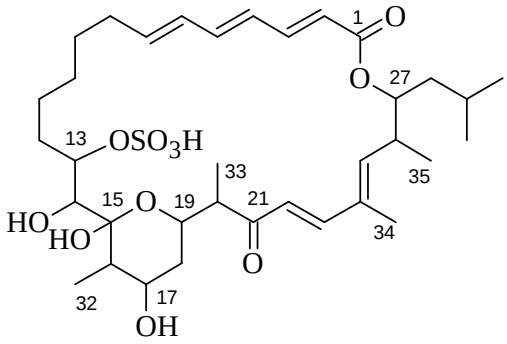

sulfangolid C (**25c**)

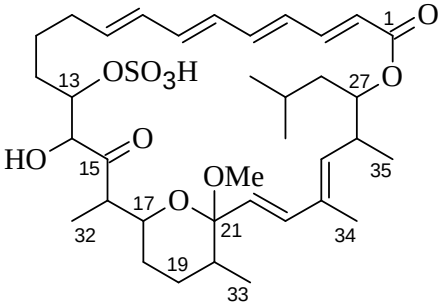

sulfangolid D (**25d**)

Figure 15. The proposed planar structures of the sulfangolid family (**25a-d**) isolated from different strains of the genus *Sorangium cellulosum* in the research groups of Prof. Dr. Reichenbach and Prof. Dr. Höfle at the HZI (former GBF).

2 Results

2.1 Roimatacene, a Polyunsaturated Carboxylic Acid from *Cystobacter ferrugineus* Cb G35

2.1.1 Development of an Isolation Procedure for Roimatacene (26)

The antibiotic activity of *Cystobacter ferrugineus*, strain Cb G35, against *E. coli* was detected in a broad antimicrobial screening. The crude extract was fractionated by HPLC and each fraction was tested against *E. coli*. Thus, the growth inhibition of *E. coli* was correlated to an unknown compound with a HRESIMS molecular ion cluster $[M-H]^-$ at *m/z* 515.3021 and a corresponding molecular formula of $C_{30}H_{44}O_7$ (calc. 515.3014). Accordingly, the unknown compound was isolated from the Amberlite XAD-16 adsorber resin of fermentation (70 L) in a bioactivity-guided procedure. Because the compound repeatedly decomposed during the isolation process, several fermentations were necessary for the development of a protective protocol for the oxygen- and light-sensitive polyene roimatacene (**26**). General aspects stabilizing the compound during the isolation were considered to finally result in the isolation strategy presented in Figure 16. Especially, all extracts had to be kept dissolved in methanol containing 4-ethoxyphenol as free radical scavenger. Prior to use, all solvents were saturated with nitrogen gas and all operations were carried out under nitrogen atmosphere. Ethyl acetate was filtered over aluminum oxide to remove peroxides, and extracts and fractions were handled in amber glassware.

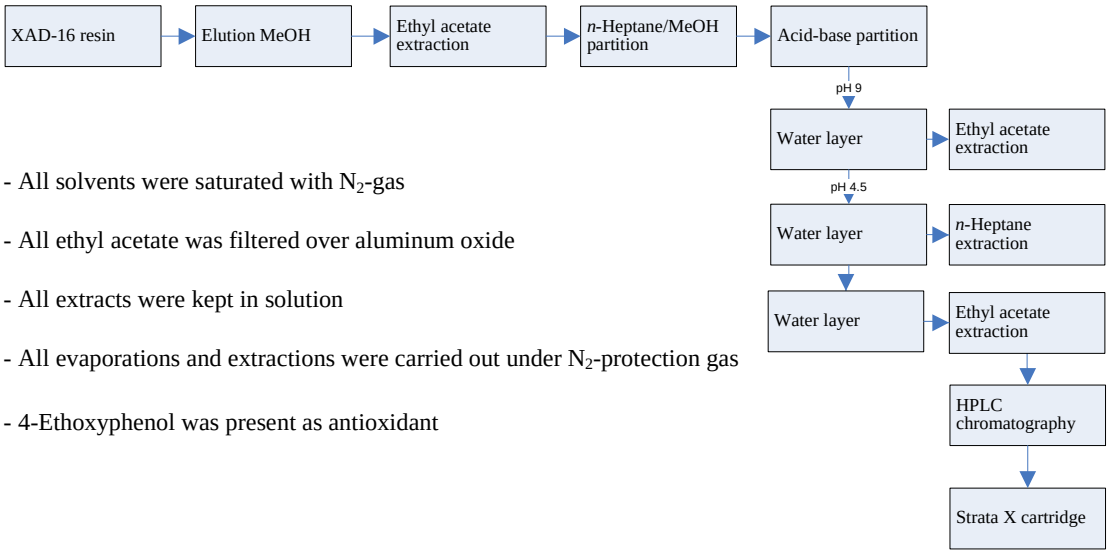

Figure 16. Isolation procedure for roimatacene (**26**), starting from Amberlite XAD-16 resin.

The Amberlite XAD-16 resin was harvested from the fermentation by sieving and was then eluted with methanol. Subsequently to evaporation of the organic solvent, the water layer was extracted with filtered ethyl acetate, and after evaporation of the ethyl acetate an *n*-heptane/methanol partition was carried out, in order to remove lipophilic by-products from the crude extract. The antibiotic **26** was further enriched by an advanced acid-base partition. The partition started with an ethyl acetate extraction of the alkaline water layer, which was subsequently acidified to pH 4.5. An additional extraction of the acidic water layer with *n*-heptane removed large amounts of fatty acid, which otherwise interfered with the further purification process by RP-chromatography. The enriched roimatacene (**26**) was extracted from the acidic water layer with ethyl acetate. The final purification was carried out by RP-chromatography using N_2-saturated solvents and providing 4-ethoxyphenol to each HPLC fraction. The methanol of the combined roimatacene (**26**) fractions was evaporated *in vacuo* and the residual water was applied on a strata-X cartridge (phenomenex) under nitrogen atmosphere. The newly established isolation procedure permitted the isolation of sufficient material for a complete structure elucidation as well as for all biological assays.

2.1.2 Structure Elucidation of the Core Structure of Roimatacene (26)

The biological active roimatacene (**26**), isolated according to the isolation protocol described in chapter 2.1.1, was analysed by HRESIMS, as well as 1D and 2D NMR spectroscopy for structure elucidation. Due to the instability of roimatacene (**26**) meaningful IR data were not obtained. HRESIMS of the molecular ion cluster $[M-H]^-$ at *m/z* 515.3021 established the molecular formula $C_{30}H_{44}O_7$ (calc. 515.3014) for **26** with 9 degrees of unsaturation. The molecular formula was supported by the NMR data, presented in Table 2.

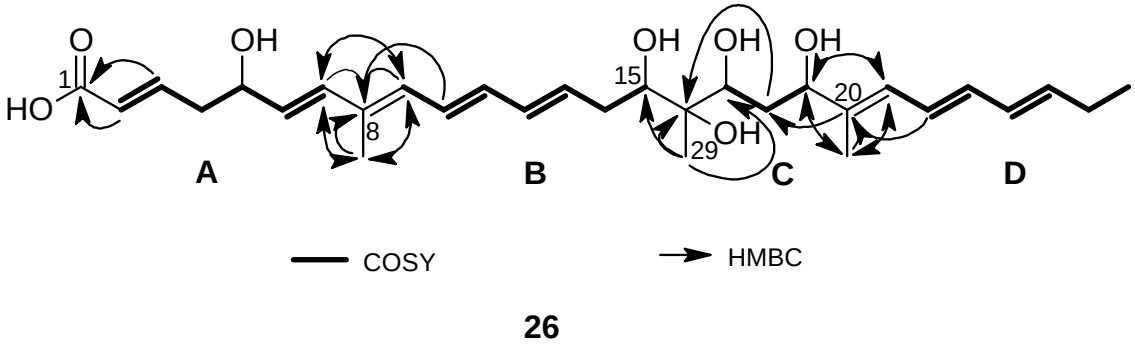

26

Figure 17. Structural elements A to D of roimatacene (**26**) assigned from the $^1H,^1H$ COSY spectrum and selected $^1H,^{13}C$ HMBC correlations.

All protons were assigned to their directly bound carbons from the $^{1}H,^{13}C$ HMQC spectrum. The interpretation of the $^{1}H,^{1}H$ COSY spectrum furnished four structural elements A to D presented in Figure 17. The connection of the structural elements was accomplished by the interpretation of the $^{1}H,^{13}C$ HMBC spectrum, allocating the carboxylic acid carbon C1 to subunit A by its HMBC correlations with 2H and 3H. The quaternary carbon C8 (δ_C 134.4 ppm) was verified by ^{13}C ATP NMR spectroscopy under the overlapping ^{13}C signal of C13 (δ_C 134.4 ppm). C8 was correlated to methyl group C28 and subsequently identified as connection between the structural fragments A and B from HMBC correlations with 7H and 9H, and correlations of methyl group C28 with the same protons (7H and 9H). Further, methines C7 and methine C9 showed mutual HMBC correlations securing the connection of subunits A and B. Similarly, the quaternary carbon C16 and the directly bound methyl group C29 showed HMBC correlations with 15H of subunit B, as well as with 17H and 18Hβ of subunit C. The final connection of structural unit D was indicated by HMBC correlations of C20 with 18H and 22H, as well as by mutual correlations of the methyl group C30 at C20 with methines 19H and 21H. In addition, methines 19H and 21H showed the expected mutual HMBC correlation between subunit C and D.

The interpretation of the ^{1}H NMR spectrum of roimatacene (**26**) clearly indicated the *trans*-configurations of the double bonds by vicinal coupling constants of 15 Hz. The *trans*-configurations were additionally supported by the corresponding nOes (Table 2).

The resulting planar structure of the polyunsaturated carboxylic acid roimatacene (**26**) is presented in Figure 18. The structure revealed an unusual accumulation of reactive functional groups, like a tertiary alcohol at C16, as well as three α-polyunsaturated alcohol groups at C5, C15 and C19, an acrylic acid residue and polyenes, altogether providing a well-founded justification for the observed sensitivity of **26**.

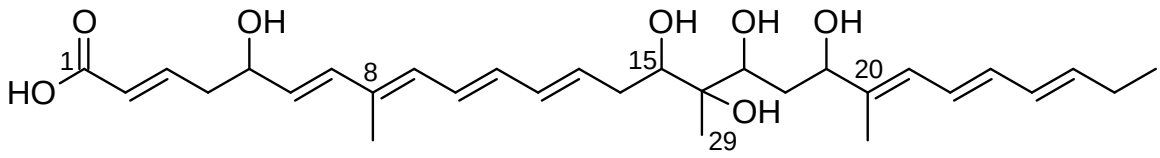

26

Figure 18. The planar structure of roimatacene (**26**).

Table 2: NMR data of roimatacene (**26**) (^{1}H 600 MHz, ^{13}C 150 MHz, [D_6]DMSO).

Atom	δ_H	H	m	*J* [Hz]	COSY	δ_C	HMBC	ROESY[d]
1	-	-	-	-	-	167.1	3, 2	-
2	5.79	1	d	16.0	3, 4	123.6	4 > 3	(3)
3	6.80	1	ddd	16.0, 7.0, 7.0	2, 4	145.6	4	(2) >(4),5
4	2.35	2	m[b]	-	3, 5[d]	40.0	3, 2, 6, 5OH	>(5), 2, (3)
5	4.18	1	ddd	11.0, 6.7, 5.5	4 > 6, 5OH	69.9	7, 6, 4 >3	7, (4,6), 3
5OH	5.01	(1)	s(br)	-	5	-	-	-
6	5.67	1	dd(br)	15.8, 5.9	7, 5	132.0	7, 4	28, (7, 5), 4
7	6.25	1	d	15.8	6	133.6	28, 6, 9, 10	9, 5, (6)
8	-	-	-	-	-	134.4[c]	28, 10, 7, 9[d]	-
28	1.80	3	s	-	9	12.6	7, 9	6, 10
9	6.10	1	m[a]	-	10, 12	131.0	7, 11, 28	7, 11
10	6.47	1	dd	14.6, 11.6	7, 9	126.9	12	28, 12
11	6.27	1	dd	14.6, 10.6	10, 12	133.9	13, 9	13, 9
12	6.16	1	m[a]	-	11, 13	131.7	10, 11 > 14α/β	10
13	5.82	1	ddd	15.1, 7.3, 7.3	12, 14β	134.4	14α/β, 11	11, 15, (14α/β)
14α	2.35	1	m[b]	-	13, 15, 14β	34.6	12, 13 > 15OH	(14β, 15, 13), 12, 17
14β	2.02	1	dddd	15.4,7.7,7.7, 1.5	14 α, 15, 13	-	-	(14α, 13)
15	3.51	1	dd[d]	9.7, 1.7[d]	15OH, 14β	73.4	29, 18β	13, 17, (14α), 29, 18α/β
15OH	4.52	(1)	s(br)	-	15	-	-	-
16	-	-	-	-	-	74.3	29, 18β	-
16OH	4.43	(1)	s(br)	-	17 > 15OH	-	-	-
29	0.93	3	s	-	-	18.2	17OH	17, 15 > 12, 18α
17	3.29	1	dd[d]	10.5, 1.5[d]	18 β[d]	73.5	29[d], 18β	19, 15, (18α), 29, 30, 21
17OH	4.08	(1)	s(br)	-	17	-	-	-
18α	1.70	1	ddd	13.8, 10.2, 1.3	19, 18 β	36.1	> 18β	(18β, 17), 15, 29
18β	1.49	1	ddd	13.8, 10.2, 6.4	19, 18 α >17	-	-	30, 15, (19)
19	4.14	1	dd	7.0, 6.4	18 α/β > 19OH	74.9	29, 30, 21, 18α/β	21, 17, (18α/β)
19OH	4.85	(1)	s(br)	-	19	-	-	-
20	-	-	-	-	-	140.2	30, 18α/β > 22	-
30	1.67	3	s	-	21	11.6	21, 19	19, 22
21	6.00	1	d(br)	11.2	22, 30	125.2	30, 23, 19	23, 19 > (22), 17
22	6.37	1	dd	14.5, 11.2	23, 21	126.9	21, 23	30, 24, (23, 21)
23	6.14	1	m[a]	-	22, 24	132.2	21, 25	21, (22) > 25, 30
24	6.14	1	m[a]	-	25, 23	129.9	22, 26	26, (23, 25)
25	5.74	1	ddd	14.3,7.1, 7.1	24, 26	135.6	27, 26, 23	(24, 26), 27
26	2.08	2	dt	7.1, 7.5	27, 25	25.2	27, 25, 24	(27, 25), 24
27	0.97	3	t	7.5	26	13.5	26, 25	(26), 25

The compound was stabilized with 4-ethoxyphenol (^{1}H NMR (600 MHz, [D_6]DMSO) δ ppm 1.26 (t, *J* = 6.97 Hz, 3 H) 3.89 (q, *J* = 6.97 Hz, 2 H) 6.65 (d, *J* = 8.80 Hz, 2 H) 6.72 (d, *J* = 8.80 Hz, 2 H); ^{13}C NMR (150 MHz, [D_6]DMSO) δ ppm 14.8, 63.3, 115.3, 115.7, 151.0, 151.3. [a] multiplet of 4 protons at 6.15 ppm, one AA'-system consisting of 23/24H and an overlap with 9H and 12H. All proton shifts were taken from the HMQC spectrum. [b] overlap of 4H and 14Hα. Proton shifts from the HMQC spectrum. [c] ^{13}C shift from APT spectrum after H/D exchange. [d] data after H/D exchange.

2.1.3 The Relative Configuration of Roimatacene (26)

In order to establish the relative configuration of the polyol fragment C15 to C19, three acetonides (**28**-**30**) were prepared from roimatacene methyl ester (**27**) by the reaction with 2,2-dimethoxypropane presented in Scheme 1.

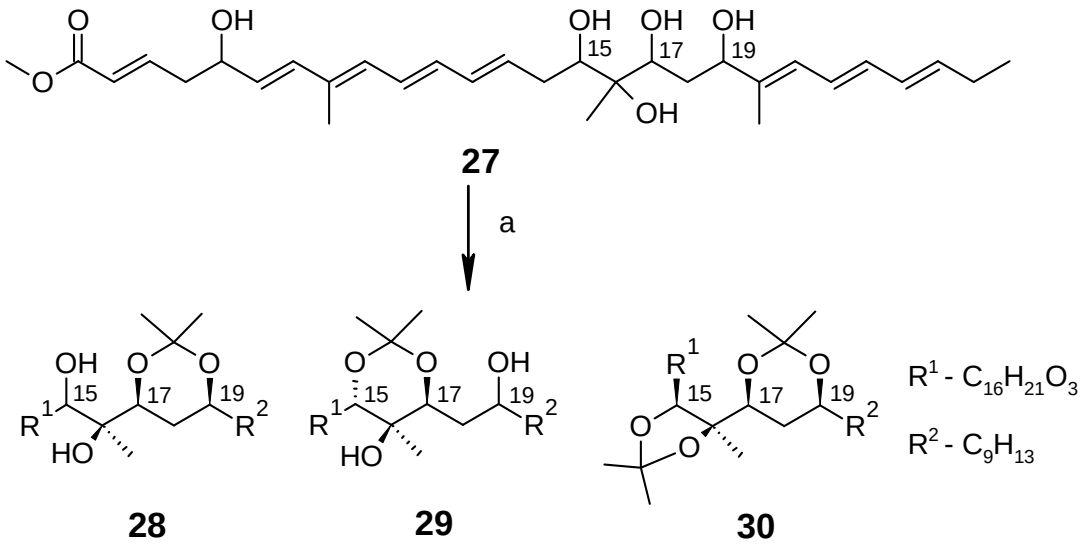

Scheme 1. Preparation of acetonides **28** to **30** from roimatacene methyl ester (**27**); a) 2,2-dimethoxypropane, PPTS, 4°C, 18h.

Subsequent to the isolation of all three acetonides, their complete NMR data were intensely studied. The analysis of the 17,19-acetonide **28** revealed a typical shift of δ_C 98.9 ppm for the quaternary carbon *C*Me$_2$ (C32) and δ_C 20.0 and 30.1 ppm (Table 3) for the methyl groups C33/34, characteristic for a chair conformation of acetonides as analyzed by Rychnovsky´s method.[72] The chair conformation was further supported by nOe correlations of 33H, 17H and 19H in coaxial positions. Supplementary, 18Hβ in the equatorial position was distinguished from the axial 18Hα by nOes with 17H and 19H. A chair conformation is only possible for *syn*-1,3-diols, and therefore 17OH and 19OH take the *syn*-configuration.

Conversely, the second product assigned as 15,17-acetonide **29**, showed chemical shifts of δ_C 100.2 ppm for the quaternary carbon *C*Me$_2$ (C32) and very similar carbon shifts of δ_C 25.2 and 23.7 ppm for the methyl groups C33/34, unambiguously indicating a twisted-boat conformation and thus the *anti*-configuration of 15OH and 17OH (see Table 4).[72] An unambiguous assignment of the relative configuration of stereocentre C16 considering the nOe correlations from the ^{1}H,^{1}H ROESY spectrum is impossible from this twisted-boat conformation.

Table 3: NMR data of 17,19-acetonide **28** (^{1}H, 600 MHz, ^{13}C 150 MHz, $CDCl_3$)

Atom	δ_H	H	m	*J* [Hz]	COSY	δ_C	HMBC	ROESY
31	3.74	3	s	-	-	51.5	-	-
1	-	-	-	-	-	166.7	31, 3 > 2	-
2	5.94	1	d	15.8	3 > 4	123.7	4	(3)
3	6.98	1	ddd	15.7, 7.2, 2.2	4, 2	144.7	4	(2, 4)
4	2.51	2	m	-	5, 3 >2	40.3	> 2, 6, 3	(3), 2, (5), 6
5	4.37	1	ddd	12.0, 7.0, 1.8	4, 6	71.8	4, 7, 6	7, (4) > 3, (6)
5OH	1.43	1	m	-	5		-	-
6	5.7	1	dd	15.4, 7.0	7, 5	129.7	4 > 7	(7, 5), 28, 4
7	6.32	1	d	15.4	6	136.1	28, 9	5, (6), 9, 4
8	-	-	-	-	-	139.7	-	-
28	1.87	3	s	-	9	12.8	9	10, 6
9	6.09	1	m	-	10, 28	132.2	28, 7, 11	7, 9
10	6.50	1	dd	13.6, 11.4	9, 11	127.7	9	(11, 9), 28
11	6.28	1	dd	15.0, 11.2	12, 10	133.7	28, 9	(10), 13
12	6.26	1	dd	15.0, 11.0	11, 13	133.2	10 > 14α/β	10, (13)
13	5.86	1	ddd	14.4, 7.3, 7.3	12, 14α/β	132.1	14α, 11, 10	11, 15, (14α/β)
14α	2.51	1	m	-	14β, 15, 13	35.9	11	29, (14β), 16OH, (15) 17, 12
14β	2.21	1	ddd	14.5, 10.1, 7.7	14α, 13, 15			(14α), 17, 29, 13, 12
15	3.58	1	ddd	10.3, 8.1, 2.2	14α/β	77.3	29, 14α/β	29, 16OH, (14α), 13, 17
15OH	2.58	1	m	-	15		-	-
16	-	-	-	-	-	73.7	15OH, 14α	-
16OH	2.84	1	s	-	29		-	-
29	1.06	3	s	-	-	18.8	16OH	17, 15, 16OH, 15OH, 18β
17	4.11	1	dd	11.6, 2.4	18α/β	72.9	29, 18α	19, 33, 18β, 29, 15OH, 16OH, 15, 18α
18α	1.84	1	m	-	19, 17, 18β	28.6	-	(18β), 29, 16OH
18β	1.45	1	m	-	18α, 19, 17			(18α), 29, 19, 17
19	4.31	1	dd	11.7, 1.8	18α/β	74.0	29, 30, 21	33, 21, 17, 30, 18β
32	-	-	-	-	-	98.9	33, 34	-
33	1.52	3	s	-	>34	20.0	34	17, 19
34	1.45	3	s	-	>33	30.1	33	-
20	-	-	-	-	-	136.4	30, 22, 21, 19	-
30	1.80	3	s	-	21	12.9	21	22, 19
21	6.09	1	m	-	22, 30	126.0	30, 22, 19	19
22	6.34	1	dd	14.5, 11.0	21, 23	126.2	23, 30	30, (21), 24
23	6.21	1	dd	15.0, 11.0	22, 24	133.6	25	25, (22, 24)
24	6.09	1	m	-	23 > 25	129.6	26	26
25	5.76	1	dt	15.0, 6.8	24, 26	136.8	26, 27, 23	23, (24, 26) > 27
26	2.13	2	quintet	7.3	27, 25	25.8	27, 25, 24	(27, 25), 24
27	1.03	3	t	7.3	26	13.5	-	

The compound was stabilized with 4-ethoxyphenol: ^{1}H NMR (600 MHz, $CDCl_3$): δ 1.39 (t, J = 7.2 Hz, 3 H) 3.99 (q, J = 7.0 Hz, 2 H) 6.78 ppm (q, J = 9.2 Hz, 4 H); ^{13}C NMR (150 MHz, $CDCl_3$): δ 14.9, 64.1, 115.6, 116.0, 149.4, 153.2 ppm.

Table 4: NMR data of 15,17-acetonide **29** (^{1}H 600 MHz, ^{13}C 150 MHz, $CDCl_3$).

Atom	δ_H	H	m	*J* [Hz]	COSY	δ_C	HMBC	ROESY
31	3.74	3	s	-	-	51.5	-	-
1	-	-	-	-	-	166.7	31, 3	-
2	5.94	1	d	15.8	3	123.6	4	(3) > 4
3	6.98	1	dt	15.4, 6.6	4, 2	144.8	4	(2), (4)
4	2.50	2	t	7.3	5, 3	40.3	2	(3), (5), 2 > 6
5	4.36	1	q(br)	6.4	4, 6, 5OH	71.8	7 > 4, 6	
5OH	1.76	1	s (br)		5			5
6	5.68	1	dd	15.8, 7.0	7, 5	129.3	4, 7	28, (7, 5)> 4
7	6.32	1	m[a]	-	6	136.2	9, 28	5, 9
8	-	-	-	-	-	135.4	28 > 9	-
28	1.88	3	s	-	>>9	12.8	7, 9	6, 10
9	6.11	1	m[a]	-	10> 28	132.4	7, 10	(10), 7, 11
10	6.44	1	dd	13.2, 11.7	9, 11	127.1	-	(9, 11), 28
11	6.26	1	m[a]	-	10, 12	134.3	9, 13	(10), 13, 9
12	6.26	1	m[a]	-	13, 11	132.5	10	(13), 10
13	5.79	1	ddd	15.0,7.5,1.5	14α, 12, 14β	132.2	14α/β	(12), 11> 15
14α	2.41	1	ddd	14.9, 7.4, 1.8	14β, 13, 15	32.1	-	(14β,15)> 29, 12, (13)
14β	2.15	1	ddd	14.9, 10.0, 7.4	15, 14α >13	-	-	(14α), 29 > (15)
15	3.65	1	s	-	14β > 14α	72.3	29	33/34 , 19, 17 > 13, (14α)
16	-	-	-	-	-	85.2	29, 18	-
29	1.18	3	s	-	-	19.3	-	17>> 30, 14β, 18
17	4.00	1	dd	6.0, 3.5	18	78.5	29, 18	(18), 33/34, 29, 15
32	-	-	-	-	-	100.2	33/34	-
33	1.35	3	m	-	-	25.2	34	15, 17
34	1.35	3	m	-	-	23.7	33	15, 17
18	1.93	2	m	-	19, 17	37.1	-	(17, 19), 30 >29
19	4.67	1	dd (br)	8.6, 6.8	18	84.0	30 > 21	21, 15, 18 > 30
20	-	-	-	-	-	133.6	> 30	-
30	1.75	3	s	-	> 21	12.1	19, 21	>22, 19
21	6.15	1	m[a]	-	22	126.5	30, 23, 19	19
22	6.33	1	m[a]	-	21, 23	126.3	30, 23	(23),30
23	6.19	1	m[a]	-	24, 22 > 30	133.4	25 > 22	19, 21
24	6.12	1	m[a]	-	25, 23	129.7	26, 22	>26
25	5.75	1	dt	7.2, 14.7	24, 26	136.7	27, 26> 23	(24), 23, (26)
26	2.13	2	quint	7.2	27 > 25	25.8	27 > 25> 24	(27) > (25), 24
27	1.02	3	t	7.3	26	13.5	26 > 25	(26)

The compound was stabilized with 4-ethoxyphenol: ^{1}H NMR (600 MHz, $CDCl_3$): δ 1.39 (t, J = 7.2 Hz, 3 H) 3.99 (q, J = 7.0 Hz, 2 H) 6.78 ppm (q, J = 9.2 Hz, 4 H); ^{13}C NMR (150 MHz, $CDCl_3$): δ 14.9, 64.1, 115.6, 116.0, 149.4, 153.2 ppm. [a] multiplet of 8 protons in between 6.35 – 6.10, proton shifts from ^{1}H,^{13}C HSQC spectrum

In order to establish the relative configuration of stereocentre C16 in roimatacene (**26**), the NMR data of bis-acetonide **30** were studied in detail (Table 5). The *syn*-configuration of the 17,19-acetonide was secured by the observation of the same chemical shifts and nOe correlations in bis-acetonide **30** as for **28**. Further, the relative configuration of the *anti*-15,17-acetonide **29** was considered, before the two possible diastereomers of C16 were modelled applying the "Conformational Search" module of HyperChem (Version 8.5) using MM+ calculations. Both optimized alternative conformers were then carefully compared with the NMR data of **30** (Table 5, Figure 19).

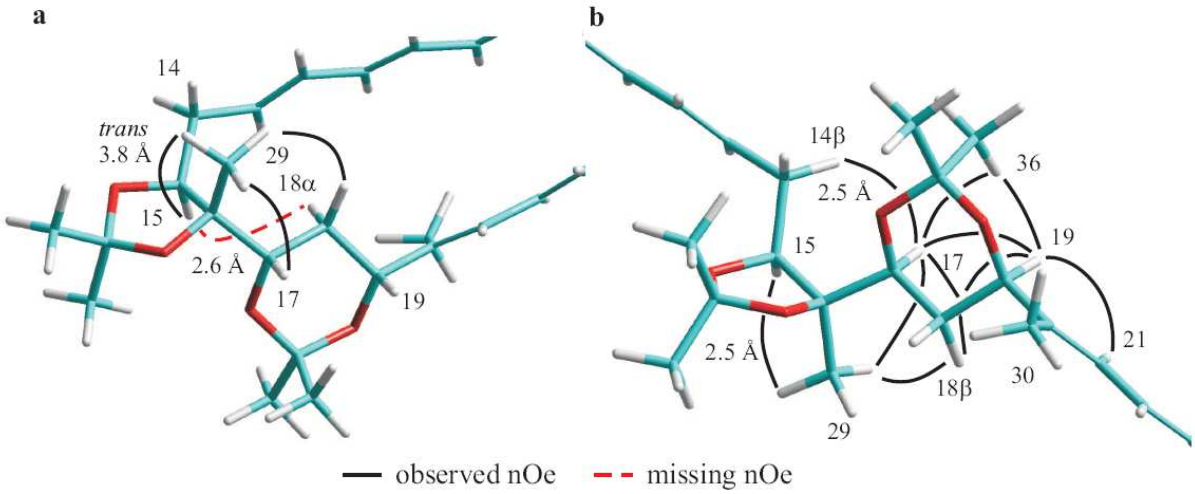

Figure 19. Partial view of **30** resulting from modelling studies with HyperChem and selected nOe of **30**, a) the relative 15*S**,16*R**,17*S**,19*R** isomer and b) the relative 15*S**,16*S**,17*S**,19*R** isomer of the bis-acetonide **30**.

The nOes of the chair conformation of the 17,19-*syn*-acetonide unit in **30**, differentiating the equatorial 18Hβ (δ_H 1.41 ppm) and axial 18Hα (δ_H 1.77 ppm) protons as in **28**, are presented in Figure 19b. The methyl group C29 at C16 in the 15,16-acetonide unit of **30** showed ROESY correlations with 18Hβ and 17H of the 17,19-*syn*-acetonide. These nOe correlations are feasible for both isomers of **30** presented in Figure 19a and b. However, the strongest nOe of methyl group C29 was indicated with 15H, thus enabling a discrimination between both isomers, because this observation is only compatible with the distance of 2.5 Å in the relative 15*S**,16*S**,17*S**,19*R** configuration in Figure 19b. The distance of 3.8 Å in the 15*S**,16*R**,17*S**,19*R** configuration (Figure 19a), besides the *trans*-orientation of methyl group C29 and 15H, would not allow a strong nOe. Instead, a strong nOe between 15H and 18Hα would be expected from a distance of 2.6 Å in the model, which is missing in the ^{1}H,^{1}H ROESY spectrum of **30** (Figure 19a). Further, a nOe between 17H and 14Hβ of the side chain was observed, which is impossible for the *S**,*R**,*S**,*R** isomer (Figure 19a), even after rotation

of the side chain. However, the observation is fully compatible with the distance of 2.5 Å between 17H and 14Hβ in the S^*,S^*,S^*,R^* configuration (Figure 19b). A strong nOe between 19H and 21H strongly supports the orientation of the triene side chain as it is presented in the S^*,S^*,S^*,R^* model, although the expected nOe between methyl group 30H (δ_H 1.79 ppm) and 18Hα (δ_H 1.71 ppm) could not be observed, due to their overlapping ^{1}H NMR signals.

The extensive NMR analyses and the comparison with the result of the molecular modelling of both possible 16R^* and 16S^*-diastereomeres strongly support the 15S^*,16S^*,17S^*,19R^* configuration of roimatacene (**26**) as presented in Figure 20.

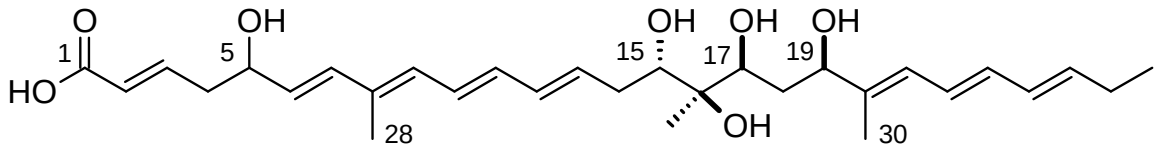

26

Figure 20. The relative 15S^*,16S^*,17S^*,19R^* configuration of roimatacene (**26**).

Table 5: NMR data of 15,16,17,19-bis-acetonide **30** (^{1}H 600 MHz, ^{13}C 100 MHz, $CDCl_3$).

Atom	δ_H	H	m	*J* [Hz]	COSY	δ_C	HMBC	ROESY
31	3.74	3	s	-	-	51.5	(31)	-
1	-	-	-	-	-	166.7	31, 3 >2	-
2	5.94	1	dd	15.8, 1.1	3	123.6	4	(3)
3	6.98	1	dt	15, 7	2, 4	144.7	4, 5	(2) > (4)
4	2.51	2	ddd	7.4, 6.2, 1.3	5, 3	40.3	2, 3, 5, 6	(5,3), 2, 6
5	4.38	1	m	-	4, 6	71.7	7,4,6>3	(4), 7
6	5.70	1	dd	15, 7	7, 5	126.6	4,7,5	28, (7),4, (5)
7	6.33	1	d	15.4	6	136.1	28, 9, 5	5, (6), (9 overlap with 22)
8	-	-	-	-	-	134.1	28, 6, 7,9	-
28	1.88	3	s	-	-	12.8	7	6, 10
9	6.12[a]	1	m[a]	-	10	132.2	28, 7	(10), 11, 7
10	6.48	1	dd	15, 11	9, 11	127.7	28	28 > (9,11)
11	6.28[a]	1	m[a]	-	10, 12	133.8	9, 13	(12), 9, 13
12	6.27[a]	1	m[a]	-	13,11	132.7	14α/β, 10	10, (13,11)
13	5.81	1	ddd	14.6,7.9,6	12 >14α	131.6	15, 14α/β	(12), 11
14α	2.74	1	ddd	15,9,6	14β,15	32.4	>12	(14β)
14β	2.55	1	m	-	14α, 15			(14α)
15	3.91	1	dd	8.1, 5.5	14α/β	84.2	29> 14α/β	33, 29
16	-	-	-	-	-	82.1	29,18α,14α	-
29	1.18	3	s	-	-	23.0	15	15 >17, 18β
32	-	-	-	-	-	108.0	33,34	-
33	1.38	3	s	-	-	26.8	34	34, 15
34	1.53	3	s	-	33	26.8	33	-
17	3.76	1	m	-	18α/β	71.6	29,18α, 15	36,19>29,14β,18β
18α	1.77	1	m	-	18β,19, 17	29.4	-	18β
18β	1.41	1	m	-	18α			18α>17,19, 29
19	4.26	1	dd	11.9, 1.7	>18α/β	74.2	30>18α,21	36,21,17,30,18β
20	-	-	-	-	-	136.9	30>22, 19	-
35	-	-	-	-	-	98.5	36,37	-
36	1.50	3	s	-	-	19.6	37	19,17,33
37	1.47	3	s	-	-	30.1	36	-
30	1.79	3	s	-	-	12.9	21,22>>19	>22, 19
21	6.10[a]	1	m[a]	-	22 >30	125.8	30>23,22,19	19, (22)
22	6.34[a]	1	dd	15,11	21,23	126.4	>23,21/24	24, (23)
23	6.20	1	dd	15,11	22,24	133.4	25, 24,22	25, (22,24)
24	6.12[a]	1	m[a]	-	25, 23	129.7	26, 22	22, (25)
25	5.75	1	dt	13.6, 6.6	26, 24	136.6	27, 26, 23	(24) >23, (26)
26	2.13	2	quin	7.2	27 >25	25.8	27, 25, 24	(27)>(25),24
27	1.02	3	t	7.3	26	13.5	26,25	(26)

The compound was stabilized with 4-ethoxyphenol: ^{1}H NMR (600 MHz, $CDCl_3$): δ 1.39 (t, J = 7.2 Hz, 3 H) 3.99 (q, J = 7.0 Hz, 2 H) 6.78 ppm (q, J = 9.2 Hz, 4 H); ^{13}C NMR (150 MHz, $CDCl_3$): δ 14.9, 64.1, 115.6, 116.0, 149.4, 153.2 ppm. [a] multiplet of 8 protons between 6.35 – 6.10 ppm, proton shifts from ^{1}H,^{13}C HSQC spectrum

2.1.4 The Absolute Stereochemistry of Roimatacene (26)

The absolute stereochemistry of roimatacene (**26**) was established applying Mosher´s method.[82] Exasperatingly, the methoxy(trifluoro-methyl)phenylacetyl (MTPA) esters prepared directly from **26** or from the acetonides **28**, **29** decomposed during isolation. In order to stabilize the MTPA esters, roimatacene (**26**) was completely hydrogenated under mild conditions, although two additional isomeric stereocentres at C8 and C20 were created. A separation of the four resulting diastereomeres was not accomplished. Neither a more selective hydrogenation procedure was successfully applied. The octahydroroimatacene (**31**) was then further esterified with *p*-bromophenacyl bromide to give the UV-active *p*-bromophenacyl octahydroroimatacene ester (**32**). Finally, the tris-(*R*)- and the tris-(*S*)-MTPA esters **33a/b** were derived by Yamaguchi esterification of *p*-bromoacetophenone-octahydroroimatacene ester **32**.[106] Without further optimization 36.6 mg of roimatacene (**26**) finally yielded 2.8 mg of the tris-(*S*)-MTPA ester and 2.1 mg of tris-(*R*)-MTPA ester of the *p*-bromoacteophenone-octahydroroimatacene ester **33a/b**. The synthesis route is presented in Scheme 2.

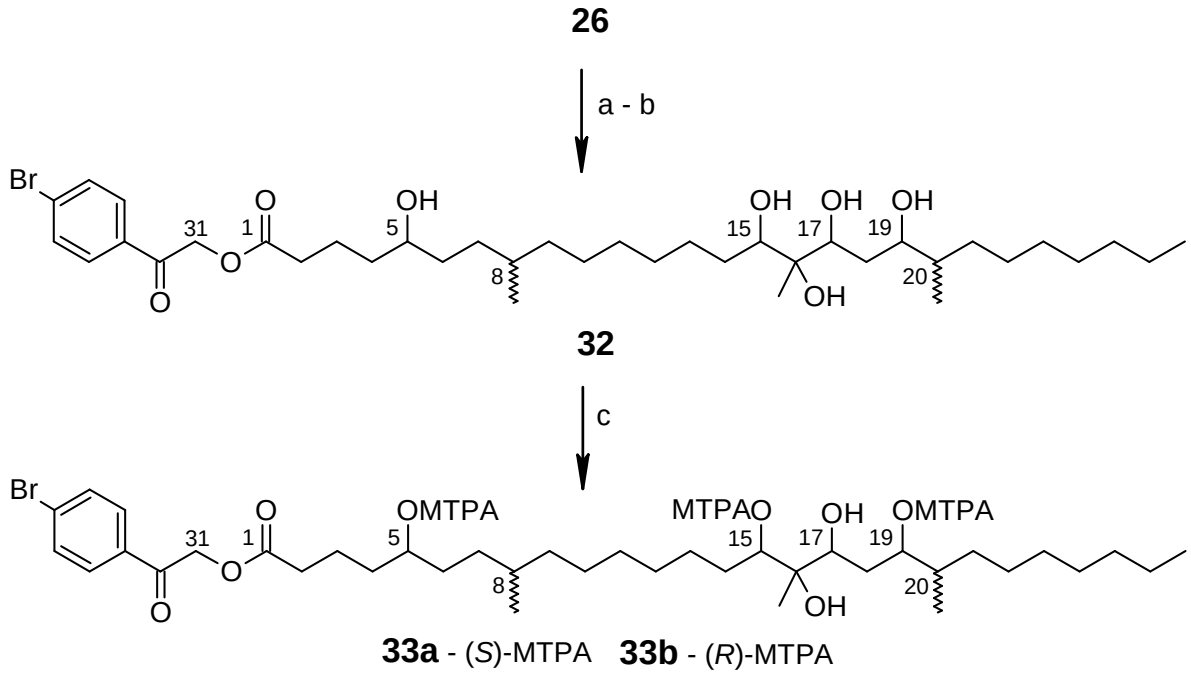

Scheme 2. Preparation of the tris-(*R*)- and the tris-(*S*)-MTPA esters of *p*-bromoacetophenone-octahydroroimatacene ester **33a**/**b**. a) Pd/C (10%), H_2, RT, 4.5 h; b) *p*-bromophenacyl bromide, 3Å mol sieve, Et_3N, acetone, 19 h; c) MTPA, 2,4,6-trichlorobenzoyl chloride, DMAP, Et_3N, 0°C to RT, 4 h.

The structure elucidations of the tris-(*R*)- and tris-(*S*)-MTPA esters of *p*-bromoacetophenone-octahydroroimatacene ester **33a**/**b** were accomplished by using complete NMR data sets of each ester. Due to the epimeric centres at C8 and C20 two of the four possible diastereomers were visible in the NMR data in the vicinity of each epimeric centre. In Table 6 and Table 7 the consequential assignments of the protons and carbons based on $^{1}H,^{13}C$ HMQC, $^{1}H,^{1}H$ COSY, $^{1}H,^{13}C$ HMBC, and $^{1}H,^{1}H$ ROESY spectra are presented. The integrals of the proton signals were defined for each visible isomer at both epimeric centres.

Table 6: Tris (*S*)-MTPA ester of *p*-bromoacetophenone-octahydroroimatacene ester (**33a**)

Atom	δ_H	H	m	*J* [Hz]	COSY	δ_C	HMBC	ROESY	calc. δ_C
36	-	-	-	-	-	128.9[b]	34,34’	-	129.1
35,35’	7.65	4	d br.	8.4	34,34’	132,3	(35,35’),35,35’	34,34’	132.3
34,34’	7.77	4	d br.	8.4	35,35’	129.2	(35,35’)	31	129.4
33	-	-	-	-	-	132.9	35,35’	-	133.0
32	-	-	-	-	-	191.1[b]	34,34’,31	-	190.7
31	5.27	4	d	0.7	-	65.7	-	2	65.5
1	-	-	-	-	-	189.2	31,2	-	173.0
2	2.44	4	t br	7.0	3	33.3	>3,4	31	33.9
3α	1.67[a]	c	m	-	2,4	20.3	2>4	5,4	20.8
β	1.59[a]	c	m	-					
4	1.71[a]	c	m	-	5,3	32.8	2	-	33.1
5	5.12[e]	2	m	-	4,6	77.3[a]	>6,3	4,3,6	74.8
6α	1.67[a]	c	m	-	-	31.3	-	(5)	32.7
β	1.60[a]	c	m	-	5,7			(5),8	
7	[f]								
8	1.35[a]	d	m	-	28,9	32.7	28	(28,9)>6	32.6
28	0.84	6	t br	7.0	8	19.4	-	(8),9	20.2
9α	1.24[a]	d	m	-	CH_2	36.8[a]	28	(9)	37.2
β	1.07[a]	d	m	-	8,CH_2		28	(9)	
10-13	CH_2								
14α	1.82	c	m	-	15	28.7[a]	-	-	30.9
β	1.57	c	m	-	15				
15	5.10[e]	2	m	-	14	78.9[a]	29	29,CH_2	77.6
16	-	-	-	-	-	74.7[b]	29	-	76.8
29	1.04	6	d	5.9	-	17.2	-	18,17,15	16.7
17	3.38[a]	1	m	-	18	70.2[b]	29	29,18,15,19	72.8
18α	1.91	d	m	-	17,19,18β	31.2	30	20,19	31.5
β	1.75[a]	c	m	-	18α	-	-	-	
19	5.25	1	m	-	20,18	78.1[b]	30	(18,20),CH_2	76.6
20	1.75[a]	c	m	-	19,CH_2	36.1	30	18,30	37.4
30	0.78	3	d	7.0	20	15.0	-	20	14.7
17’	3.40[a]	1	m	-	18’	71.0[b]	29	29,15	72.8
18’	1.86[a]	c	m	-	17’,19’	30.7[a]	-	(18’)	31.5
19’	5.12[e]	1	m	-	30’,18’α	79.8[a]	-	30’	76.6
20’	1.62[a]	c	m	-	19`	35.3	30’	30’	37.4
30’	0.80	3	d	6.6	20`	13.4	-	20’	14.7
21-24	CH_2								
25α	1.24[b]	d	m	-	25,CH_2	31.8	27,26	-	32.0
β	1.29[b]	d	m	-	CH_2			-	
26	1.30[a]	d	m	-	27,25	22.6	27,25	(27)	22.7
27	0.89	6	td	7.1, 1.3	26	14.1	-	(26)	14.1
37	[f]								168.9
38	-	-	-	-	-	84.4[b]	44>40,40’	-	84.0
39	-	-	-	-	-	128.3	41,41’	-	132.5
40,40’	7.56	12	m	-	41,41’,42	127.4	-	41,41’,42	127.4
41,41’	7.40	12	m	-	42,40,40’	129.5, 128.4	-	-	128.4
42	7.43	6	m	-	41,41’,40,40’	129.9, 128.6	41,41’,40,40’	-	128.7
43	[f]								127.5
44	3.56, 3.50	18	m	-		55.5, 55.4		40,40’	55.5

33a contains two isomeric centres at C8 and C20 and the integrals are normalized for each visible isomer at each epimeric centre; some signals are doubled or broad, the signals from C15 to C20 could be assigned to each isomer. [a] proton shift from $^1H,^{13}C$ HSQC; [b] ^{13}C shift from the $^1H,^{13}C$ HMBC; [c] integral of overlapping protons between 1.90 – 1.55 ppm of 26 protons; [d] integral of overlapping protons between 1.35 – 1.15 ppm of 53 protons; [e] ^1H shift from the *J*-resolved spectrum; [f] not assigned, due to the low amount of compound.

Table 7: Tris (*R*)-MTPA ester of *p*-bromoacetophenone-octahydroroimatacene ester (**33b**)

Atom	δ_H	H	m	*J* [Hz]	COSY	δ_C	HMBC	ROESY	calc. δ_C
36	-	-	-	-	-	129.3[b]	34,34',35,35'	-	129.1
35,35'	7.65	4	d	8.4	34,34'	132.3	35,35'	35,35'	132.3
34,34'	7.77	4	d	8.4	35,35'	129.2	34,34',35,35'	34,34',31	129.4
33	-	-	-	-	-	133.1[b]	35,35'	-	133.0
32	-	-	-	-	-	191.0[b]	31,34,34'	-	190.7
31	5.29	4	s	-	-	65.6[a]	-	34,34'	65.5
1	-	-	-	-	-	172.3[b]	31,2,3	-	173.0
2	2.51	4	t br	6.6	3	33.4	4	4	33.9
3α	1.79[b]	[c]	m	-	2,4	20.4[a]	2,4,5	5,2	20.8
β	1.74[b]								
4	1.76[b]	[c]	m	-	5	32.9[b]	2,3,6	4,5	33.1
5	5.11[d]	[e]	m	-	4,6	77.2[a]	3,7	3,8	74.8
6α	1.60[d]	[c]	m	-	5,7	30.9	-	5,4	32.7
β	1.56[d]								
7α	1.22[a]	[c]	m	-	6,7β,8	31.6[b]	28,5	-	33.1
β	1.01[a]	[c]	m	-	7α			-	
8	1.26[f]	[g]	m	-	7	32.5[b]	28,28',6	>28,28',9	32.6
28	0.80	3	d	6.6	-	19.5	9	8	20.2
28'	0.78	3	d	6.6	-	19.3	9	8	
9α	1.20[a]	[g]	m	-	8	36.7[a]	28,28'	-	37.2
β	1.02	[g]	m	-	-	-	-	-	
10-13	CH_2								
14α	1.85[a]	[c]	m	-	15	28.8	CH_2	-	30.9
β	1.58[a]	[c]	m	-	15				
15	5.10[a]	[c]	m	-	14	78.7[a]	29,CH_2	CH_2	77.6
16	-	-	-	-	-	75.0[b]	29,15,17	-	76.8
29	0.97	6	d	6.6	-	16.9+16.8	>15	CH_2	16.7
17	3.31[a]	1	m	-	18	70.2[a]	29>18	15	72.8
18α	1.85[a]	[c]	m	-	17,18β,19	28.8	-	18β	31.5
β	1.58[a]	[c]	m	-	18α,19			18α,19	
19	5.20	1	m	-	18	78.4	30,18α	17,18β	76.6
20	1.67	[c]	m	-	30,19	35.3[a]	30	30,18	37.4
30	0.84	3	d	6.6	20	13.1	-	20	14.7
17'	3.28	1	m	-	18'	71.0	29,18'	19',20'>30'	72.8
18'	1.68[a]	[c]	m	-	17',19'	30.7	17'	19',17',30'	31.5
19'	5.07[d]	[e]	m	-	18'	79.9	30'	17',30'	76.6
20'	1.76	[c]	m	-	30'	36.0	30',18'	19`	37.4
30'	0.90[b]	[h]	m	-	20`	13.5	-	20`	14.7
21-24	CH_2								
26	1.29	[g]	m	-	27,CH_2	22.6	27,CH_2	(27),CH_2	22.7
27	0.90	[h]	m	-	26	15.3+14.1	CH_2	(26)	14.1
37	-	-	-	-	-	167.2+166.8+166.1[b]	5,15,19	-	168.9
38	-	-	-	-	-	84.7[b]	44, Aromatic	-	84.0
39	-	-	-	-	-	128.7+132.3+131.7[b]	Aromatic	-	132.5
40,40'	7.57	12	m	-	Aromatic	127.6+127.5+127.4	Aromatic	Aromatic	127.4
41,41',42	7.41	18	m	-	Aromatic	129.5-128.4	Aromatic	Aromatic	128.4
43	-	-	-	-	-	[i]	-	-	127.5
44	3.57	6	s br	-	-	55.4	-	-	55.5
	3.53	12	m	-	-	55.3	-	-	

33b contains two isomeric centres at C8 and C2; integrals were normalized for each visible isomer at the epimeric centre; some signals are doubled or broad; the signals from C15 to C20 could be assigned to each isomer. [a] proton shift from $^1H,^{13}C$ HSQC; [b] carbon shift from $^1H,^{13}C$ HMBC; [c] integral of overlapping protons 1.88- 1.57 ppm = 26 protons; [d] proton shift from $^1H,^1H$ COSY correlation; [e] integral of overlapping protons 5.13 – 5.06 ppm = 5 protons; [f] no assignment, due to low amount of compound, proton shift from $^1H,^1H$ ROESY; [g] integral of overlapping protons from 1.32- 0.99 ppm = 70 protons; [h] integral of 9 protons at 0.90 ppm; [i] could not be assigned.

The presence of the *p*-bromophenacyl residue was indicated by the expected signals in the ^{1}H and ^{13}C NMR spectra as well as several HMBC correlations presented in Figure 21. Between 31H and 16H only very small shift differences were visible and for both MTPA esters **33a/b** the common values of this structural element were noted in the NMR tables (Table 6 and Table 7). The partial structure between C17 and C20 including methyl group C30, the two isomeric structures were separately identified in both esters **33a/b**.

Figure 21 shows the structural elements assigned from the $^{1}H,^{1}H$ COSY spectra and selected HMBC correlations of the tris-(*S*)-MTPA esters of *p*-bromoacetophenone-octahydroroimatacene ester **33a**. The position of the MTPA ester residues were indicated by their characteristic acyl shifts of 5H (δ_H 5.12 ppm), 15H (δ_H 5.10 ppm) and 19H (δ_H 5.25 and 5.12 ppm). A COSY sequence between 2H and 6H was assigned and supported by HMBC correlations (Table 6). The COSY sequence between methyl group C28 and 9H was allocated from unambiguous correlations between 28H and 8H, as well as 8H with 9Hβ. All protons between 31H of the *p*-bromophenacyl residue and 9H showed a doubling of their ^{1}H signals with small shift differences due to isomerisation at C8.

The doublet signals of methyl groups 30H (δ_H 0.78 ppm) and 30'H (δ_H 0.80 ppm) were used as starting points to establish the COSY sequence between C17 and C20 of both isomers, which were confirmed by mutual HMBC correlations. The further connection was revealed by the HMBC cross correlations of C17 with 29H and 29'H. The methyl groups C29/29' identified the quaternary carbon C16 by a broad HMBC cross peak. The signal of C15 was identified from its HMBC correlation with methyl group C29. Additionally, 15H showed a COSY correlation with 14H ($\delta_{H/C}$ 1.82 and 1.57/28.7 ppm).

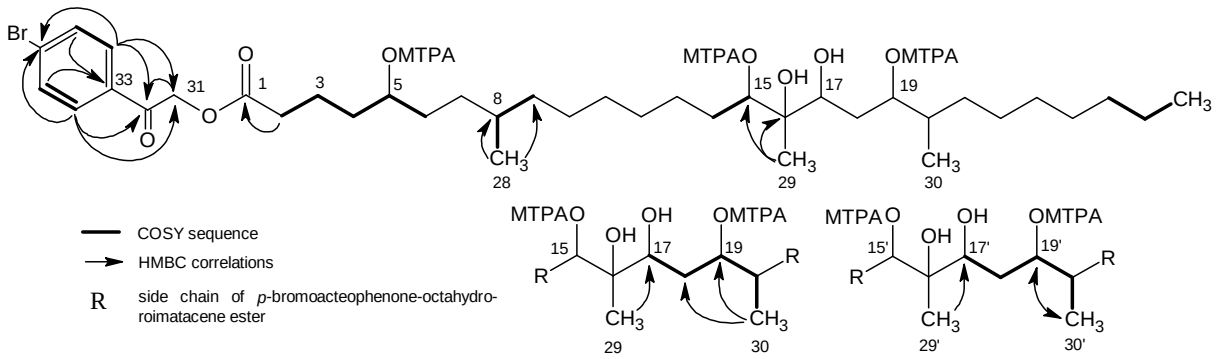

Figure 21. COSY sequences of the tris-(*S*)-MTPA esters of *p*-bromoacetophenone-octahydroroimatacene ester **33a** and selected HMBC correlations. The two separately assigned isomers from C15/C15' to C20/C20' are presented with their COSY sequence and selected HMBC correlations.

The (*R*)-MTPA ester of *p*-bromoacetophenone-octahydroroimatacene ester **33b** was assigned analogously to **33a** (Figure 22). The methylene group C7 was identified from HMBC correlations with methyl group 28C and 5H, as well as 7H revealed a COSY correlation with 6H and 8H. The methyl groups C30 (δ_H 0.84 ppm) and C30' (δ_H 0.90 ppm) were separately assigned and used as starting point for the COSY sequences of each isomer up to 17/17'H. The quaternary carbon C16 was assigned from HMBC correlations with 15H, 17H and 29/29'H. The ^{1}H chemical shift of the narrow singlets of methyl group 29H and 29'H was averaged to δ_H 0.97 ppm. Oxymethine C15 was assigned from HMBC correlations with C16 and mutual HMBC correlations with the methyl groups C29/29'. In addition 15H showed COSY cross peaks with 14H at δ_H 1.85 and 1.58 ppm.

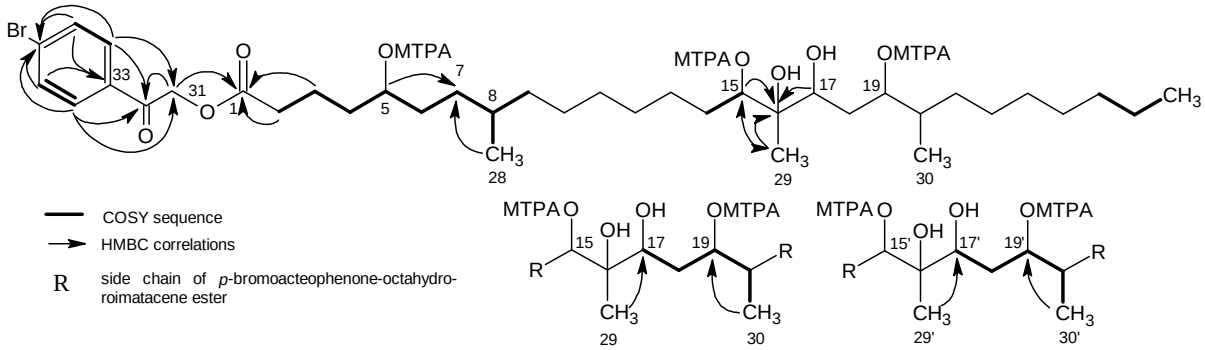

Figure 22. COSY sequences of the tris-(*R*)-MTPA esters of *p*-bromoacetophenone-octahydroroimatacene ester **33b** and selected HMBC correlations. The two separately assigned isomers from C15/C15' to C20/C20' are presented with their COSY sequence and selected HMBC correlations.

After detailed NMR assignment of the diastereomeric MTPA-esters **33a** and **33b**, the ^{1}H chemical shifts of the two Mosher esters **33a/b** were compared to calculate the $\Delta\delta^{SR}$ values in the vicinity of the MTPA esters (Table 8).

Table 8: $\Delta\delta^{SR}$ values of the tris-(*S*)- and tris-(*R*)-MTPA esters of *p*-bromoacetophenone-octahydroroimatacene ester (**33a/b**)

H	Ø $\delta_{H(S\text{-MTPA})}$	Ø $\delta_{H\ (R\text{-MTPA})}$	$\Delta\delta^{SR}$	H	Ø $\delta_{H(S\text{-MTPA})}$	Ø $\delta_{H\ (R\text{-MTPA})}$	$\Delta\delta^{SR}$
31	5.27	5.29	-0.02	14α	1.82	1.85	-0.03
2	2.44	2.51	-0.07	14β	1.57	1.58	-0.01
3α	1.67	1.79	-0.12	15	5.10	5.10	0.00
3β	1.59	1,74	-0.15	29	1.04	0.97	0.07
4	1.71	1.76	-0.05	17	3.39	3.30	0.07
5	5.12	5.11	0.01	18α	1.91	1.83	0.08
6α	1.67	1.60	0.07	18β	1.75	1.66	0.09
6β	1.60	1.56	0.04	18`	1.80	1.68	0.12
8	1.35	1.26	0.09	19	5.19	5.14	0.05
28	0.84	0.79	0.05	20	1.69	1.72	-0.03
9α	1.24	1.20	0.04	30	0.79	0.87	-0.08
9β	1.07	1.02	0.05				

Consequently, the absolute configuration of the stereocentres C5, C15 and C19 were assigned. The (*S*)-configuration of C5 was indicated by negative $\Delta\delta^{SR}$ values for 31H to 4H and positive values for 6H, 8H, 9H and methyl group 28H (Figure 23). Similarly, the 15*S*- and 19*R*-configurations were identified from completely positive $\Delta\delta^{SR}$ values between both stereocentres C15 and C19, and from negative $\Delta\delta^{SR}$ values of 14H, 20H and 30H on both sides (Figure 23,Table 8).

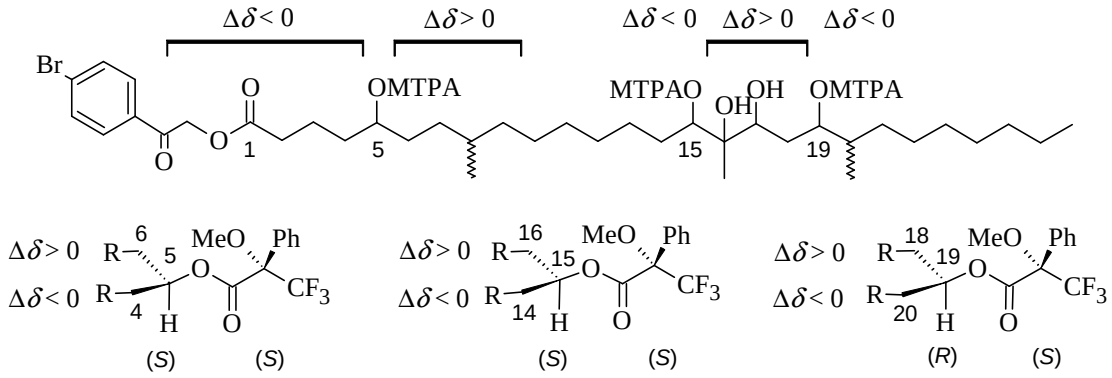

R - side chain of the tris-MTPA esters of *p*-bromoacetophenone-octahydroroimatacene as numbered

Figure 23. $\Delta\delta^{SR}$ values after comparison of the ^{1}H NMR data of the tris-MTPA esters 8a/b and the evaluation of the stereocentres C5, C15, C19.

The Mosher-derived 15*S*,19*R*-configuration agrees with the relative configuration of **26** assigned from the acetonide derivatives **28**-**30** of roimatacene methyl ester (**27**) described in chapter 2.1.3. Thus, the absolute configuration of roimatacene (**26**) was unambiguously derived as all-*trans*-5*S*,15*S*,16*S*,17*S*,19*R* configuration presented in Figure 24.

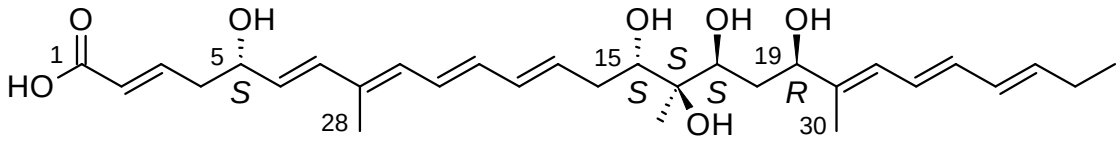

26

Figure 24. The absolute configuration of all-*trans*-5*S*,15*S*,16*S*,17*S*,19*R* roimatacene (**26**).

2.1.5 The Biosynthetic Precursors of Roimatacene (26)

In order to determine the biosynthetic precursors of roimatacene (**26**), *Cystobacter ferrugineus* strain Cb G35 was fed with different amounts of acetate, methionine and propionate in pre-experiments to evaluate the optimal feeding concentration for the labelled precursors. For this reason 100 mL cultures of Cb G35 were fed with 25, 50, and 100 mg of the precursors. The roimatacene (**26**) production of these cultures are presented in Figure 25. Feeding acetate increased the roimatacene (**26**) production from 1.08 mg/L to 1.20 mg/mL in 100 mL cultures. This observation was transferred to the up-scale fermentation feeding 1.15-1.75 g/h sodium acetate (100g/kg). The feeding experiments were conducted with 100 mg of [1-^{13}C]- and [2-^{13}C]-labelled acetate and 50 mg of labelled [$^{13}CH_3$]-methionine and [1-^{13}C]-propionate.

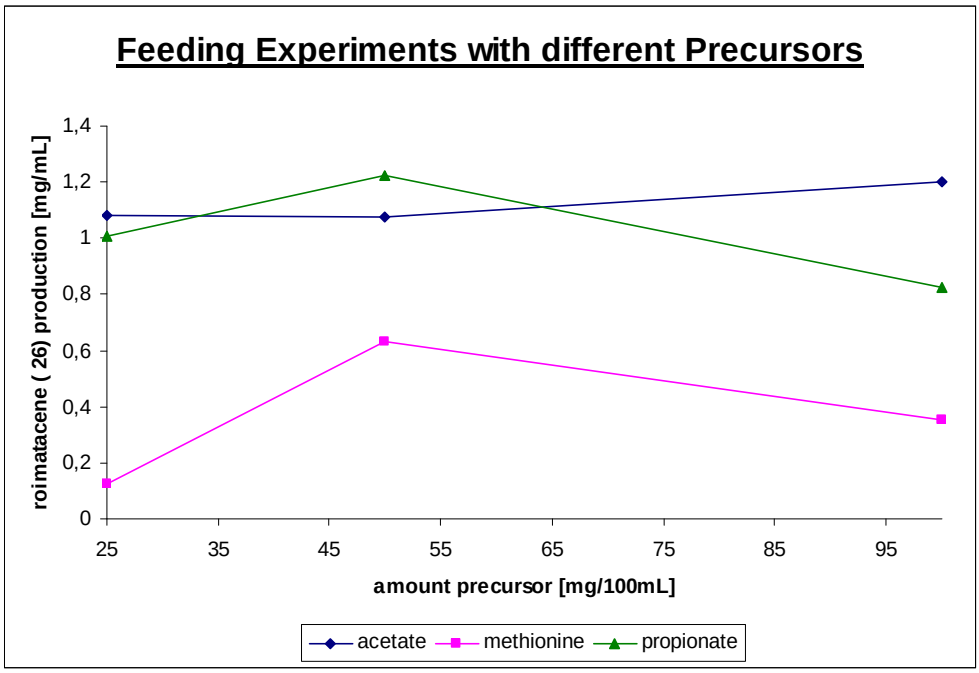

Figure 25. Different concentrations of acetate, methionine and propionate were fed to a Cb G35 culture, controlling the roimatacene (**26**) production under feeding conditions to evaluate the limiting concentration of the labelled precursors.

After feeding [1-^{13}C]- and [2-^{13}C]-labelled acetate, as well as [$^{13}CH_3$]-methionine and [1-^{13}C]-propionate to 100 mL cultures of strain Cb G35, the labelled roimatacene (**26**) was isolated and ^{13}C NMR spectra were measured. According to ^{13}C NMR analysis, the C_3 starter unit derives from S-adenosyl-L-methionine (SAM) and acetate as in the case of the biosynthesis of apicularen.[107] The remaining carbon chain of roimatacene (**26**) was exclusively assembled from acetyl-CoA. The labelling of all methyl groups originated from [$^{13}CH_3$]-methionine. For

this reason, roimatacene (**26**) derived from the [1-^{13}C]-propionate feeding showed no enriched ^{13}C signals. The results of the feeding experiments are summarized in Figure 26.

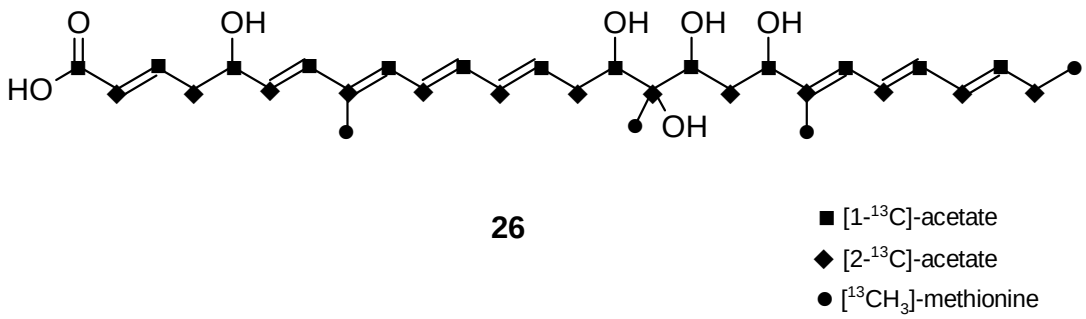

26

■ [1-^{13}C]-acetate
◆ [2-^{13}C]-acetate
● [$^{13}CH_3$]-methionine

Figure 26. Incorporation of ^{13}C-labelled precursors in roimatacene (**26**).

2.1.6 Biological Activity of Roimatacene (26)

Roimatacene (**26**) was screened against various Gram-positive and Gram-negative bacteria, yeasts and the fungus *Mucor hiemalis* (Table 9).[108] **26** exclusively showed antimicrobial activity against Gram-negative bacteria. Due to the instability of roimatacene (**26**), **26** was introduced in methanolic as well as in DMSO solution into the serial dilution test assays. In addition, the supernatant of an *E. coli* tolC assay was analysed by HPLC-HRESIMS to prove the stability of roimatacene (**26**) during incubation of the assays (Appendix, Spectrum 16). Accessorily, the test solutions were stabilized by the radical scavenger 4-ethoxyphenol. The radical scavenger showed no growth inhibition up to a concentration of 3.4 µg/mL. Thus, the maximum concentration of 4-ethoxyphenol used in the roimatacene-test solutions was limited to 3.0 µg/mL. The MICs of roimatacene (**26**) in the µg/mL range are rather moderate.

In the proliferation assay of the mouse fibroblast cell line L-929 the IC_{50} of roimatacene is ≥ 18 µg/mL. At this dilution the IC_{50} (8.8 µg/mL) of the radical scavenger 4-ethoxyphenol in the roimatacene (**26**)-test solution limited the experiment and therefore no explicit results are available.

Table 9: MIC of roimatacene (**26**) in DMSO (1.28 mg/mL + 0.46 mg/mL 4-ethoxyphenol) and in methanol (1.34 mg/mL + 0.44 mg/mL 4-ethoxyphenol)

organism	MIC (µg/mL, DMSO)	MIC (µg/mL, MeOH)	organism	MIC (µg/mL, MeOH and DMSO)
Escherichia coli 2 DC 14 PS	2.2	2.3	*Micrococcus luteus*	>9.0
Pseudomonas stutzeri	4.2	4.4	*Schizosaccharomyces pombe*	>9.0
Escherichia coli tolC	0.1	0.1	*Pichia anomala*	>9.0
Escherichia coli CG	8.6	9.0	*Rhodotorula glutinis*	>9.0
Chromobacterium violaceum	0.3	0.3	*Candida albicans*	>9.0
Klebsiella pneumonia	>8.6	>9.0	*Mucor hiemalis*	>9.0
Bacillus subtilis	>8.6	>9.0	*Nocardia flava*	>9.0
Staphylococcus aureus	>8.6	>9.0	*Pseudomonas aeruginosa*	>9.0

2.2 Six *p*-Hydroxyacetophenone Amides Isolated from *Cystobacter ferrugineus* Cb G35

2.2.1 Isolation of the *p*-Hydroxyacetophenone Amides 34a-f

In addition to roimatacene (**26**), *Cystobacter ferrugineus* strain Cb G35 was found to produce myxalamide C (**24c**) and a family of six novel *p*-hydroxyacetophenone amides **34a-f**. These were isolated from one fermentation (70 L), which showed a significantly decreased production of roimatacene (**26**). A chromatogram of the crude extract, showing the UV spectra of *p*-hydroxyacetophenone *iso*-butanamide **34a** at 8.2 min, a tremendously decreased roimatacene (**26**) signal at 13.5 min and the myxalamide C (**24c**), peak at 21.5 min, presented in Figure 27.

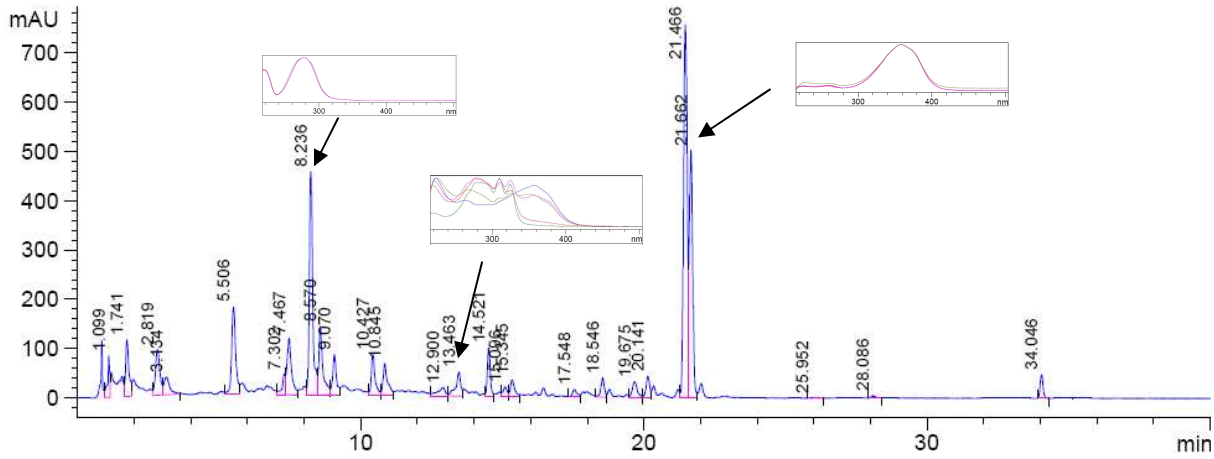

Figure 27. Standard analytical HPLC of the crude extract of fermentation KVT 268, showing signals of roimatacene (**26**) (peak at 13.5 min), *p*-hydroxyacetophenone *iso*-butanamide (**34a**) (8.2 min) and myxalamide C (**25c**) (21.5 min), detected at 200-500 nm.

The Amberlite XAD-16 absorber resin was recovered from the culture broth by sieving and was eluted with methanol. After evaporation of the organic solvent the remaining aqueous mixture was extracted with ethyl acetate. Lipophilic by-products were removed from the raw extract by a methanol/*n*-heptane partition yielding 17.5 g of polar raw material. 1.0 g of the methanol extract was fractionated by silica gel flash chromatography and further purified by RP-HPLC to yield 59.6 mg of **34a**, 7.1 mg of **34b**, 3.3 mg of **34c** and 6.9 mg of **34d**, respectively. In order to isolate the minor metabolites, 4.4 g of the polar crude extract was processed similarly to yield 0.8 mg of **34e** and 1.1 mg of **34f** after RP-chromatography. The isolation process is displayed in Figure 28.

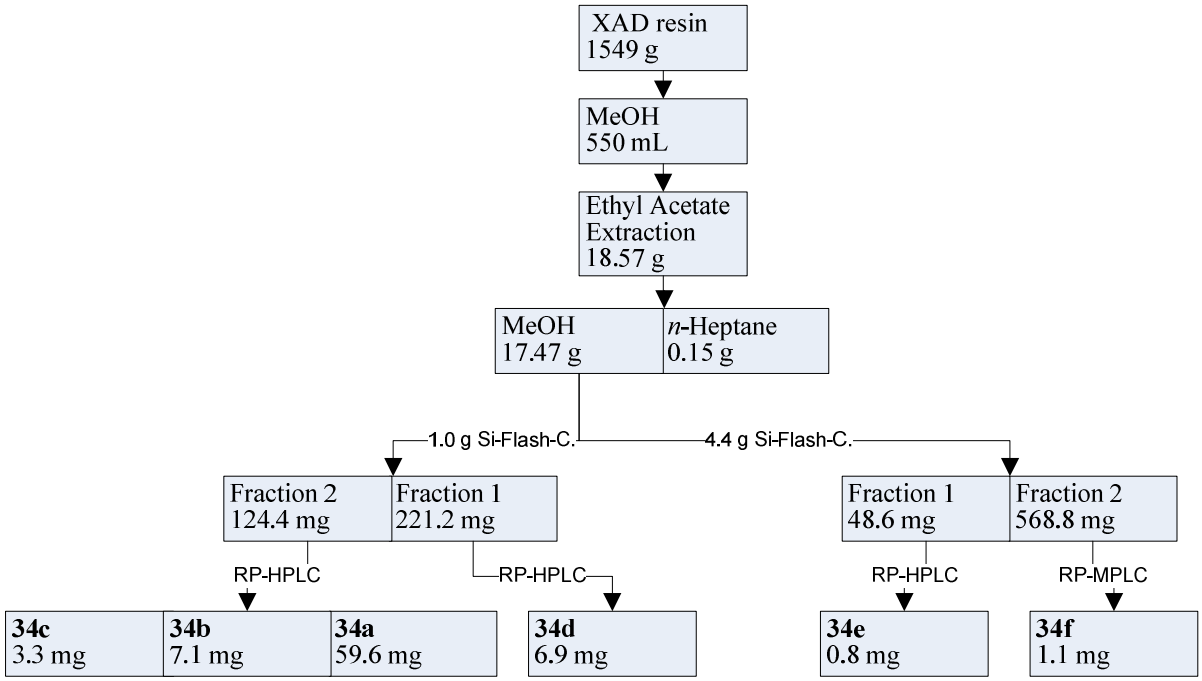

Figure 28. Isolation of the six *p*-hydroxyacetophenone amides **34a-f** from XAD-16 resin of the Cb G35 fermentation KVT 268

2.2.2 Structure Elucidation of the *p*-Hydroxyacetophenone Amides 34a-f

The structures of the *p*-hydroxyacetophenone amides **34a-f** were unambiguously elucidated using a combination of HRESIMS, as well as 1D and 2D NMR spectroscopic data.

Table 10: NMR data of *p*-hydroxyacetophenone *iso*-butanamide (**34a**)

				34a			
No.	**δ_H**	**H**	**m**	***J* [Hz]**	**COSY**	**δ_C**	**HMBC**
1						164.2	3/5 > 2/6
2/6	6.90	2	d	8.7	3/ 5	116.4	
3/5	7.94	2	d	8.7	2/ 6 > 8	131.6	
4						128.2	2/6
7						194.6	8 > 3/5
8	4.66	2	s		> 3/ 5	46.6	
9						176.0	8, 10 >11
10	2.21	2	d	7.1	11 > 8	46.2	12/13 > 11
11	2.14	1	m		12/13 > 10	27.4	12/13, 11
12/13	1.03	6	d	6.6	11	22.8	12/13, 11

The main component **34a** was crystallized from methanol as white needles and had a molecular formula of $C_{13}H_{17}NO_3$ for the $[M+H]^+$ ion at *m/z* 236.1287 (calcd. 236.1281) according to HRESIMS analysis. Subsequent to the assignment of the directly bound protons to the corresponding carbons from $^1H,^{13}C$ HSQC, the $^1H,^1H$ COSY and $^1H,^{13}C$ HMBC NMR

data revealed two substructures, a *p*-hydroxybenzoyl and a 3-methylbutanoyl unit (Table 10, Figure 29). One characteristic key fragment in the HRESIMS was found at *m/z* 152.0710 with an elemental composition $C_8H_{10}NO_2$ indicating the presence of an amidic nitrogen linking the two subunits. This observation was confirmed by characteristic chemical shifts of the attached carbon atoms C8 ($\delta_{H/C}$ 4.66/46.6 ppm) and the amide C9 (δ_C 176.0 ppm), as well as congruent long-range HMBC correlations shown in Figure 29. Of particular importance, the position of the carbonyl group C7 in the aromatic subunit was unambiguously evident from the HMBC correlations with 3/5H and 8H as well as from the characteristic chemical shift at δ_C = 194.6 ppm. Compatible observations were reported for hibispeptin A (**39**), a cyclic peptide containing an analogous aromatic ketone unit.[109]

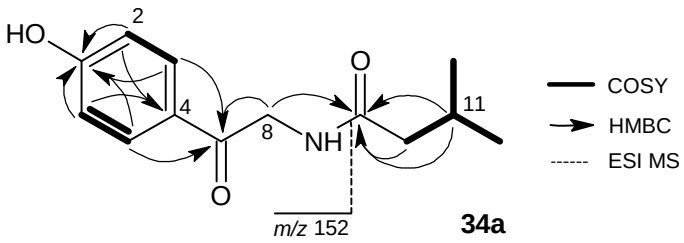

Figure 29. The structure of *p*-hydroxyacetophenone *iso*-butanamide **34a** with COSY derived structural elements, selected HMBC correlations and the key fragment in the ESI mass spectrum.

In addition to **34a**, five secondary metabolites of this family were isolated from the crude extract of strain Cb G35 presented in Figure 30. The structures of *p*-hydroxyacetophenone amides **34b-f** derived from NMR studies analogously to **34a** and the NMR data are presented in Table 11-12.

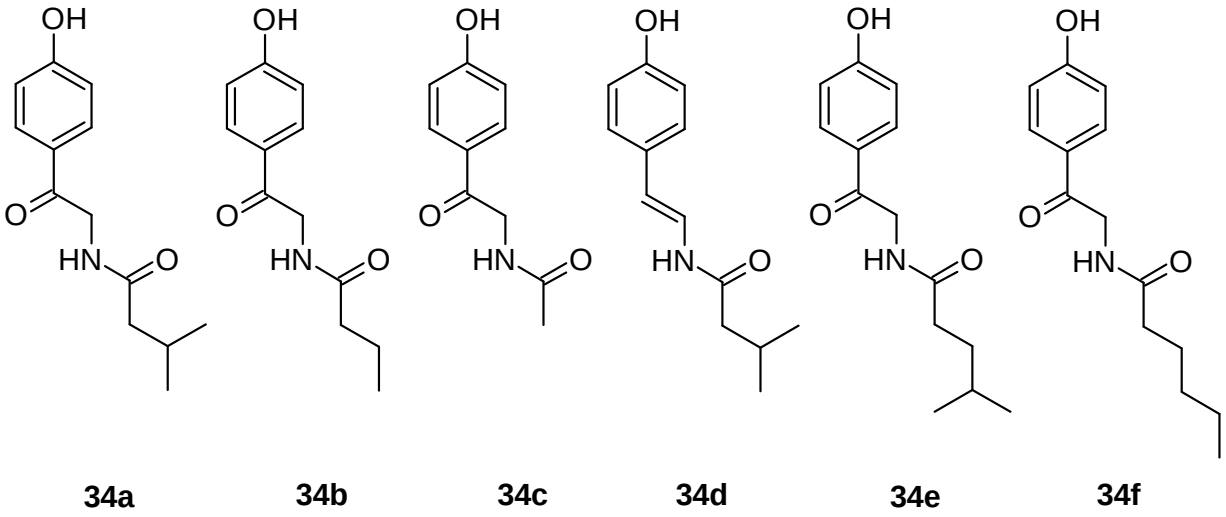

Figure 30. *p*-Hydroxyacetophenone amides **34a-f** isolated from *Cystobacter ferrugineus*, strain Cb G35.

Metabolite **34b** had a HRESIMS molecular ion at *m/z* 222.1125 and a corresponding molecular formula of $C_{13}H_{17}NO_3$ for the $[M+H]^+$ ion (calc. *m/z* 222.1125). In **34b** an *n*-propyl residue replaced the *iso*-butyl side chain of **34a**. The smallest metabolite **34c** with an HRESIMS molecular ion at *m/z* 194.0809 for the molecular formula $C_{10}H_{11}NO_3$ (calc. 194.0812) showed an acetyl residue with the characteristic methyl singlet at δ_H = 2.05 ppm as amide side chain. The main UV absorption of compound **34d**, which had a HRESIMS molecular ion at *m/z* 220.1331 and a corresponding molecular formula of $C_{13}H_{17}NO_2$ (calc. 220.1332), shifted from 278 nm to 285 nm due to the replacement of the C7 carbonyl group by a *trans*-double bond (^3J = 14.5 Hz) conjugated to the aromatic system (Appendix, Spectrum 17 and 18). Analogously to **34a**, the amide moiety of **34d** was an *iso*-butyl residue. The minor compounds **34e** and **34f** were lipophilic isomers with a common molecular formula of $C_{14}H_{19}NO_3$ corresponding to their $[M+H]^+$ ions at *m/z* 250.1447 (calc. 250.1438). Their NMR structure elucidation revealed the difference of their side chains, i.e. an *iso*-pentyl group in **34e** and an *n*-pentyl group in **34f**.

Table 11: NMR data of *p*-hydroxyacetophenone *n*-butanamide (**34b**) and *p*-hydroxyacetophenone acetamide (**34c**) (^{1}H 300 MHz, ^{13}C 75 MHz, CD_3OD)

	34b							**34c**						
No.	**δ_H**	**H**	**m**	***J* [Hz]**	**COSY**	**δ_C**	**HMBC**	**No.**	**δ_H**	**H**	**m**	***J* [Hz]**	**COSY**	**δ_C**	**HMBC**
1						164.2	3/5, 2/6	1						164.4	3/5, 2/6
2/6	6.90	2	d	8.7	3/5	116.4	2/6 >3/5	2/6	6.86	2	d	8.8	3/5	116.6	2/6 >3/5
3/5	7.93	2	d	8.7	2/6 > 8	131.6	3/5	3/5	7.90	2	d	8.8	2/6	131.7	3/5
4						128.1	2/6 > 8	4						128.2	2/6 > 8
7						194.6	3/5, 8	7						194.7	3/5, 8
8	4.66	2	s		> 10, 3/5	46.6		8	4.62	2	s		> 10	46.9	
9						176.5	10, 8, 11	9						173.8	8, 10
10	2.33	2	t	7.4	11, 8 > 12	38.8	11, 12	10	2.05	3	s		> 8	22.5	
11	1.72	2	tq	7.4, 7.4	12, 10	20.3	10, 12								
12	1.03	3	t	7.4	11	14.0	10, 11								

Table 12: NMR data of *p*-hydroxyethenphenyl *iso*-butanamide (**34d**) (^{1}H 400 MHz, ^{13}C 100 MHz, CD_3OD)

	34d					
No.	**δ_H**	**H**	**m**	***J* [Hz]**	**COSY**	**δ_C**	**HMBC**
1						157.6	3/5, 2/6
2/6	6,75	2	d	8.7	3/5	116.5	2/6
3/5	7.19	2	d	8.7	2/6	127.7	7, 3/5
4						129.2	2/6, 8
7	6.18	1	d	14.5	8	114.8	3/5 > 8
8	7.31	1	d	14.5	7	121.5	7
9						172.9	11, 8
10	2.18	2	m		11	46.2	12/13 > 11
11	2.16	1	m		12/13, 10	27.5	10, 12/13
12/13	1.02	6	d	6.6	11	22.7	12/13 > 10, 11

Table 13. NMR data of *p*-hydroxyacetophenone *iso*-pentanamide (**34e**) and *p*-hydroxyacetophenone *n*-pentanamide (**34f**) (^{1}H 600 MHz, ^{13}C 150 MHz, CD_3OD)

	34e								**34f**							
No.	δ_H	**H**	**m**	***J* [Hz]**	**COSY**	δ_C	**HMBC**		**No.**	δ_H	**H**	**m**	***J* [Hz]**	**COSY**	δ_C	**HMBC**
1						164.5	2/6,3/5		1	-	-	-	-	-	164.4	3/5,2/6
2/6	6.91	2	d	8.8	3/5	116.6	3/5		2/6	6.86	2	d	8.8	3/5	116.6	3/5
3/5	7.95	2	d	8.8	2/6	131.7	2/6		3/5	7.90	2	d	8.8	2/6	131.7	2/6
4						128.2	2/6		4	-	-	-	-	-	128.3	2/6
7						194.8	8,3/5		7	-	-	-	-	-	194.4	3/5,8
8	4.66	2	s			46.8			8	4.62	2	s	-	-	46.8	-
9						177.0	10,8,11		9	-	-	-	-	-	176.9	8,7>11
10	2.38	2	m		11>12	35.2	11>12		10	2.31	2	t	7.5	11	37.1	11
11	1.60	2	m		10,13/14,12	36.1	10,13/14,12		11	1.66	2	quintet	7.5	12,10	26.8	10
12	1.66	1	m		13/14, 11	29.1	13/14,11,10		12	1.39	2	m	-	11,13,14	32.7	14,12,11
13/14	0.99	6	d	6.6	12,11, 13/14	22.9	13/14,11,12		13	1.38	2	m	-	14,12	23.6	14,12,11
									14	0.93	3	t	6.6	13,12	14.4	-

2.2.3 Biosynthetic Precursors of *p*-Hydroxyacetophenone *iso*-Butanamide (34a)

The biosynthetic precursors of the main metabolite **34a** were determined by feeding experiments with D-, ^{13}C- and ^{15}N-labelled amino acids in 100 mL cultures. These were supplemented with traces of unlabelled methionine to increase the production of **34a** in strain Cb G35 under feeding conditions.

Feeding [D_{10}]-leucine resulted in HRESIMS molecular ion clusters at *m/z* 236.1268 for $[M+H]^+$ of the unlabelled compound **34a** and at *m/z* 245.1834 for $[C_{13}H_7D_9NO_3+H]^+$ of the [D_9]-labelled metabolite **34a** showing an incorporation of 65% of the precursor (Appendix, Spectrum 59). Consistent with the high incorporation of deuterium, the ^1H NMR spectrum of the raw sample showed decreased intensities of the ^1H signals for the *N*-acyl residue of **34a** (Appendix, Spectrum 58).

Table 14: ^{13}C Incorporation in labelled **34a** from feeding experiments with [$^{13}C_9$,^{15}N]-tyrosine.

Position	**^{13}C incorporation [%]** from ^{13}C NMR	**^{13}C incorporation [%]** from ^1H NMR
1	53	-
2/6	53	51[c]
3/5	53	53[c]
4	53	-
7	53[a]	-
8	53	n.a.
9	8[b]	n.a.
10	7-8	n.a.
11	7-8	n.a.
12/13	7[b]	n.a.

n.a. = signals were not analyzed; [a] calculation with reference C9; [b] calculated from labelled to natural ^{13}C signal ratio;[110] [c] calculated ^{13}C incorporation from the ^1H NMR spectrum.

After feeding [$^{13}C_9$,^{15}N]-tyrosine the complete molecule **34a** was found to be ^{13}C-enriched in the ^{13}C NMR analysis, which is presumably due to partial scrambling of the precursor by primary metabolism via fumarylacetoacetate to doubly ^{13}C-labelled acetate. The NMR analysis of the [$^{13}C_9$,^{15}N]-tyrosine labelled *p*-hydroxyacetophenone *iso*-butanamide (**34a**) are presented in Table 14. Due to the scrambling, the acyl residue showed a low ^{13}C incorporation of 7-8%, which was calculated from the doublet signals of the ^{13}C-labelled C9 and the methyl groups C12 and C13 compared to their corresponding natural singlet signals (Appendix, Spectrum 57).[110] In contrast, the ^{13}C signals of the *p*-hydroxyacetophenone unit in **34a** showed complex signal patterns due to the intact incorporation of the completely ^{13}C-labelled tyrosine (Appendix, Spectrum 57). Representative for this structural unit, a 53% ^{13}C incorporation of carbonyl C7 was calculated, compared to the natural singlet signal of C9, the

second carbonyl group in **34a**. Reference ^{13}C signals for the other carbon types were not available. In addition, the ^{1}H NMR spectrum showed broad doublets for the aromatic protons of the ^{13}C-labelled part of the sample with a direct CH coupling of $^{1}J_{C,H}$ ~ 150 Hz.[111] Compared to the unlabelled aromatic proton signals, the doublets indicated 52% ^{13}C incorporation, fully supporting the ^{13}C NMR result (Appendix, Spectrum 56). In order to assess the incorporation of ^{15}N, the ^{1}H doublet signal of the ^{15}N-labelled NH proton with a direct coupling of $^{1}J_{N,H}$ ~ 95 Hz was compared to the unlabelled singlet NH signal in the ^{1}H NMR spectrum to give a ^{15}N incorporation of 30% (Appendix, Spectrum 56). This result was supported by HRESIMS of the sample, which showed the natural key fragment $[C_8H_9NO_2+H]^+$ at *m/z* 152.0701 and two labelled monoisotopic ions (Appendix, Spectrum 60). One peak at *m/z* 161.0938 for $[^{13}C_8H_9{}^{15}NO_2+H]^+$ with 29% incorporation of the complete labelled fragment and a second ion with 30% at *m/*z 160.0966 for $[^{13}C_8H_9NO_2+H]^+$ missing the labelled nitrogen. The total ^{13}C incorporation of 59% for the fragment ion of **34a** is in good agreement with the results from the NMR analyses.

2.2.4 Biological Activity of *p*-Hydroxyacetophenone Amides 34a-f

The *p*-hydroxyacetophenone amides **34a-f** were tested up to a concentration of 100 µg/mL but did not show any significant antibiotic activity against *Mucor hiemalis*, Gram-positive bacteria (*Staphylococcus aureus*, *Nocardia flava*, *Micrococcus luteus*), Gram-negative bacteria (*Escherichia coli*, *Chromobacterium violaceum*) or yeasts (*Candida albicans*, *Rhodotorula glutinis*, *Pichia anomala*, *Schizosaccharomyces pombe*). In addition **34a-f** were screened against various micro algae (*Scenedesmus bajacalifornicus*, *Chlamydomonas sp*., *Bracteacoccus sp*., *Pseudococcomyxa simplex* and *Botryococcus brauni*), and only **34d** induced growth inhibition of *Pseudococcomyxa simplex* at the highest concentration tested (100 µg/mL). Similarly, **34a-f** showed no cytotoxic effect or growth inhibition in cell culture assays with human leukemic U-937 cells up to a concentration of 100 µg/mL.

2.3 Sulfangolids, Macrolide Sulfate Esters from *Sorangium cellulosum*

2.3.1 Verification of the Proposed Structures of Sulfangolids 25a-d

Sulfangolid A (**25a**) was isolated from *Sorangium cellulosum* strain So ce666 during my diploma thesis. In the HRESIMS **25a** showed a molecular ion cluster $[M-H]^-$ at *m*/*z* 663.3208 for the molecular formula $C_{35}H_{51}O_{10}S$ (calc. 663.3206). In the direct chemical ionisation mass spectrum **25a** provided a highly abundant negative charged fragment ion at *m*/*z* 566 (100%). The characteristic loss of 97 u suggested the elimination of a HSO_4^- residue. The sulfate residue was also present in the IR spectrum with strong bands at 1252 (s) and 1011 (s) cm^{-1}. The absorption at 342 nm in the UV spectrum indicated a tetraene chromophore conjugated with a carbonyl group and a second absorption at 283 nm suggested a dienone chromophore.

The detailed structure was elucidated by 1D and 2D NMR spectroscopy (Table 15). A $^1H,^{13}C$ HMQC spectrum correlated the protons to their directly bound carbons and the analysis of the $^1H,^1H$ COSY spectrum furnished four structural elements A–D (Figure 31). The exchangeable protons of the alcohols were assigned to oxygenated methines C14 and C17 from their $^1H,^1H$ COSY correlations, thus locating the sulfate moiety to the oxygenated methine C13 ($\delta_{H/C}$ 4.36/77.4 ppm). The lactone carbon C1 (δ_C 165.1 ppm) showed HMBC correlations with 2H and 3H of subunit A. Due to the high order spin system of the olefinic protons, the coupling constants in Table 15 were deduced from a simulated ^1H spectrum using ACD/C+H Predictor (Version 11) to match the observed ^1H NMR signal pattern of **25a** (Appendix, Spectrum 69). All double bonds of the tetraene in subunit A were *trans*-configured according to their vicinal coupling constants ^3J of 15 Hz.

The structural elements A and B were connected via carbonyl C15 (δ_C 217.5 ppm) by HMBC correlations with 14H, 14OH of subunit A and 16H and methyl group C32 of subunit B. Carbonyl C21 (δ_C 202.2 ppm) displayed cross peaks in the HMBC spectrum with methyl group C33 of subunit B and with the unsaturated methines 22H and 23H of subunit C. Subunit C was further connected to the quaternary carbon C24 (δ_C 134.2 ppm) and subunit D following several HMBC correlations: the mutual HMBC correlations between methyl group C34 and methines 23H and 25H, as well as between methines 23H and 25H, and the quaternary C24 with 22H and 34H. The *trans*-configuration of the double bonds was unravelled from the vicinal coupling constant $^3J_{22,23}$ of 15.4 Hz and the $^1H,^1H$ ROESY correlation of methyl group C34 with 22H and 25H, as well as correlations between 23H and 25H. The last double bond equivalent was used to close the macrolide ring of sulfangolid A

(**25a**) at position C27, which was indicated by a characteristic acyl shift of 27H ($\delta_{H/C}$ 4.91/74.2 ppm).

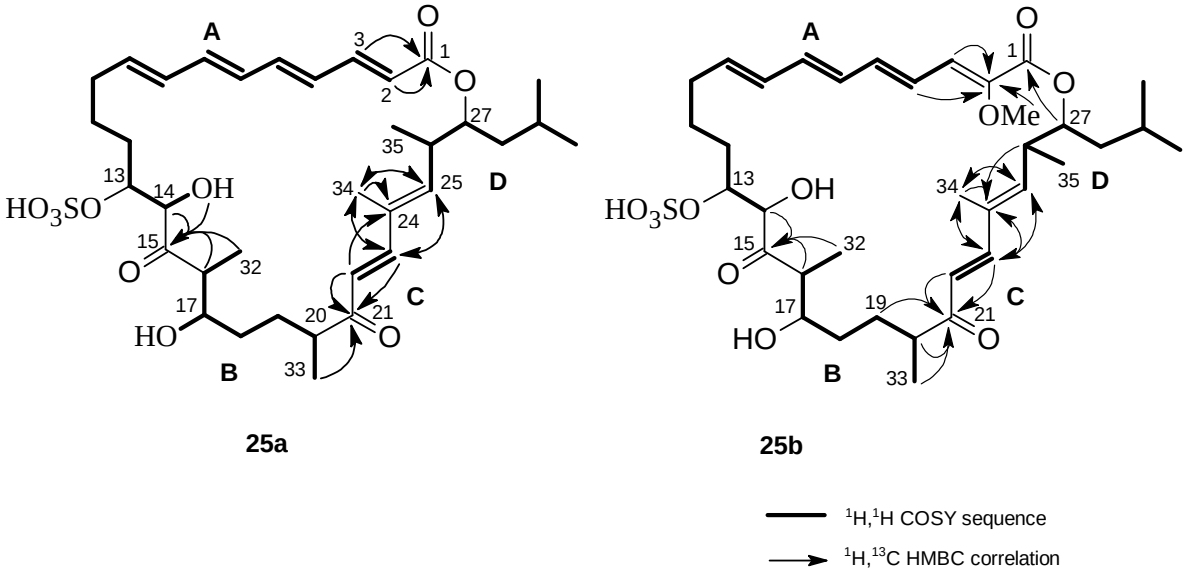

Figure 31. The structures of sulfangolid A (**25a**) and sulfangolid B (**25b**) with the COSY sequences and selected HMBC correlation.

Sulfangolid B (**25b**) was isolated from *Sorangium cellulosum* strain So ce192 (H. Irschik, R. Jansen) and showed a molecular ion cluster $[M-H]^-$ at *m/z* 693.3314 in the HRESIMS establishing the molecular formula of $C_{36}H_{53}O_{11}S$ (calc. 693.3308). Similar to sulfangolid A (**25a**), variant B (**25b**) showed analogue COSY sequences and HMBC correlations presented in Figure 31. Sulfangolid B (**25b**) differed from **25a** by an additional methoxy group in the unusual position at C2 (Table 16). The position of the methoxy group was indicated by the chemical shift of quaternary carbon C2 at δ_C 145.5 ppm showing HMBC correlations with the methoxy group ($\delta_{H/C}$ 3.75/60.8 ppm) and with methines 3H and 4H (Figure 31).

Sulfangolid C (**25c**) was isolated from *Sorangium cellulosum* strain So ce12 during my diploma thesis. The compound **25c** showed a molecular ion $[M-H]^-$ at *m/z* 681.3314 in the HRESIMS establishing the molecular formula $C_{35}H_{53}O_{11}S$ (calc. 681.3317). The UV maximum at 311 nm indicated the loss of one conjugated double bond from the unsaturated lactone chromophore compared to **25a**. Subsequently to $^1H,^{13}C$ HSQC analysis, the $^1H,^1H$ COSY data revealed five structural fragments A-E (Figure 32). The lactone C1 was connected with fragments A and D from HMBC correlations with 2H and the acyl proton 27H ($\delta_{H/C}$ 4.94/74.4 ppm). The quaternary carbon C15 was correlated with 13H and 14H of fragment A and 16H and methyl group C31 of fragment B. In addition, C15 showed a characteristic carbon shift of a hemiketal at δ_C 100.4 ppm. A six-membered ketal ring was formed with the

oxymethine C19 ($\delta_{H/C}$ 3.84/68.3 ppm) of fragment B, which was supported by nOe correlations between 15OH, 17H and 19H. Further carbonyl C21 showed HMBC correlations with methyl group C32 and 23H of subunit C. The quaternary carbon C24 connected fragment C and D, evident from various HMBC correlations of C24 with 22H and 23H, as well as with 25H. In addition the directly bound methyl group C34 showed HMBC correlations with 23H, and the mutual HMBC cross peaks between C23 of subunit C and C25 of subunit D (Figure 32). The final connection of the *iso*-butyl side chain was accomplished by HMBC correlations of C27 and C29, as well as mutual HMBC cross peaks between the methyl groups C30, C31 and C28.

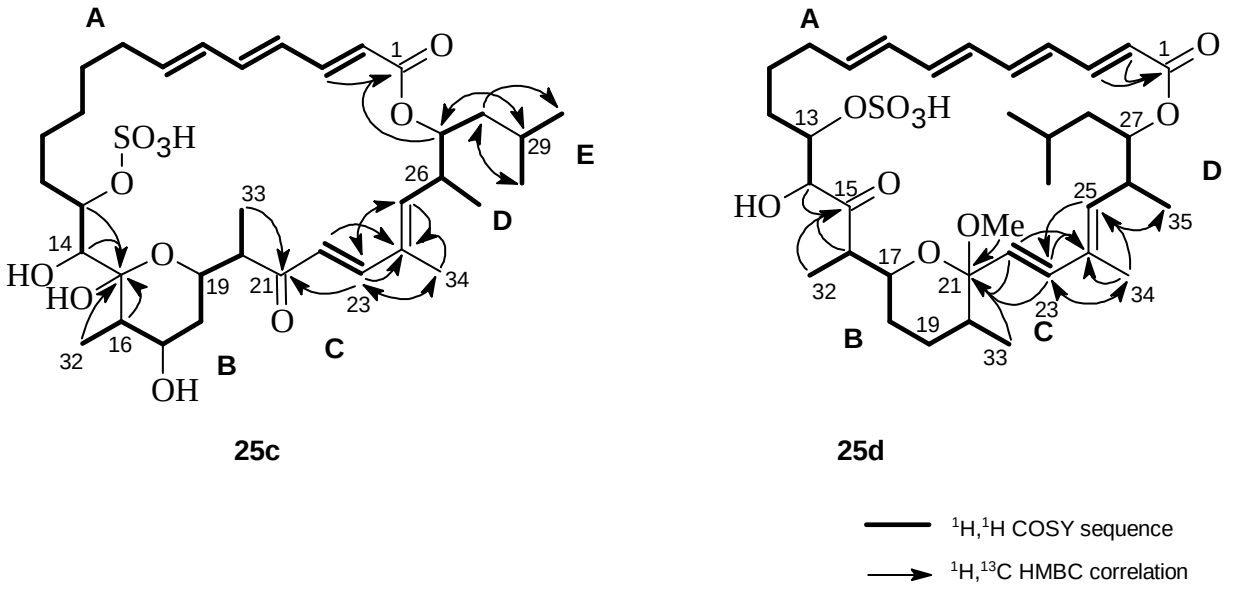

Figure 32. The structures of sulfangolid C (**25c**) and sulfangolid D (**25d**) with the COSY sequences and selected HMBC correlations important for the structure elucidation.

Sulfangolid D (**25d**) was isolated from *Sorangium cellulosum* strain So ce1375 (K. Gerth, M. Herrmann). The HRESIMS analysis showed a molecular ion cluster $[M\text{-}H]^-$ at *m/z* 677.3343 for the elemental composition $C_{36}H_{53}O_{10}S$ (calc. 677.3365). After $^1H,^{13}C$ HSQC analysis, four structural subunits were assigned from the $^1H,^1H$ COSY spectrum of **25d**. Subunit A was correlated by HMBC correlations of C1 with 2H and 3H, and on the other side to carbonyl C15 by HMBC cross peaks of C15 with 14H. On the other hand, C15 showed HMBC correlations with 16H and 32H of fragment B. The quaternary carbon C21 was HMBC correlated with a methoxy group ($\delta_{H/C}$ 3.15/49.8 ppm) while its characteristic carbon shift at δ_C 103.2 ppm indicated a ketal carbon. This ketal was formed within subunit B as six-membered ring with the ether at C17, due to the characteristic chemical shifts of δ_H 3.63 ppm and δ_C 72.5 ppm. Further C21 was connected to fragment C by HMBC correlations of 22H

and 23H. The quaternary carbon C24 and the methyl group C33 interconnected fragment C and fragment D according to various HMBC correlations of C24 with 22H and 23H, as well as mutual HMBC correlations of methyl group C34 with 23H and 25H presented in Figure 32.

Table 15: NMR data of sulfangolid A (**25a**) (^{1}H 600 MHz; ^{13}C 150 MHz, [D_6]DMSO)

Atom	δ_H	m	*J* [Hz]	COSY[a]	ROESY[a,b]	δ_C	HMBC[c]
1	-	-	-			165.1	2>>3
2	5.76	d	14.8[d]	3	4 o. 5>>34	119.8	
3	6.88	m	14.8, 11.0[d]	4 o. 5, 2	4 o. 5>>34	145.2	
4	6.35	m	11.0, 15.0[d]	3, 6 o. 7	2 o. 3>>33, 34	128.4	2
5	6.36	m	15.0, 11.0[d]	3, 6 o. 7	2 o. 3>>33, 34	142.1	6 o. 7
6	6.23	m	15.0, 11.0[d]	4 o. 5, 8	4 o. 5, 9>33	128.9	4 o. 5
7	6.22	m	15.0, 11.0[d]	4 o. 5, 8	4 o. 5, 9>33	138.6	
8	6.14	m	14.8, 11.0[d]	7 o. 6, 9	(9), 10β	130.6	
9	5.67	ddd	14.8, 10.1, 4.8	8, 10α/β	(10α),10β, 6 o. 7	139.0	
10α	2.30	m		10β, 9, 11α/β	(10β)	32.1	
10β	1.92	m		10α, 9	(10α, 9), 8		
11α	1.69	m		11β, 12β>10α/β	(10α), 9, 8	24.9	
11β	1.26	m		11α, 12β>10 α /β, 12α	13>9		
12α	1.00	m		12β, 11β>13	(13)>9	28.4	14
12β	1.47	m		12α, 11α/β, 13	(13)		
13	4.36	dd	10.0, 2.1	14, 12α/β	14_{OH}, 12β, 11β>12α>11α>10α	77.4	14_{OH}
14	4.46	dd	6.6, 2.1	13, 14_{OH}	32, (14_{OH}), 16	77.2	
14_{OH}	5.76	d	6.6	14			
15	-	-	-			217.5	32, 16, 14, 14_{OH}
16	3.01	dq	9.3, 7.2	17, 32	(32), 14_{OH}, 18β>18α, 14, 17_{OH}	47.9	32
32	1.00	d	7.2	16	(16), 17>17_{OH}, 14	14.6	
17	3.34	dddd(br)	9.3, 7.3, 1.3, 9.5	16, 18α>18β	32, 19β, 18α, 19α	71.3	32
17_{OH}	4.39	d	7.3	17	32, 16>19α		
18α	1.33	m		18β, 19α, 17	33	33.8	17_{OH}
18β	0.83	m	Σ32.2[f]	18α, 19α/β, 17	(19α), 16>20		
19α	1.92	m		19β, 18α>11α/β, 18β	(20, 19β), 22, 14_{OH}	28.9	33
19β	0.89	m	Σ31.4[f]	19α, 18α/β	>17		
20	2.34	ddq	9.5, 7.0, 2.5	33, 19α/β	22, 19α>18β	45.6	33
33	0.95	d	7.0[e]	20	(20), 22>4 o. 5	15.4	
21	-	-	-			202.2	33>22, 23
22	6.20	d	15.4	23	34, 20>19α	122.8	
23	7.20	d	15.4	22	25	145.9	34>25
24	-	-	-			134.2	34>22
34	1.52	s		25	26, 22>3>2>4 o. 5	12.6	23, 25
25	5.98	d	11.2	26, 34	23, 28α, 35	142.3	35, 34>23
26	2.93	ddq	11.2, 11.5, 7.0	25, 35>27	34, (27>35)	35.4	30, 31, 35
35	0.95	d	7.0[e]	26	25>27, 28β, (26)	15.9	26, 25
27	4.91	ddd	11.5, 4.5, 2.0	26, 28α/β	35, 31, 26, 29, (28β)	74.2	35
28α	1.58	m		28β, 27	25	35.3	35
28β	1.33	m		28α, 27, 29	35, (27)		
29	1.47	m		28β, 30, 31	27	24.2	30, 31
30	0.85	d	6.4	29	(29)	23.4	31
31	0.81	d	6.4	29	(29), 27	21.0	30
NH_4^+	7.03	s(br)					

[a] signals are sorted by intensity. [b] vicinal nOe are indicated by brackets. [c] sorted by intensity of the cross peaks. [d] overlapping signals of higher order, coupling constants were calculated by ACD/C+H NMR Predictor (Version 11). [e] overlapping signals. [f] data from *J*-resolved spectrum.

Table 16: NMR data of sulfangolid B (**25b**) (^{1}H 600 MHz; ^{13}C 150 MHz, CD_3OD)

Atom	δ_H	m	*J* [Hz]	COSY	δ_C	HMBC
1	-	-	-	-	164.6	3, 27
2	-	-	-	-	145.5	3, OMe
OMe	3.75	s	-	-	60.8	-
3	6.55	m[a]	-	4	128.2	5,4
4	6.55	m[a]	-	3,5	125.2	6
5	6.36	m	-	4,6	140.6	3,7
6	6.29	m[b]	-	5,7	131.1	4,8
7	6.29	m[b]	-	6,8	138.6	5,9
8	6.19	m	-	7,9	132.5	6, 10
9	5.78	ddd	14.8, 10.1, 4.7	8,10	139.1	10β, 11β
10α	2.46	m	-	9, 11	33.7	-
10β	2.08	m[d]	-			
11α	1.80	m	-	10,12	26.1	9
11β	1.50	m	-			
12α	1.63	m	-	11, 13	29.6	14, 10
12β	1.28	m	-			
13	4.75	dt	10.1, 2.2	12, 14	81.6	-
14	4.79	d	2.2	13	78.8	-
15	-	-	-	-	217.5	14,16,32
16	3.18	m[c]	-	32,17	48.7	-
32	1.20	d	7.1	16	14.4	17,16
17	3.66	ddd	10.5,9.3,1.9	16, 18	73.7	32,19
18α	1.57	m	-	17,19	35.0	16
18β	1.12	m	-			
19α	2.08	m[d]	-	18, 20	30.7	17, 33
19β	1.23	m	-			
20	2.58	qt	7.0, 6.7	19,33	47.3	-
33	1.14	d	6.7	20	16.5	19
21	-	-	-	-	205.9	22,23,20,33,19
22	6.34	d	15.5	23	124.1	-
23	7.37	d	15.5	22	148.4	25, 34
24	-	-	-	-	136.3	22,26,34
34	1.70	d	3.9	-	13.1	26,25,23
25	6.03	d	10.9	26	143.7	27,35, 34, 23
26	3.18	m[c]	-	27,25,35	37.0	-
35	1.09	d	6.9	26	16.3	25,26
27	5.12	ddd	11.4, 4.8, 2.0	26,28	77.3	25
28α	1.68	m	-	27,29	37.1	30,31,26
28β	1.50	m	-			
29	1.63	m	-	30,31,28	25.9	27
30	0.99	d	6.6	29	24.0	28,31
31	0.96	d	6.6	29	21.6	29,30

[a] multiplet of 3H and 4H at 6.55 ppm; [b] multiplet of 6H and 7H at 6.29 ppm; [c] multiplet of 16H and 26H at 3.18 ppm; [d] multiplet of 10Hβ and 19Hα in between 2.12 and 2.03 ppm.

Table 17: NMR data of sulfangolid C (**25c**) (^{1}H 600 MHz, ^{13}C 150 MHz, [D_6]DMSO)

Atom	δ_H	m	*J* [Hz]	COSY[a]	ROESY[a,b]	δ_C	HMBC[c]
1	-	-	-			165.1	2, 3>27
2	5.81	d	15.2	3	(3), 4, 33	120.3	4
3	6.91	dd	15.2, 11.2	2,4	(2, 4), 5, 33	144.4	5
4	6.31	dd	14.7, 11.2	3,5	(3, 5), 2>6	127.5	2>3,6
5	6.44	dd	14.7, 10.6	4, 6	(4, 6), 3, 7>>8α, 32	141.3	3, 4, 7
6	6.19	dd	15.1, 10.6	5, 7	(5), 4>8α	130.3	4>8α
7	5.87	ddd	15.1, 9.3, 5.3	6, 8α/β	(6, 8α/β), 5 >>32	140.8	5>8α
8α	2.08	m		7, 8β, 9α/β	(7, 9α/β), 6	31.0	6
8β	2.19	m		7, 8α, 9α/β	(8α, 9α/β), 6>5		
9α	1.45	m		8α/β, 10		28.9	>>8α/β
9β	1.32	m		8α/β, 11α, 10			
10	1.26	m		11, 9α/β	13	27.7	8α/β
11α	1.41	m		12, 10	13	26.3	
11β	1.26	m		12			
12	1.51	m		13		30.7	13, 6
13	4.39	t (br)	6.4	12, 14	(14), 15_{OH}, (12β), 11, 33	78.1	11
14	3.87	d (br)	7.55, (1.1[d])	14_{OH} > 13 > 15_{OH}	(13, 14_{OH}), 15_{OH}, 32, 16	75.1	14_{OH}, 15_{OH}
14_{OH}	4.73	d (br)		14	(14>15_{OH}), 16		
15	-	-	-			100.4	32, 16, 14_{OH}, 15_{OH} > 14, 13
15_{OH}	5.49	s			13, 14, 19 (17, 32)		
16	1.65	dq (br)	10.4, 6.6	17, 31, 14_{OH}	(32, 17), 17_{OH}, 14_{OH}, 14	41.6	15_{OH}, 14_{OH}, 14
32	0.86	d	6.6	16	14, 17_{OH}>15_{OH}>14_{OH}	11.2	16>>17
17	3.39	ddd (br)	10.4, 10.8, 5.3	18α, 16, 18β	(18α, 17_{OH}), 19, 32>15_{OH}	67.6	32, 17_{OH}, 16
17_{OH}	4.33	d	5.3	17	(>17, 18α), 16		
18α	1.77	ddd(br)	11.7, 4.5, 1.8	18β, 19, 17	(17_{OH}, 19, 17)	39.0	
18β	0.88	ddd[e]	11.7, 11.8, 10.8[e]	18α, 19, 17	(19, 17), 20		
19	3.84	ddd(br)	11.8, 10.0, 1.8	20, 18α/β	(20, 18α), 17, 33	68.3	33
20	2.68	dq	10.0, 7.2	19, 33	(33, 19), 22, 18β, 23	51.4	33
33	1.05	d	7.2	20	(20), 19, 22, 5, 13>7	15.2	20>>19
21	-	-	-			201.5	33>23, 22>20
22	6.34	d	15.5	23	(23), 34, 20>32	124.2	
23	7.18	d	15.5	22	(22), 25, 34>>20	146.2	34>25
24						134.2	34, 22>23, 26
34	1.61	d(br)	0.8	25	22, 26>3	12.6	23>25
25	6.0	d	11.0	26, 33	23>(26), 34, 28α	142.7	34, 23>27
26	3.01	ddd	11.0, 7.2, 4.6	27, 25, 35	(35, 25, 27), 34, 30, 28β	35.2	35
35	1.00	d	7.2	26	27, 25, (26), 28β	15.8	26, 25
27	4.94	ddd	11.5, 4.6, 2.8	26, 28α/β	34, 35, 30, 29, (28β, 26)	74.4	35, 26>28α
28α	1.58	ddd(br)	14.2, 11.5, 4.2	27, 28β	(28β), 25, 27	35.6	30, 31, 26
28β	1.36	m		27, 28α	(27), 35>>25, 26		
29	1.49	m		30, 34, 28β	27	24.2	30, 35, 27
30	0.88	d	6.8	29		23.4	31, 28α/β
31	0.84	d	6.8	29	27, 26	21.1	30>28α/β
NH_4^+	7.06	s(br)			15_{OH}, 14_{OH}, 17_{OH}		

[a] signals are sorted by intensity. [b] vicinal nOe are indicated by brackets. [c] signals are sorted by intensity of the cross peaks. [d] after H/D-exchange. [e] data from *J*-resolved spectrum.

Table 18: NMR data of sulfangolid D (**25d**) (^{1}H 300 MHz, ^{13}C 75 MHz, CD_3OD)

Atom	δ_H	m	*J* [Hz]	COSY[a]	δ_C	HMBC[b]
1	-	-	-	-	168.3	2 >3
2	5.80	d	15.5	3	121.5	-
3	7.11	m	-	2, 4 o. 5	147.0	-
4	6.46[c]	m	-	[d]	130.5	3,2
5	6.45[c]	m	-	[d]	143.3	3 >6 o. 7
6	6.33[c]	m	-	[d]	131.1	4 o. 5
7	6.34[c]	m	-	[d]	139.2	-
8	6.26[c]	m	-	[d], 9	132.9	-
9	5.69	ddd	14.2, 10.6, 3.7	10α/β, 8	140.2	-
10α	2.52	m	-	9, 10β, 11α	34.2	-
10β	2.02	m	-	9,10β, 11α/β		
11α	1.98	m	-	12α/β, 11β, 10α/β	26.3	-
11β	1.36	m	-	12α/β,11α		
12α	1.60	m	-	11α/β, 13,12β	30.5	14
12β	1.30	m	-	11α/β, 13,12α		
13	4.40	dt	10.7, 1.5	14, 12α >β	83.1	14
14	4.76	d	1.5	13	80.6	-
15	-	-	-	-	218.3	14,32>16
16	3.12	dq	9.6,6.9	17, 32	49.3[e]	32, 17
32	1.20	d	6.9	16	15.4	>16
17	3.63	m	-	16,18α/β	72.5	32>16
18α	1.60	m	-	17, 19, 18β	32.1	-
18β	1.09	m	-	19,18α		
19	1.64	m	-	18α, 20	28.7	33
20	1.57	m	-	19, 33	40.3	33
33	1.04	d	6.8	20	16.4	>20
21	-	-	-	-	103.2	23,22,33 >>OMe
OMe	3.15	s	-	-	49.8[e]	>20
22	5.15	d	16.4	23	128.0	>23
23	6.22	d	16.4	22	138.2	35, 22
24	-	-	-	-	136.2	35, 23, 22
34	1.60	d	0.9	-	13.7	23
25	5.44	d	10.5	26>35, 23	133.5	35,36,23
26	3.06	m	-	25,36> 27	36.2	36
35	1.07	d	6.8	26	16.7	>26,25
27	5.04	ddd	10.5,4.7,2.4	26,28 α/β	77.1	36
28α	1.63	m	-	27,29	37.4	30,31
28β	1.46	m	-	27		
29	1.65	m	-	30,31,28α	26.1	30,31
30	0.98	d	6.4	29	24.1	31 >29
31	0.94	d	6.4	29	21.9	30 >29

[a] signals are sorted by intensity. [b] signals are sorted by intensity of the cross peaks. [c] multiplet from 6.46 to 6.26 ppm containing 5 protons. [d] Overlapping COSY cross correlations in the multiplet from 6.46 to 6.26 ppm. [e] ^{13}C shift from the HMBC correlation.

2.3.2 The Relative Configuration of Sulfangolid C (25c)

The relative configuration of sulfangolid C (**25c**) was determined utilizing 1D and 2D NMR studies (Table 17) assisted by molecular modelling with HyperChem (Version 8.5). The 28-membered macrolide ring of sulfangolid C (**25c**) contains three large inflexible structural elements, the triene lactone, the six-membered hemiketal ring and the dienone, which alleviated the modelling. Analogously to sulfangolid A (**25a**), the double bonds of the lactone and the unsaturated ketone of **25c** maintain the all-*trans*-configuration. The six-membered hemiketal formed the basis for the elucidation of the relative configuration. Initially, the seat conformation of the hemiketal was assigned from nOe correlations of 15OH, 17H, 19H indicating their coaxial positions (Figure 33). Further nOes of 15OH, 17H and 19H with 18Hα and methyl group C32 defined the equatorial positions of 18Hα and C32 in the hemiketal. The axial position of 18Hβ (δ_H 0.88 ppm, ddd) was supported by three *trans* coupling constants between 11.8 and 10.8 Hz for $^3J_{17,18\beta}$, $^3J_{19,18\beta}$, and the geminial $^2J_{18\alpha,18\beta}$ coupling constants observed in the *J*-resolved NMR spectrum (Appendix, Spectrum 91). Further, the vicinal coupling constant $^3J_{16,17}$ of 10.4 Hz between 16H and 17H was only feasible for a coaxial relation of both protons. Another large vicinal coupling constant $^3J_{19,20}$ of 10.0 Hz positioned 20H *anti* to 19H, which is realized in the model (Figure 33) by a dihedral angle $\varphi_{19H,20H}$ of 165.9°. This *anti*-position was supported by the nOe of 20H with the axial 18Hβ (2.4 Å) while the methyl group C33 at C20 points into the macrolide ring as indicated by nOe correlations with 19H, 13H, 5H and 7H. The nOe observations are fully compatible with the modelled configuration (Figure 33) by the calculated distances of 2.4 Å between 33H and 13H, as well as 1.7 Å between 33H and 5H and 2.4 Å between 33H and 7H across the macrolide ring. The methyl group C34 substituting the *trans*-diene inclines towards the lactone ring according to the nOe correlation with 3H. The vicinal coupling $^3J_{25,26}$ of 11.0 Hz indicates a *transoid*-relation between both methines 25H/26H which is compatible with the dihedral angle $\varphi_{25H,26H}$ of 167.3° in the model. This position is additionally indicated by the nOe between 26H and methyl group C34. Consequently, the exocyclic orientation of methyl group C35 was supported by the nOe with 25H. The position of the macrolide at C27 was assigned on the basis of the small coupling constant $^3J_{26,27}$ of 4.6 Hz compatible with a calculated torsion angle $\varphi_{26H,27H}$ of 57.2° and the nOe correlation between 27H and 35H.

On the opposite side of the ketal ring, the position of 14H was indicated by nOe correlations with the axial 16H and the equatorial methyl group C32 feasible for an *anti*-orientation of 14H and 15OH. The small coupling constant $^3J_{13,14}$ of 1.1 Hz observed after H/D-exchange

reflects the calculated torsion angle $\varphi_{13H,14H}$ of 75.5° in the model. In addition, the nOe between 13H and 33H crossing the lactone ring was observed in the $^{1}H,^{1}H$ ROESY spectrum of sulfangolid C (**25c**). Both relative configurations, the 13*R** and the 13*S** of **25c,** were modelled with HyperChem (Figure 33 and Figure 34). In each case the configuration with the lowest global minimum showed very similar torsion angles for $\varphi_{13H,14H}$ (13*R** = 75.5°, 13*S** = 82.9°) and a similar distance between 13H and 33H with 2.6 and 2.4 Å (Table 19 and Table 20), well matching the observed nOes. However, in the 13*R**-model the smaller distances across the macrolide ring between methyl group C33 with 5H (1.7 Å) and 7H (2.4 Å) agree with the observed nOes of 33H far better than the corresponding distances of 3.7 and 4.2 Å in the 13*S**-model (Table 20). Additionally, the 13*R**-configuration included two hydrogen bonds stabilizing the position of the sulfate ester residue. For these reasons the 13*R** configuration of sulfangolid C (**25c**) is favoured. The resulting all-*trans* 13*R**,14*S**,15*R**,16*R**,17*S**,19*S**,20*R**,26*R**,27*R** configuration of sulfangolid C (**25c**) is presented in Figure 35.

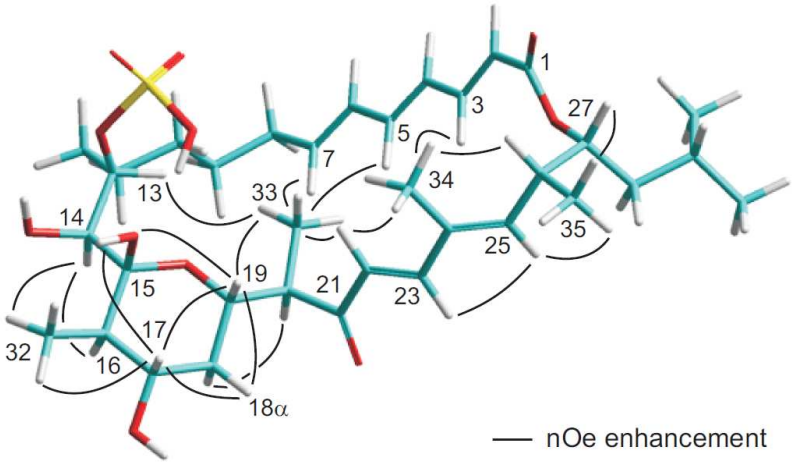

Figure 33. The model of all-*trans* 13*R**,14*S**,15*R**,16*R**,17*S**,19*S**,20*R**,26*R**,27*R** sulfangolid C (**25c**) with selected nOe correlations. Two hydrogen bonds are formed between the sulfate group at C13 and 15OH and between 15OH and 14OH.

Table 19. The proton/proton distances and dihedral angles φ of all-*trans* 13R^*,14S^*,15R^*,16R^*,17S^*,19S^*, 20R^*,26R^*,27R^* model of sulfangolid C (**25c**) presented in Figure 33.

Position	dihedral angle φ [degree]	atom distance [Å]	Position	dihedral angle φ [degree]	atom distance [Å]
13H,14H	75.5		33H,5H		1.7
13H,33H		2.4	33H,7H		2.4
14H,32H		3.3	22H,34H		1.8
14H,16H		2.4	23H,25H		2.4
16H,17H	169.2		34H,3H		3.8
17H,18Hβ	174.1		34H,26H		1.8
17H,18Hα		2.5	25H,35H		2.8
18Hβ,19H	176.7		25H,26H	167.3	
18Hβ,20H		2.4	25H,28Hα		2.5
19H,33H		2.7	26H,27H	57.2	
19H,20H	165.9		35H,27H		2.6
33H,22H		2.8	27H,29H		2.3

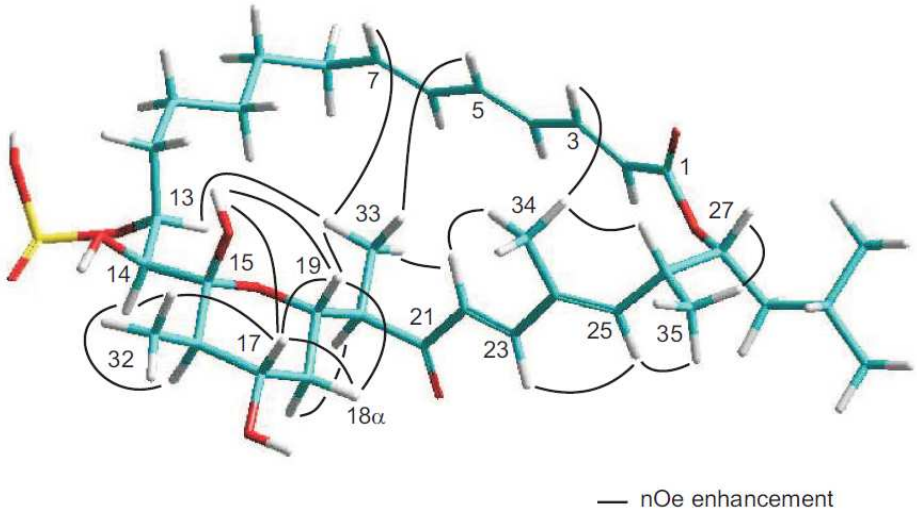

Figure 34. Model with the lowest global minimum of sulfangolid C (**25c**) with 13S^*,14S^*,15R^*,16R^*,17S^*, 19S^*,20R^*,26R^*,27R^* configuration and selected nOe enhancements.

Table 20: The measured proton/proton distances and dihedral angles φ of the modelled 13S^*,14S^*,15R^*,16R^*,17S^*,19S^*,20R^*,26R^*,27R^* configuration of sulfangolid C (**25c**) presented in Figure 34.

Position	dihedral angle φ [degree]	atom distance [Å]	Position	dihedral angle φ [degree]	atom distance [Å]
13H,14H	82.9		33H,5H		3.7
13H,33H		2.6	33H,7H		4.2
14H,32H		3.0	22H,34H		1.8
14H,16H		2.2	23H,25H		2.4
16H,17H	171.5		34H,3H		3.7
17H,18Hβ	173.8		34H,26H		1.8
17H,18Hα	56.9		25H,35H		2.6
18Hβ,19H	176.6		25H,26H	174.5	
18Hβ,20H		2.6	25H,28Hα		2.2
19H,33H		2.6	26H,27H	46.7	
19H,20H	173.5		35H,27H		2.6
33H,22H		1.8	27H,29H		2.6

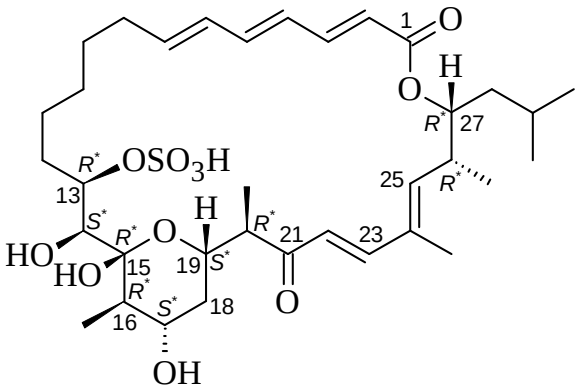

25c

Figure 35. The relative configuration of all-*trans* 13R^*,14S^*,15R^*,16R^*,17S^*,19S^*,20R^*,26R^*,27R^* sulfangolid C (**25c**).

2.3.3 Studies towards the Biosynthetic Precursors of Sulfangolid C (25c)

Two sulfangolid C (**25c**) producer strains So ce757 and So ce804 were analysed for their sulfangolid C (**25c**) production and found to synthesise 19 mg/L and 8.5 mg/L, respectively. Subsequently, strain So ce757 was used to inoculate a 70 L fermentation to observe the production kinetics of **25c** presented in Figure 36. Sulfangolid C (**25c**) is produced during days 2-8 in the exponential growth phase of the strain. In addition, the increasing glucose concentration in the supernatant was correlated to the **25c** production (Figure 36). As the strain grew in lumps this observation was used to determine the beginning of feeding the labelled precursor. In order to have a high incorporation, the precursors were fed in equal portions during sulfangolid C (**25c**) production starting at a glucose content of 0.25% in the medium.

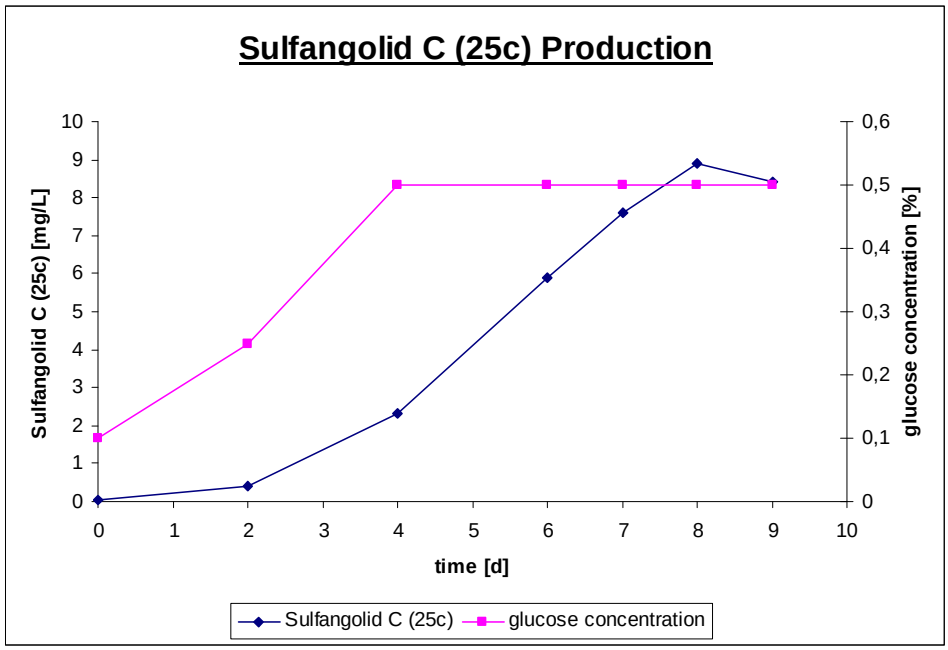

Figure 36. Sulfangolid C (**25c**) production in a 70 L fermentation of strain So ce757, measuring the glucose concentration in the media.

[1-^{13}C]-, [2-^{13}C]- and [1,2-^{13}C]-acetate, as well as [1-^{13}C]-propionate, and [D_{10}]-leucine were fed as biosynthetic precursors to *Sorangium cellulosum* strain So ce757. Subsequent to purification from the crude extract, ^{13}C NMR spectra of each isolated compound were measured. The resulting ^{13}C enriched NMR signals of sulfangolid C (**25c**) are listed in Table 21.

The starter unit of the sulfangolid C (**25c**) biosynthesis was identified as isovaleryl-CoA derived from leucine followed by two extensions with methylmalonyl-CoA precursors.[112,113]

The following ketone at C21 originates from C1 of malonyl-CoA. The metabolite **25c** is then elongated by units derived from propionate, acetate and the last propionate unit within the hemiketal, synthesising all methyl groups from propionate. The remaining part of **25c** is assembled from acetate exclusively. The sulfate residue at C13 presumable originates from sulfate in the medium, since the production of **25c** decreased dramatically from 19 to 2 mg/L after two passages in the same but sulfate-free medium. The final product **25c** is presumably released from the polyketide synthase assembly line (PKS) by lactonization.[51]

Table 21: Results of the feeding experiments: ^{13}C enriched NMR signals of labelled acetate (table) and propionate (table footnote) as well as HRESIMS and ^{1}H NMR analysis of [D_{10}]-leucine feeding experiments (table footnote).

Pos.	[1-^{13}C] acetate enrichment[a]	[2-^{13}C] acetate enrichment [%][b]	[1,2-^{13}C] acetate enrichment [%, m, $^{1}J_{c,c}$ Hz][c]	Pos.	[1-^{13}C] acetate enrichment[a]	[2-^{13}C] acetate enrichment [%][b]	[1,2-^{13}C] acetate enrichment [%, m, $^{1}J_{c,c}$ Hz][c]
1	30	n.e.	2, d, 75.7	18	n.e.[d]	n.e.	n.e.
2	n.e.[d]	6	2, d, 75.7	19	n.e.[d]	n.e.	n.e.
3	27.5	n.e.	1, d, 55.8	20	n.e.[d]	n.e.	n.e.
4	n.e.[d]	5	1, d, 55.8	33	n.e.[d]	n.e.	n.e.
5	33.5	n.e.	1, d, 54.6	21	29.5	n.e.	3, d, 52.8
6	n.e.[d]	7	1, d, 54.6	22	n.e.[d]	4	2, d, 52.8
7	27	n.e.	1, d, 42.2	23	n.e.[d]	n.e.	n.e.
8	n.e.[d]	in.[e]	1, d, 42.2	24	n.e.[d]	n.e.	n.e.
9	27	n.e.	2, d, 36.0	34	n.e.[d]	n.e.	n.e.
10	n.e.[d]	in.[e]	1, d, 36.0	25	n.e.[d]	n.e.	n.e.
11	25	n.e.	2, d, 35.7	26	n.e.[d]	n.e.	n.e.
12	n.e.[d]	in.[e]	1, d, 35.7	35	n.e.[d]	n.e.	n.e.
13	26	n.e.	1, d, 42.8	27	n.e.[d]	n.e.	n.e.
14	n.e.[d]	in.[e]	2, d, 42.8	28	n.e.[d]	n.e.	n.e.
15	n.e.[d]	n.e.	n.e.	29	n.e.[d]	n.e.	n.e.
16	n.e.[d]	n.e.	n.e.	30	n.e.[d]	n.e.	n.e.
32	n.e.[d]	n.e.	n.e.	31	n.e.[d]	n.e.	n.e.
17	27	n.e.	1, d, 34.7				

n.e. = not enriched carbon signal, [a] high enrichment ratio signal/noise (= 1), [b] enrichment calculated with unlabelled reference signal; [c] enrichment calculated by the ratio of labelled doublet signal to unlabelled singulett signal of the respective carbon; [d] signal was not observed, [e] in. = incorporation, no reference carbon available for the calculation of the enrichment, [f] ^{13}C signal is overlapping with DMSO signal and no analysis was possible. [1-^{13}C] propionate labelled carbons (enrichment) [a]: C15 (43.8), C19 (35.8), C23 (33.8) and C25 (29.5); [D_{10}]-leucine incorporation as $[M-H+9D]^-$ in HRESIMS obsd. 690.3867 (calc. 690.3879 for $[C_{35}H_{44}D_9O_{11}S]^-$) and decreased ^{1}H NMR signals for 30H (δ_H 0.88 ppm) and 31H (δ_H 0.84 ppm).

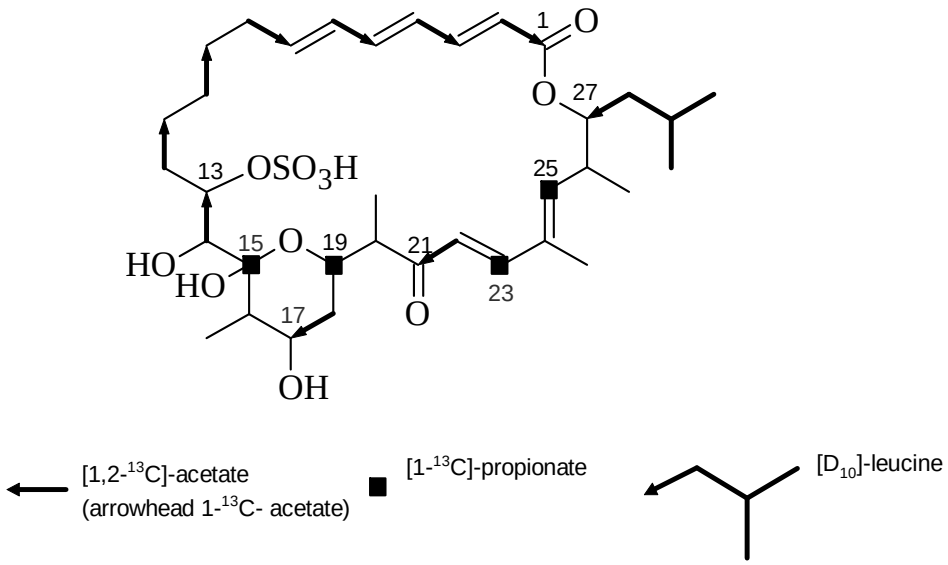

Figure 37. Biosynthetic precursors of sulfangolid C (**25c**) according to feeding experiments with labelled precursors.

3 Conclusion

3.1 General Scope of this Work

The present thesis deals with the isolation and identification of secondary metabolites from myxobacteria. At first, a protective isolation strategy for the light- and oxygen- sensitive polyunsaturated carboxylic acid roimatacene (**26**) has been developed. Furthermore the absolute configuration of **26** was established by chemical derivatization techniques, detailed NMR analyses and molecular modelling. Besides roimatacene (**26**) and traces of the known myxalamid C (**24c**) *Cystobacter ferrugineus* strain Cb G35 was found to produce six novel *p*-hydroxyacetophenone amides **34a-f**, which were isolated and characterised.

A further project included the verification of the proposed structures of the four natural sulfangolid variants **25a-d** by elucidation of their NMR data. These compounds were previously isolated from different *Sorangium cellulosum* strains. The relative configuration of sulfangolid C (**25c**) was finally established by comparison of detailed NMR data and the calculated diastereomeres from molecular modelling.

The biosynthetic precursors of roimatacene (**26**), *p*-hydroxyacetophenone *iso*-butanamide (**34a**) and sulfangolid C (**25c**) were studied by feeding experiments with D-, ^{13}C- and ^{15}N-labelled precursors.

3.2 Novel Secondary Metabolites from *Cystobacter ferrugineus* Cb G35

3.2.1 Roimatacene (26), a Novel Polyunsaturated Carboxylic Acid

The activity guided isolation of the oxygen- and light- sensitive polyunsaturated carboxylic acid **26** often terminated prematurely due to the decomposition of roimatacene (**26**). The compound decomposed during silica flash chromatography, exposure to oxygen of dried extracts, and due to traces of peroxides in solvents. The compound rearranged under acidic conditions (below pH 3). MPLC or size exclusion chromatography (Sephadex LH-20) were also unfavourable for the isolation of roimatacene (**26**). The first enriched sample of **26** contained about 50% fatty acids, which stabilized the compound and allowed measurement of a complete set of NMR data for structure elucidation. The structure elucidation revealed numerous sensitive structural elements in close proximity, e.g. an unsaturated carboxylic acid, a high degree of unsaturation, three α-polyunsaturated alcohol moieties and one tertiary

alcohol group (Figure 39). These structural elements are all combined in one carbon chain consisting of only 27 carbons, thus explaining the instability of roimatacene (**26**). The acryl acid residue in **26** led to use an antioxidant for stabilization. Different stabilization agents were tested and 4-ethoxyphenol proved to be slightly more effective compared to 4-brenzcatechol, which was previously used for the stabilization of etnangien (**35**).[114] The stabilizer did not exhibit growth inhibition of the antimicrobial screening. In addition, it could be removed by chromatography and was commercial available. Advantageously, the NMR signals of 4-ethoxyphenol did not overlap with the signals of roimatacene (**26**), thus permitting a straightforward structure elucidation.

Subsequent to the first structural analysis of roimatacene (**26**), the protective isolation strategy described in chapter 2.1.1 was successfully developed. Amber glass ware was used in order to protect roimatacene (**26**) against light, and the extracts were kept dissolved in methanol supplemented with the free radical scavenger 4-ethoxyphenol. During chromatography the mobile phases were buffered with ammonium acetate and saturated with nitrogen gas. The free radical scavenger 4-ethoxyphenol was added to each fraction during chromatography, since the separation could not be carried out under nitrogen gas. An advanced acid-base partition plays an important role in this isolation. Herewith the majority of by-products are selectively removed from the crude extract and roimatacene (**26**) is strongly enriched using the acidic character of the carboxylic acid. Previously, acid-base partition proved to be a very powerful tool in the isolation of sorangicins (**13**), as well as of etnangien (**35**).[114,115] In the case of the roimatacene (**26**) isolation fatty acids were co-purified and also showed a similar retention time in the RP-chromatography. In the advanced partition process an additional *n*-heptane extraction was carried out, in order to remove the large amount of fatty acids and to facilitate the following chromatography, before the acidic water layer was extracted with ethyl acetate. The newly developed isolation strategy and several 70 L fermentations finally provided sufficient material for a complete structure elucidation and for a biological screening of roimatacene (**26**).

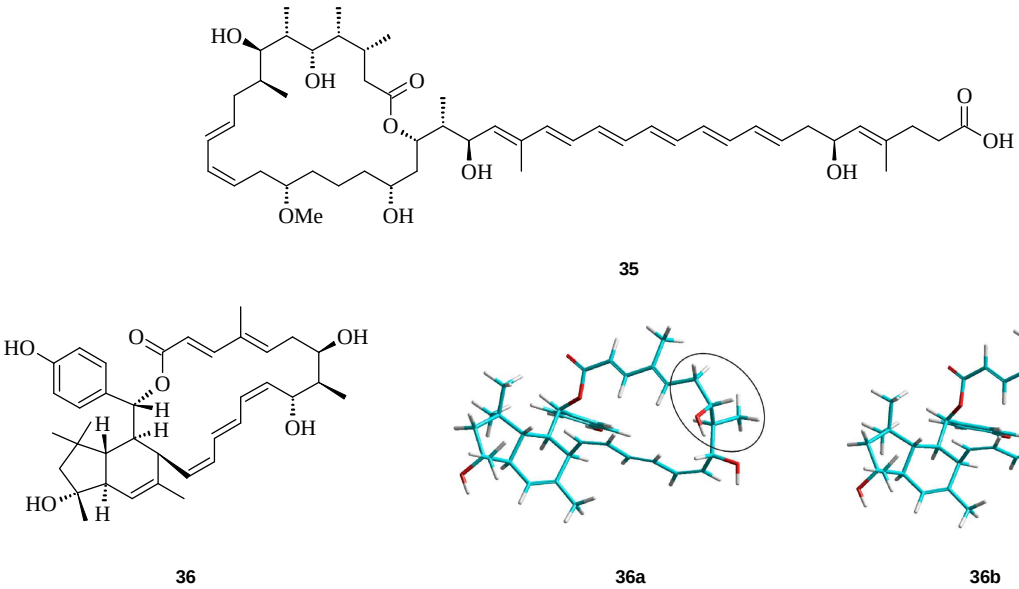

Figure 38. The secondary metabolite etnangien (**35**) isolated from myxobacteria and the atropisomeres elansolid A1 and A2 (**36a** and **36b**) isolated from Chitinophaga sancti.[87,116]

Chemical derivatization of a sensitive compound like roimatacene (**26**) usually involves difficulties. In order to synthesize the roimatacene methyl ester (**27**) the diazomethane solution had to be purified from the initial reaction mixture by distillation, in order to prevent decomposition of **26** by alkaline impurities. This observation also proved useful for the repeated esterification of etnangien (**35**) (R. Jansen; personal communication).[87] Subsequently, the derivatization to the corresponding acetonides **28**-**30** from **27** was straightforward.

The relative configuration of C15, C17, and C19 of the polyol fragment in roimatacene (**26**) was unambiguously established as 15OH, 17OH *anti*-, and 17OH, 19OH *syn*-configuration from the corresponding acetonides **28** and **29** analyzed by Rychonovsky´s method (chapter 2.1.3). The assignment of the relative configuration of the stereocentre C16 from either **28** or **29** comprising coupling constants and nOe correlations alone remained unconvincing. Finally, the relative configuration of roimatacene (**26**) was established from the resulting relative configuration of C15, C17 and C19 from **28** and **29**, as well as from a detailed study of the NMR data of the bis-acetonide **30** combined with molecular modelling. The comparison of the NMR data with the two possible diastereomeres at C16 of roimatacene bis-acetonide **30** revealed a very good agreement of observed nOes and calculated distances in the 15*S**,16*S**,17*S**,19*R**-isomere (Figure 19b, chapter 2.1.3). Detailed NMR analysis supported by molecular modelling studies was also used for the assignment of the absolute stereochemistry of etnangien (**35**), and for the elucidation of the two atropisomeres of elansolid (**36**) presented in Figure 38.[87,116]

The definition of the relative configuration of roimatacene (**26**) was essential for the assignment of the absolute stereochemistry of the natural product. The synthesis and isolation of MTPA esters from the acetonides **28** and **29** or directly from roimatacene (**26**) was impossible. For this reason, **26** was gently hydrogenated to the octrahydroroimatacene (**31**) by Pd/C catalysis under H_2 atmosphere. The formation of two additional stereocentres at C8 and C20 could not be avoided, e.g. by using Raney-nickel, or $Ru(PPh_3)_3Cl$ catalyst. After esterification of the carboxylic acid with *p*-bromophenacyl bromide, the tris-(*R*)- and the tris-(*S*)-MTPA ester **33a/b** were derived by Yamaguchi esterification.[106] The elucidation of the structures of the tris-MTPA esters **33a/b** from complete NMR data sets was rather complex as presented in chapter 2.1.4. The observed $\Delta\delta^{SR}$ values of the ^{1}H chemical shifts of the tris-(*S*)-MTPA ester of octahydroroimatacene (**33a**) and the tris-(*R*)-MTPA ester of octahydroroimatacene (**33b**), revealed the absolute configuration of the stereocentres C5, C15 and C19 as 5*S*, 15*S* and 19*R*, which was followed by the assignment of the relative configuration of the polyol fragment of C15 to C19 found in chapter 2.1.3. The absolute configuration of roimatacene (**26**) was determined as all-*trans*-5*S*,15*S*,16*S*,17*S*,19*R*, shown in Figure 39.

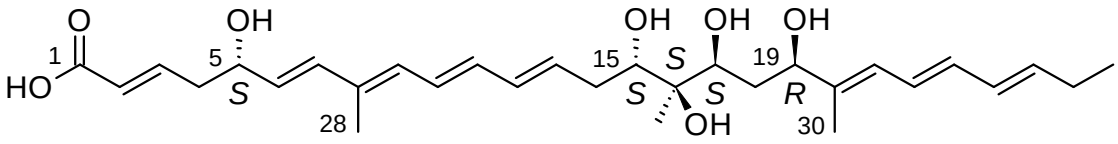

26

Figure 39. The absolute configuration of all-*trans*-5*S*,15*S*,16*S*,17*S*,19*R* roimatacene (**26**).

Subsequent to the isolation, roimatacene (**26**) was screened against various microorganisms and a mouse fibroblast cell line as described in chapter 2.1.6. Roimatacene (**26**) showed biological activity against Gram-negative bacteria summarized in Table 22.

Table 22: Minimum inhibitory concentration (MIC) of roimatacene (**26**) against selected Gram-negative bacteria.

test organism	MIC [μg/mL]
Escherichia coli tolC	0.1
Escherichia coli CG	8.6
Escherichia coli 2 DC 14 PS	2.2
Chromobacterium violaceum	0.3
Pseudomonas stutzeri	4.2
Pseudomonas aeruginosa	>9.0
Klebsiella pneumoniae	>9.1

The MICs in the μg/mL range are rather moderate. The lowest MIC (0.1 μg/mL) was found against *E. coli* tolC, which can be expected due to the inactivation of the major RND (resistance-nodulation-cell division) efflux pumps in this strain. One mechanism known for multi-drug resistance of Gram-negative bacteria is the ability to drain off drugs by the efflux pump systems of the outer membrane.[117] Since **26** was also active against the *E. coli* 2 DC14PS mutant (MIC = 2.2 μg/mL), which shows an overexpression of one RND efflux pump,[118] the target of roimatacene (**26**) is most likely not related to the resistance against the tripartite efflux pump systems of the RND family. *Chromobacterium violaceum* is prevalently used as model strain for simple analysis of quorum sensing activity. The biosynthesis of the quorum sensing indicator violacein was inhibited by **26** with a MIC of 0.3 μg/mL. The mode-of-action against *Pseudomonas stutzeri*, (MIC = 4.2 μg/mL) was further investigated against the *Pseudomonas aeruginosa*, because of the rapidly increasing clinical multi-drug resistance, but **26** showed no significant growth inhibition.[7,119-121]

The sensitivity of roimatacene (**26**) and the origin of the soil sample motivated the name for the carboxylic acid **26**. The conserved soil sample, from which the strain was isolated, was collected in New Zealand at the Franz Josef glacier. The Franz Josef glacier is called *Kā Roimata o Hine Hukatere* in Māori, with "Roimata" meaning tear. Therefore the name roimatacene (**26**) translates to **tear** of the ***C****ystobacter ferrugineus* poly**ene**.

The work on roimatacene (**26**) can be seen as a representative example of the development of an activity-guided isolation, starting with a biologically active crude extract of a myxobacterium to finally establish the absolute configuration of the active secondary metabolite.

3.2.2 A Family of Six Novel *p*-Hydroxyacetophenone Amides 34a-f

In addition to the polyunsaturated carboxylic acid roimatacene (**26**), a family of six *p*-hydroxyacetophenone amides **34a-f** was isolated and described from *Cystobacter ferrugineus* Cb G35 in the course of this thesis. The *p*-hydroxyacetophenone acetamide **34c** has previously been described as synthetic product in the partial synthesis of chloramphenicol derivatives and in the total synthesis of tyrosine kinase inhibitors.[122,123] Further the two closely related natural product families, the arylethylamides **37a-n** and the acylated tyramides **38a-j**, are presented in Figure 40. The first arylethylamines **37a-f** were isolated from three limnic strains of a new subspecies of bacillus,[124] while the arylethylamines **37g-n** were obtained in a screening of numerous *Cytophaga*, *Frigoribacter*, and marine *Streptomyces* extracts.[125] In this screening of 500 bacterial isolates ten acylated tyramides **38a-j** were found, produced by different *Vibrio* sp.

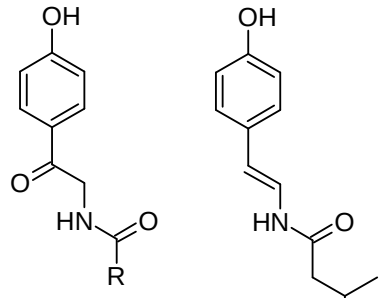

34

34d

R :
a *iso*-Bu
b Pr
c Me
e *iso*-Pe
f Pe

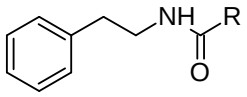

37

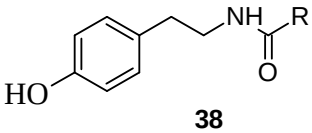

38

R :

a Me	**h** $Me(CH_2)_{12}$
b Et	**i** $Me_2CH(CH_2)_{11}$
c *iso*-Pr	**j** $MeCH_2CH(Me)(CH_2)_{10}$
d *iso*-Bu	**k** $Me(CH_2)_{13}$
e Pe	**l** $Me_2CH(CH_2)_{12}$
f $MeCH_2CH(Me)$	**m** $Me(CH_2)_{14}$
g $Me_2C=CH$	**n** $Me_2CH(CH_2)_{13}$

R :

a Me	**f** Me_2CHCH_2
b Et	**g** $Me_2C=CH$
c *iso*-Pr	**h** $Me_2CH(CH_2)_2$
d Pr	**i** $MeS(CH_2)_2$
e $MeCH_2CH(Me)$	**j** $PhCH_2$

Figure 40: The *p*-hydroxyacetophenone amides **34a-f** and the closely related families of acylated arylethylamides (**37a-n**) and tyramides (**38a-j**).

Of particular importance in the family *p*-hydroxyacetophenone amides is the carbonyl group at C7, which was unambiguously identified by the chemical shifts of C7 and C8, as well as the corresponding HMBC correlations described in chapter 2.2.2. These data correspond well with the observed chemical shifts and correlations of the cyclic peptide hibispeptin A (**39**) isolated from *Hibiscus syriacus*, which contained an analogous aromatic ketone moiety (Figure 41).[109]

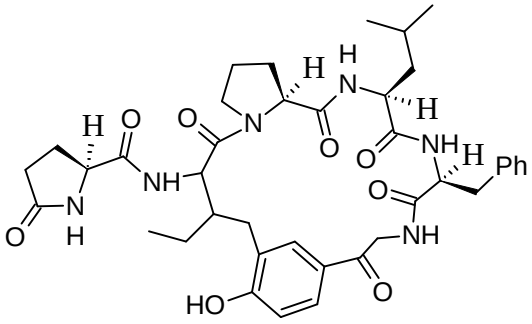

39

Figure 41: The structure of hibispeptin A (**39**), a cyclic peptide isolated from *Hibiscus syriacus*.[109]

The biosynthetic precursors of **34a** were studied by feeding experiments with D, ^{13}C and ^{15}N-labelled leucine and tyrosine, presented in chapter 2.2.3. The combined ^{13}C and ^{1}H NMR as well as HRESIMS data indicate tyrosine as precursor of the complete *p*-hydroxyacetophenone amine moiety, including the amide nitrogen, and leucine as precursor of the aliphatic *iso*-butyl residue of **34a**. Thus, *Cystobacter ferrugineus* strain Cb G35 is able to oxidize tyrosine to the atypical carbonyl at C7, revealed from the high significant incorporation of ^{13}C-labelled tyrosine. A degradation pathway discussed in biosynthesis studies of ubiquinone (**41**, coenzyme Q) involves the formation of 4-hydroxycinnamate (**40d**) and 4-hydroxybenzoate (**40g**), which could be conceivable precursors for **34d** and the carbonyl group of C7 in the other *p*-hydroxyacetophenone amides (Figure 42).[126] However, the amine of tyrosine is lost in the first step of this pathway, which is not correlating with the observed significant incorporation of the ^{15}N originating from the [^{15}N,$^{13}C_9$]-labelled tyrosine in the feeding experiments, as well as the high incorporation of C8. For this reason the biosynthetic pathway of tyrosine to form the *p*-hydroxyacetophenone amides should be further investigated. The side chains of **34a** originated from leucine, while the modified side chains of **34b**-**f** can be suggested to derive from different amino acid or fatty acid precursors.

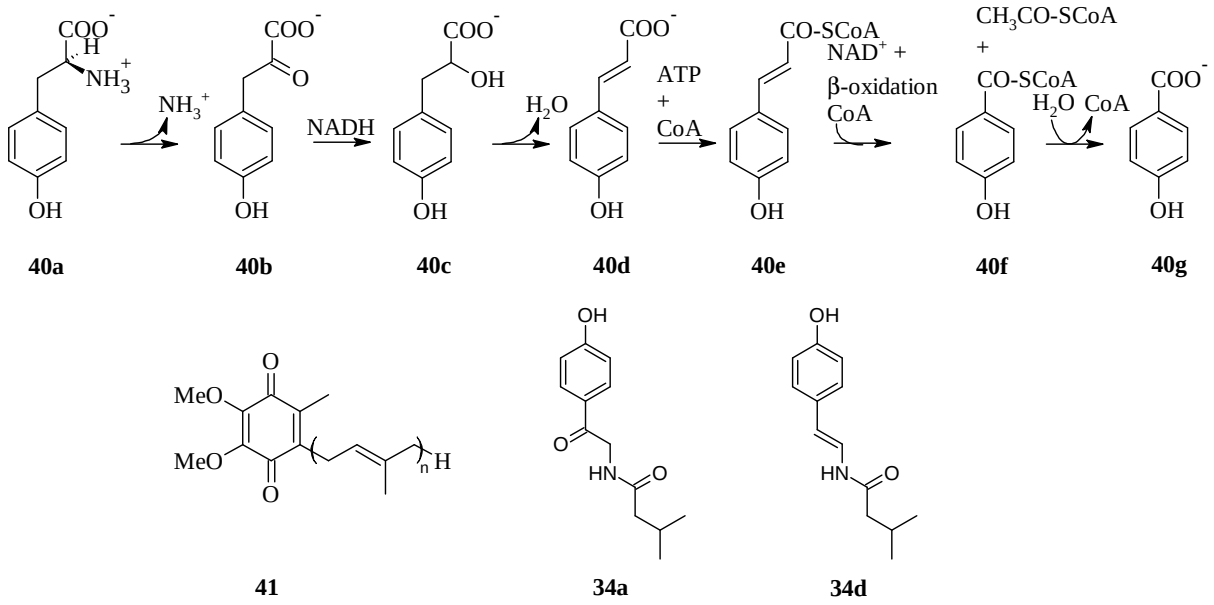

Figure 42. Proposed pathway of tyrosine for the biosynthesis of ubiquinone (**41**, coenzyme Q) and the structures of *p*-hydroxyacetophenone amides **34a** and **d**. Tyrosine (**40a**); 4-hydroxyphenylpyruvate (**40b**); 4-hydroxy-phenyllacetate (**40c**); 4-hydroxycinnamate (**40d**), *p*-coumaroyl-CoA (**40e**); 4-hydroxybenzoyl-CoA (**40f**); 4-hydroxybenzoate (**40g**).[126]

An antimicrobial screening of the *p*-hydroxyacetophenone amides **34a-f** showed no significant growth inhibition of the tested microorganisms. Due to the described biological activity of arylethylamide **37e** against the microalgae *Chlorella sorokiniana*, *Chlorella vulgaris* and *Scenedesmus subspicatus*,[124] the *p*-hydroxyacetophenone amides **34a-f** were further tested against various microalgae presented in chapter 2.2.4. In this screening of microalgae only **34d** inhibited growth of *Pseudococcomyxa simplex* at a concentration of 100 µg/mL.

3.3 Sulfangolids 25a-d from *Sorangium cellulosum*

The four sulfangolid derivatives **25a-d** were isolated from different strains of the species *Sorangium cellulosum*. In a screening of 1700 *Sorangium cellulosum* strains remarkably 90% of the isolates were found to produce biologically active secondary metabolites. Especially members of the genus *Sorangium* are versatile multiproducers, for example strain So ce1525 produces chivosazoles,[127,128] disorazols,[129,130] sorangicins,[37,38] soraphens,[32,131] sorangolide,[132] chlorotonil[133] and sulfangolid simultaneously.[31] The sulfangolids **25a-d** were isolated as side-products during the investigation of biologically active metabolites from *Sorangium cellulosum*. Sulfangolid A (**25a**) and D (**25d**) were isolated from strain So ce1375, at that time investigated for fungicidal soraphen derivatives (unpublished data K. Gerth, H. Reichenbach M. Herrmann, G. Höfle). So ce666 and So ce192 produced the cytotoxic chivosazols and disorazols as biologically active metabolites, as well as traces of sulfangolid A (**25a**) and B (**25b**). Whereas strain So ce12 mainly synthesised sorangicin, diszorasol, chivosazol and sorangolid derivatives in addition to traces of sulfangolid C (**25c**) (unpublished data K. Gerth, H. Reichenbach, R. Jansen, G. Höfle). All the NMR data for the structure elucidation, as well as from the previous isolations of the four sulfangolids **25a-d** have been assembled. The NMR data were analyzed to verify the proposed structures for sulfangolid A to D (**25a-d**) as presented in chapter 2.3.1. The final NMR data are combined in this thesis and the manuscript "Sulfangolids, Macrolide Sulfate Esters from *Sorangium cellulosum*" (W. Zander, H. Irschik, H. Augustiniak, M. Herrmann, R. Jansen, H. Steinmetz, K. Gerth, W. Kessler, M. Kalesse, G. Höfle, R. Müller, to be submitted).

The structure of sulfangolid C (**25c**) containing three inflexible structural elements in the 28-membered macrolide ring, i.e. the polyunsaturated ester, the α,β-unsaturated ketone at C21, and the six-membered hemiketal, altogether stabilize the conformation of the macrolide ring, thus allowing elucidation of the relative stereochemistry. The relative all-*trans* $\underline{13S^*}$,14S^*,15R^*,16R^*,17S^*,19S^*,20R^*,26R^*,27R^* configuration of sulfangolid C (**25c**) proposed in my diploma thesis was revised to the all-*trans* $\underline{13R^*}$,14S^*,15R^*,16R^*,17S^*,19S^*,20R^*, 26R^*,27R^* configuration, due to the better agreement of interatomic distances of the modelled diastereomere in comparison with the NMR data presented in chapter 2.3.2. In addition the biosynthetic precursors of sulfangolid C (**25c**) were studied as a basis for further genetic research of the frequently observed sulfangolids.

The four sulfangolid derivatives **25a**-**d** present an extraordinary group of polyketides, because they are the first group of myxobacterial secondary metabolites containing a sulfate ester residue. A sulfate-free analogue of the sulfangolids is the myxobacterial kulkenon (**42**) isolated from *Sorangium cellulosum* So ce1426 (unpublished data R. Jansen, H. Irschik, G. Höfle, H. Reichenbach). Comparing kulkenon (**42**) to the family of sulfangolids **25a**-**d**, **42** has one additional methyl group at position C2, while the southern fragment shows high similarity to sulfangolid C (**25c**). The 26-membered macrolide of **42** is reduced by two carbons compared to the 28-membered macrolide rings of the sulfangolid family, and the sulfate ester moiety is absent. Further the northern fragment of kulkenon (**42**) is identical to sulfangolid A (**25a**). Due to the high similarity of kulkenon (**42**) to the sulfangolids, **42** can be considered as a sulfate-free analogue.

Commonly, sulfate ester residues are known from *Streptomyces* sp. or marine microorganisms, like the earlier described marine polyether maitotoxin (**23**). Structural similarities are found in the *Streptomyces* natural products clethramycins (**43c**) and the analogue family of mediomycins, here represented by mediomycin A (**43a**) and B (**43b**) in Figure 43.[134,135] These secondary metabolites are highly functionalized polyketides containing a sulfate ester residue at C29, multiple hydroxyl groups and a ketone at C31 in addition to several double bonds. Of special interest are the differences between the secondary metabolites from *Streptomyces* and the sulfangolid family. A sulfate-free derivative with identical carbon skeleton of these metabolites was described with mediomycin B (**43b**). In addition, a derivative of mediomycin A (**43a**) with hydrogenated double bonds was characterised, while such derivatives have not been found for the sulfangolids. The ketal found in sulfangolid C (**25c**) and D (**25d**) would also be feasible between 35OH and the carbonyl group at C31 in **43a**-**c**, but such a derivative has not been described to data.

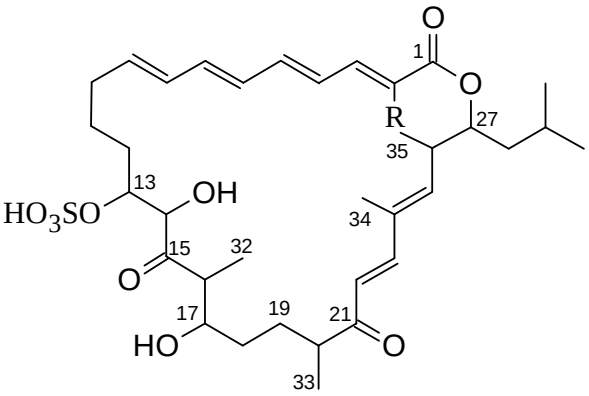

sulfangolid A (**25a**) R = H

sulfangolid B (**25b**) R = OMe

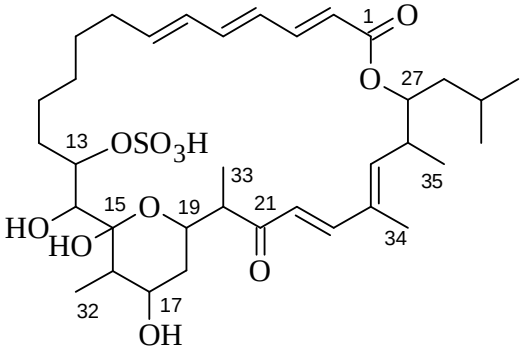

sulfangolid C (**25c**)

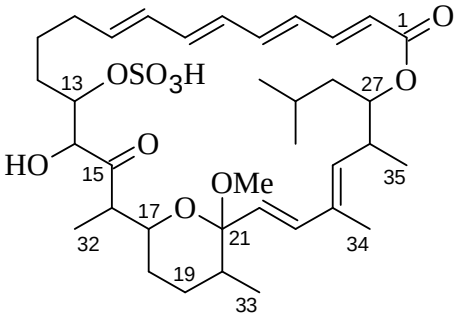

sulfangolid D (**25d**)

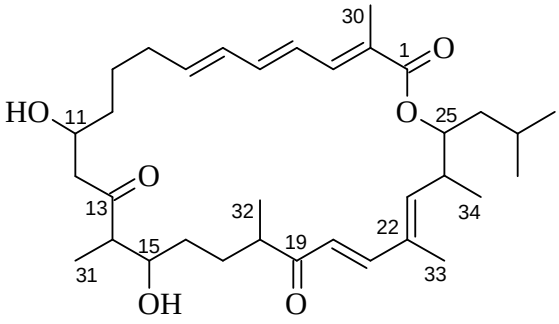

kulkenone (**42**)

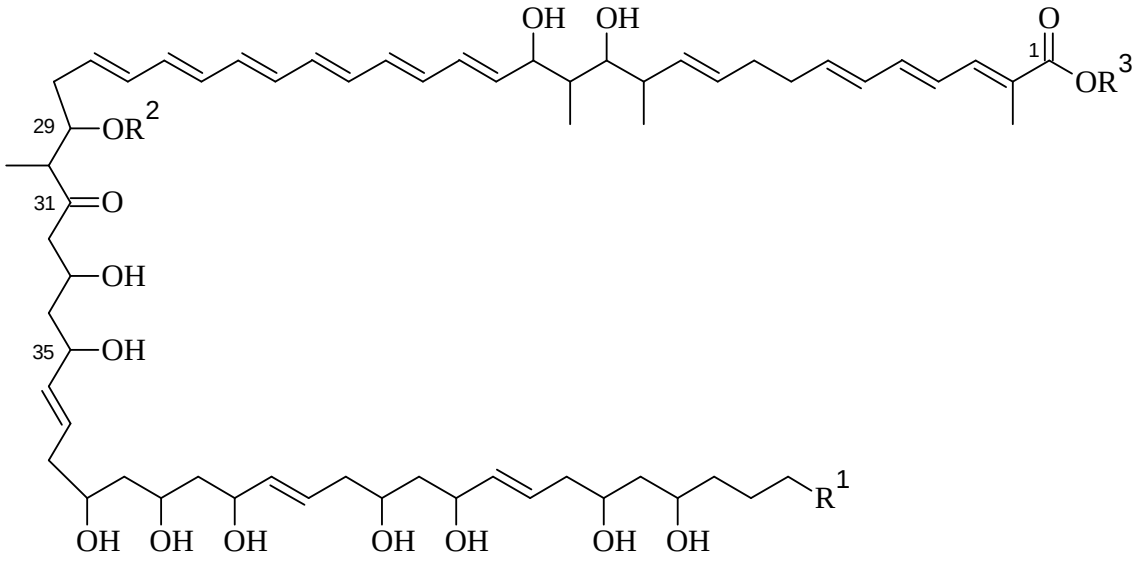

43

mediomycin A (**43a**) $R^1 = NH_2$, $R^2 = SO_3H$, $R^3 = H$

mediomycin B (**43b**) $R^1 = NH_2$, $R^2 = H$, $R^3 = H$

clethramycin (**43c**) $R^1 = CN_3H_4$, $R^2 = SO_3H$, $R^3 = H$

Figure 43 The secondary metabolites mediomycin A (**43a**) and B (**43b**) and the analogue clethramycin (**43c**) isolated from *Streptomyces*, the myxobacterial sulfangolids **25a-d** and the analog kulkenon (**42**).[135]

3.4 Summary and Future Aspects

The thesis presents results of extensive studies in the field of structure elucidation of labile secondary metabolites. On the one hand, the assignment of the relative configuration of sulfangolid C (**25c**) based mainly on detailed NMR studies and molecular modelling, while on the other hand the absolute configuration of roimatacene (**26**) is supported by derivatization techniques coupled to NMR analysis and sustained by molecular modelling. The structure analysis of roimatacene (**26**) lead to the development of a protective isolation strategy creating the basis for solving the relative and later the absolute configuration of a compound that already proved problematic during isolation. The assignment of the absolute stereochemistry of the novel secondary metabolite roimatacene (**26**) is the basis for a total synthesis, and required for the synthesis of stable derivatives of **26**, for example by selective hydrogenation of double bonds. In addition to SAR-studies, the evaluation of the biological target would be indicated as next step.

The *p*-hydroxyacetophenone amides **34a**-**f** with the atypical oxidation of the tyrosine moiety and the family of sulfangolids **25a**-**d** with the sulfate ester residue present two novel motives of myxobacterial biosynthesis worthy of further investigations.[136] The high biodiversity of myxobacteria is also unambiguously revealed in the genome sequencing projects of *Sorangium cellulosum* (strain So ce56, 13.0 Mbp),[53] *Myxococcus xanthus* (strain DK1622, 9.1 Mbp),[54] *Stigmatella aurantiaca* (10.2 Mbp)[137] and *Anaeromyxobacter dehalogenans* (strain 2CP-C, 5.1 Mbp).[138] The *Sorangium cellulosum* genome with 13.0 Mbp is the largest genome sequenced from any bacterium so far. In *Myxococcus xanthus* DK1622 over 8.5% of the genome are dedicated to secondary metabolism, which is more than it has been observed in other microorganisms.[139] This observation leads to the conclusion, that still a high number of natural products can be discovered from myxobacteria in the future and will reveal more of the true potential of these gliding bacteria.[27]

4 Experimental

4.1 Material

4.1.1 Instruments

The standard **analytical reversed phase liquid chromatography (RP-HPLC)** system was a Agilent 1100 series HPLC system [column 125×2 mm, Nucleosil 120 EC, 5 µm, C_{18}, (Macherey-Nagel); temperature 40°C; solvent A: H_2O/ACN (95/5) + 5 mM/L of NH_4Ac + 40 µL/L of acetic acid; solvent B: H_2O/ACN (5/95) + 5 mM/L of NH_4Ac + 40 µL/L of acetic acid, gradient: 10% B increasing to 100% B in 30 min, maintained 100% B for 10 min; flow rate (FR) = 0.3 mL/min; UV detection 210-500 nm].

The **HPLC- high resolution mass spectrometry (HPLC-HRESIMS)** was done on a Agilent 1200 series RRLC system, ESI-TOF-MS Maxis (Bruker) [column 50×2.1 mm, Acquity UPLC BEH C-18, 1.7 µm (Waters), solvent A: 0.1% formic acid in water; solvent B: 0.1% formic acid in ACN, gradient 5% B for 0.5 min, increasing to 100% B in 19.5 min and continued at 100% B for 5 min, FR = 0.6 mL/min; NH_4Ac-buffer gradient: column 100×2.1 mm, XBridge^{TM} C18 3.5 µm, (Waters), solvent A: H_2O/ACN (95/5) + 5 mM/L of NH_4Ac + 40 µL/L of acetic acid; solvent B: H_2O/ACN (5/95) + 5 mM/L of NH_4Ac + 40 µL/L of acetic acid, gradient from 10% B increasing to 100% B in 30 min and continued at 100% B for 10 min, FR = 0.3 mL/min, UV detection 210-500 nm].

The **preparative reversed phase high pressure liquid chromatography (RP-HPLC)** system was a preparative Agilent 1100 series HPLC system or the HPLC system consisting of a manual injection system (Rheodyne), the preparative K-1800 pump system with mixing chamber (Knauer) connected to an UV-detector (Techlab).

The **preparative reversed phase- medium pressure liquid chromatography (RP-MPLC)** system consisted of two pumps C-605, control unit C-620, fraction collector C-660 and photometer C-635 (Büchi).

Silica-gel-flash chromatography was carried out with the silica-gel-flash system from Biotage and the cartridge Si 40 S 2976-1 (Biotage), or with open-glass columns packed with silica gel 60, particle size 0.063-0.200 mm (Merck).

Thin-layer chromatography (TLC) in analytical scale was carried out with TL-Silica-Gel 60 F254-Aluminium (Merck), staining was done with aqueous cer-dye (10 g cer(IV)-sulfate, 25 g phosphor-molybdäne acid, 80 mL sulphuric acid in 1 L) and heating 120°C. For semi-preparative scale PSC-plates (20×20×0.1 cm, silica gel 60 F_{254}, Merck) with concentration zone were used. The **RP-cartridge system** of strata-X cartridges (0.5 g and 1.0 g, Phenomenex) were used for concentration from water layers.

Optical rotation was determined with a Perkin-Elmer 241 instrument, **UV spectra** were recorded with a Shimadzu UV-Vis spectrophotometer UV-2450, and **IR spectra** were measured with a Nicolet 20DXB FT-IR spectrometer.

Centrifugation was carried out with a Varifuge 20RS (Heraeus Sepatech).

NMR spectra were recorded with Bruker NMR spectrometer DPX-300 (^{1}H 300 MHz, ^{13}C 75 MHz), ARX-400 (^{1}H 400 MHz, ^{13}C 100 MHz); AVANCE DMX-600 (^{1}H 600 MHz, ^{13}C 150 MHz) with the assistance of C. Kakoschke, B. Jaschok-Kenter and M. Rettstadt (University Hannover).

The **up-scale fermentation** was carried out in a 100 L fermentor (Giovanola Frères SA, Monthey, Switzerland) with an inoculation volume of 70 L in the presence of Amberlite XAD-16 (Rohm & Haas) with the assistance of K. I. Mohr, H. Irschik, K. Gerth, D. Telkemeyer, W. Kessler, B. Ebert, A. Perreth, A. Schulz and R. Sterlinski.

4.1.2 General Chemicals

Table 23. Chemicals used (in alphabetical order) and the supplying company

Chemicals	Supplying Company
acetic acid	Roth
acetone	Merck
acetone, dry	Merck
acetonitrile, p.a.	J.T. Baker
ammonia	Riedel-de Haen
ammonium acetate	Roth
buffer, pH 7	Roth
celite	Merck
diazald®	Aldrich
dichloromethane	J.T. Baker
diethyl ether	J.T. Baker
dimethoxypropanne	Sigma-Aldrich
DMAP	Fluka
ethanol	J.T. Baker
4-ethoxyphenol	Aldrich
ethyl acetate	J.T. Baker
formic acid	Roth
H_2SO_4	Roth
KOH	Merck
methanol	Merck
methanol p.a.	J.T. Baker
methanol (Uvasol)	Merck
Milli-Q-Wasser	Millipore
mol sieve (3Å)	Merck
(R)/(S)-MTPA	Fluka
NaCl	Roth
$NaHCO_3$	Fluka
n-heptane	Roth
p-dibromoacetophenone	Aldrich
Pd/C	Merck

continuing Table 23:

Chemicals	**Supplying Company**
pyridin-*p*-toluenesulfonic acid	Fluka
sodium acetate	Roth
TEA	Fluka
toluene	Merck
2,4,6-trichlorobenzoyl chloride	Aldrich
water, p.a.	J.T. Baker
Media	
Amberlide XAD-16	Rohm and Haas
$CaCl_2 \times 2H_2O$	Merck
casitone	BD
1-docosanol	Merck
fructose	Fluka
glucose	Cerestar
glycerine (87%)	Merck
HEPES	Roth
H_2SO_4	AppliChem
leucine	Merck
methionine	Merck
$MgSO_4 \times 7H_2O$	Merck
Na-Fe-EDTA	Fluka
$NaNO_3$	Merck
skim milk	AppliChem
sodium acetate	Merck
sodium propionate	Merck
soyabean flour	Cargill
starch 12018	Cargill
tegosipon antifoam	Evonik
tyrosine	Merck
yeast extract	Ohly

continuing Table 23:

Chemicals	**Supplying Company**
Feeding Experiments	
[1-^{13}C]-acetate (99%)	Cambridge Isotope Laboratories
[1,2-^{13}C]-acetate (99%)	Cambridge Isotope Laboratories
[2-^{13}C]-acetate (99%)	Cambridge Isotope Laboratories
[D_{10}]-leucine (98%)	Campro Scientific
[$^{13}CH_3$]-methionine (98%)	Cambridge Isotope Laboratories
[1-^{13}C]-propionate (97%)	Cambridge Isotope Laboratories
[$^{13}C_9$,^{15}N]-tyrosine(98% ^{13}C, 98% ^{15}N)	Campro Scientific
NMR-solvents	
$CDCl_3$	Deutero GmbH
CD_3OD	Deutero GmbH
[D_6]DMSO	Deutero GmbH
[D_3]trifluoroethanol	Deutero GmbH

4.2 Fermentation of Cb G35 and Isolation of Roimatacene (26)

4.2.1 Fermentation of Cb G35 for the Isolation of Roimatacene (26)

Cystobacter ferrugineus strain Cb G35 (deposited at Deutsche Sammlung von Mikroorganismen und Zellkulturen GmbH; DSM 24415) was transferred to a liquid medium consisting of soybean flour 4 g/L, glucose 2 g/L, starch 8 g/L, $CaCl_2 \times 2\ H_2O$ 1 g/L, $MgSO_4 \times 7\ H_2O$ 1 g/L, HEPES 11.9 g/L and Na-Fe-EDTA 8 mg/L at pH 7.4. 5 L of a 4 day old pre-culture was used to inoculate a volume of 70 L of the same medium in a 100 L fermentor in the presence of 1.4 kg adsorber resin Amberlite XAD-16. The culture was supplemented with 1.15-1.75 g/h of NaAc solution (100 g/kg) during seven days of cultivation (blade impeller 150 rpm, aeration 7 L/min, 30°C, pO_2 20%, pH regulated between pH 7.15 and 7.25 with 10% KOH and 5% H_2SO_4). For harvesting the culture broth was passed through a process filter collecting the absorber resin. Residual cells were floated from the recovered XAD-16 resin with water.

4.2.2 Isolation Procedure of Roimatacene (26)

General remark: Handling of roimatacene (**26**) extracts and ethyl acetate: Extracts containing roimatacene (**26**) were kept in solution (methanol) supplemented with 4-ethoxyphenol. As far as possible N_2-gas was used at all times. Ethyl acetate was filtrated over aluminium oxide before use. Amber glassware was used for handling and for storage at 4°C.

The XAD-16 absorber resin was eluted with methanol/water (3/7), methanol and acetone (4 L each) saturated with N_2-gas. After addition of saturated NaCl solution (250 mL), the water layer (300 mL) remaining after evaporation of the methanol was adjusted to pH 4.2 with formic acid and extracted with ethyl acetate (5 portions of 100 mL). The ethyl acetate was supplemented with 0.1 M 4-ethoxyphenol (100 µL) and methanol (100 mL). The ethyl acetate layer was evaporated and dissolved to a 140 mL methanol layer, without drying the samples. The extract was analysed by HPLC to contain 504 mg of roimatacene (**26**) in 13.4 g of crude extract. The extract was partitioned between methanol and *n*-heptane to provide 12.9 g of polar raw material, containing 440 mg roimatacene (**26**) according to HPLC analyses (supplemented with 200 µL of 0.1 M 4-ethoxyphenol). The methanol extract was stored in 142 mL of methanol (c = 3.1 mg/mL) at 4°C. After 6 weeks HPLC analysis showed degradation to 256 mg of **26** (58%, c = 1.8 mg/mL) in the crude extract. Half of the extract was dissolved in 2 N ammonia (75 mL) and methanol was evaporated. The pH of the water

layer was adjusted to pH 9.5 with 2N ammonia and extracted with ethyl acetate (3 portions of 95 mL). The water layer was acidified to pH 4.2 with formic acid and then extracted twice with *n*-heptane (55 mL) to remove fatty acids from the crude extract. The acidic water layer was then extracted with ethyl acetate (4 portions of 75 mL) supplemented with 4-ethoxyphenol (200 µL, 0.1 M), methanol and toluene before evaporation of the ethyl acetate. The methanol/toluene solution yielded 99.4 mg enriched roimatacene (**26**) according to HPLC analyses. **26** was further purified by preparative RP-HPLC in 7 batches [column VP250/21 Nucleodur 100-10 C-18 ec (Macherey-Nagel), solvent methanol/water (6:4) containing 50 mM/L of NH_4Ac and 400 µL/L of acetic acid; the solvents were saturated with N_2-gas and 10 µL of 0.1 M 4-ethoxyphenol were provided in each test tube of the fraction collector]. **26** eluted at R_t = 34 min. The fraction was evaporated and the water layer was passed through a strata-X cartridge (1.0 g) under N_2-protection gas, washed with water, and eluted with methanol. 4-Ethoxyphenol (200 µL, 0.1 M) was added to the methanol layer before the concentration was adjusted to 50 mL containing 38.5 mg of roimatacene (**26**).

Roimatacene (**26**): Pale yellow solution in methanol; $[\alpha]_D^{RT}$ = + 58.4 (*c* = 0.65, methanol); NMR data (^{1}H NMR 600 MHz, ^{13}C NMR 150 MHz, [D_6]DMSO): Table 2; UV (methanol) λ_{max} (lg ε) = 276 (4.323), 286 (4.332), 308 (4.369), 323 nm (4.309); HRESIMS: *m*/*z*: calcd. for $C_{30}H_{43}O_7$: 515.3014, found 515.3021.

4.2.3 Derivatization of Roimatacene (26)

Roimatacene methyl ester (27): Diazald$^{(R)}$ (5.3 g) was dissolved in ether (20 mL) and ethanol (3 mL), and was stirred with aqueous KOH (2.0 g in 3.2 mL H_2O). After heating to 35°C the ether/diazomethane solution was distilled and then added drop-wise to a stirred solution of roimatacene (**26**) and 4-ethoxyphenol in methanol at room temperature. After 20 min ether and diazomethane were evaporated under nitrogen gas to the crude product in methanol. The product was purified by preparative RP-HPLC [column VP250/21 Nucleodur 100-10 C-18 ec (Macherey-Nagel); solvent A: methanol water (6/4) supplemented with 50 mM/L NH_4Ac and 400 µL/L formic acid, solvent B: methanol same buffer concentration; gradient: 100% A increasing to 100% B in 50 min, continued for 15 min, FR = 20 mL/min, UV detection 278 nm, R_t = 60 min]. After evaporation of the methanol, the water layer was diluted and passed through a strata-X cartridge (1.0 g) under nitrogen atmosphere. The cartridge was rinsed with water and roimatacene ester (**27**) was eluted with methanol (supplemented with 40 µL of 0.1 M 4-ethoxyphenol).

Roimatacene methyl ester (**27**): Pale yellow solution in methanol; ^{1}H NMR (600 MHz, [D_6]DMSO): δ = 0.92 (s, 4 H) 0.93 - 0.95 (m, 1 H) 0.95 (t, *J* = 7.52 Hz, 4 H) 1.45 - 1.52 (m, 2 H) 1.66 (s, 4 H) 1.67 - 1.72 (m, 2 H) 1.79 (s, 4 H) 1.90 (s, 2 H) 1.98 - 2.04 (m, 1 H) 2.07 (t, *J* = 7.34 Hz, 3 H) 2.32 - 2.43 (m, 5 H) 2.50 (dt, *J* = 3.67, 1.83 Hz, 2 H) 3.32 (d, *J* = 10.27 Hz, 2 H) 3.48 - 3.55 (m, 7 H) 3.63 (s, 4 H) 4.12 - 4.22 (m, 3 H) 5.66 (dd, *J*=15.59, 6.05 Hz, 1 H) 5.70 - 5.76 (m, 1 H) 5.81 (dt, *J* = 14.95, 7.38 Hz, 1 H) 5.89 (d, *J* = 15.41 Hz, 1 H) 5.97 (d, *J* = 11.00 Hz, 1 H) 6.08 - 6.19 (m, 5 H) 6.24 (dd, *J* = 15.22, 8.25 Hz, 2 H) 6.36 (dd, *J*=13.94, 11.37 Hz, 1 H) 6.46 (dd, *J* = 14.67, 11.74 Hz, 1 H) 6.87 ppm (d, *J* = 15.77 Hz, 1 H); ^{13}C NMR (150 MHz, [D_6]DMSO): δ = 172.4, 166.3, 146.8, 140.2, 135.9, 134.5, 134.1, 133.8, 132.4, 132.4, 132.0, 131.9, 131.2, 130.0, 127.0, 125.5, 122.4, 75.0, 74.5, 73.6, 70.0, 63.5, 51.4, 48.8, 40.0, 36.2, 34.7, 25.4, 21.2, 18.3, 13.6, 12.8, 11.7 ppm; 4-ethoxyphenol: ^{1}H NMR (600 MHz, [D_6]DMSO): δ = 1.25 (t, *J* = 6.97 Hz, 4 H) 3.88 (q, *J* = 6.97 Hz, 3 H) 6.63 - 6.66 (m, 2 H) 6.69 - 6.73 ppm (m, 2 H); ^{13}C NMR (150 MHz, [D_6]DMSO): δ = 151.5, 151.1, 115.9, 115.5, 15.0 ppm; HRESIMS: *m*/*z*: calcd. for $C_{31}H_{46}O_7Na$ 553.3136, found 553.3128.

Acetonides of roimatacene methyl ester (28-30): 31.7 mg of **27** were dried and dissolved in 2,2-dimethoxypropane (4 mL). Pyridium-*p*-tolouenesulfonic acid (12.5 mg) was added and the reaction was stirred over night at 4°C. After quenching with 5% $NaHCO_3$ solution the reaction was extracted with DCM (3 portions of 50 mL). After evaporation of DCM the crude extract was further purified by RP-HPLC [column VP250/21 Nucleodur 100-10 C-18 ec (Macherey-Nagel), solvent A: methanol/water 1/1; solvent B: methanol; gradient: 70% B increasing to 100% B in 50 minutes and maintained at 100% B for 10 minutes, FR = 20 mL/min, UV detection 210-500 nm] yielding 17,19-acetonide **28** (5.5 mg, R_t = 9.1 min), 15,17-acetonide **29** (2.4 mg, R_t = 22.9 min) and the bis-acetonide **30** (4.2 mg, R_t = 20.9 min).

17,19 acetonide of roimatacene methyl ester (**28**): yellow oil, NMR data (^{1}H NMR 600 MHz, ^{13}C NMR 150 MHz, $CDCl_3$): Table 3; HRESIMS *m*/*z*: calcd. for $C_{34}H_{50}O_7Na$ 593.3449, found 593.3448.

15,17 acetonide of roimatacene methyl ester (**29**): yellow oil, NMR data (^{1}H NMR 600 MHz, ^{13}C NMR 150 MHz, $CDCl_3$): Table 4; HRESIMS *m*/*z*: calcd. for $C_{34}H_{54}O_7N$ 570.3789, found 570.3801.

15,16,17,19-bis-acetonide of roimatacene methyl ester (**30**): yellow oil, NMR data (^{1}H NMR 600 MHz, ^{13}C NMR 150 MHz, $CDCl_3$): Table 5; HRESIMS *m*/*z*: calcd. for $C_{37}H_{54}O_7Na$ 633.3762, found 633.3768.

Tris-(*S*)-MTPA ester of *p*-bromoacetophenone-octahydroroimatacene ester (33a): For the (*S*)-Mosher ester about 25 mg of roimatacene (**26**) were hydrogenated in methanol in presence of Pd/C (10%, 31.4 mg) under H_2-atmosphere at RT for 4.5 h. The reaction mixture was filtered over celite and dried *in vacuo* to yield 35.2 mg extract of octahydroroimatacene (**31**). The extract was dissolved in dry acetone (2 mL) and stirred for 19 h at RT with TEA (15 µL) and *p*-dibromoacetophenone (24.1 mg) in the presence of 3Å mol sieve. The mixture was filtered over celite and dried to give 66.9 mg. *p*-Bromoacetophenone-octahydroroimatacene ester (**32**) was separated by silica gel plate chromatography [two PSC-plates 20×20×0.1 cm, silica gel 60 F_{254} with concentration zone (Merck), solvent ethyl acetate/*n*-heptane 8/2]. The UV active zone (R_f = 0.42) was eluted with ethyl acetate to give 5.3 mg of *p*-bromoacetophenone-octahydroroimatacene ester (**32**). 2,4,6-trichlorobenzoyl chloride (12.5 µL) and 5.3 mg of **32** were dissolved in dry toluene (0.7 mL) and added to a solution of (*S*)-MTPA (16.2 mg), DMAP (14.4 mg) and TEA (12.5 µL) in dry toluene (0.4 mL) at 0°C. The reaction mixture was stirred for 15 min at 0°C and 4 h at RT. The reaction

was quenched with buffer (pH 7) and extracted with ethyl acetate (3 portions of 50 mL) to yield 14.6 mg crude product. The tris-(*S*)-MTPA derivative **33a** was further purified by RP-HPLC [column VP 250/10 Nucleodur 100-7 C-18 ec (Macherey-Nagel); solvent A: methanol/water 1/1, solvent B: methanol, gradient: 85% B in 20 min to 86% B, in 3 min to 90% B, maintained at 90% B; FR = 6 mL/min, UV detection at 259 nm, R_t = 49 min] to yield 2.8 mg of **33a**.

Tris-(*R*)-MTPA ester of *p*-bromoacetophenone-octahydroroimatacene ester (**33b**): Tris-(*R*)-MTPA ester of *p*-bromoacetophenone-octahydroroimatacene ester (**33b**) was prepared analogously starting with 11.6 mg of roimatacene (**26**) and obtaining 2.1 mg of tris-(*R*)-MTPA ester **33b** for NMR spectroscopy.

Octahydroroimatacene (**31**): yellowish oil; ^{1}H NMR (300 MHz, CD_3OD): δ = 0.88 - 0.93 (m, 10 H) 1.06 - 1.17 (m, 5 H) 1.31 – 1.35 (m, 24 H) 1.56 -1.84 (m, 10 H) 2.44 (m, 4 H) 3.35 (br. s, 1 H) 3.54 (m, 2 H) 3.65 ppm (br. s, 1 H); ^{13}C NMR (75 MHz, CD_3OD): δ = 177.8, 76.6, 76.6, 76.5, 76.4, 76.2, 76.1, 76.1, 76.0, 72.6, 72.6, 38.4, 38.2, 37.9, 37.8, 36.0, 36.0, 34.4, 34.3, 34.2, 34.1, 33.8, 33.2, 32.2, 31.3, 31.2, 31.0, 30.9, 30.7, 30.6, 28.7, 28.7, 28.3, 28.1, 23.9, 20.4, 20.2, 15.68, 15.5, 14.5 ppm; doubling of signals due to isomers at C8 and C20; 4-ethoxyphenol ^{1}H NMR (300 MHz, CD_3OD): δ = 3.94 (q, *J* = 6.97), 6.71 (m, Hz, 4 H), CH_3 in 1.31 – 1.35 ppm (m, 24 H); ^{13}C NMR (75 MHz, CD_3OD): δ = 153.8, 152.4, 116.9, 116.8, 65.3, 14.6 ppm; HRESIMS *m*/*z*: calcd. for $C_{30}H_{60}O_7Na$ 555.4231, found 555.4233.

p-bromoacetophenone-octahydroroimatacene ester (**32**): yellowish oil, ^{1}H NMR (300 MHz, $CDCl_3$) δ = 0.85 - 0.96 (m, 11 H) 1.05 (s, 3 H) 1.08 - 1.18 (m, 4 H) 1.27 – 1.33 (m, 17 H) 1.39 - 1.51 (m, 8 H) 1.63 - 1.81 (m, 4 H) 2.55 (t, *J* = 7.25 Hz, 2 H) 3.45 (m, 1 H) 3.62 (m, 1 H) 3.83 (m, 1 H) 3.98 (m, 1 H) 5.31 (s, 2 H) 7.65 (d, *J* = 8.7 Hz, 2 H) 7.79 ppm (d, *J* = 8.7 Hz, 2 H), ^{13}C NMR (75 MHz, $CDCl_3$) δ = 191.5, 173.2, 133.0, 132.3, 129.3, 129.2, 80.3, 77.3, 74.0, 74.0, 71.9, 71.8, 65.7, 39.8, 39.6, 36.9, 36.8, 36.7, 36.6, 35.1, 34.9, 33.8, 33.4, 32.9, 32.7, 32.1, 32.0, 31.9, 29.9, 29.8, 29.6, 29.3, 27.4, 27.3, 26.9, 22.7, 21.2, 21.0, 19.8, 19.7, 14.9, 14.1 ppm; doubling of signals due to the isomers at C8 and C20; HRESIMS *m*/*z*: calcd. for $C_{38}H_{66}BrO_8$ 729.3936, found 729.3972.

Tris-(*S*)-MTPA ester of *p*-bromoacetophenone-octahydroroimatacene ester (**33a**): oil; NMR data (^{1}H NMR 600 MHz, ^{13}C NMR 150 MHz, $CDCl_3$): Table 6; HRESIMS *m*/*z*: calcd. for $C_{68}H_{90}BrF_9O_{14}N$ 1394.5395, found 1394.5404.

Tris-(*R*)-MTPA ester of *p*-bromoacetophenone-octahydroroimatacene ester (**33b**): oil; NMR data (^{1}H NMR 600 MHz, ^{13}C NMR 150 MHz, $CDCl_3$): Table 7; HRESIMS *m*/*z*: calcd. for $C_{68}H_{86}BrF_9O_{14}Na$ 1399.4949, found 1399.4957.

4.2.4 Biosynthetic Studies of Roimatacene (26) by Feeding Experiments

100 mL cultures of strain Cb G35 of the described medium were supplemented with 25 mg, 50 mg and 100 mg of methionine, acetate and propionate additionally to 1% XAD-16 absorber resin. After 7 days of incubation at 30°C the XAD-16 resin of each culture was harvested, eluted with methanol and acetone supplemented with 4-ethoxyphenol (100 µL, 0.1 M) and analysed by HPLC.

50 mg of [$^{13}CH_3$] sodium methionine (98%), 50 mg of [2-^{13}C] sodium propionate (97%), 100 mg of [1-^{13}C]- and [2-^{13}C] sodium acetate (99%, all Cambridge Isotope Laboratories) were fed in two portions after 16 and 40 hours of incubation to shaken cultures (100 mL) of strain Cb G35. The cultures were incubated at 30°C for 7 days. After washing with water each XAD-16 resin was eluted twice with 3 bed volumes of methanol and twice with acetone. The organic layers of each experiment were evaporated to a small volume before adjusting their concentration to 100:1 under the addition of 4-ethoxyphenol (50 µL, 0.1 M). All extracts were partitioned between methanol and *n*-heptane. The methanol layers were subjected to acid-base partition. They were dissolved in 2 N ammonia (10 mL) and the methanol was evaporated. The aqueous layer was extracted with ethyl acetate (3 portions of 10 mL). The water layers were acidified to pH 3.3 with formic acid and extracted with *n*-heptane (10 mL) and then with ethyl acetate (3 portions of 10 mL). 4-ethoxyphenol (20 µL, 0.1 M) was added to the ethyl acetate layers of each experiment. Ethyl acetate was evaporated after addition of toluene and methanol. The solvents were evaporated after addition of [D_6]DMSO and ^{13}C-NMR spectra of all samples of the feeding experiments were measured.

[$^{13}CH_3$]-methionine labelled roimatacene (**26**): ^{13}C NMR (100 MHz, [D_6]DMSO): δ (signal/noise) = 18.3 (16.5/1), 13.6 (19.2/1), 12.7 (13.2/1), 11.7 ppm (14.4/1).

[1-^{13}C]-acetate labelled roimatacene (**26**): ^{13}C NMR (100 MHz, [D_6]DMSO): δ (signal/noise) = 167.3 (4.3/1), 145.8 (5.1/1), 135.8 (3.5/1), 134.5 (2.1/1), 134.0 (2.7/1), 133.8 (2.9/1), 132.4 (3.5/1), 131.2 (3.1/1), 125.4 (2.2/1), 75.1 (2.3/1), 73.6 (2.3/1), 70.1 ppm (3.1/1).

[2-^{13}C]-acetate labelled roimatacene (**26**): ^{13}C NMR (100 MHz, [D_6]DMSO): δ (signal/noise) = 140.3 (5.0/1), 133.7 (5.5/1), 132.1 (5.5/1), 131.8 (6.0/1), 130.0 (9/1), 127.0 (9.5/1), 123.7 (11/1), 74.4 (9/1), 36.1 (5.5/1), 34.7 (5.0/1), 25.3 ppm (10/1).

[2-^{13}C]-acetate labelled roimatacene (**26**): APT ^{13}C NMR (100 MHz, [D_6]DMSO): δ ppm (signal/noise) = 134.4 (1.4/1).

[1-^{13}C]-propionate labelled roimatacene (**26**): no enriched signals.

4.3 Fermentation of Cb G35 and Isolation of *p*-Hydroxyacetophenone Amides 34a-f

4.3.1 Fermentation of Cb G35 for the Isolation of *p*-Hydroxyacetophenone Amides 34a-f

Cystobacter ferrugineus, strain Cb G35 was transferred to a liquid medium consisting of soybean flour 4 g/L, glucose 2 g/L, starch 8 g/L, $CaCl_2$ x 2 H_2O 1 g/L, $MgSO_4$ x 7 H_2O 1 g/L, HEPES 11.9 g/L and Fe-EDTA 8 mg/L at pH 7.4. 70 L of the same medium in a 100 L fermentor (blade impeller 150 rpm, aeration 9 L/min, 30°C, pO_2 20%, pH regulated between pH 7.15 and 7.25) were inoculated in the presence of 1.4 kg of XAD-16 resin. After 7 days the culture broth was passed through a process filter to collect the absorber resin. Residual cells were floated from recovered XAD-16 resin with water.

4.3.2 Isolation of *p*-Hydoxyacetophenone Amides 34a-f

Isolation of *p*-hydroxyacetophenone amides 34a-c: The XAD resin was eluted with 4 L of methanol/H_2O (30/70), methanol (4 L) and acetone (4 L) in a column. The organic solvent was evaporated from the methanol fraction to give 550 mL of an aqueous mixture, which was extracted with ethyl acetate (5 portions of 250 mL). The combined ethyl acetate layer was dried *in vacuo* to give 18.6 g crude extract. The extract was dissolved in methanol and partitioned between methanol and *n*-heptane, to provide 17.5 g of more polar raw material. 1.0 g of this extract was separated by silica gel flash chromatography [Flash40 (Biotage), cartridge Si 40 S 2976-1 (Biotage); solvent DCM/methanol/*n*-heptane (18/1/1)]. 4 main fractions were collected according to the analysis of all fractions by thin layer chromatography (TLC). Fraction 3 yielded 124.4 mg which were further purified in 3 batches by preparative RP-HPLC [column 250×21 mm, Nuleodur 100 EC (10 µm, C_{18}) (Macherey-Nagel); solvent A: methanol/H_2O (10/90 + 0.01% acetic acid), solvent B: methanol/H_2O

(90/10 + 0.01% acetic acid); gradient 25% B for 5 min, increasing to 45% B over 35 min, maintained at 45% for 10 min, increasing to 100% B over 5 min; FR = 20 mL/min, UV detection 210-500 nm]. Fractions were combined peak wise. The organic solvent was evaporated from the fractions after addition of toluene and the water layer was extracted with ethyl acetate yielding compound **34c** (R_t = 7 min, 3.3 mg), **34b** (R_t = 19 min, 7.1 mg) and **34a** (R_t = 29 min, 59.6 mg).

Isolation of *p*-hydroxyacetophenone amide 34d: Fraction 2 (221.2 mg) from the silica gel flash chromatography was separated by preparative RP-HPLC in 5 batches [column 250×21 mm, Nuleodur 100 EC (10 µm, C_{18}) (Macherey-Nagel); solvent A: methanol/H_2O 10/90 + 0.01% acetic acid, solvent B: methanol/H_2O 90/10 + 0.01% acetic acid; gradient 25% B for 5 min, increasing to 35% B in 25 min, increasing to 100% B in 1 minutes maintained at 100% B for 20 minutes; FR = 20 mL/min, UV detection at 210-500 nm]. Compound **34d** (6.9 mg) eluted at R_t = 38 min.

Isolation of *p*-hydroxyacetophenone amide 34e and 34f: 4.4 g of the methanol extract were subjected to silica gel flash chromatography (300 g silica gel 60, particle size 0.063-0.200 mm, Merck) and eluted stepwise with ethyl acetate/DCM/*n*-heptane (3/3/4) (3 L) and ethyl acetate (6 L). 15 fractions were collected and dried *in vacuo* according to TLC analyses. Fraction 5 (48.6 mg) was further separated in 3 batches by preparative RP-HPLC [column 250×21 mm, Nuleodur 100 EC (10 µm, C_{18}) (Macherey-Nagel); gradient 37% B for 30 min, increasing to 100% B over 20 min; solvent A: methanol/H_2O (10/90), solvent B: methanol; FR = 20 mL/min, UV detection 210-500 nm]. Compound **34e** eluted at 33.5 min (0.8 mg). Fraction 9 (314 mg) of the silica gel chromatography was separated by preparative RP-MPLC [column 480×30 mm, ODS-AQ, 120 Å, S 16 µm, C-18 (Macherey-Nagel); solvent A: H_2O/methanol (90/10), solvent B: methanol, gradient: 35% B to 38% B in 3 h, to 100% B in 30 min, isocratic 30 min; FR = 30 mL/min, UV detection 280 nm). 11 fractions were collected and evaporated. The remaining aqueous layers were extracted with ethyl acetate. Compound **34f** (1.1 mg) eluted at R_t = 185 min.

p-Hydroxyacetophenone *iso*-butanamide (**34a**): white needles; mp 188°C; analytical TLC: R_f = 0.07; UV (methanol): λ_{max} (lg ε) = 202 (4.864), 218 (4.724), 278 (4.893) nm; IR (KBr): ν = 3356, 3195, 2960, 1649, 1577, 1546, 1245, 1170 cm^{-1}; NMR (CD_3OD): Table 10; HRESIMS *m/z*: calcd. for $C_{13}H_{18}NO_3$ 236.1281, found: 236.1287.

p-Hydroxyacetophenone *n*-butanamide (**34b**): white needles; mp 184°C; analytical TLC: R_f = 0.05. UV (methanol): λ_{max} (lg ε) = 201 (4.736), 219 (4.553), 278 (4.721) nm; IR (KBr): ν = 3358, 3101, 2962, 1633, 1581, 1519, 1243, 1174 cm^{-1}; NMR (CD_3OD): Table 11; HRESIMS *m/z*: calcd. for $C_{12}H_{16}NO_3$ 222.1125, found 222.1125.

p-Hyroxyacetophenone acetamide (**34c**): white needles; mp 187°C; analytical TLC: R_f = 0.02; UV (methanol): λ_{max} (lg ε) = 201 (4.363), 219 (4.211), 278 (4.396) nm; IR (KBr): ν = 3344, 3200, 2931, 1652, 1577, 1548, 1243, 1170 cm^{-1}; NMR (CD_3OD): Table 11; HRESIMS *m/z*: calcd. for $C_{10}H_{12}NO_3$ 194.0812, found 194.0809.

p-Hydroxyethenphenyl *iso*-butanamide (**34d**): oil; analytical TLC: R_f = 0.24; UV (methanol): λ_{max} (lg ε) = 200 (4.330), 219 (4.454), 285 (4.747) nm; IR (KBr): ν = 3289, 3074, 2969, 1670, 1539, 1228, 1170 cm^{-1}; NMR (CD_3OD): Table 12; HRESIMS *m/z*: calcd. for $C_{13}H_{18}NO_2$ 220.1332, found 220.1331.

p-Hyrdoxyacetophenone *iso*-pentanamide (**34e**): analytical TLC: R_f = 0.07; UV (ethanol) λ_{max} (lg ε) = 219 nm (4.228), 279 nm (4.350), 331 nm (3.388); NMR (CD_3OD): Table 13; (+)-HRESIMS *m/z*: calcd. for $C_{14}H_{20}NO_3$ 250.1438, found 250.1447.

p-Hydroxyacetophenone *n*-pentanamide (**34f**): analytical TLC: R_f = 0.09; UV (ethanol): λ_{max} (lg ε) = 218 (4.021), 279 (4.111), 331 (3.150) nm; NMR (CD_3OD): Table 13; HRESIMS *m/z*: calcd. For $C_{14}H_{20}NO_3$ 250.1438, found 250.1447.

4.3.3 Biosynthetic Studies of *p*-Hydroxyacetophenone Amide 34a by Feeding Experiments

Three cultures (100 mL medium described above) were provided with XAD 16 resin (2 mL). The cultures were supplemented with [$^{13}CH_3$]-sodium methionine (50 mg, 98%, Cambridge Isotope Laboratories), [D_{10}]-leucine (50 mg, 98%, Campro Scientific) or [$^{13}C_9$,^{15}N]-tyrosine (50 mg, 98% ^{13}C, 98% ^{15}N, Campro Scientific). The cultures were incubated at 30°C with shaking at 180 rpm for 6 days. After sieving off the XAD resin, the resin was eluted with acetone (60 mL) for 16 h. The extracts were evaporated and re-dissolved in methanol (1 mL) for HPLC-HRESIMS or CD_3OD for NMR spectroscopy analysis.

p-Hydroxyacetophenone *iso*-butanamide (**34a**) from feeding [$^{13}C_9$,^{15}N]-tyrosine: ^{13}C NMR (CD_3OD, 75.5 MHz): δ = 194.6 (m, 1 C, C-7, labelled, calculated 50% incorporation rate (ir)), 176.0 (m, 0.16 C, C-9, labelled, 8% ir), 176.0 (s, 0.02 C, C-9, unlabelled), 164.2 (m, 0.93 C, C-1, labelled), 131.6 (m, 5.33 C, C-3,5, labelled), 128.0 (m, 3.02 C, C-4, labelled), 116.4 (m, 5.63 C, C-2,6, labelled), 46.5 (m, 3.13 C, C-8,10, labelled), 27.4 (m, 0.86 C, C-11, labelled), 22.8 (d, *J* = 34.9, 0.81 C, C-12,13, labelled, 7% ir), 22.8 (s, 0.11 C, C-12,13, unlabelled), % ^{13}C incorporation = 1.1 × ($integral_{labelled}$/$integral_{unlabelled}$) - 1.1; ^1H NMR ([D_3]trifluoroethanol/H_2O 1/1, 600MHz): reference spectrum δ = 0.99 (d, J = 6.6 Hz, 6 H, H-12,13) 2.08 (dq, *J* = 7.7, 6.6 Hz, 1 H, H-11) 2.23 (d, *J* = 7.7 Hz, 2 H, H-10) 4.68 (d, *J* = 5.0 Hz, 2 H, H-8) 7.00 (d, *J* = 8.8 Hz, 2 H, H-2,6) 7.56 (t, *J* = 5.0 Hz, 1 H, N-H) 7.94 (d, *J* = 8.8 Hz, 2 H, H-3,5); labelled spectrum δ = 7.00 (d, 8.8 Hz, 3.74 H, H-2,6, unlabelled), 7.00 (dm, *J* = 150 Hz, 3.81 H, H-2,6, labelled, 51% ir), 7.56 (m, 1.0 H, N-H, unlabelled), 7.56 (dm, *J* = 95 Hz, 0.42 H, N-H, labelled, 30% ir), 7.94 (d, *J* = 8.8 Hz, 2.88 H, H-3,5, unlabelled), 7.94 (dm, *J* = 150 Hz, 3.22 H, H-3,5, labelled, 53% ir); (% ir = ($integral_{labelled}$/ ($integral_{labelled}$ + $integral_{unlabelled}$))× 100); (+)-HRESIMS: *m/z* (%) = 250.1677 (2), 249.1647 (14), 248.1663 (11), 247.1584 (10), 246.1584 (9), 245.1515 (42), 244.1537 (51), 237.1272 (27), 236.127 (94), 161.0938 (69), 160.0966 (70), 153.0688 (24), 152.0701 (100%). (% ir = $intensity_{labelled}$/ ($intensity_{labelled}$ + $intensity_{unlabelled}$) × 100)

p-Hydroxyacetophenone *iso*-butanamide (**34a**) from feeding [D_{10}]-leucine: ^1H NMR (CD_3OD, 300 MHz): identified signals from the crude extract δ = 1.03 (d, *J* = 6.4 Hz, 2.2 H, H-12,13), 4.66 (s, 2.0 H, H-8), 6.91 (d, *J* = 8.8 Hz, 2.0 H, H-2,6), 7.94 (d, *J* = 8.8 Hz, 1.9 H, H-3,5); (+)-HRESIMS: *m/z* (%) = 245.1834 (100), 236.1268 (53). (% ir = $\%_{labelled}$ / ($\%_{labelled}$ + $\%_{unlabelled}$) × 100)

4.4 Isolation of Sulfangolids 24a-d

4.4.1 Isolation of Sulfangolid A (25a)

Sulfangolid A (**25a**) was produced by the *Sorangium cellulosum* strain So ce666 in a 60 L fermentor at 30°C containing the following medium: Starch 6 g/L, soybean flour 2 g/L, skim milk 1 g/L, casitone 1 g/L, glucose × H_2O 1 g/L, $CaCl_2$ × 2 H_2O 1 g/L, $MgSO_4$ × 7 H_2O 1 g/L, Na-Fe-EDTA 8 mg/L at pH 7.4 in the presence of 1 % of adsorber resin Amberlite XAD-16 and 1-docosanol 55 mg/L. The pH was regulated between pH 7.0 and 7.8. After 14 days of cultivation, starch and glucose were used up and the culture broth was passed through a process filter to collect the absorber resin. Residual cells were floated from the XAD-16 resin with water. The resin was eluted with MeOH/acetone 1/1 (3 L) and acetone (4 L). The organic solvents were evaporated and the remaining water/oil mixture (350 mL) was extracted with ethyl acetate (5 portions of 500 mL) after addition of saturated NaCl solution (150 mL). The ethyl acetate-layer yielded 30.0 g crude extract after evaporation. A MeOH/*n*-heptane partition was carried out to remove 10.9 g lipophilic by-products in the *n*-heptane layer (4 portions of 200 mL). The remaining methanol layer was evaporated and dissolved in Et_2O (200 mL) and 2 M ammonia. The ammonia layer was extracted with Et_2O (5 portions of 200 mL) at 0°C (centrifugation at 0°C, 5 min, 3000 rpm). After evaporation the Et_2O-layer yielded 2.1 g of lipophilic material. The ammonia layer was acidified to pH 4 and extracted with Et_2O (3 portions of 200 mL) to yield 18.5 g of crude extract after evaporation. The water layer was finally extracted with ethyl acetate (3 portions of 250 mL) to give 10.2 g. In order to remove format salts this fraction was partitioned between water and DCM to yield 5.3 g in the DCM layer. This fraction was purified by RP-MPLC [column 480×30 mm (Kronlab), RP-ODS-AQ C18 (Macherey-Nagel), solvent A: H_2O/ACN 95/5 + 50 mM/L NH_4Ac + 400 µL/L acetic acid; solvent B: H_2O/ACN 5/95 + 10 mM/L NH_4Ac + 80 µL/L acetic acid, gradient: 35% B for 20 min, increasing to 40% B in 80 min, maintaining for 60 min, FR = 20 mL/min, UV detection 278 nm]. The fractions at R_t = 44 min were combined and neutralized with 2 M ammonia before the organic solvent was evaporated. The water layer was passed through a strata-X cartridge (0.5 g). After washing with water, the product was eluted from the cartridge with methanol to give 74.8 mg of dried material, which was further purified by RP-HPLC [column 250×21 mm, 10 µm, C_{18} RP-Nucleodur 100-EC (Macherey-Nagel), solvent A: H_2O/ACN 95/5 + 50 mM/L NH_4Ac + 400 µL/L acetic acid; solvent B: H_2O/ACN 5/95 + 10 mM/L NH_4Ac + 80 µL/L acetic acid, gradient: 35% B for 5 min, increasing to 40% B in 20 min, maintaining for 40 min, FR = 20.0 mL/min, UV detection 278 nm]. Sulfangolid A (**25a**)

had a R_t = 36 min and yielded 2.8 mg as ammonium salt after work up analogously to the RP-MPLC chromatography.

Sulfangolid A (**25a**): yellowish oil; analytical TLC: DCM/MeOH 8.5/1.5: R_f = 0.16; $[\alpha]_D^{RT}$ = + 74.3 (*c* = 0.7 in methanol); NMR data (^{1}H 600 MHz, ^{13}C 150 MHz, [D$_6$]DMSO): Table 15; UV/Vis (methanol): λ_{max} (lg ε) = 283 (4.462), 342 nm (4.435); IR (KBr): ν = 3431 (b, s), 2958 (m), 2932 (m), 1704 (s), 1624 (m), 1252 (s), 1011 (s) cm^{-1}; MS (DCI): reactant gas ammonia, *m*/*z* (%): 548 (25), 566 (100), 567 (35), 568 (10), 584 (15); HRESIMS *m*/*z*: for $C_{35}H_{51}O_{10}S$ calcd. 663.3208; found 663.3206.

4.4.2 Isolation of Sulfangolid B (25b)

Sulfangolid B (**25b**) was produced by strain So ce192 in a 100 L fermentor at 30°C in a medium consisting of starch 8 g/L, soybean meal 2 g/L, yeast extract 2 g/L, glucose × 2 H_2O 2 g/L, $CaCl_2$× 2 H_2O 1 g/L, $MgSO_4$ × 7 H_2O 1 g/L, Na-Fe-EDTA 8 mg/L at pH 7.4 in the presence of 2% Amberlite XAD-16 and 10 mL of tegosipon antifoam. The pH was regulated analogue to the sulfangolid A (**25a**) production. After 7 days of cultivation the culture broth was passed through a process filter to collect the absorber resin. Residual cells were floated from XAD-16 resin with water. The resin was eluted with MeOH/H_2O 6/4 and MeOH (each 5 L). The methanol layer was evaporated *in vacuo* to give 22.0 g of crude extract. Lipophilic by-products were removed by MeOH/*n*-heptane partition to give 20.0 g MeOH extract and 1.0 g of by-products. The methanol extract was dissolved in DCM and filtered over celite before silica-gel-flash chromatography (column 80 mL). The silica gel chromatography was eluted step wise with DCM (yield 9.0 g), DCM/MeOH 19/1 (yield 6.65 g), DCM/MeOH 9/1 (yield 0.72 g) and finally with MeOH (yield 0.22 g) (500 mL of each solvent). The DCM/MeOH 9/1 extract was further purified by silica-flash chromatography [column 37×420 mm HD-Sil 15µ, 60Å (Macherey-Nagel), gradient: 10 min with petroleum ether/DCM/MeOH 50/48/2, increasing the MeOH proportion to 4% in 120 min, maintaining 4% for 30 min, increasing to 5% MeOH in 30 min, maintaining 5% for 30 min, rinsing the column with DCM/MeOH 7/3, FR = 35 mL/min, UV detection 278 nm]. The sulfangolid B (**25b**) containing fraction had a R_t of 124 min and a dry weight of 114 mg after evaporation. This fraction was further purified by RP-HPLC chromatography [column 20.5×250 mm Nucleosil 100-7 C18 (Macherey-Nagel), 65% MeOH isocratic, FR = 18 mL/min, UV detection 278 nm]. Sulfangolid B (**25b**) (8 mg) was isolated at R_t = 11 min.

Sulfangolid B (**25b**): yellowish oil, analytical TLC: DCM/MeOH 8.5/1.5: R_f = 0.16; NMR data (^{1}H 600 MHz, ^{13}C 150 MHz, CD_3OD): Table 16; HRESIMS *m/z*: calcd. for $C_{36}H_{53}O_{11}S$ 693.3314, found 693.3308.

4.4.3 Isolation of Sulfangolid C (25c)

Sulfangolid C (**25c**) was produced by *Sorangium cellulosum* strain So ce12 in the same medium as So ce192, supplemented with fructose 1 g/L and KNO_3 1 g/L. Two fermentors with 70 L media each were performed. They were supplemented with 1% of adsorber resin XAD-16 and 100 mg/L 1-docosanol. The pH was regulated between pH 7.0 and 7.8. After 9 days the culture broths were passed through a process filters. Residual cells of the combined XAD-16 resin were floated with water. The absorber resin was then eluted with MeOH/H_2O 1/1 (3.5 L) and MeOH (4.5 L). The organic solvent was evaporated from the layers *in vacuo* and the water layers of each fraction were extracted with ethyl acetate (5 portions of 250 mL) after addition of saturated NaCl solution (150 mL). The layers were combined and the solvent was evaporated *in vacuo* to give 33.8 g of crude extract. Lipophilic by-products were extracted by MeOH/*n*-heptane partition to yield 22.5 g methanol extract and 1.8 g *n*-heptane extract. The methanol extract was dissolved in Et_2O (250 mL) and 2 M ammonia (125 mL). The Et_2O-layer was extracted with 2 M ammonia (3 portions of 300 mL). The Et_2O-layer yielded 11.8 g non-polar compounds. The combined ammonia layers were neutralized with formic acid to pH 7 and then extracted with Et_2O (3 portions of 300 mL), yielding 6.2 g residue after evaporation. The water layer was further extracted with ethyl acetate (3 portions of 300 mL), yielding 5.9 g of enriched sulfangolid C (**25c**). This crude extract was dissolved in Et_2O and H_2O and acidified with formic acid to pH 4 to be extracted with Et_2O (3 portions of 150 mL) at 0°C (centrifugation at 0°C, 8 min, 3000 rpm), yielding 2.6 g of the enriched carboxylic acid sorangicin A (**13**). The water layer was neutralized with 2M ammonia and extracted with ethyl acetate (3 portions of 200 mL) under the addition of saturated NaCl solution (80 mL). The ethyl acetate extract was evaporated *in vacuo* to yield 1.4 g enriched sulfangolid C (**25c**). This fraction was further purified by LH-20 chromatography (50×1000 mm column, solvent: MeOH, FR = 4.0 mL/min, UV detection 278 nm) in 3 batches. The fractions were combined according to the UV-chromatogram and fraction 7 at R_t = 560 min with 85 mg product contained the highest concentration of sulfangolid C (**25c**). This fraction was further purified by RP-HPLC in three batches [column 250×21 mm, 10 µm, C_{18} RP-Nucleodur 100-EC (Macherey-Nagel), solvent A: H_2O/ACN 95/5 + 50 mM/L NH_4Ac + 400 µL/L acetic acid; solvent B: H_2O/ACN 5/95 + 10 mM/L NH_4Ac + 80 µL/L acetic acid,

gradient: 25% B maintaining for 15 min, increasing to 50% B in 90 min, maintaining 15 min, FR = 20.0 mL/min, UV detection 278 nm]. The UV peak at R_t = 81 min was neutralized with 2 M ammonia, the organic solvent was evaporated and the water layer passed through a strata-X cartridge (0.5 g, Phenomenex). After washing with water the compound was eluted from the cartridge with methanol to yield 29.6 mg. Sulfangolid C (**25c**) was further purified by RP-HPLC [column 250×21 mm, 10 µm, C_{18} RP-Nucleodur 100-EC (Macherey-Nagel), solvent A: H_2O/ACN 95/5 + 50 mM/L NH_4Ac + 400 µL/L acetic acid; solvent B: H_2O/ACN 5/95 + 10 mM/L NH_4Ac + 80 µL/L acetic acid, gradient: 30% B maintaining for 5 min, increasing to 40% B in 40 min, maintaining at 40% B for 20 min, FR = 20 mL/min, UV detection 278 nm]. Sulfangolid C (**25c**) had a R_t = 17 min and yielded 17.7 mg of the ammonium salt after work up by strata-X cartridge (1.0 g).

Sulfangolid C (**25c**): yellowish oil; analytical TLC: DCM/MeOH 8.5/1.5, R_f = 0.15; $[\alpha]_D^{RT}$ = + 153.3 (*c* = 0.5 in methanol); NMR data (^{1}H 600 MHz, ^{13}C 150 MHz, [D_6]DMSO): Table 17; UV/Vis (methanol): λ_{max} (lg ε) = 288 nm (4.446); IR (KBr): ν = 3421 (b, s), 2957 (s), 2931 (s), 1705 (s), 1616 (m), 1255 (s), 1006 (s) cm^{-1}; HRESIMS *m/z*: calcd. for $C_{35}H_{53}O_{11}S$ 681.3314, found 681.3317.

4.4.4 Isolation of Sulfangolid D (25d)

Sulfangolid D (**25d**) was produced by *Sorangium cellulosum*, strain So ce1375, in a 70 L fermentor at 30°C with medium consisting of soybean meal 5 g/L, glucose × H_2O 1 g/L, starch 10 g/L, $CaCl_2$ × 2 H_2O 1 g/L, $MgSO_4$ × 7 H_2O 1 g/L, $NaNO_3$ 80 mg/L and Na-Fe-EDTA 8 mg/L at pH 7.2. The fermentor was additionally supplemented with 0.1% of Amberlite XAD-16 resin and 100 mg/L 1-docosanol. The pH was regulated as described above. After 10 days the resin was collected by sieving in a process filter. The recovered XAD resin containing residual cells (3.25 kg) was stirred for 1 h in methanol (15 L) before the organic solvent was passed through a celite filter. The organic solvent was evaporated and the water was extracted with ethyl acetate to yield 21.5 g of crude extract, which was dissolved in methanol and partitioned between methanol and *n*-heptane to remove 8.7 g lipophilic by-products. The methanol layer yielded 12.1 g after evaporation. The methanol extract was separated by silica gel chromatography (1.2 L silica gel 60 (Merck)) and stepwise eluted with DCM (2 L), DCM + 10% methanol (2.5 L) and DCM + 20% methanol. Sulfangolid D (**25d**) eluted in the last fraction to give 1.6 g of residue after evaporation. The extract was further purified by silica gel MPLC in two batches [column 500×70 mm HD-Sil 18-20-60, MeOH/H_2O (85/15) supplemented with 50 mM/L NH_4Ac, FR = 8 mL/min, UV

detection 365 nm]. Sulfangolid A (**25a**) was recovered at R_t = 105 min (yield 566 mg) and Sulfangolid D (**25d**) at R_t = 210 min (yield 281 mg) as ammonium salts.

Sulfangolid D (**25d**): yellowish oil; TLC: DCM/MeOH (85/15): R_f = 0.27; NMR data (^{1}H 300 MHz, ^{13}C 75 MHz, CD_3OD): Table 18; UV/Vis (methanol): λ_{max} (lg ε) = 237 (3.954), 339 nm (5.741); IR (KBr): ν = 3447 (b, s), 2959 (s), 2935 (s), 1704 (s), 1617 (m), 1597 (s), 1457 (m), 1256 (s), 1227 (s), 1165 (m), 1124 (m), 1079 (m), 1045 (m), 1008 (s), 980 (m), 922 (m) cm^{-1}; HRESIMS *m/z*: calcd. for $C_{36}H_{53}O_{10}S$ 677.3365, found 677.3343.

4.4.5 Fermentation of So ce757 for the Production Kinetics of Sulfangolid C (25c)

Sorangium cellulosum strain So ce757 inoculated a 70 L fermentor at 30°C containing the following medium: starch 10 g/L, soybean meal 2 g/L, skim milk 2 g/L, glycerine (87%) 1 g/L, $CaCl_2 \times 2\ H_2O$ 1 g/L, $MgSO_4 \times 7\ H_2O$ 1 g/L, glucose $\times 2\ H_2O$ 0.5 g/L, Na-Fe-EDTA 8 mg/L at pH 7.8, supplemented with 1% Amberlite XAD-16. The pH was regulated between pH 7.0 and 7.8. A sample of about 100 mL culture was taken on day 2, 4, 6, 7, 8 and 9, the glucose concentration of the supernatant was tested with Diabur-Test 5000 (Roche), the XAD-16 was eluted twice with methanol and twice with acetone. The organic layers of each sample were combined and the solvent evaporated. The residue was concentrated 1:100 and analysed for the sulfangolid C (**25c**) concentration by HPLC. The XAD-resin was harvested on day 9 of cultivation.

4.4.6 Biosynthetic Studies of Sulfangolid C (25c) by Feeding Experiments

Sorangium cellulosum strain So ce757 producing 19 mg/L sulfangolid C (**25c**) was used in the feeding experiments with the following medium: starch 10 g/L, soybean meal 2 g/L, milk powder 2 g/L, glycerine 87% 1 g/L, $CaCl_2 \times 2\ H_2O$ 1 g/L, $MgSO_4 \times 7\ H_2O$ 1 g/L, glucose × H_2O 0.5 g/L, Na-Fe-EDTA 8 mg/L at pH 7.8 and Amberlite XAD 16 resin 10 g/L. For the ^{13}C-labelled acetate and [D_{10}]-leucine 4 Erlenmeyer flasks with 350 mL medium and for propionate a 700 mL culture were provided. As the strain grew in lumps, start of the cultivation with an exact inoculum was not possible. Alternatively, the kinetic of the production was correlated with the glucose content of the medium. Feeding was started with the beginning of the production at a glucose concentration of 0.25%. During 4 days the precursors were added in equal portions with a final amount of 252 mg [1-^{13}C]-sodium acetate (99%), 251 mg of [2-^{13}C-D_3]-sodium acetate (99%, 98%), 250 mg [1,2-^{13}C]-sodium acetate (99%), 504 mg [1-^{13}C]-sodium propionate (97%) (Cambridge Isotope Laboratories) and 253 mg [D_{10}]-leucine (98%, Campro Scientific, under the addition of HCl). The XAD resin of each culture was harvested after starch and glucose consumption by sieving and then eluted with methanol and acetone. The extracts of each experiment were combined and partitioned between methanol and *n*-heptane. The methanol layers were further purified by RP-HPLC [column 250×21 mm, 10 µm, C_{18} RP–Nucleodur 100-EC (Macherey-Nagel), solvent A: 95/5 H_2O/ACN + 50 mM/L + 400 µL/L acetic acid, solvent B: 5/95 H_2O/ACN + 10 mM/L + 80 µL/L acetic acid, gradient: 10% B in 60 min to 65% B, FR = 20 mL/min, UV detection 287 nm] and **3** was recovered at a R_t = 45 min. After evaporation of the organic solvent the water layers were extracted with ethyl acetate. Yields: [1-^{13}C]-acetate labelled **25c** 5.4 mg, [2-^{13}C-D_3]-acetate labelled **25c** 2.6 mg, [1,2-^{13}C]-acetate labelled **25c** 3.6 mg, [1-^{13}C]-propionate labelled **25c** 7.3 mg and [D_{10}]-leucine labelled **25c** 9.5 mg. The summarized NMR data are presented in Table 21. In addition, strain So ce757 was transferred to an analogous but sulfate-free medium and the sulfangolid C (**25c**) production decreased from 19 mg/L to 2 mg/L after two passages.

5 References

[1] Li, J. W.-H.; Vederas, J. C. *Science*. **2009**, *325*, 161-165.

[2] Newman, D. J.; Cragg, G. M.; Snader, K. M. *J. Nat. Prod.* **2003**, *66*, 1022-37.

[3] Andermann, A. A. J. *McGill J. Med.* **1996**, 115-120.

[4] Demain, A. L. *J. Ind. Microbiol. Biotechnol.* **2006**, *33*, 486-95.

[5] Demain, A. L. *Med. Res. Rev.* **2009**, *29*, 821-842.

[6] Nathan, C. *Nature*. **2004**, *431*, 899-902.

[7] Nordmann, P.; Naas, T.; Fortineau, N.; Poirel, L. *Curr. Opin. Microbiol.* **2007**, *10*, 436-40.

[8] Boyce, J. M. *Lancet Infect Dis*. **2005**, *5*, 653-663.

[9] Dixon, N.; Wong, L. S.; Geerlings, T. H.; Micklefield, J. *Nat. Prod. Rep.* **2007**, *24*, 1288-310.

[10] Newman, D. J.; Cragg, G. M. *J. Nat. Prod.* **2007**, *70*, 461-77.

[11] Kneller, R. *Nat. Rev. Drug Discovery*. **2010**, *9*, 867-882.

[12] Koehn, F. E.; Carter, G. T. *Nat. Rev. Drug Discovery*. **2005**, *4*, 206-20.

[13] Weissman, K. J.; Leadlay, P. F. *Nat. Rev. Microbiol.* **2005**, *3*, 925-36.

[14] Niggemann, J.; Michaelis, K.; Frank, R.; Zander, N.; Höfle, G. *J. Chem. Soc., Perkin Trans. 1*. **2002**, 2490-2503.

[15] Cordier, C.; Morton, D.; Murrison, S.; Nelson, A.; OLeary-Steele, C. *Nat. Prod. Rep.* **2008**, *25*, 719-37.

[16] Raghunand, T. R.; Bishai, W. R.; Chen, P. *Int. J. Antimicrob. Agents*. **2006**, *28*, 36-41.

[17] Jayasuriya, H.; Herath, K. B.; Zhang, C.; Zink, D. L.; Basilio, A.; Genilloud, O.; Diez, M. T.; Vicente, F.; Gonzalez, I.; Salazar, O.; Pelaez, F.; Cummings, R.; Ha, S.; Wang, J.; Singh, S. B. *Angew. Chem. Int. Ed.* **2007**, *46*, 4684-8.

[18] Davis, G. F.; Downs, T. R.; Farmer, J. A.; Pierson, C. R.; Roesgen, J. T.; Cabrera, E. J.; Nelson, S. L. *J. Biolmol. Screening*. **2002**, *7*, 67-77.

[19] Clardy, J.; Walsh, C. *Nature*. **2004**, *432*, 829-37.

[20] Hamad, B. *Nat. Rev. Drug Discovery*. **2010**, *9*, 675-676.

[21] Reichenbach, H. *J. Ind. Microbiol. Biotechnol.* **2001**, *27*, 149-56.

[22] Shimkets, L. J.; Dworkin, M.; Reichenbach, H. *Prokaryotes*, Dworkin, M.; Falkov, S.; Rosenberg, C.; Schleifer, K.; Stackebrandt, E., Eds.; 7th ed.; Springer: New York; 2006.

[23] Dworkin, M. *Microbiol. Rev.* **1996**, *60*, 70-102.

[24] Iizuka, T.; Jojima, Y.; Fudou, R.; Yamanaka, S. *FEMS Microbiol. Lett*. **1998**, *169*, 317-22.

[25] Fudou, R.; Jojima, Y.; Iizuka, T.; Yamanaka, S. *J. Gen. Microbiol.* **2002**, *48*, 109-16.

[26] Dawid, W. *FEMS Microbiol. Rev.* **2000**, *24*, 403-27.

[27] Wenzel, S. C.; Müller, R. *Curr. Opin. Drug Discovery & Devel.* **2009**, *12*, 220-230.

[28] Weissman, K. J.; Müller, R. *Nat. Prod. Rep.* **2010**, *27*, 1276-95.

[29] Niggemann, J.; Bedorf, N.; Flörke, U.; Steinmetz, H.; Gerth, K.; Reichenbach, H.; Höfle, G. *Eur. J. Org. Chem.* **2005**, *2005*, 5013-5018.

[30] Gerth, K.; Washausen, P.; Gerhard, H.; Irschik, H.; Reichenbach, H. *J. Antibiot.* **1995**, *49*, 71-75.

[31] Gerth, K.; Pradella, S.; Perlova, O.; Beyer, S.; Müller, R. *J. Biotech.* **2003**, *106*, 233-253.

[32] Höfle, G.; Bedorf, N.; Schomburg, D.; Gerth, K.; Reichenbach, H. *Liebigs Ann. Chem.* **1993**, *LIV*, 1017- 1021.

[33] Kohl, W.; Irschik, H.; Reichenbach, H.; Höfle, G. *Liebigs Ann. Chem.* **1983**, *XVII*, 1656 - 1667.

[34] Irschik, H.; Jansen, R.; Höfle, G.; Gerth, K.; Reichenbach, H. *J. Antibiot.* **1985**, *XXXVIII*, 145-152.

[35] Jansen, R.; Irschik, H.; Reichenbach, H.; Höfle, G. *Liebigs Ann. Chem.* **1985**, 822-836.

[36] Ho, M. X.; Hudson, B. P.; Das, K.; Arnold, E.; Ebright, R. H. *Curr. Opin. Struct. Biol.* **2009**, *19*, 715-23.

[37] Irschik, H.; Jansen, R.; Gerth, K.; Höfle, G.; Reichenbach, H. *J. Antibiot.* **1986**, *XL*, 7-13.

[38] Jansen, R.; Wray, V.; Irschik, H.; Reichenbach, H.; Höfle, G. *Tetrahedron Lett.* **1985**, *26*, 6031-6034.

[39] Mukhopadhyay, J.; Das, K.; Ismail, S.; Koppstein, D.; Jang, M.; Hudson, B. P.; Sarafianos, S.; Tuske, S.; Patel, J.; Jansen, R.; Irschik, H.; Arnold, E.; Ebright, R. H. *Cell*. **2008**, *135*, 295-307.

[40] Sousa, R. *Cell*. **2008**, *135*, 205-7.

[41] Höfle, G.; Bedorf, N.; Steinmetz, H.; Schomburg, D.; Gerth, K.; Reichenbach, H. *Angew. Chem. Int. Ed.* **1996**, *35*, 1567-1569.

[42] Hardt, I. H.; Steinmetz, H.; Gerth, K.; Sasse, F.; Reichenbach, H.; Höfle, G. *J. Nat. Prod.* **2001**, *64*, 847-856.

[43] Ibrahim, N. K. *Cancer Manag. Res.* **2010**, *2*, 169-179.

[44] Khalil, M. W.; Sasse, F.; Lünsdorf, H.; Elnakady, Y. A.; Reichenbach, H. *ChemBioChem*. **2006**, *7*, 678-83.

[45] Chai, Y.; Pistorius, D.; Ullrich, A.; Weissman, K. J.; Kazmaier, U.; Müller, R. *Chem. Biol.* **2010**, *17*, 296-309.

[46] Ullrich, A.; Chai, Y.; Pistorius, D.; Elnakady, Y. A.; Herrmann, J. E.; Weissman, K. J.; Kazmaier, U.; Müller, R. *Angew. Chem. Int. Ed.* **2009**, *48*, 4422-5.

[47] Leamon, C. P.; Reddy, J. A.; Vetzel, M.; Dorton, R.; Westrick, E.; Parker, N.; Wang, Y.; Vlahov, I. *Cancer Res.* **2008**, *68*, 9839-44.

[48] Vlahov, I. R.; Wang, Y.; Kleindl, P. J.; Leamon, C. P. *Bioorg.Med.Chem.Lett.* **2008**, *18*, 4558-61.

[49] Reddy, J. A; Dorton, R.; Dawson, A.; Vetzel, M.; Parker, N.; Nicoson, J. S.; Westrick, E.; Klein, P. J.; Wang, Y.; Vlahov, I. R.; Leamon, C. P. *Mol. Pharmaceutics*. **2009**, *6*, 1518-25.

[50] Vollbrecht, L.; Steinmetz, H.; Höfle, G. *J. Antibiot.* **2002**, *55*, 715-721.

[51] Wenzel, S. C.; Müller, R. *Nat. Prod. Rep.* **2009**, *26*, 1385-407.

[52] Weissman, K. J.; Müller, R. *Bioorg. Med. Chem.* **2009**, *17*, 2121-36.

[53] Schneiker, S.; Pavlova, O.; Kaiser, O.; Gerth, K.; Alici, A.; Altmeyer, M. O.; Bartels, D.; Bekel, T.; Beyer, S.; Bode, E.; Bode, H. B.; Bolten, C. J.; Choudhuri, J. V.; Doss, S.; Elnakady, Y. A.; Frank, B.; Gaigalat, L.; Goesmann, A.; Groeger, C.; Gross, F.; Jelsbak, L.; Jelsbak, L.; Kalinowski, J.; Kegler, C.; Knauber, T.; Konietzny, S.; Kopp, M.; Krause, L.; Krug, D.; Linke, B.; Mahmud, T.; Martinez-Arias, R.; McHardy, A. C.; Merai, M.; Meyer, F.; Mormann, S.; Muñoz-Dorado, J.; Perez, J.; Pradella, S.; Rachid, S.; Raddatz, G.; Rosenau, F.; Rückert, C.; Sasse, F.; Scharfe, M.; Schuster, S. C.; Suen, G.; Treuner-Lange, A.; Velicer, G. J.; Vorhölter, F.-J.; Weissman, K. J.; Welch, R. D.; Wenzel, S. C.; Whitworth, D. E.; Wilhelm, S.; Wittmann, C.; Blöcker, H.; Pühler, A.; Müller, R. *Nat. Biotechnol.* **2007**, *25*, 1281-9.

[54] Goldman, B. S.; Nierman, W. C.; Kaiser, D.; Slater, S. C.; Durkin, A. S.; Eisen, J. A.; Ronning, C. M.; Barbazuk, W. B.; Blanchard, M.; Field, C.; Halling, C.; Hinkle, G.; Iartchuk, O.; Kim, H. S.; Mackenzie, C.; Madupu, R.; Miller, N.; Shvartsbeyn, A.; Sullivan, S. A.; Vaudin, M.; Wiegand, R.; Kaplan, H. B. *Proc. Natl. Acad. Sci. USA.* **2006**, *103*, 15200-15205.

[55] Garcia, R. O.; Krug, D.; Müller, R. *Methods Enzymol.* **2009**, *458*, 59-91.

[56] Nicolaou, K. C.; Snyder, S. A. *Angew. Chem. Int. Ed.* **2005**, *44*, 1012-44.

[57] Kwan, E. E.; Huang, S. G. *Eur. J. Org. Chem.* **2008**, *2008*, 2671-2688.

[58] Molinski, T. F. *Nat. Prod. Rep.* **2010**, *27*, 321-9.

[59] Godejohann, M.; Daolio, C.; Tseng, L.-H.; Heintz, L. *LaborPraxis.* **2009**, *33*, 46-48.

[60] Molinski, T. F. *Curr. Opin. Biotechnol.* **2010**, *21*, 819-26.

[61] Fukushi, E. *Biosci. Biotechnol. Biochem.* **2006**, *70*, 1803-1812.

[62] Berger, S.; Braun, S. *200 and More NMR Experiments*, 1st ed.; WILEY-VCH: Weinheim; 2004.

[63] Bifulco, G.; Dambruoso, P.; Gomez-Paloma, L.; Riccio, R. *Chem. Rev.* **2007**, *107*, 3744-79.

[64] Butts, C. P.; Jones, C. R.; Towers, E. C.; Flynn, J. L.; Appleby, L.; Barron, N. J. *Org. Biomol. Chem.* **2011**, *9*, 177-84.

[65] Karplus, M. *J. Chem. Phys.* **1959**, *30*, 11.

[66] Matsumori, N.; Kaneno, D.; Murata, M.; Nakamura, H.; Tachibana, K. *J. Org. Chem.* **1999**, *64*, 866-876.

[67] Hoye, T. R.; Suhadolnik, J. C. *J. Am. Chem. Soc.* **1987**, *109*, 4402-4403.

[68] Lee, J.; Kobayashi, Y.; Tezuka, K.; Kishi, Y. *Org. Lett.* **1999**, *1*, 2181-4.

[69] Kobayashi, Y.; Lee, J.; Tezuka, K.; Kishi, Y. *Org. Lett.* **1999**, *1*, 2177-80.

[70] Di Micco, S.; Chini, M. G.; Riccio, R.; Bifulco, G. *Eur. J. Org. Chem.* **2010**, *2010*, 1411-1434.

[71] Jung, M. E.; Johnson, T. W. *Org. Lett.* **1999**, *1*, 1671-4.

[72] Rychnovsky, S. D.; Skalitzky, D. J. *Tetrahedron Lett.* **1990**, *31*, 945-948.

[73] Rychnovsky, S. D.; Richardson, T. I.; Rogers, B. N. *J. Org. Chem.* **1997**, *62*, 2925-2934.

[74] Jundt, L.; Steinmetz, H.; Luger, P.; Weber, M.; Kunze, B.; Reichenbach, H.; Höfle, G. *Eur. J. Org. Chem.* **2006**, *2006*, 5036-5044.

[75] Perez, L. J.; Faulkner, D. J. *J. Nat. Prod.* **2003**, *66*, 247-50.

[76] Yamada, T.; Kitada, H.; Kajimoto, T.; Numata, A.; Tanaka, R. *J. Org. Chem.* **2010**, *75*, 4146-53.

[77] Hungeling, M.; Lechtenberg, M.; Fronczek, F. R.; Nahrstedt, A. *Phytochem.* **2009**, *70*, 270-7.

[78] Kobayashi, Y.; Hayashi, N.; Kishi, Y. *Org. Lett.* **2001**, *3*, 2253-5.

[79] Hayashi, N.; Kobayashi, Y.; Kishi, Y. *Org. Lett.* **2001**, *3*, 2249-52.

[80] Kobayashi, Y.; Hayashi, N.; Tan, C. H.; Kishi, Y. *Org. Lett.* **2001**, *3*, 2245-8.

[81] Duddeck, H.; Diaz Gomez, E. *Chirality*. **2009**, *68*, 51-68.

[82] Dale, J. A.; Dull, D. L.; Mosher, H. S. *J. Org. Chem.* **1969**, *34*, 2543-2549.

[83] Sullivan, G. R.; Dale, J. A.; Mosher, H. S. *J. Org. Chem.* **1973**, *38*, 2143-2147.

[84] Seco, J. M.; Quiñoá, E.; Riguera, R. *Chem. Rev.* **2004**, *104*, 17-118.

[85] Reid, R.; Piagentini, M.; Rodriguez, E.; Ashley, G.; Viswanathan, N.; Carney, J.; Santi, D. V.; Hutchinson, C. R.; McDaniel, R. *Biochem.* **2003**, *42*, 72-9.

[86] Caffrey, P. *ChemBioChem*. **2003**, *4*, 654-7.

[87] Menche, D.; Arikan, F.; Pavlova, O.; Horstmann, N.; Ahlbrecht, W.; Wenzel, S. C.; Jansen, R.; Irschik, H.; Müller, R. *J. Am. Chem. Soc.* **2008**, *130*, 14234-43.

[88] Dalisay, D. S.; Morinaka, B. I.; Skepper, C. K.; Molinski, T. F. *J. Am. Chem. Soc.* **2009**, *131*, 7552-3.

[89] Gross, L.; Mohn, F.; Moll, N.; Meyer, G.; Ebel, R.; Abdel-Mageed, W. M.; Jaspars, M. *Nat. Chem.* **2010**, *2*, 821-825.

[90] Nicolaou, K. C.; Frederick, M. O.; Aversa, R. J. *Angew. Chem. Int. Ed.* **2008**, *47*, 7182-225.

[91] Kita, M.; Uemura, D. *Chem. Rec.* **2010**, *10*, 48-52.

[92] Murata, M.; Naoki, H.; Iwashita, T.; Matsunaga, S.; Sasaki, M.; Yokoyama, A.; Yasumoto, T. *J. Am. Chem. Soc.* **1993**, *115*, 2060-2062.

[93] Zheng, W.; DeMattei, J. A; Wu, J.-P.; Duan, J. J.-W.; Cook, L. R.; Oinuma, H.; Kishi, Y. *J. Am. Chem. Soc.* **1996**, *118*, 7946-7968.

[94] Nonomura, T.; Sasaki, M.; Matsumori, N.; Murata, M.; Tachibana, K.; Yasumoto, T. *Angew. Chem. Int. Ed.* **1996**, *35*, 1675-1678.

[95] Sasaki, M.; Matsumori, N.; Maruyama, T.; Nonomura, T.; Murata, M.; Tachibana, K.; Yasumoto, T. *Angew. Chem. Int. Ed.* **1996**, *35*, 1672-1675.

[96] Gallimore, A. R.; Spencer, J. B. *Angew. Chem. Int. Ed.* **2006**, *45*, 4406-13.

[97] Nicolaou, K. C.; Frederick, M. O. *Angew. Chem. Int. Ed.* **2007**, *46*, 5278-82.

[98] Nicolaou, K. C.; Frederick, M. O.; Burtoloso, A. C. B.; Denton, R. M.; Rivas, F.; Cole, K. P.; Aversa, R. J.; Gibe, R.; Umezawa, T.; Suzuki, T. *J. Am. Chem. Soc.* **2008**, *130*, 7466-76.

[99] Song, H. Y.; Joo, J. M.; Kang, J. W.; Kim, D.-S.; Jung, C.-K.; Kwak, H. S.; Park, J. H.; Lee, E.; Hong, C. Y.; Jeong, S.; Jeon, K.; Park, J. H. *J. Org. Chem.* **2003**, *68*, 8080-8087.

[100] Gerth, K.; Jansen, R.; Kunze, B.; Reifenstahl, G.; Höfle, G.; Irschik, H.; Reichenbach, H.; Thierbach, G. *J. Antibiot.* **1983**, *XXXVI*, 1150-1156.

[101] Jansen, R.; Reifenstahl, G.; Gerth, K.; Reichenbach, H. *Liebigs Ann. Chem.* **1983**, *7*, 1081 - 1095.

[102] Jansen, R.; Sheldrick, W. S.; Höfle, G. *Liebigs Ann. Chem.* **1984**, 78 - 84.

[103] Silakowski, B.; Nordsiek, G.; Kunze, B.; Blöcker, H.; Müller, R. *Chem. Biol.* **2001**, *8*, 59-69.

[104] Höfle, G. *Annual Report GBF 1996*, **1996**.

[105] Weissman, K. J.; Müller, R. *Bioorg. Med. Chem.* **2009**, *17*, 2121-36.

[106] Inanaga, J.; Hirata, K.; Saeki, H.; Katsuki, T.; Yamaguchi, M. *Bull.Chem.Soc.Jpn*. **1979**, *52*, 1989-1993.

[107] Jansen, R.; Kunze, B.; Reichenbach, H.; Höfle, G. *Eur. J. Org. Chem.* **2000**, 913-919.

[108] Irschik, H.; Gerth, K.; Kemmer, T.; Steinmetz, H.; Reichenbach, H. *J. Antibiot.* **1983**, *36*, 6-12.

[109] Yun, B.; Ryoo, I.; Lee, I.; Yoo, I. *Tetrahedron Lett.* **1998**, *39*, 993-996.

[110] Scott, A. I.; Townsend, C. A.; Okada, K.; Kajiwara, M.; Cushley, R. J.; Whitman, P. J. *J. Am. Chem. Soc.* **1974**, 8069

[111] Schraml, J.; Cigler, P. *Mag. Reson. Chem.* **2008**, *46*, 748-55.

[112] Mahmud, T.; Wenzel, S. C.; Wan, E.; Wen, K. W.; Bode, H. B.; Gaitatzis, N.; Müller, R. *ChemBioChem*. **2005**, *6*, 322-30.

[113] Mahmud, T.; Bode, H. B.; Silakowski, B.; Kroppenstedt, R. M.; Xu, M.; Nordhoff, S.; Höfle, G.; Müller, R. *J. Biol. Chem.* **2002**, *277*, 32768-74.

[114] Irschik, H.; Schummer, D.; Höfle, G.; Reichenbach, H.; Steinmetz, H.; Jansen, R. *J. Nat. Prod.* **2007**, *70*, 1060-3.

[115] Jansen, R.; Irschik, H.; Reichenbach, H.; Wray, V.; Höfle, G. *Liebigs Ann. Chem.* **1989**, 213-222.

[116] Steinmetz, H.; Gerth, K.; Jansen, R.; Schläger, N.; Dehn, R.; Reinecke, S.; Kirschning, A.; Müller, R. *Angew. Chem. Int. Ed.* **2011**, *50*, 532-6.

[117] El`Garch, F.; Jeannot, K.; Hocquet, D.; Llanes-Barakat, C.; Plésiat, P. *Antimicrob. Agents Chemother.* **2007**, *51*, 1016-21.

[118] Kern, W. V.; Jürgen A. Bohnert *Antimicrob. Agents Chemother.* **2005**, *49*, 849-852.

[119] Drapeau, C. M. J.; Grilli, E.; Petrosillo, N. *Int. J. Antimicrob. Agents*. **2010**, *35*, 39-44.

[120] Mesaros, N.; Nordmann, P.; Plésiat, P.; Roussel-Delvallez, M.; Van Eldere, J.; Glupczynski, Y.; Van Laethem, Y.; Jacobs, F.; Lebecque, P.; Malfroot, A.; Tulkens, P. M.; Van Bambeke, F. *Clin. Microbiol. Infect.* **2007**, *13*, 560-78.

[121] Falagas, M. E.; Bliziotis, I. A. *Int. J. Antimicrob. Agents*. **2007**, *29*, 630-6.

[122] Franklin, C. S.; Morris, D. S.; Smith, S. D. *Chem. Soc.* **1952**, 4-7.

[123] Widler, L.; Green, J.; Missbach, M.; Susa, M.; Altmann, E. *Bioorg. Med. Chem. Lett.* **2001**, *11*, 849-852.

[124] Maskey, R. P.; Asolkar, R. N.; Kapaun, E.; Wagner-Döbler, I.; Laatsch, H. *J. Antibiot.* **2002**, *55*, 643-649.

[125] Böröczky, K.; Laatsch, H.; Wagner-Döbler, I.; Stritzke, K.; Schulz, S. *Chem. Biodivers.* **2006**, *3*, 622-34.

[126] Meganathan, R. *FEMS Microbiol. Lett.* **2001**, *203*, 131-9.

[127] Jansen, R.; Irschik, H.; Reichenbach, H.; Höfle, G. *Liebigs Ann. Chem.* **1997**, *LXXX*, 1725- 1732.

[128] Irschik, H.; Jansen, R.; Gerth, K.; Höfle, G.; Reichenbach, H. *J. Antibiot.* **1995**, *48*, 962-966.

[129] Jansen, R.; Irschik, H.; Reichenbach, H.; Wray, V.; Höfle, G. *Liebigs Ann. Chem.* **1994**, *LIX*, 759-773.

[130] Irschik, H.; Jansen, R.; Gerth, K.; Höfle, G.; Reichenbach, H. *J. Antibiot.* **1995**, *48*, 31-35.

[131] Gerth, K.; Bedorf, N.; Irschik, H.; Reichenbach, H.; Höfle, G. *J. Antibiot.* **1993**, *47*, 23-31.

[132] Irschik, H.; Jansen, R.; Gerth, K.; Höfle, G.; Reichenbach, H. *J. Antibiot.* **1995**, *48*, 886-887.

[133] Gerth, K.; Steinmetz, H.; Höfle, G.; Jansen, R. *Angew. Chem. Int. Ed.* **2008**, *47*, 600-602.

[134] Igarashi, Y.; Iwashita, T.; Fujita, T.; Naoki, H.; Yamakawa, T.; Yoshida, R.; Furumai, T. *J. Antibiot.* **2003**, *56*, 705-708.

[135] Cai, P.; Kong, F.; Fink, P.; Ruppen, M. E.; Williamson, R. T.; Keiko, T. *J. Nat. Prod.* **2007**, *70*, 215-219.

[136] Wenzel, S. C.; Müller, R. *Nat. Prod. Rep.* **2007**, *24*, 1211-24.

[137] Ronning, C. M.; Nierman, W. C. In *Myxobacteria: Multicellularity and Differentiation*; Whitworth, D., Ed.; ASM Press: Washington DC, 2007; pp. 285-298.

[138] Thomas, S. H.; Wagner, R. D.; Arakaki, A. K.; Skolnick, J.; Kirby, J. R.; Shimkets, L. J.; Sanford, R. A.; Löffler, F. E. *PloS one*. **2008**, *3*, e2103.

[139] Bode, H. B.; Müller, R. In *Myxobacteria: Multicellularity and Differentiation.*; Whitworth, D., Ed.; ASM Press: Washington DC, 2077; pp. 259-282.

6 Appendix

6.1 Author´s Effort in Publication

Roimatacene, a Polyunsaturated Carboxylic Acid from *Cystobacter ferrugineus* Cb G35

WZ monitored the production of roimatacene (**26**) during all fermentations, developed the isolation strategie, as well as planed and carried out all derivatization experiments. The molecular modelling was done by R. Jansen, while the complete structure elucidation and the comparison of the modelling results were done by WZ. The feeding experiments were done by K. I. Mohr, while the isolation and analyses was done by WZ. The antimicrobial screening was conducted by K. I. Mohr and the proliferation assays in the lab of Florenz Sasse. WZ wrote the manuscript.

Six *p*-Hydroxyacetophenone Amides from *Cystobacter ferrugineus* Cb G35

The secondary metabolite production during fermentation was monitored by WZ. The isolation and the structure elucidation, as well as planning and analysing the feeding experiments were done by the author. WZ wrote the manuscript.

Sulfangolids, Macrolide Sulfate Esters from Sorangium cellulosum

The fermentation of strain So ce666 (sulfangolid A), So ce192 (sulfangolid B) and So ce12 (sulfangolid C) were done by H. Irschik. The fermentation of So ce1375 was carried out by K. Gerth. The isolation of sulfangolid B was done by R. Jansen and of sulfangolid D by M. Herrmann. The isolation of sulfangolid A and C as it is presented here and in the manuscript was planned by R. Jansen and carried out by WZ during the Diploma Thesis. The verification of the proposed structures of **25a-d** by NMR data and the presented NMR tables were done by the author. The relative configuration was done by WZ and extensively discussed with R. Jansen. The molecular modelling was done by R. Jansen. The feeding experiments were carried out and analysed by WZ. The manuscript was written by WZ.

6.2 Spectra

6.2.1 Spectra of Roimatacene (26)

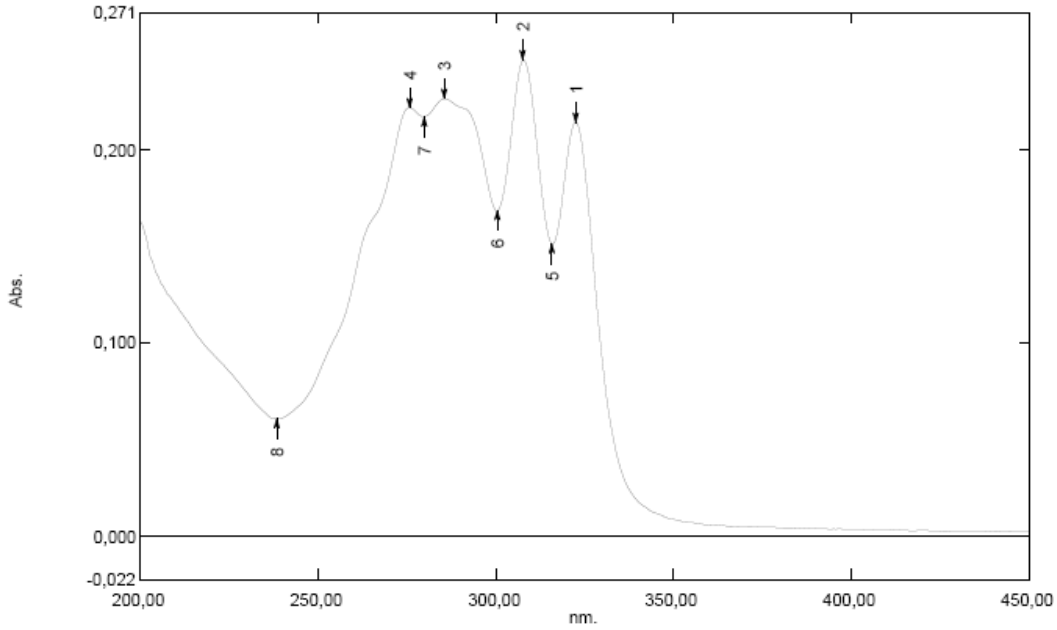

Spectrum 1: UV spectrum of roimatacene (**26**) in methanol (*c* = 0.5 mg/100 mL).

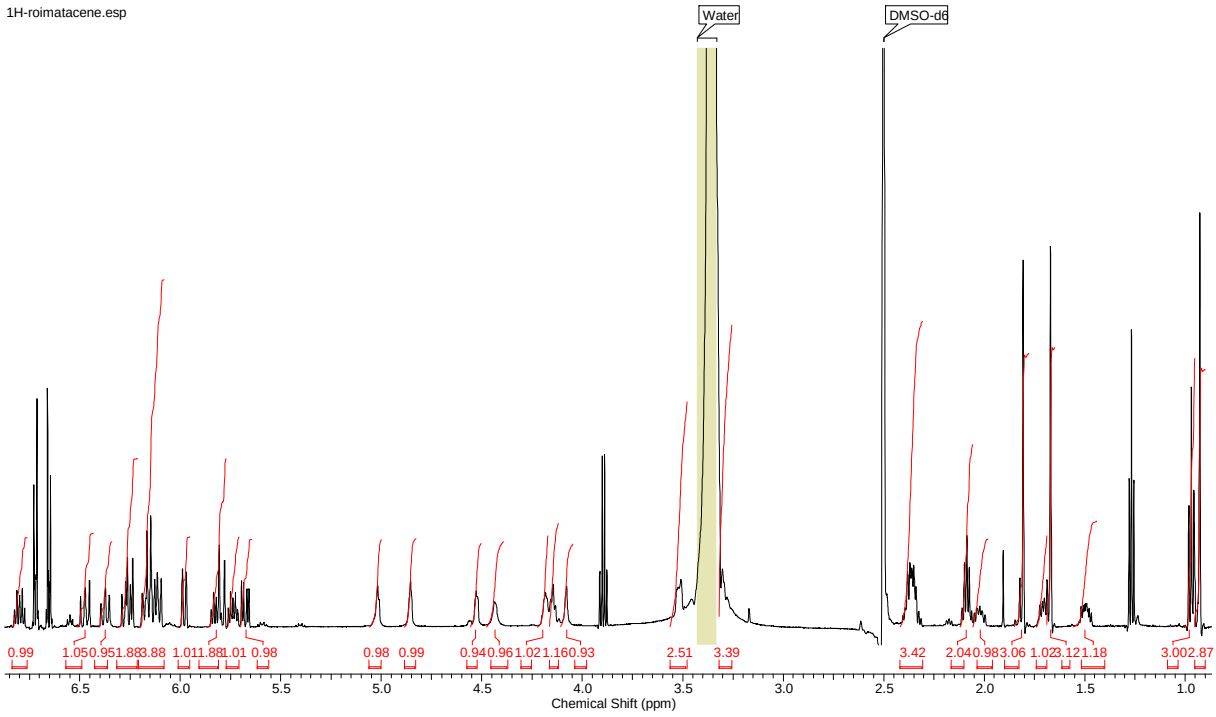

Spectrum 2: ^{1}H NMR spectrum of roimatacene (**26**) (^{1}H 600MHz, ^{13}C 150 MHz, [D_6]DMSO).

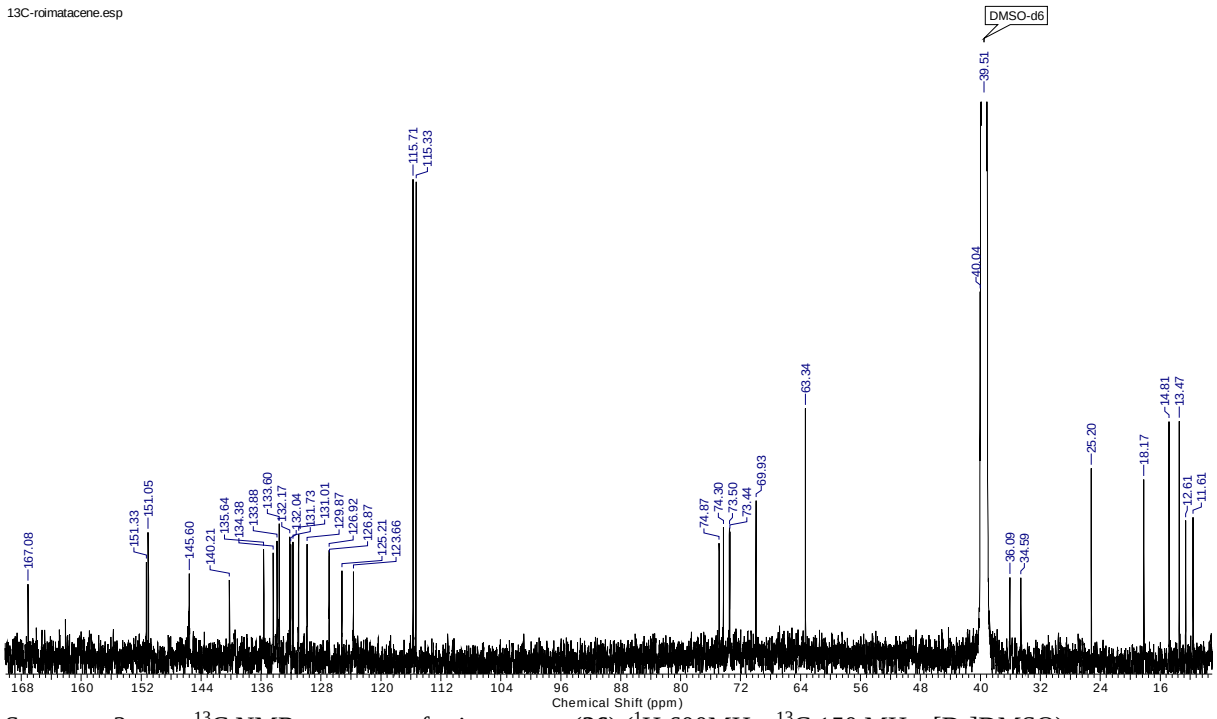

Spectrum 3: ^{13}C NMR spectrum of roimatacene (**26**) (^{1}H 600MHz, ^{13}C 150 MHz, [D_6]DMSO).

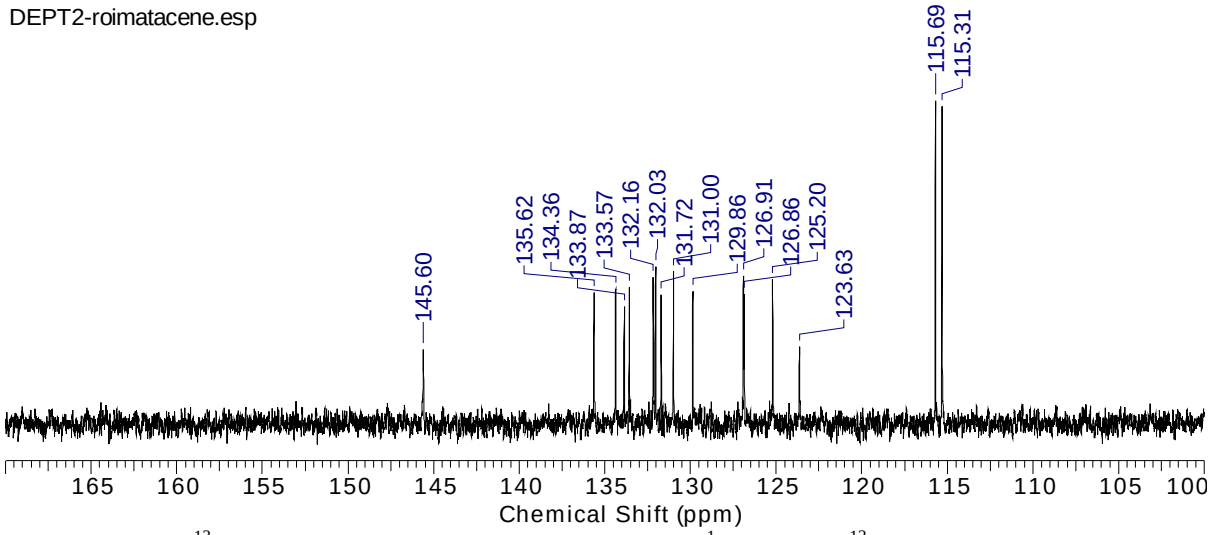

Spectrum 4: ^{13}C DEPT NMR spectrum of roimatacene (**26**) (^{1}H 600MHz, ^{13}C 150 MHz, [D_6]DMSO).

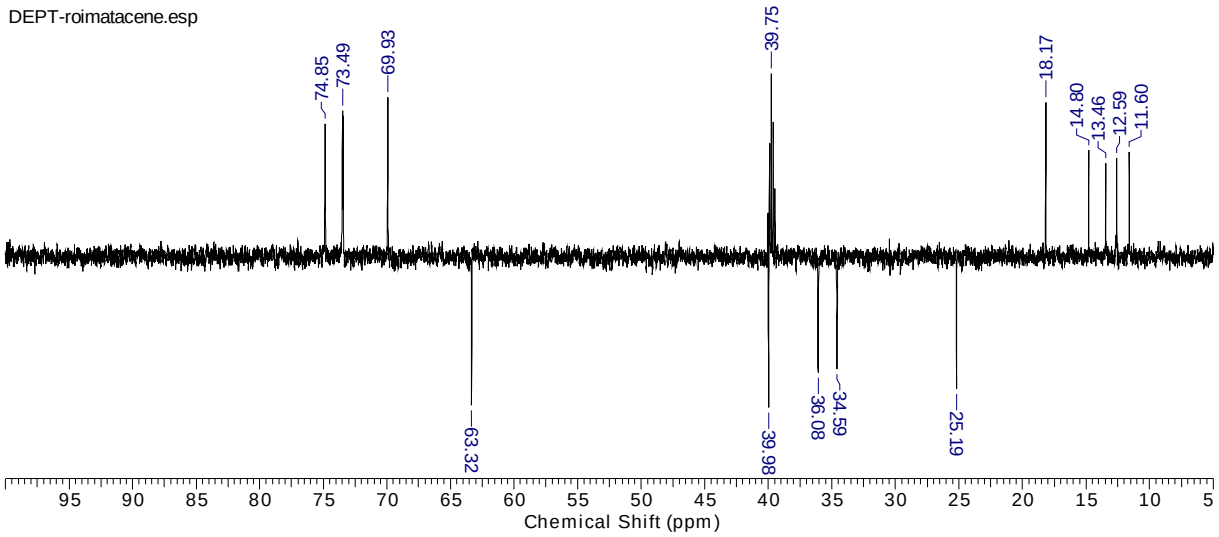

Spectrum 5: ^{13}C DEPT NMR spectrum of roimatacene (**26**) (^{1}H 600MHz, ^{13}C 150 MHz, [D_6]DMSO).

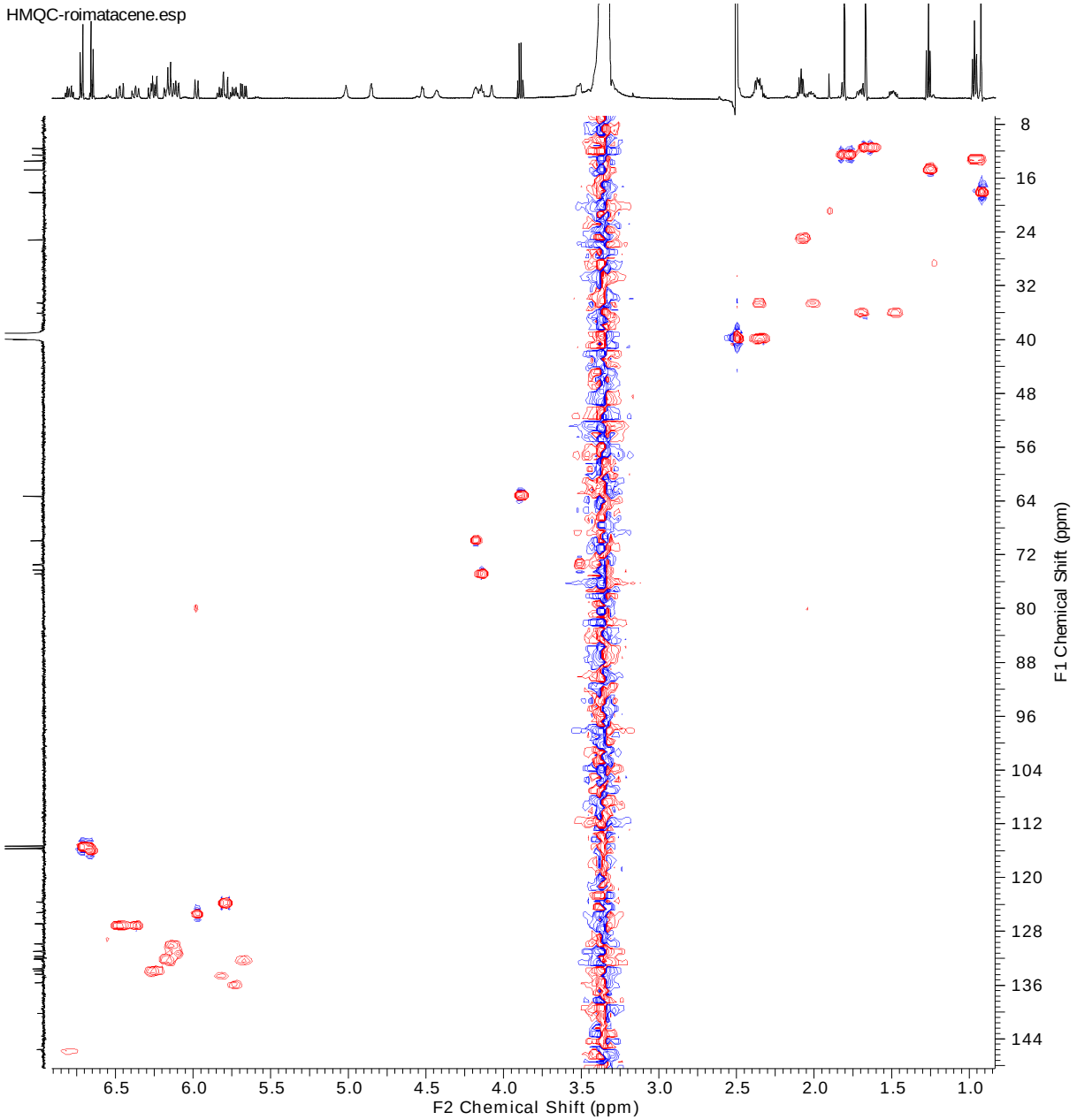

Spectrum 6: $^{1}H,^{13}C$ HMQC NMR spectrum of roimatacene (**26**) (^{1}H 600MHz, ^{13}C 150 MHz, [D_6]DMSO).

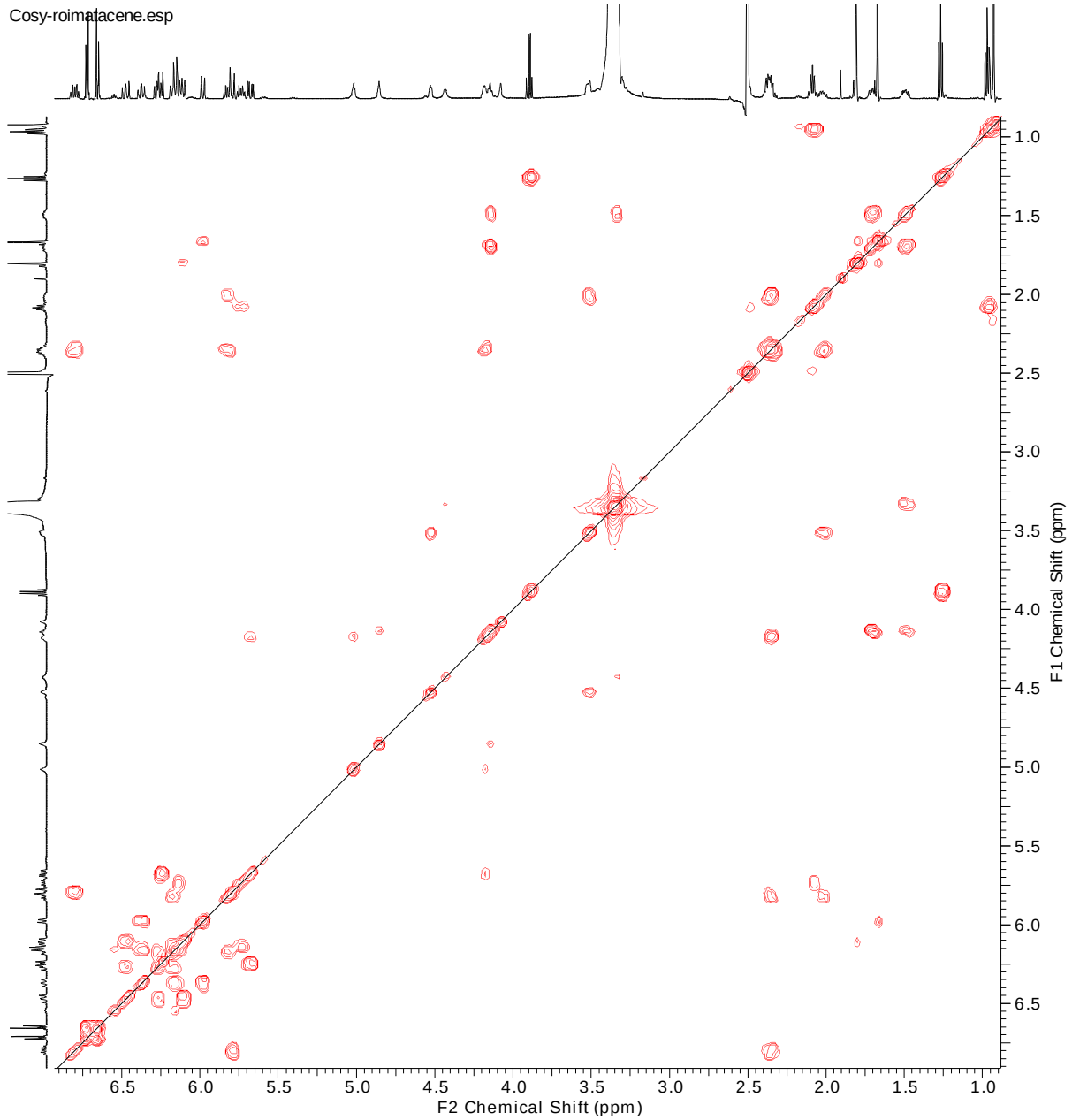

Spectrum 7: $^{1}H,^{1}H$ COSY NMR spectrum of roimatacene (**26**) (^{1}H 600MHz, ^{13}C 150 MHz, [D_6]DMSO).

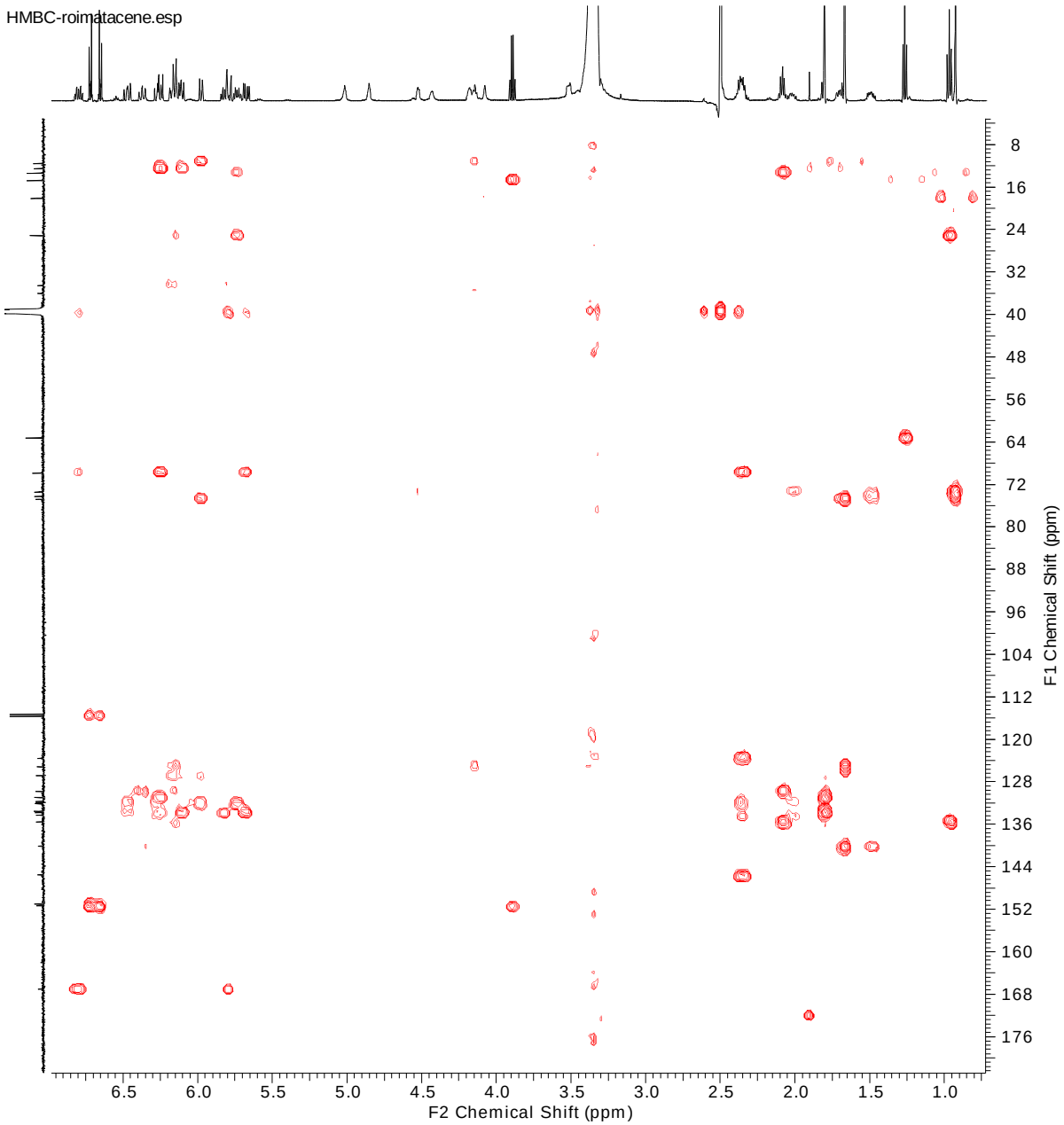

Spectrum 8: $^{1}H,^{13}C$ HMBC NMR spectrum of roimatacene (**26**) (^{1}H 600MHz, ^{13}C 150 MHz, [D_6]DMSO).

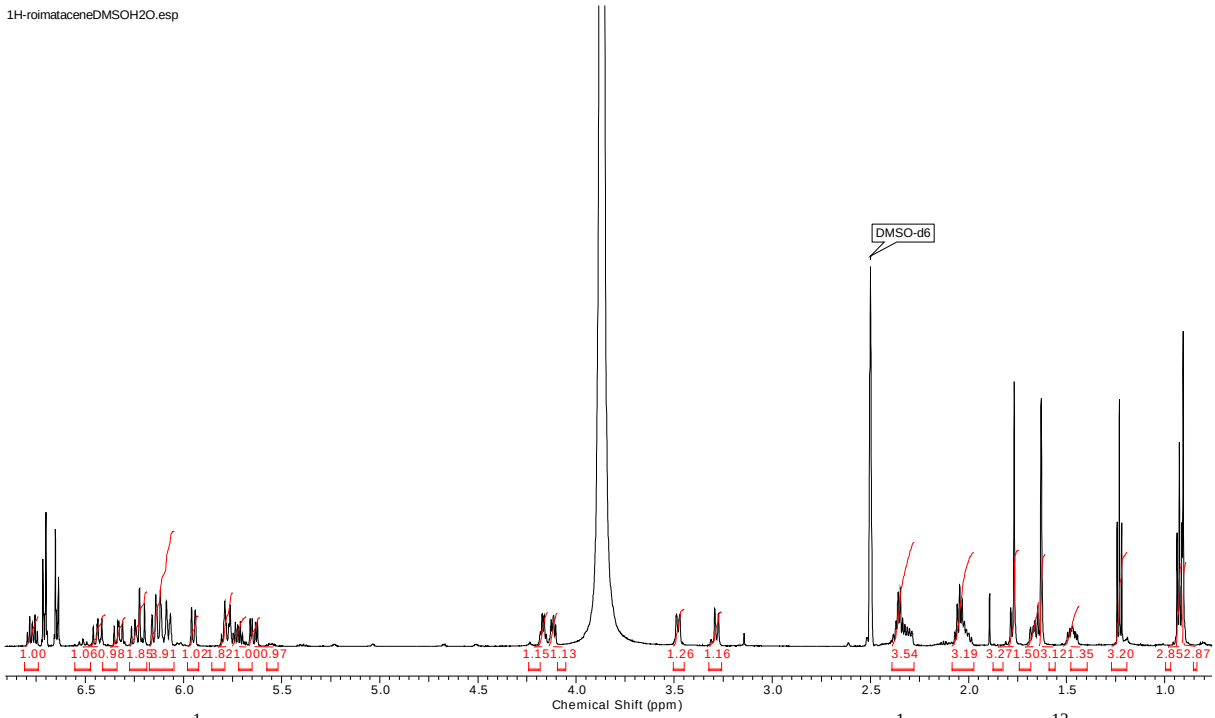

Spectrum 9: ^{1}H NMR spectrum of roimatacene (**26**) after H/D exchange (^{1}H 600 MHz,^{13}C 150 MHz, [D_6]DMSO).

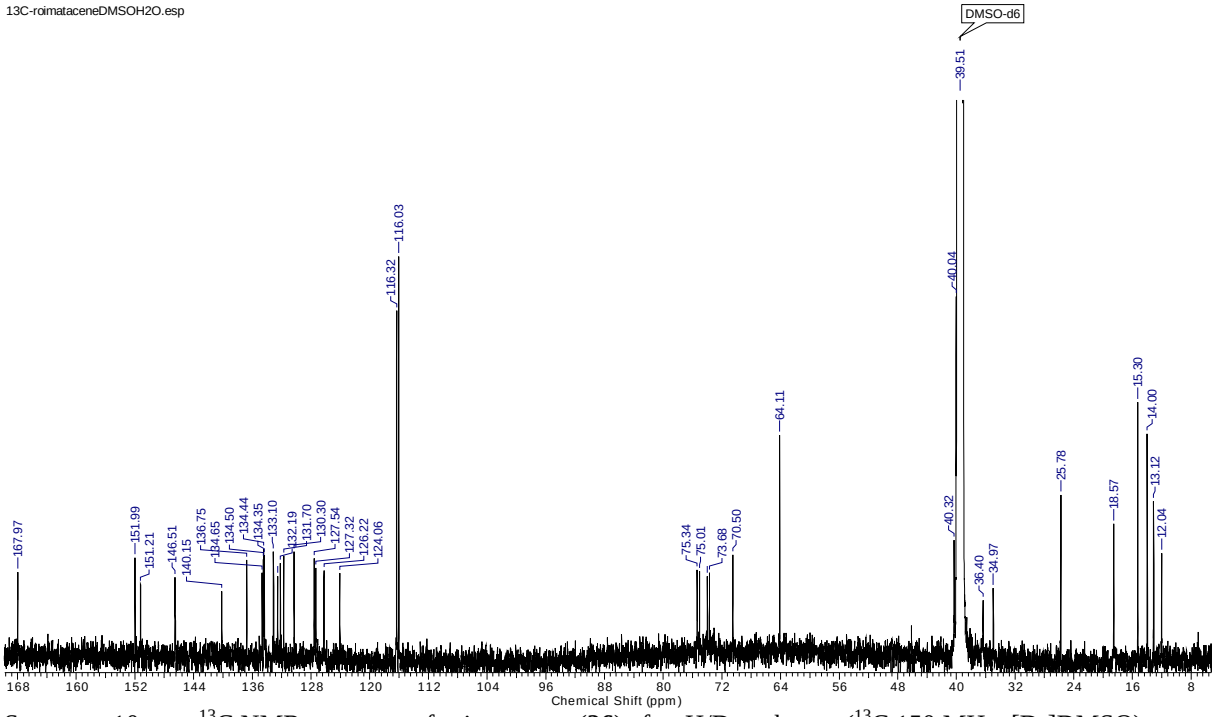

Spectrum 10: ^{13}C NMR spectrum of roimatacene (**26**) after H/D exchange (^{13}C 150 MHz, [D_6]DMSO).

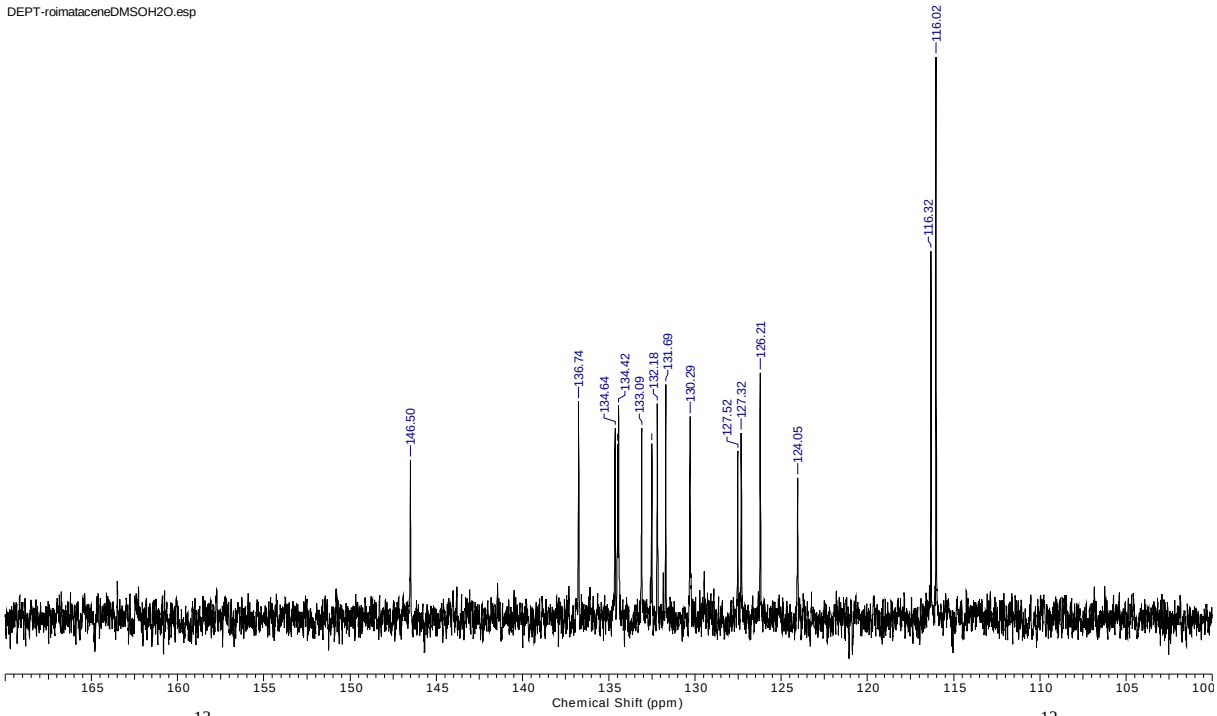

Spectrum 11: ^{13}C DEPT NMR spectrum of roimatacene (**26**) after H/D exchange (^{13}C 150 MHz, [D6]DMSO).

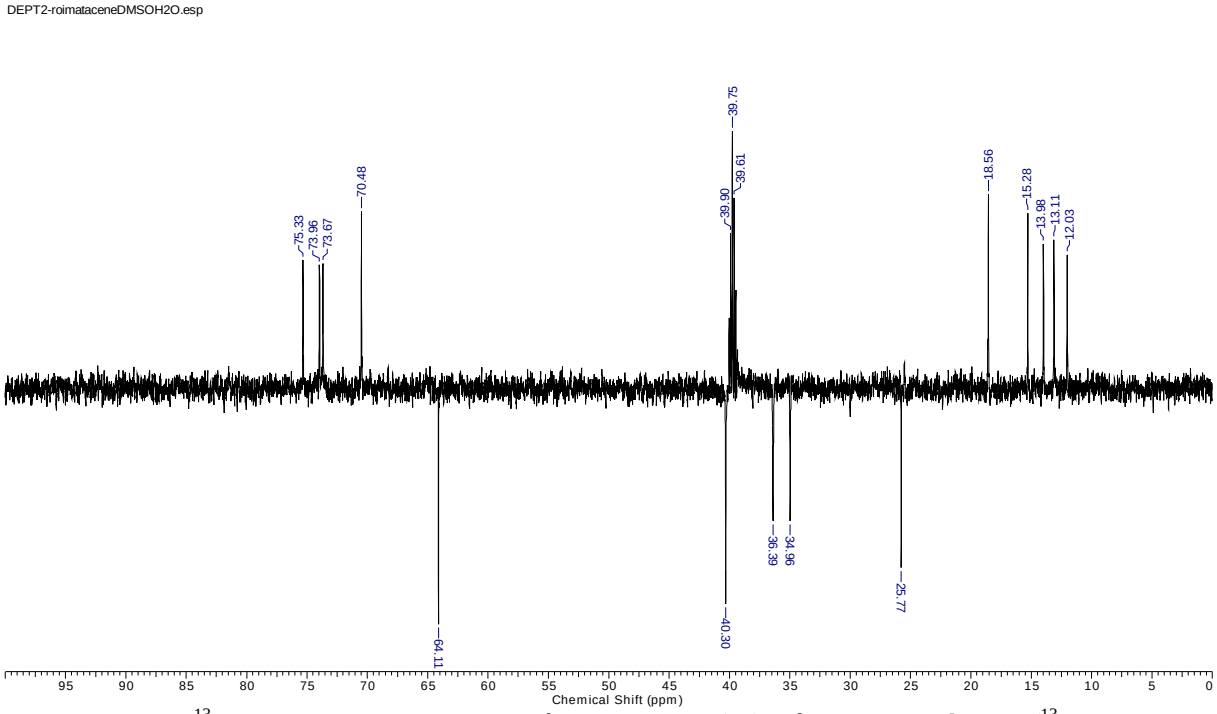

Spectrum 12: ^{13}C DEPT NMR spectrum of roimatacene (**26**) after H/D exchange (^{13}C 150 MHz, [D_6]DMSO).

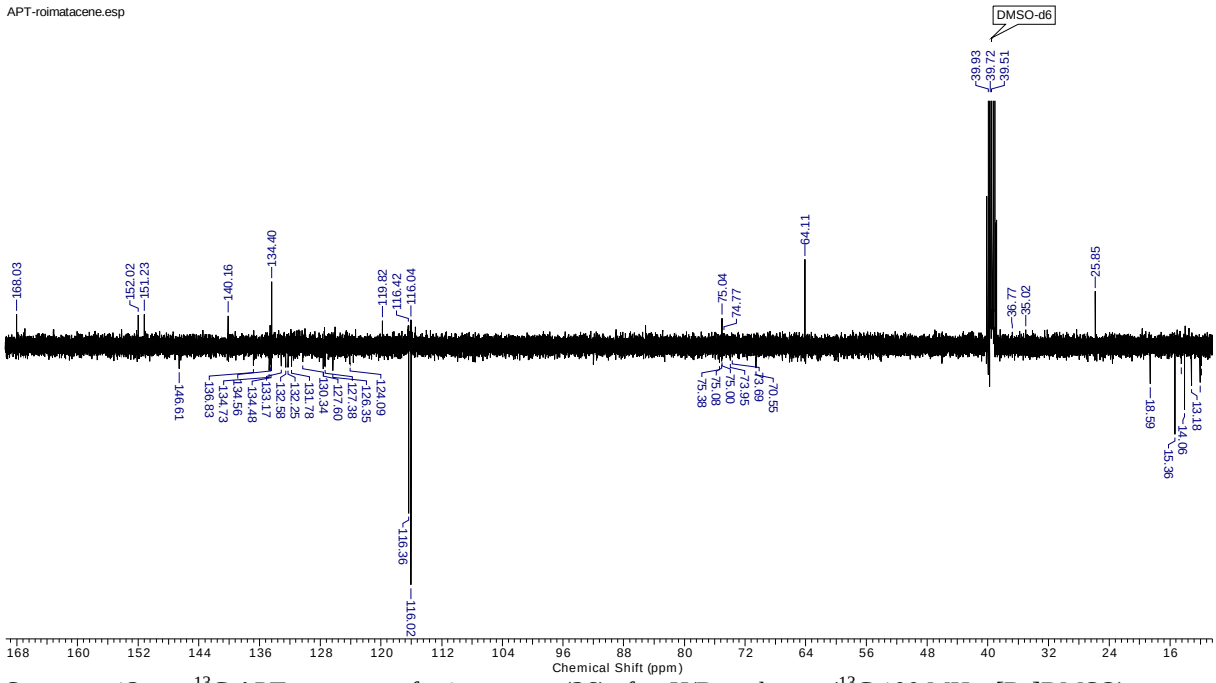

Spectrum 13: ^{13}C APT spectrum of roimatacene (**26**) after H/D exchange (^{13}C 100 MHz, [D_6]DMSO).

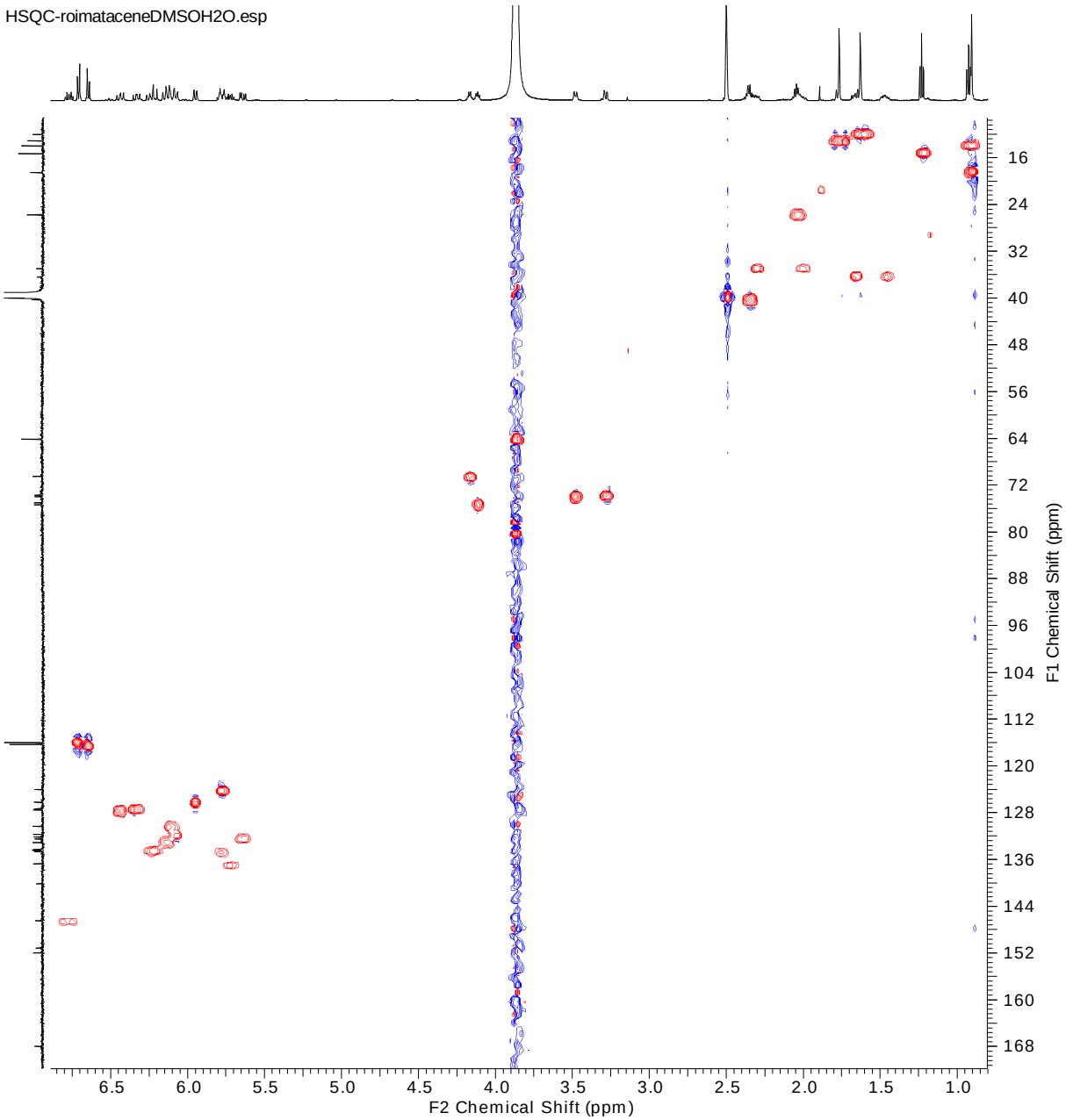

Spectrum 14: $^{1}H,^{13}C$ HSQC NMR spectrum of roimatacene (**26**) after H/D exchange (^{1}H 600 MHz, ^{13}C 150 MHz, [D_6]DMSO).

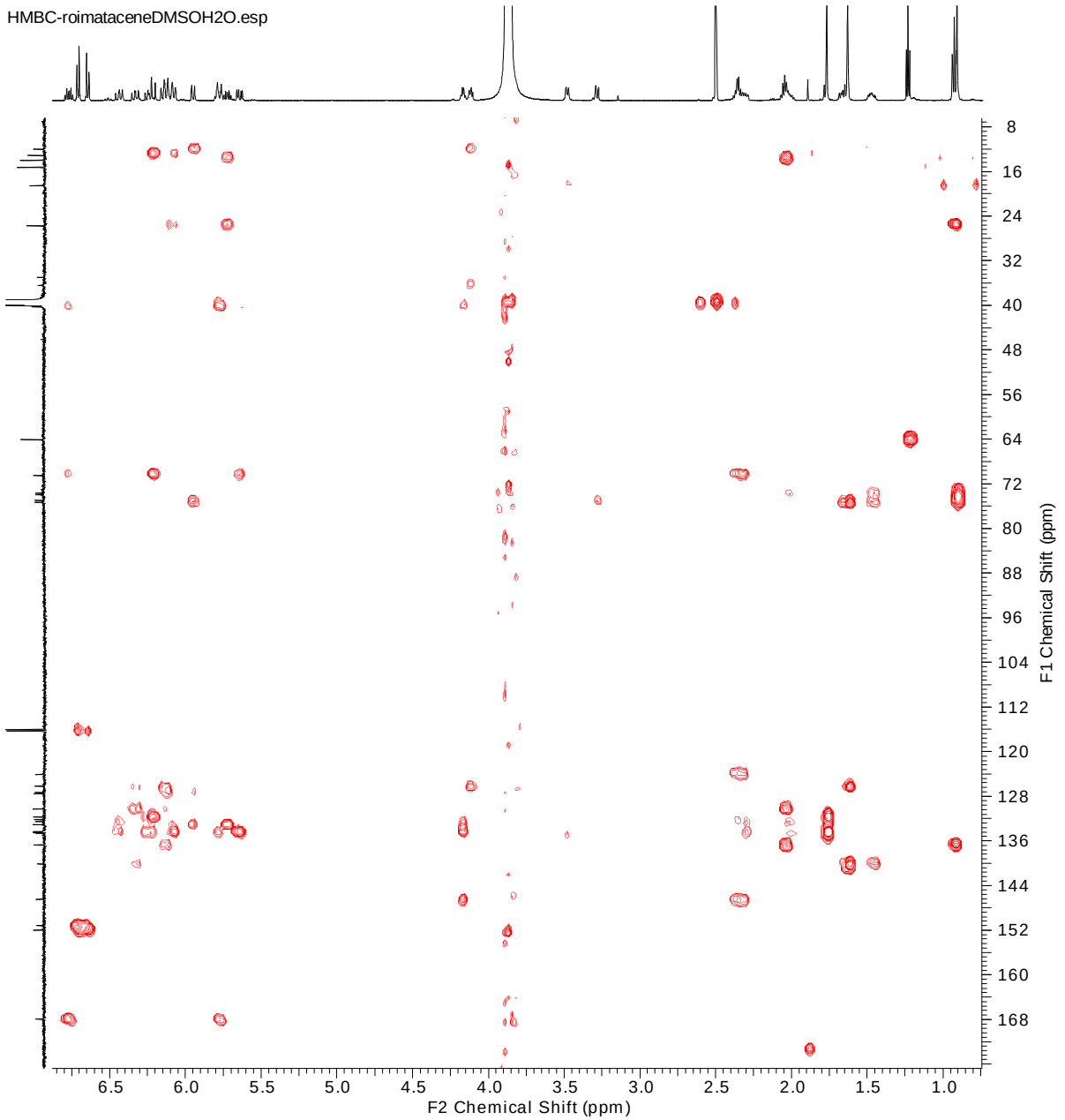

Spectrum 15: $^{1}H,^{13}C$ HMBC NMR spectrum of roimatacene (**26**) after H/D exchange (^{1}H 600 MHz,^{13}C 150 MHz, [D_6]DMSO).

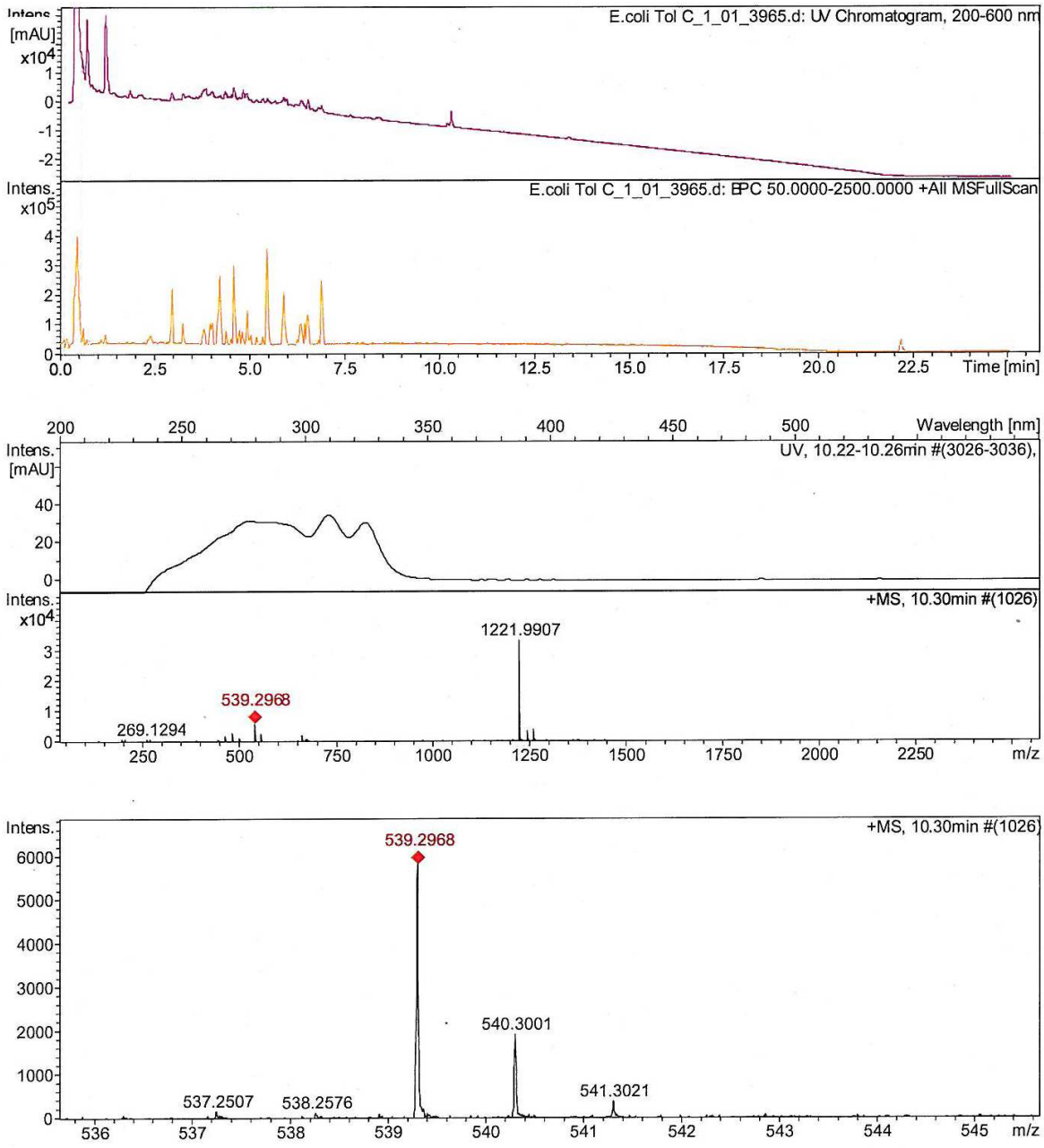

Spectrum 16. HPLC-HRESIMS chromatogram of the supernatant of the *E. coli* tolC MIC dilution assay after incubation, the supernatant was centrifuged (5 min, 3000 g) and 5 µL were analyzed. The peak at 10.3 min showed the roimatacene (**26**) characteristic chromophore and the mass spectrum represented the molecular ion of $[M+Na]^+$ (calc. 539.2979).

6.2.2 Spectra of *p*-Hydroxyacetophenones (34a-f)

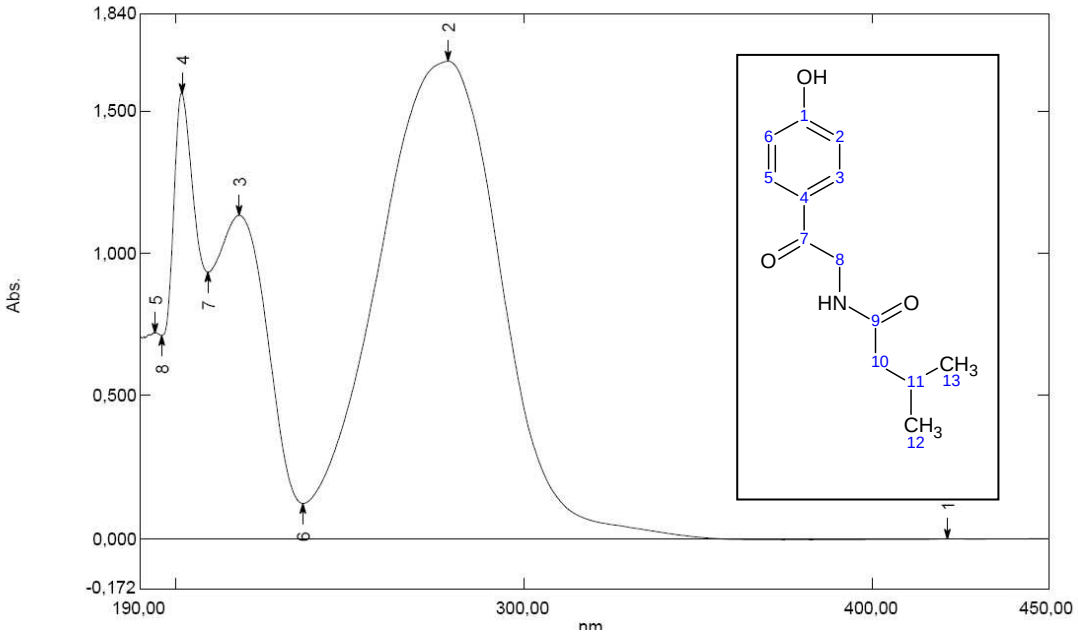

Spectrum 17: UV spectrum of *p*-hydroxyacetophenone *iso*-butanamide (**34a**) in methanol (*c* = 0.5 mg/100 mL).

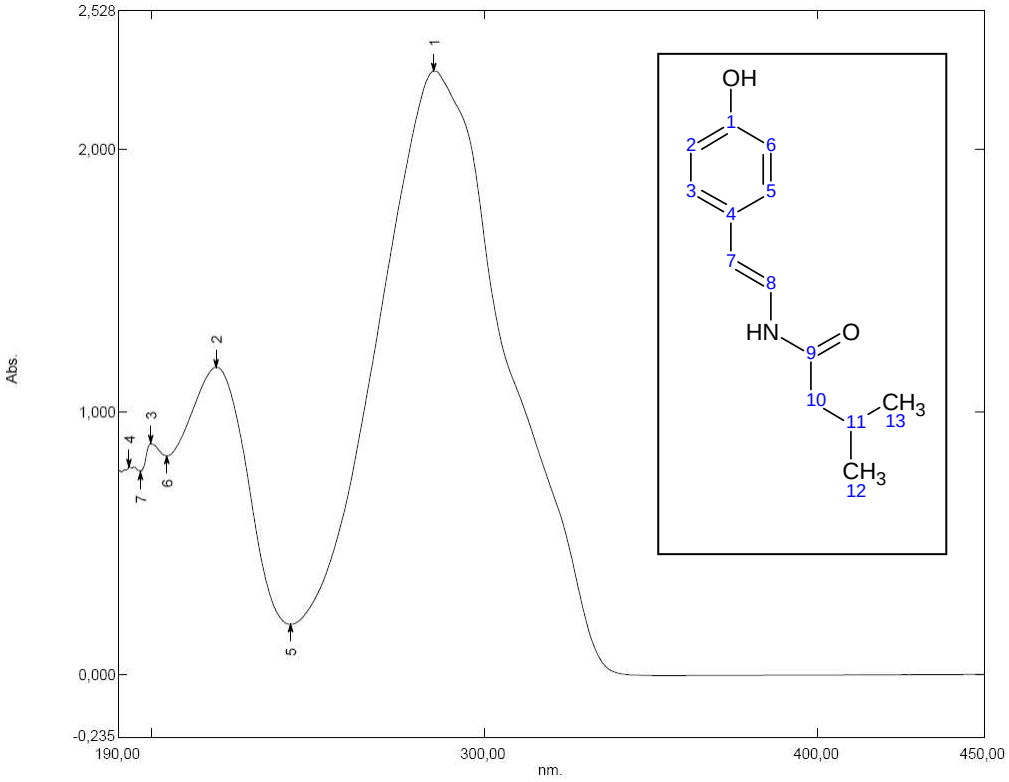

Spectrum 18: UV spectrum of *p*-hydroxyethenphenyl-*iso*-butanamide (**34d**) in methanol (*c* = 1 mg/100mL).

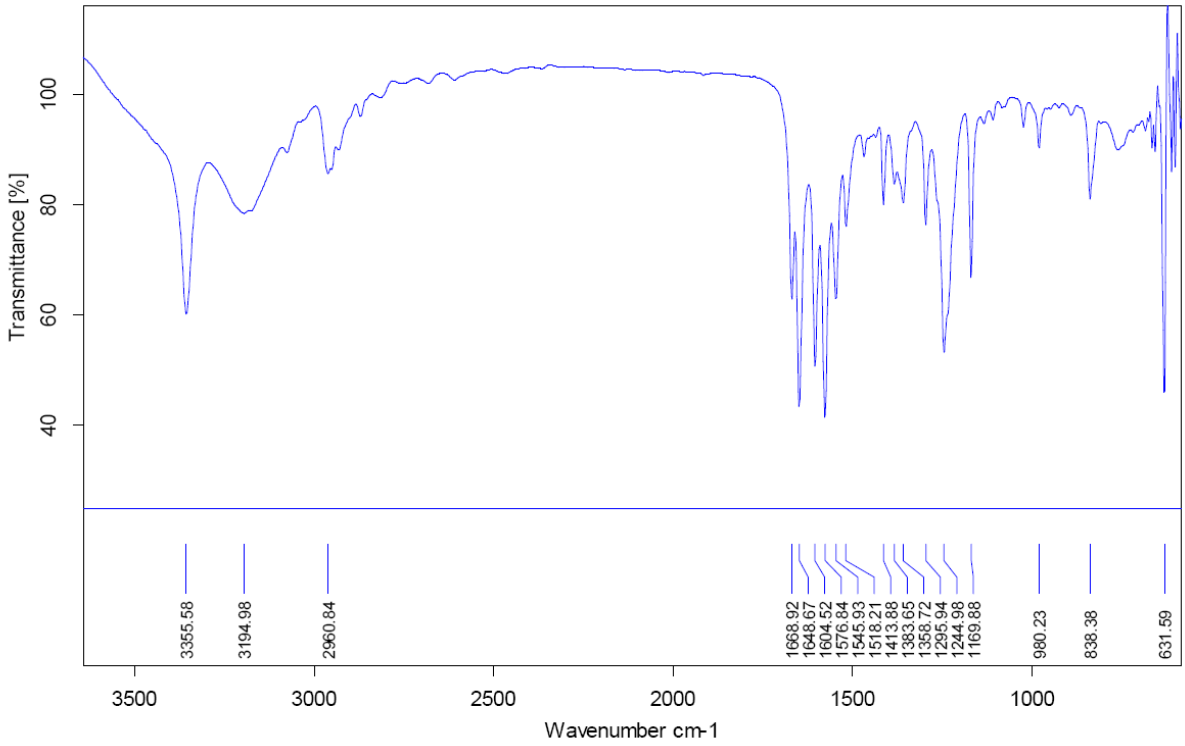

Spectrum 19: IR spectrum of compound *p*-hydroxyacetophenone *iso*-butanamide (**34a**) (0.5 mg, KBr).

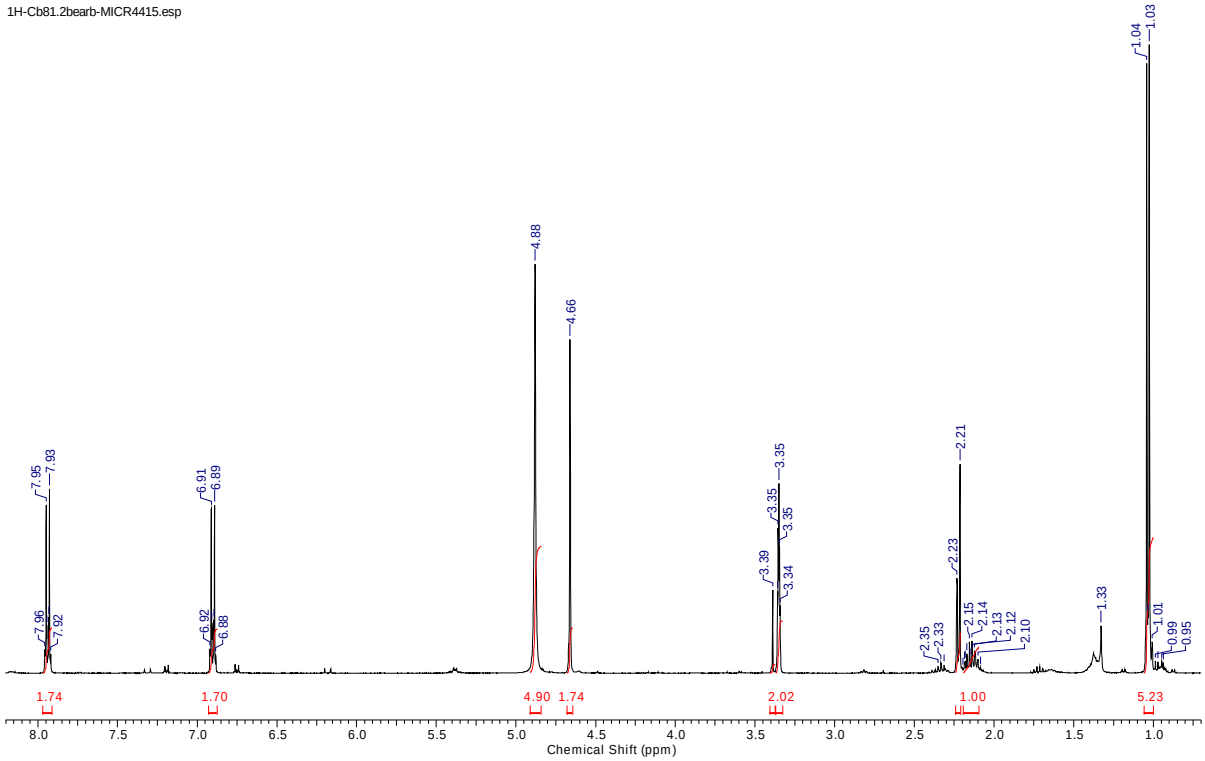

Spectrum 20: ^{1}H NMR spectrum of *p*-hydroxyacetophenone *iso*-butanamide (**34a**) (^{1}H 400 MHz, CD_3OD).

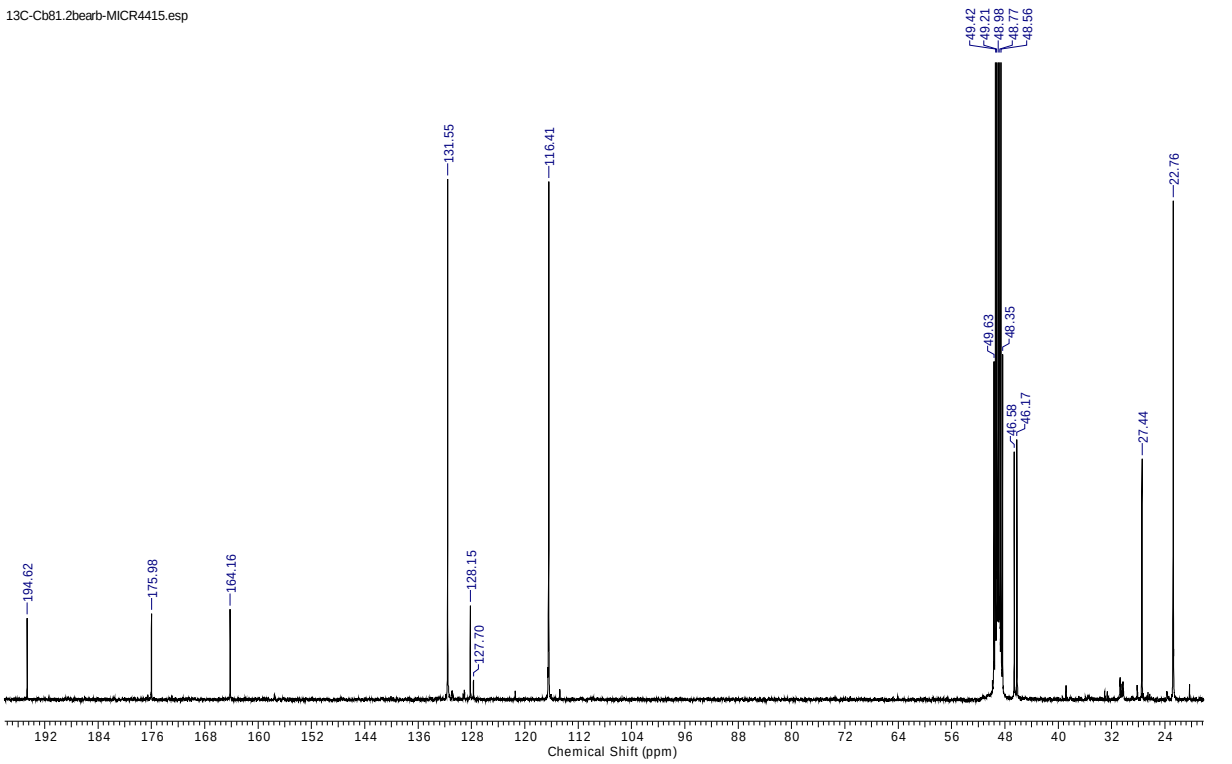

Spectrum 21: ^{13}C NMR spectrum of *p*-hydroxyacetophenone *iso*-butanamide (**34a**) (^{13}C 100 MHz, CD_3OD).

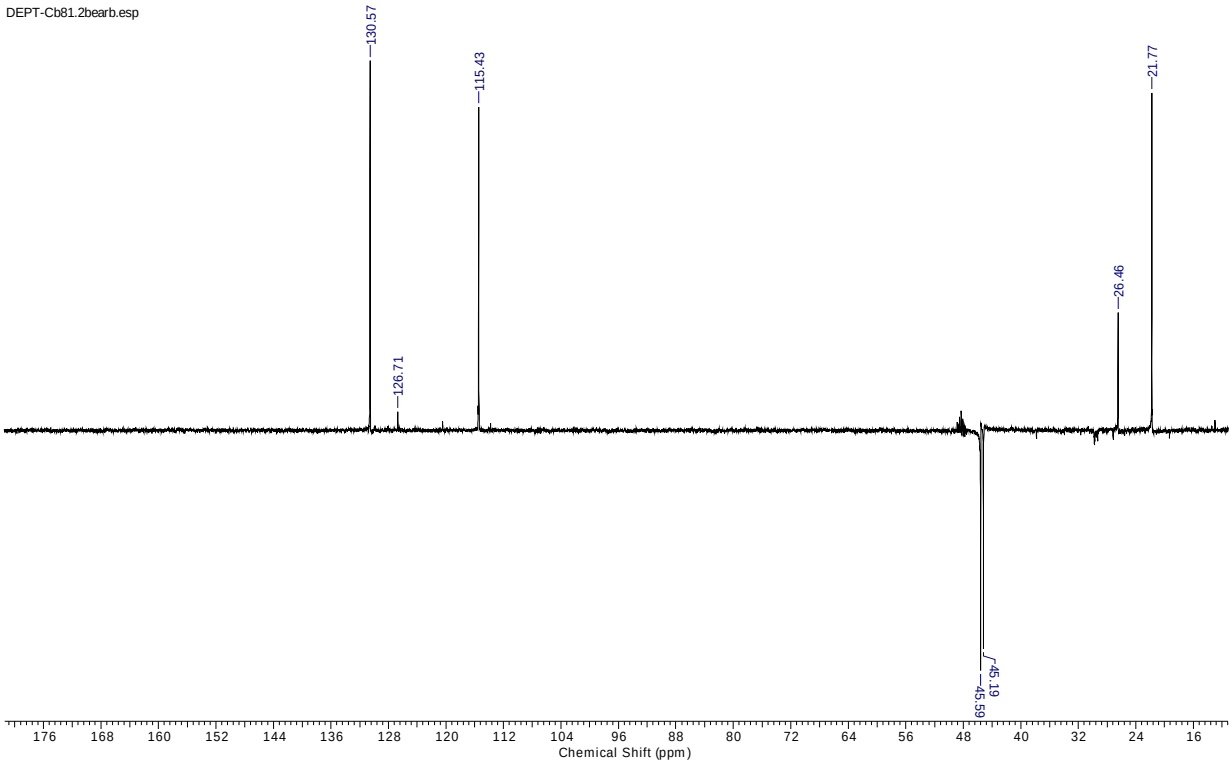

Spectrum 22: DEPT NMR spectrum of *p*-hydroxyacetophenone *iso*-butanamide (**34a**) (^{1}H 400 MHz, ^{13}C 100 MHz, CD_3OD).

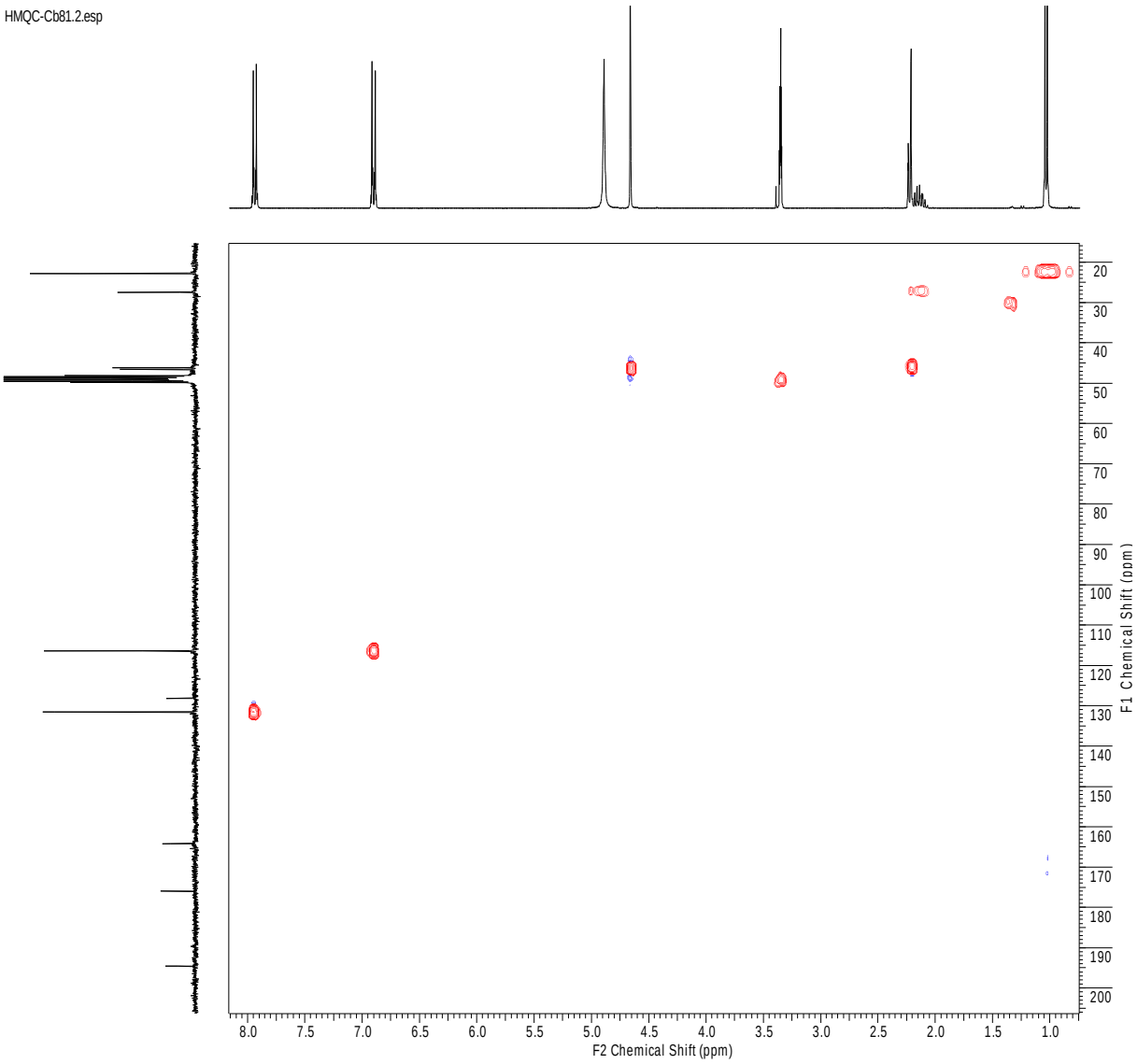

Spectrum 23: $^{1}H,^{13}C$ HMQC NMR spectrum of *p*-hydroxyacetophenone *iso*-butanamide (**34a**) (^{1}H 400 MHz, ^{13}C 100 MHz, CD_3OD).

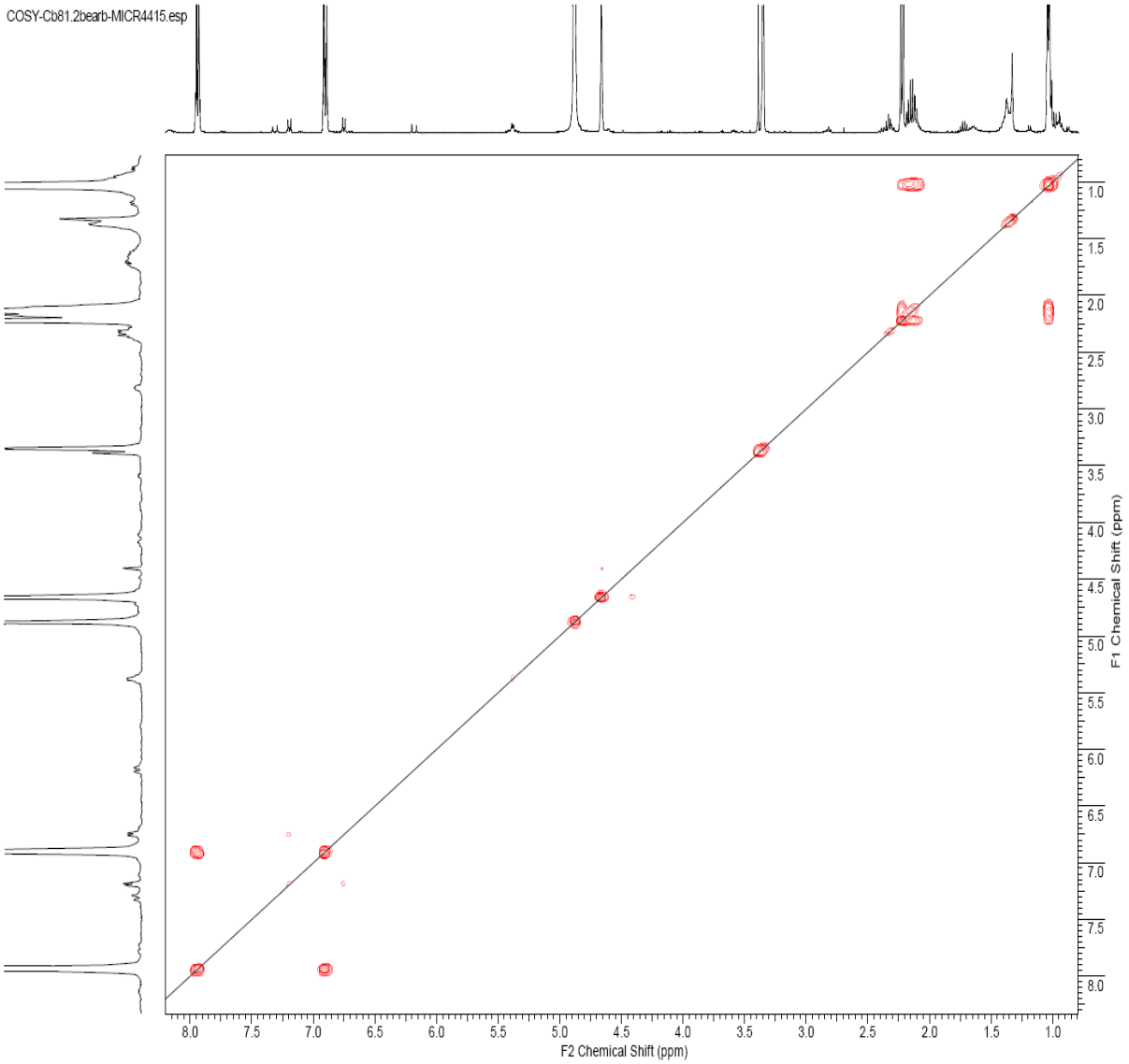

Spectrum 24: $^{1}H,^{1}H$ COSY NMR spectrum of *p*-hydroxyacetophenone *iso*-butanamide (**34a**) (^{1}H 400 MHz, ^{13}C 100 MHz, CD_3OD).

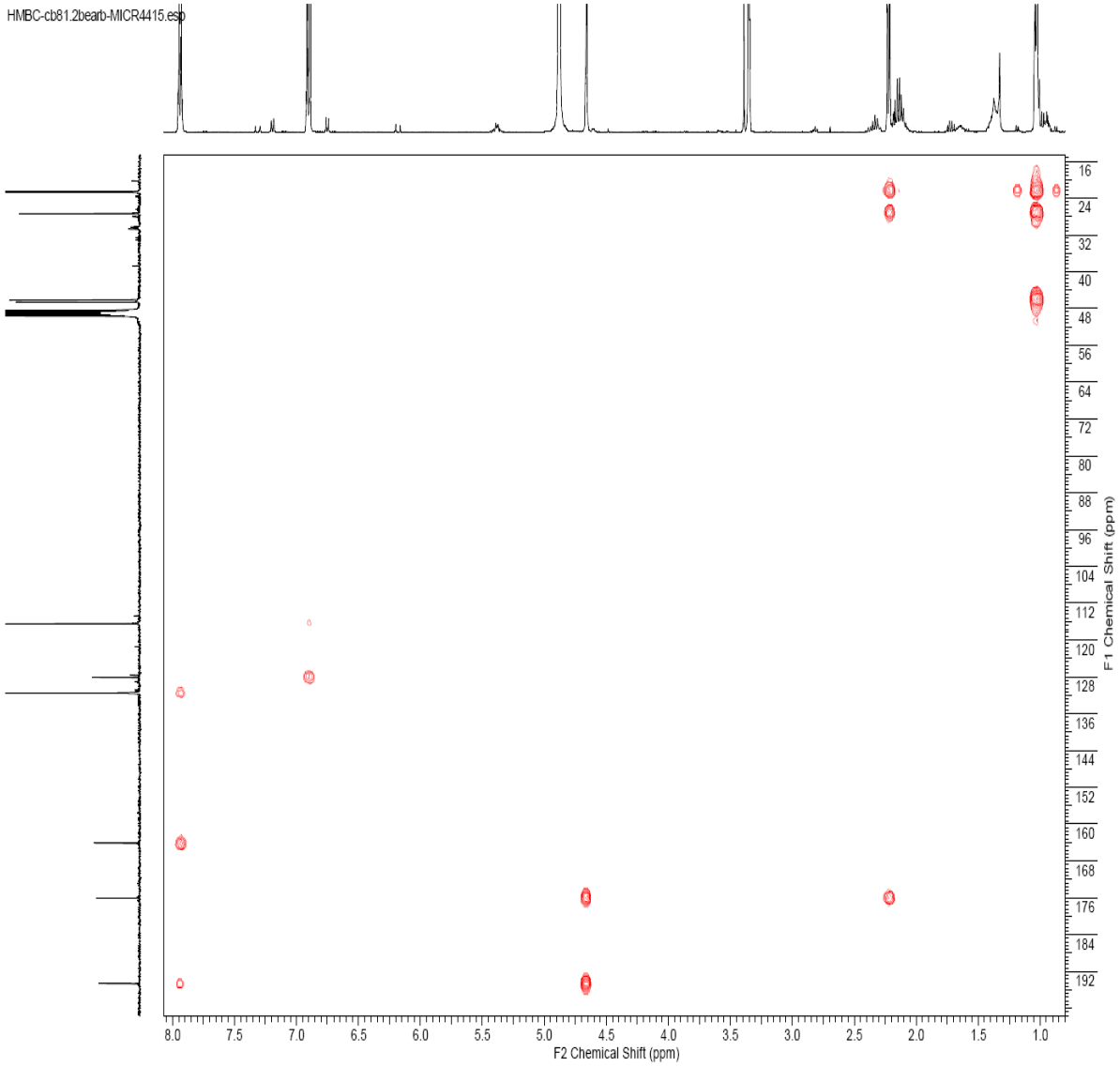

Spectrum 25: $^{1}H,^{13}C$ HMBC NMR spectrum of *p*-hydroxyacetophenone *iso*-butanamide (**34a**) (^{1}H 400 MHz, ^{13}C 100 MHz, CD_3OD).

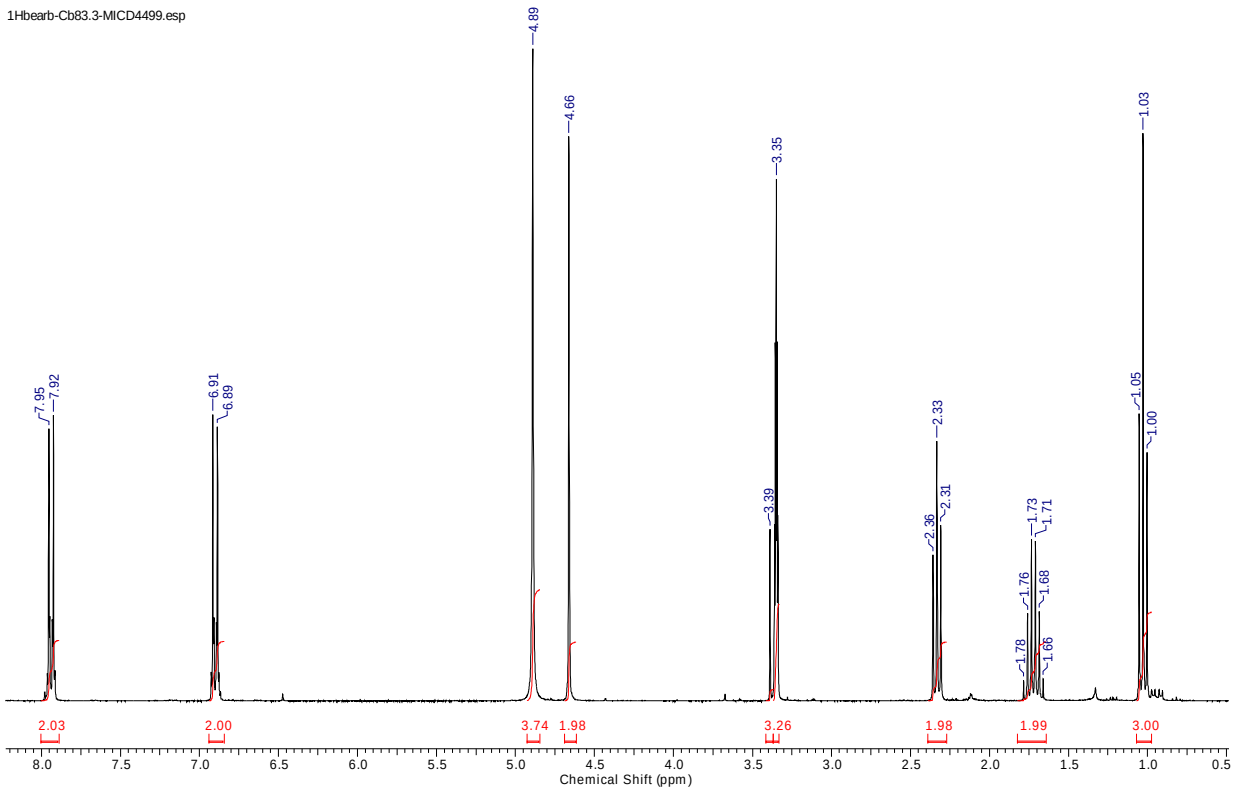

Spectrum 26: ^{1}H NMR spectrum of *p*-hydroxyacetophenone *n*-butanamide (**34b**) (^{1}H 300 MHz, CD_3OD).

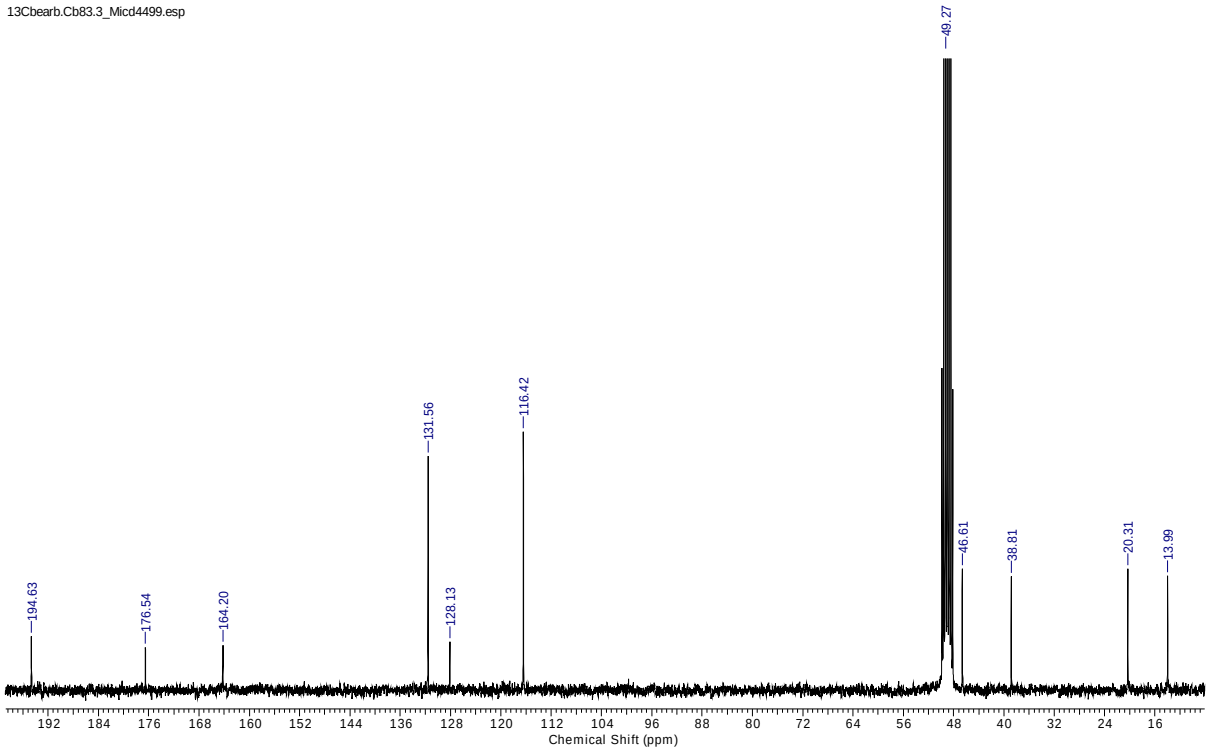

Spectrum 27: ^{13}C NMR spectrum of *p*-hydroxyacetophenone *n*-butanamide (**34b**) (^{13}C 75 MHz, CD_3OD).

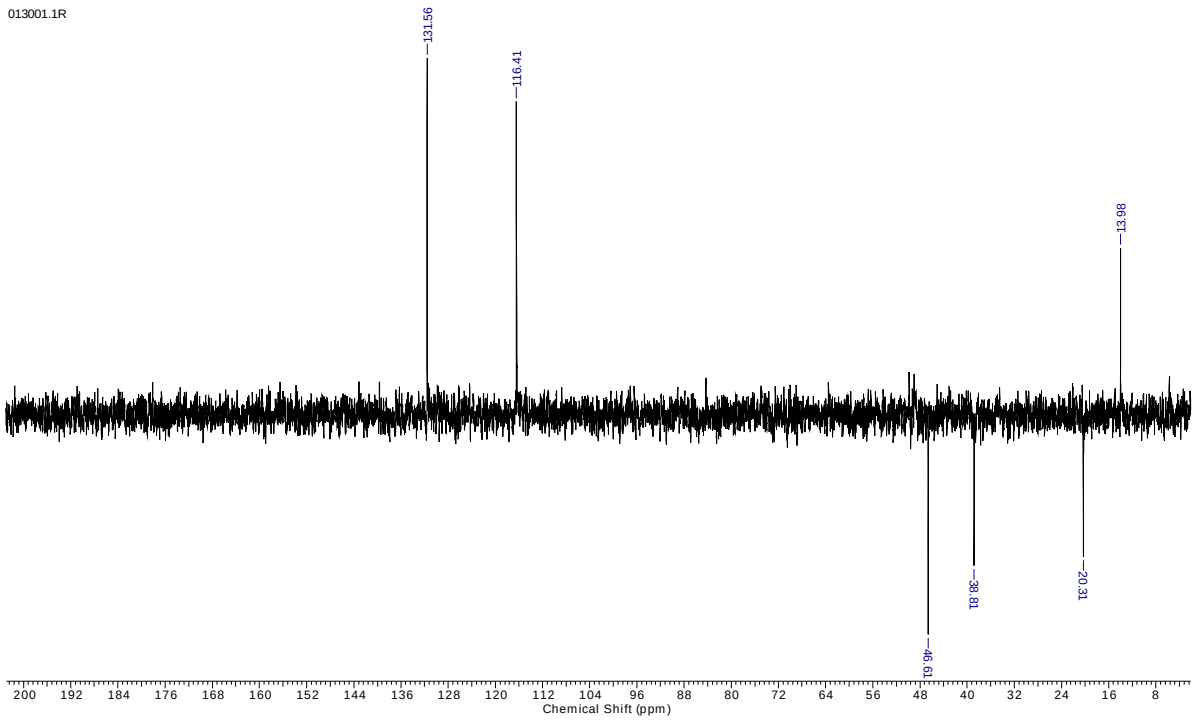

Spectrum 28: ^{13}DEPT NMR spectrum of *p*-hydroxyacetophenone *n*-butanamide (**34b**) (^{1}H 300 MHz, ^{13}C 75 MHz, CD_3OD).

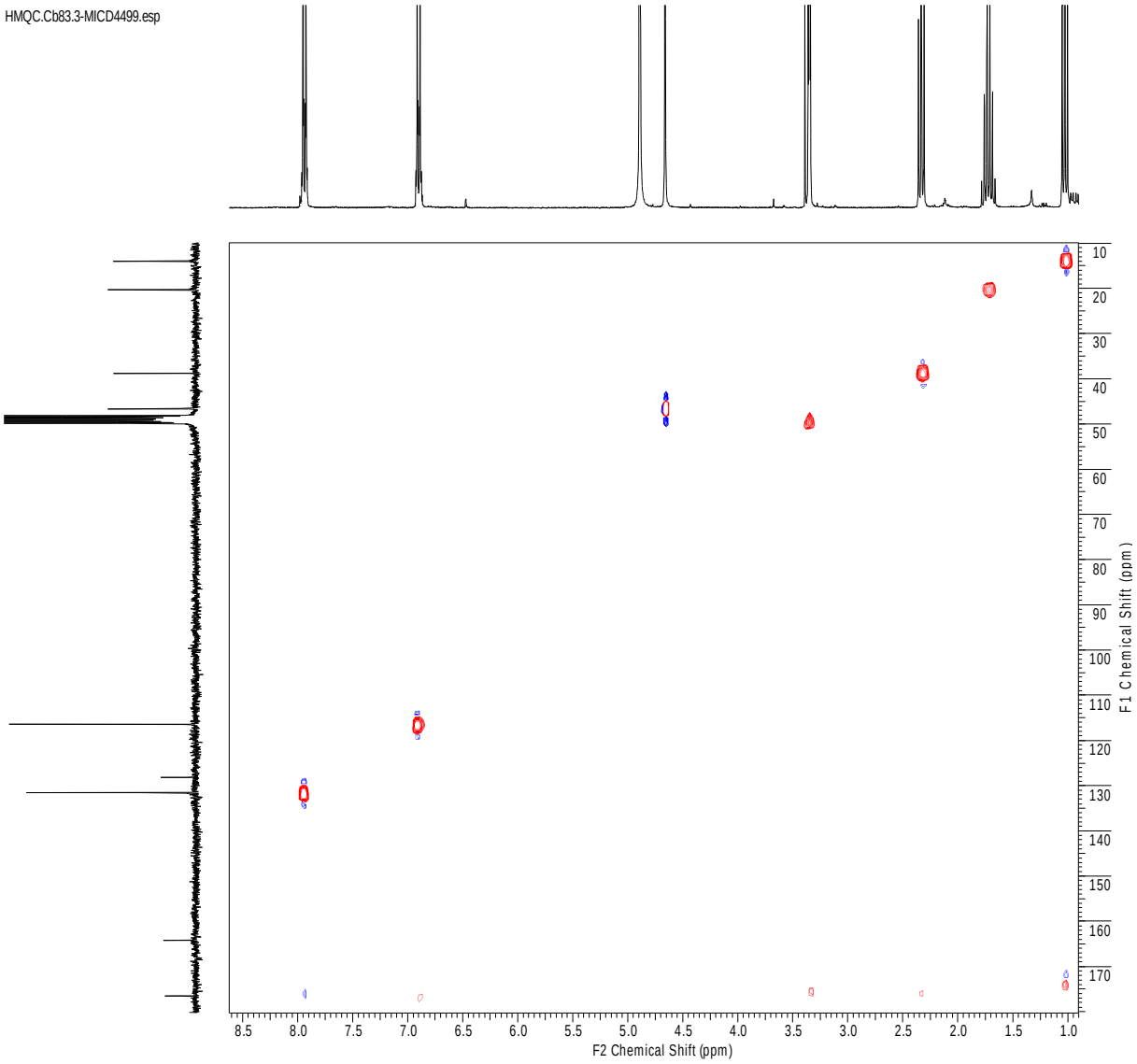

Spectrum 29: $^{1}H,^{13}C$ HMQC NMR spectrum of *p*-hydroxyacetophenone *n*-butanamide (**34b**) (^{1}H 300 MHz, ^{13}C 75 MHz, CD_3OD).

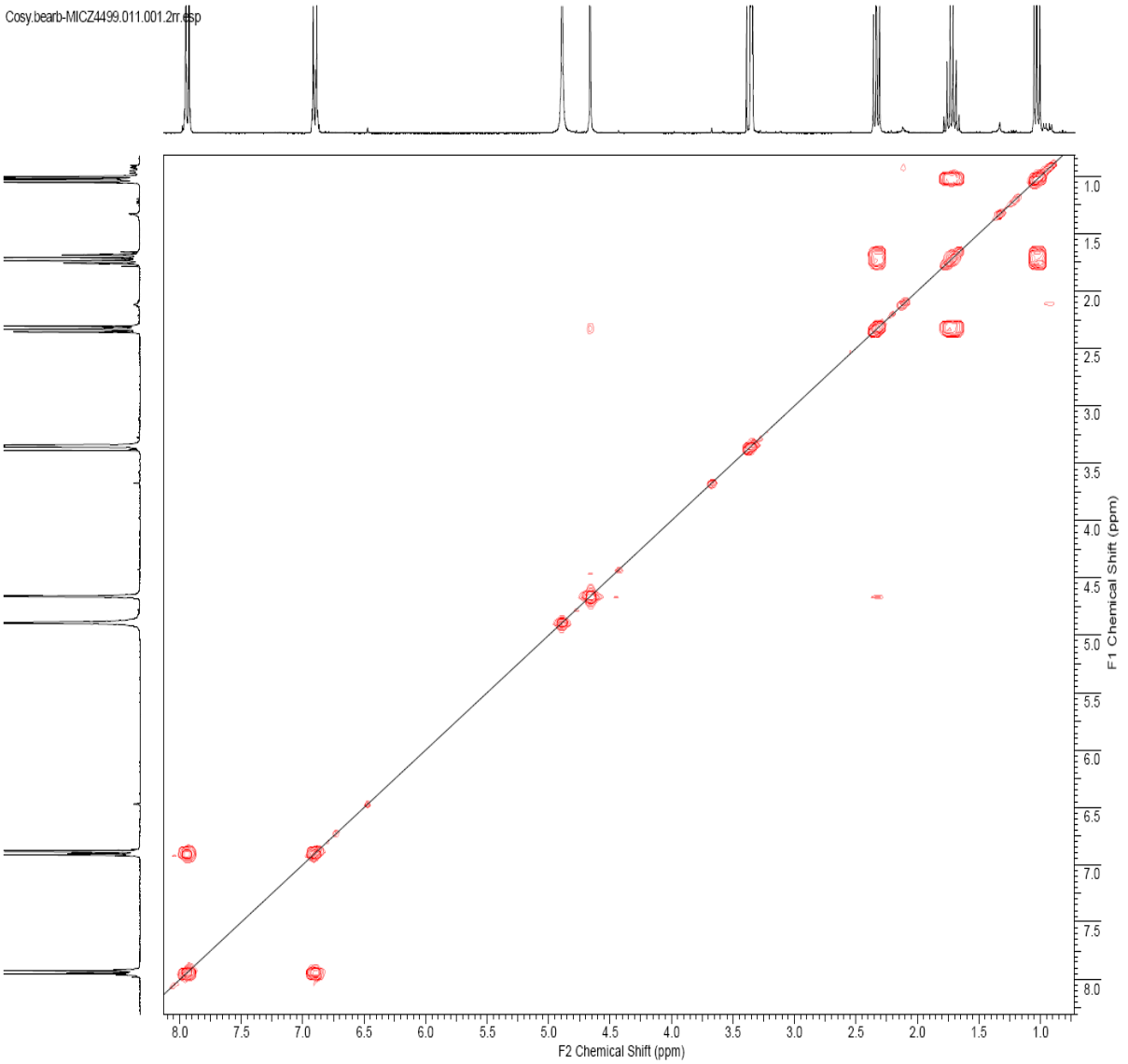

Spectrum 30: $^{1}H,^{1}H$ COSY NMR spectrum of *p*-hydroxyacetophenone *n*-butanamide (**34b**) (^{1}H 300 MHz, ^{13}C 75 MHz, CD_3OD).

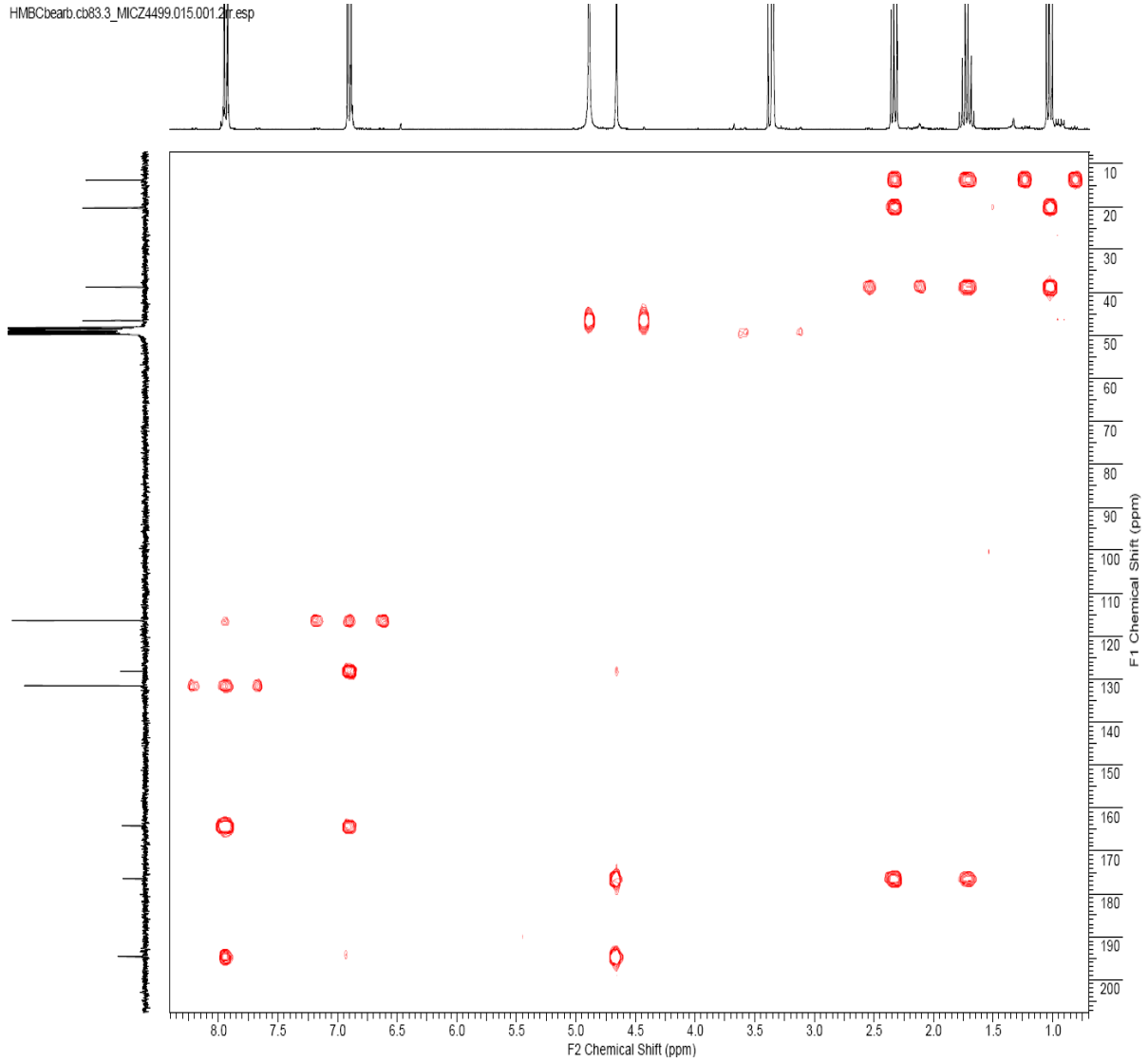

Spectrum 31: $^{1}H,^{13}C$ HMBC NMR spectrum of *p*-hydroxyacetophenone *n*-butanamide (**34b**) (^{1}H 300 MHz, ^{13}C 75 MHz, CD_3OD).

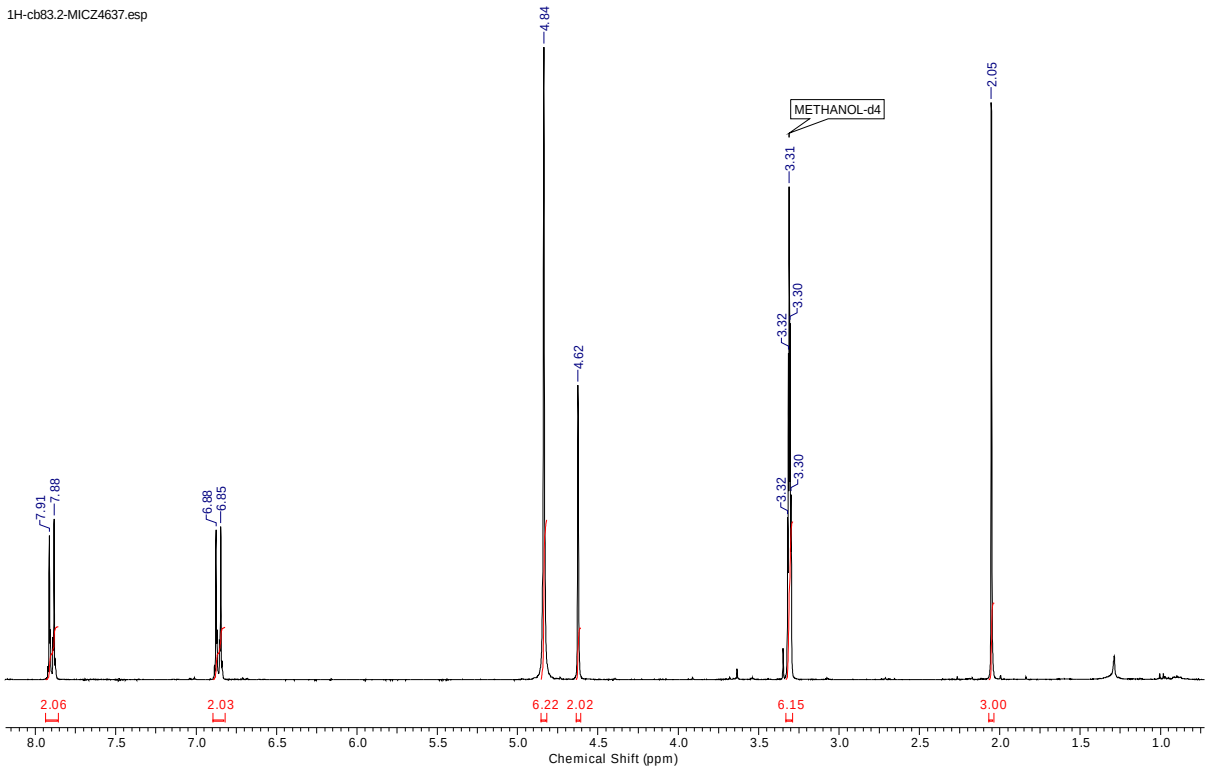

Spectrum 32: ^{1}H NMR spectrum of *p*-hydroxyacetophenone acetamide (**34c**) (^{1}H 300 MHz, ^{13}C 75 MHz, CD_3OD).

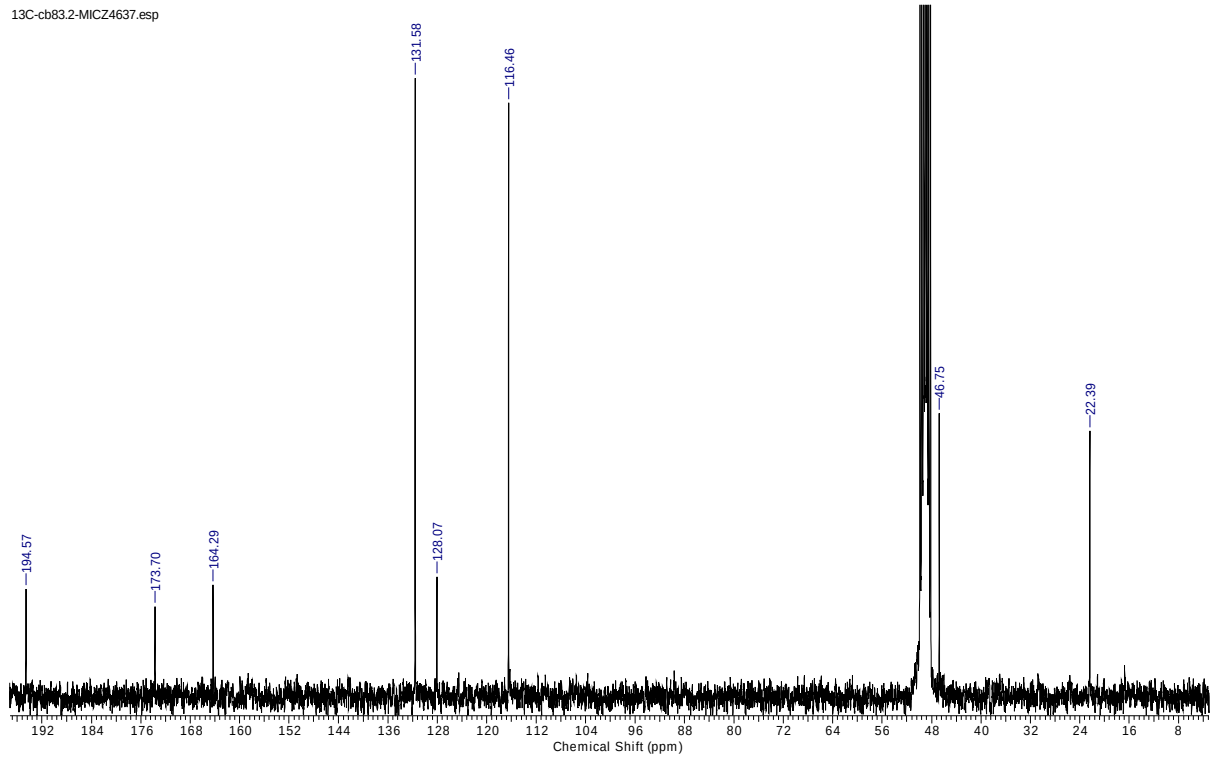

Spectrum 33: ^{13}C NMR spectrum of *p*-hydroxyacetophenone acetamide (**34c**) (^{1}H 300 MHz, ^{13}C 75 MHz, CD_3OD).

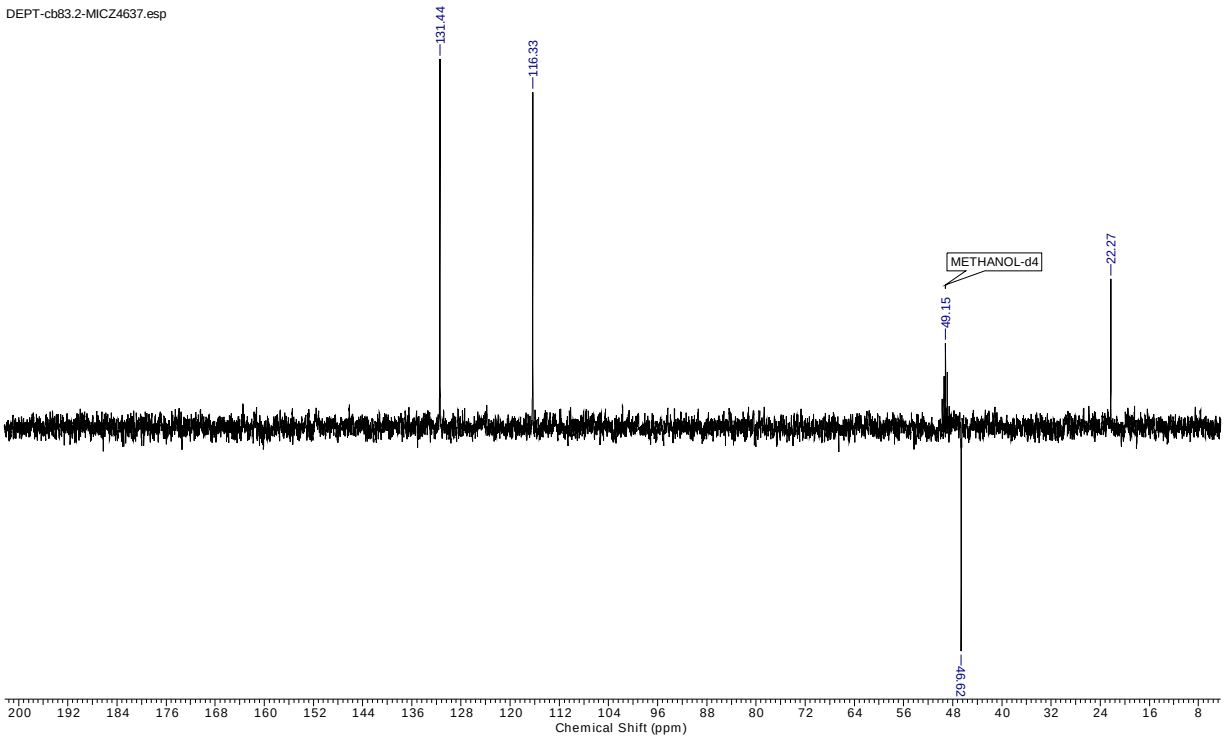

Spectrum 34: ^{13}C DEPT NMR spectrum of *p*-hydroxyacetophenone acetamide (**34c**) (^{1}H 300 MHz, ^{13}C 75 MHz, CD_3OD).

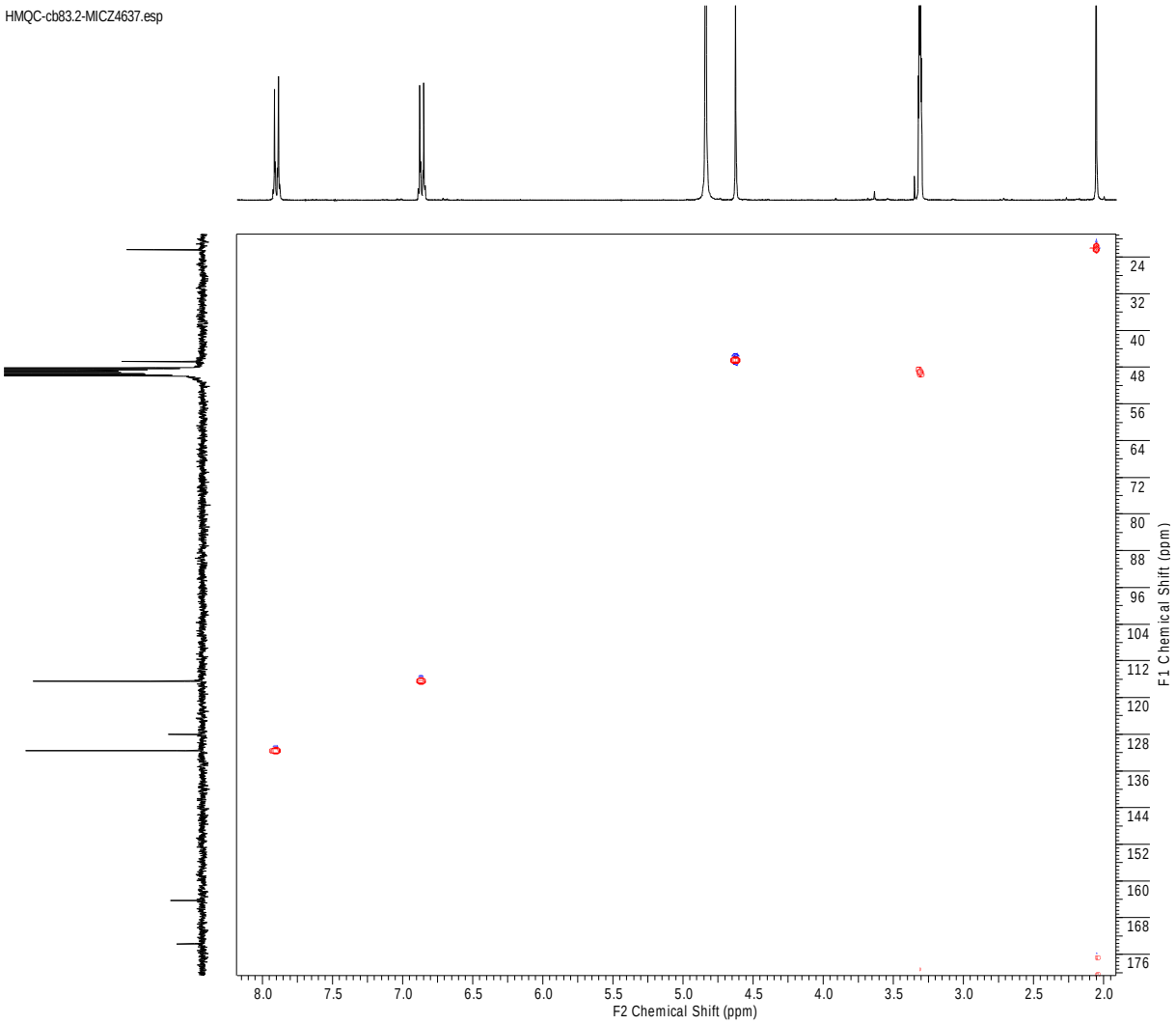

Spectrum 35: $^{1}H,^{13}C$ HMQC NMR spectrum of *p*-hydroxyacetophenone acetamide (**34c**) (^{1}H 300 MHz, ^{13}C 75 MHz, CD_3OD).

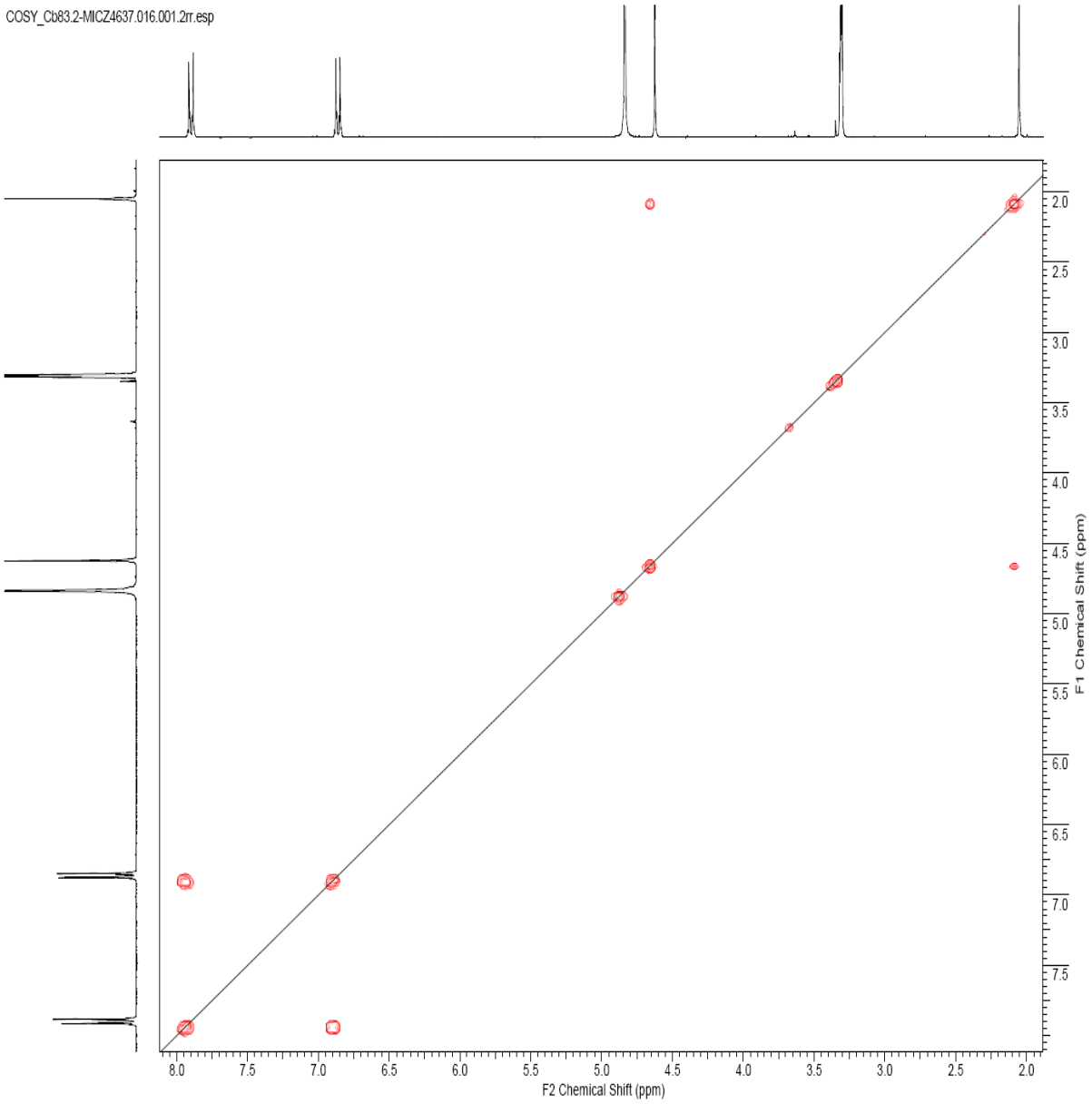

Spectrum 36: $^{1}H,^{1}H$ COSY NMR spectrum of *p*-hydroxyacetophenone acetamide (**34c**) (^{1}H 300 MHz, ^{13}C 75 MHz, CD_3OD).

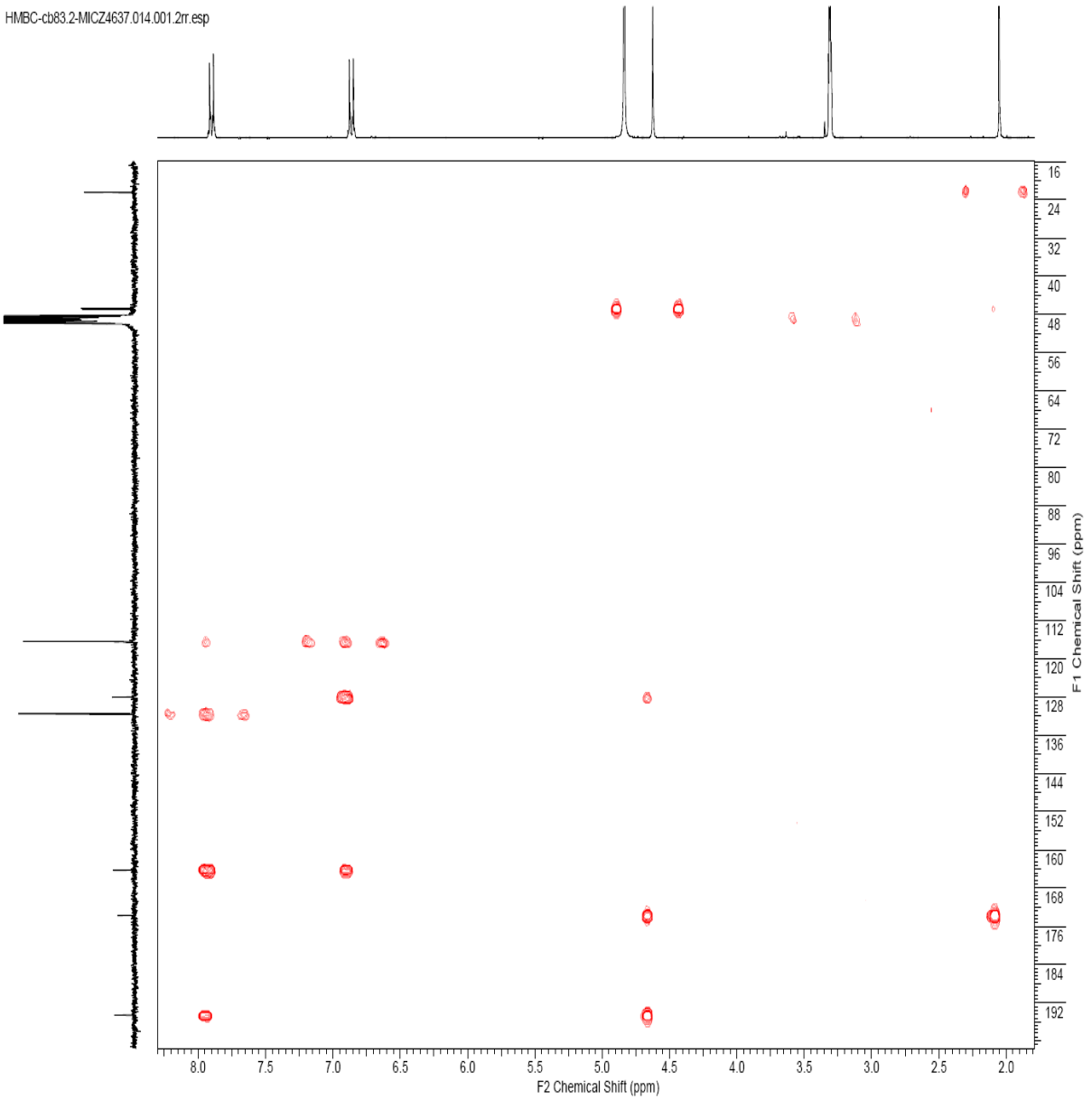

Spectrum 37: $^{1}H,^{13}C$ HMBC NMR spectrum of *p*-hydroxyacetophenone acetamide (**34c**) (^{1}H 300 MHz, ^{13}C 75 MHz, CD_3OD).

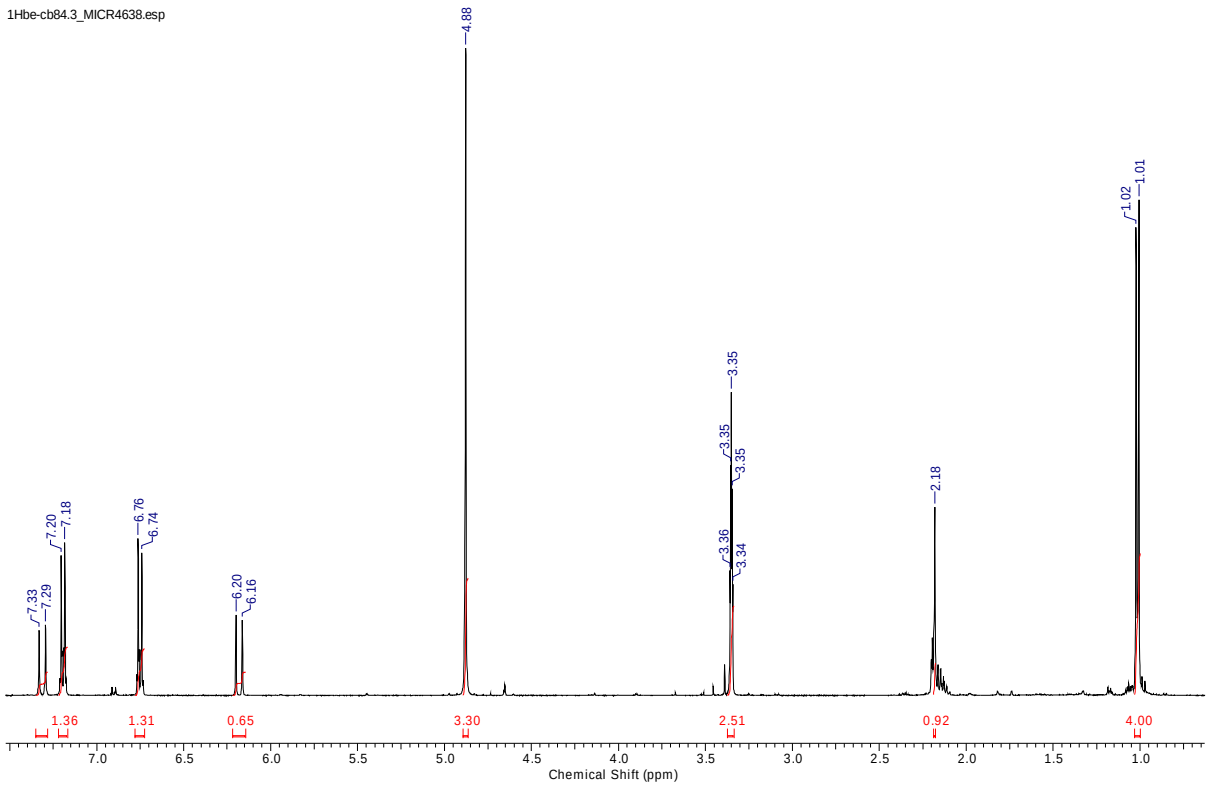

Spectrum 38: ^{1}H NMR spectrum of *p*-hydroxyethenphenyl *iso*-butanamide (**34d**) (^{1}H 400 MHz, ^{13}C 100 MHz, CD_3OD).

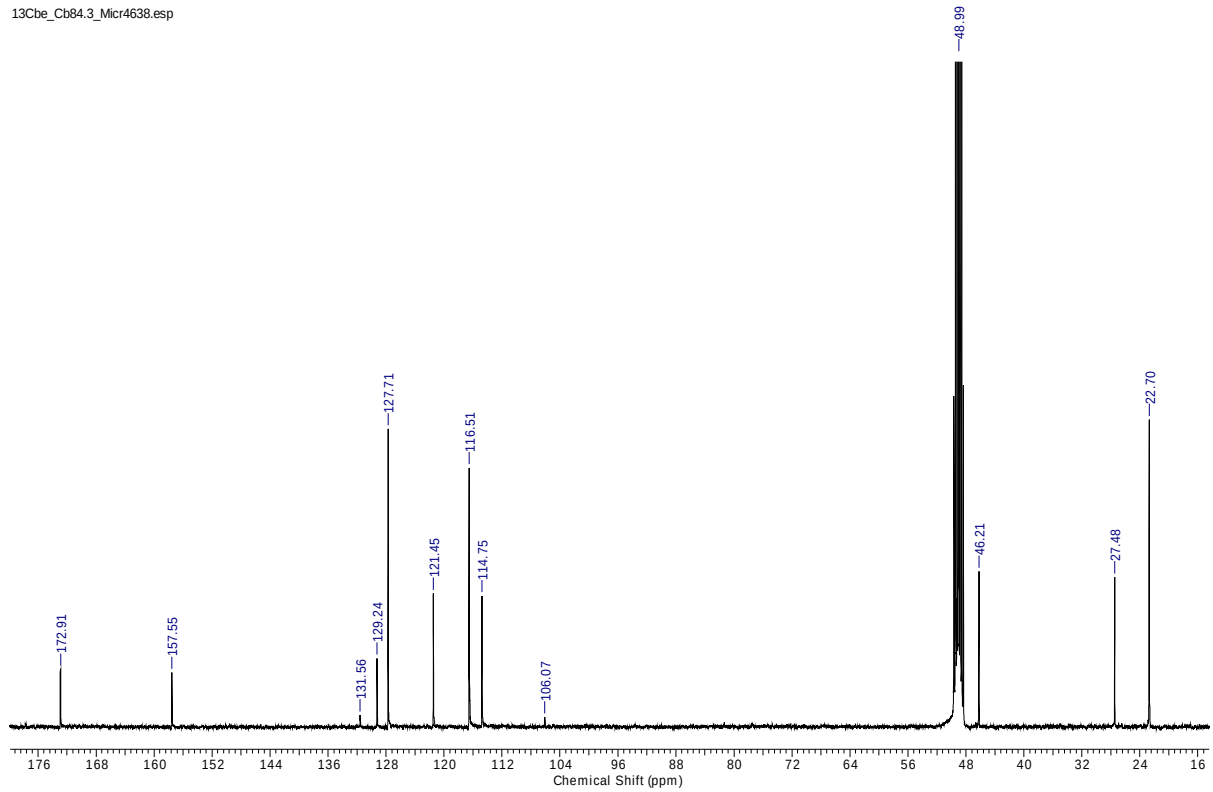

Spectrum 39: ^{13}C NMR spectrum of *p*-hydroxyethenphenyl *iso*-butanamide (**34d**) (^{1}H 400 MHz, ^{13}C 100 MHz, CD_3OD).

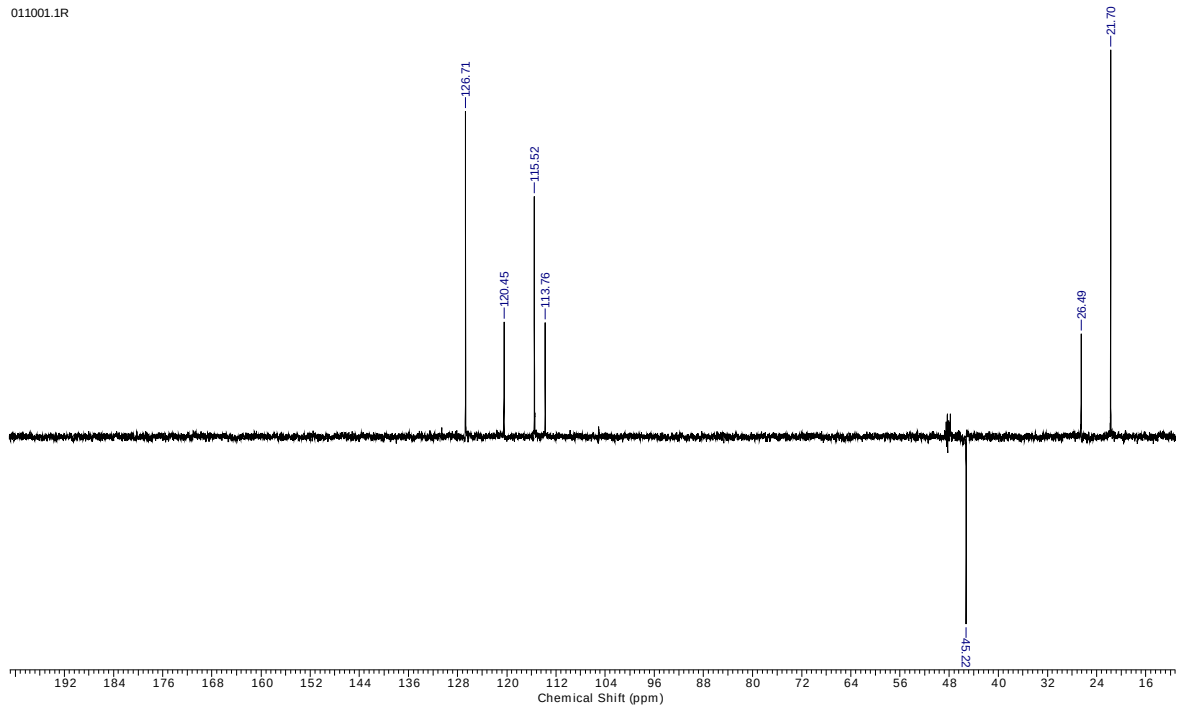

Spectrum 40: ^{13}C DEPT NMR spectrum of *p*-hydroxyethenphenyl *iso*-butanamide (**34d**) (^{1}H 400 MHz, ^{13}C 100 MHz, CD_3OD).

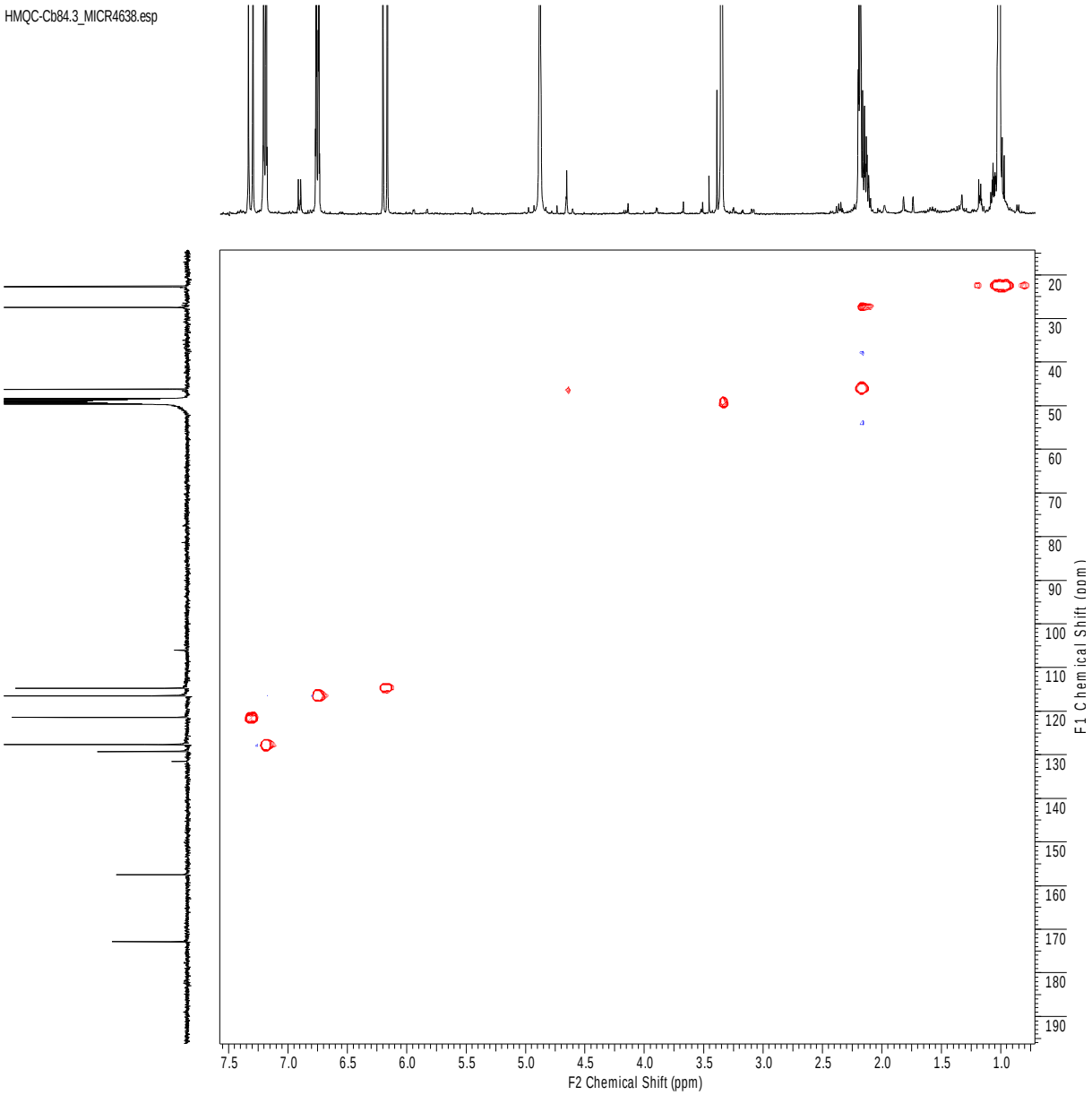

Spectrum 41: $^{1}H,^{13}C$ HMQC NMR spectrum of *p*-hydroxyethenphenyl *iso*-butanamide (**34d**) (^{1}H 400 MHz, ^{13}C 100 MHz, CD_3OD).

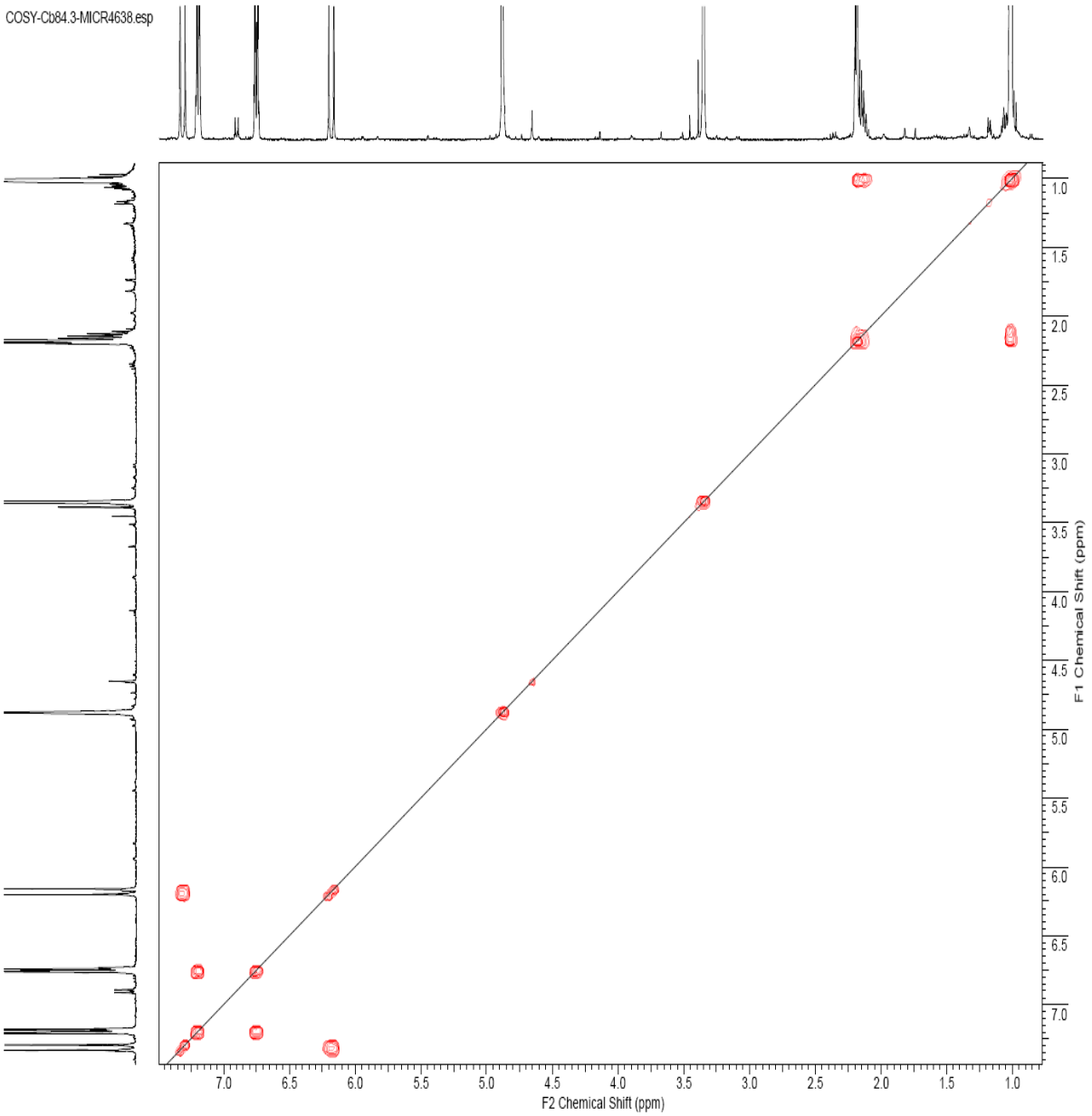

Spectrum 42: $^{1}H,^{1}H$ COSY NMR spectrum of *p*-hydroxyethenphenyl *iso*-butanamide (**34d**) (^{1}H 400 MHz, ^{13}C 100 MHz, CD_3OD).

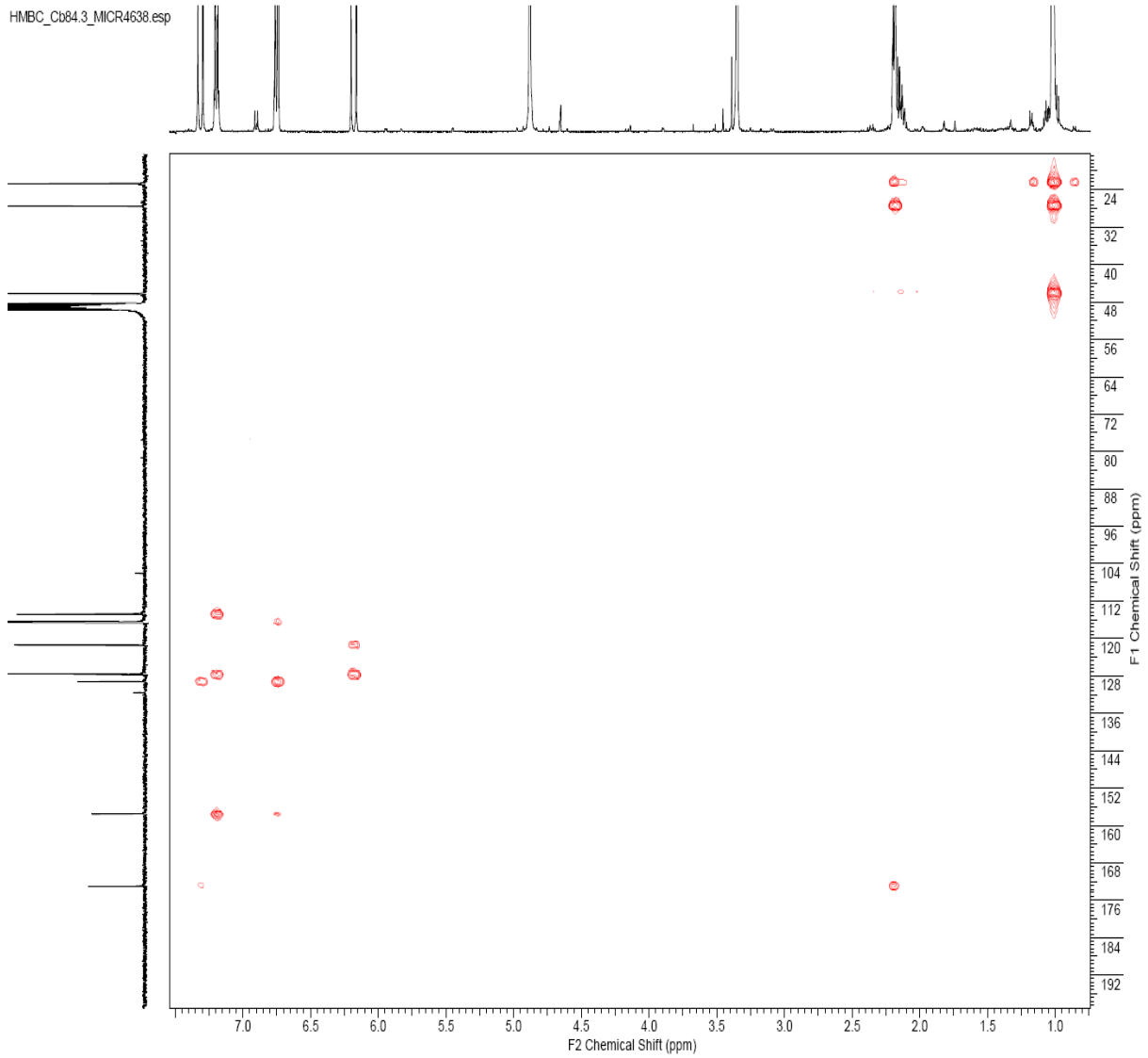

Spectrum 43: $^{1}H,^{13}C$ HMBC NMR spectrum of *p*-hydroxyethenphenyl *iso*-butanamide (**34d**) (^{1}H 400 MHz, ^{13}C 100 MHz, CD_3OD).

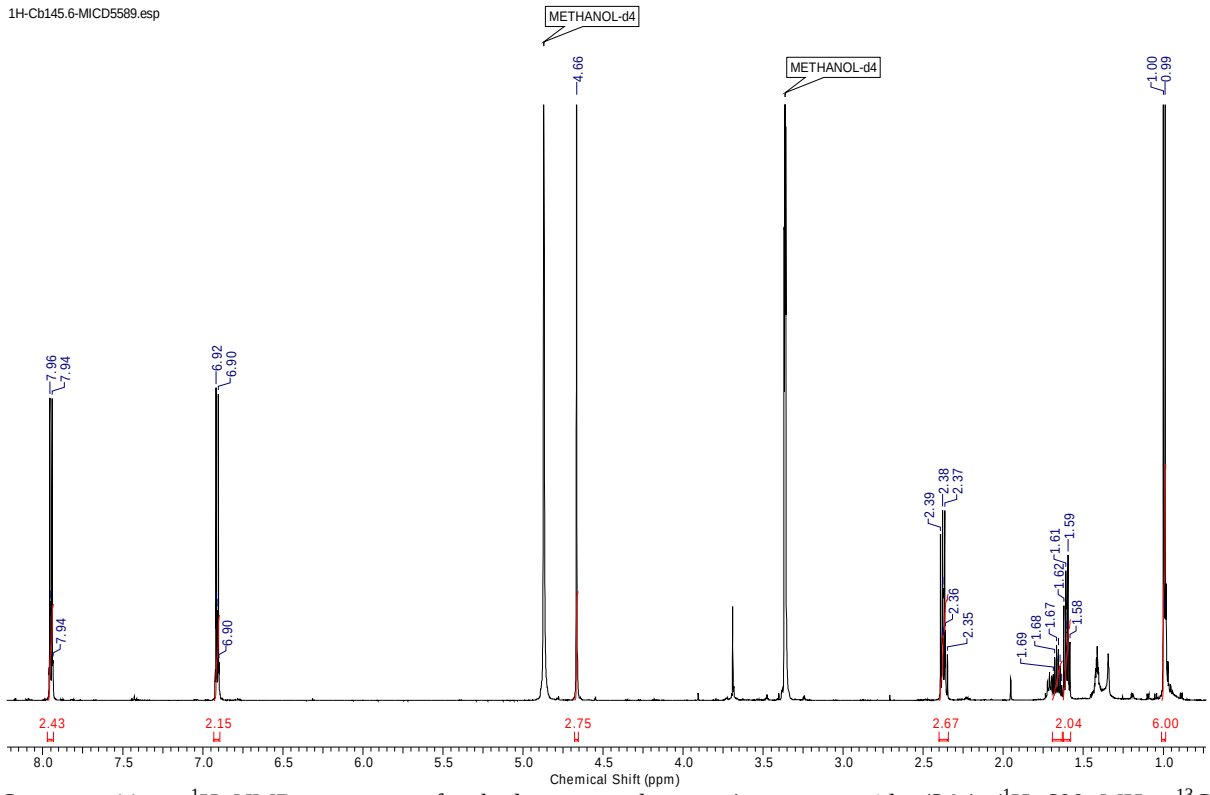

Spectrum 44: ^{1}H NMR spectrum of *p*-hydroxyacetophenone *iso*-pentanamide (**34e**) (^{1}H 600 MHz, ^{13}C 150 MHz, CD_3OD).

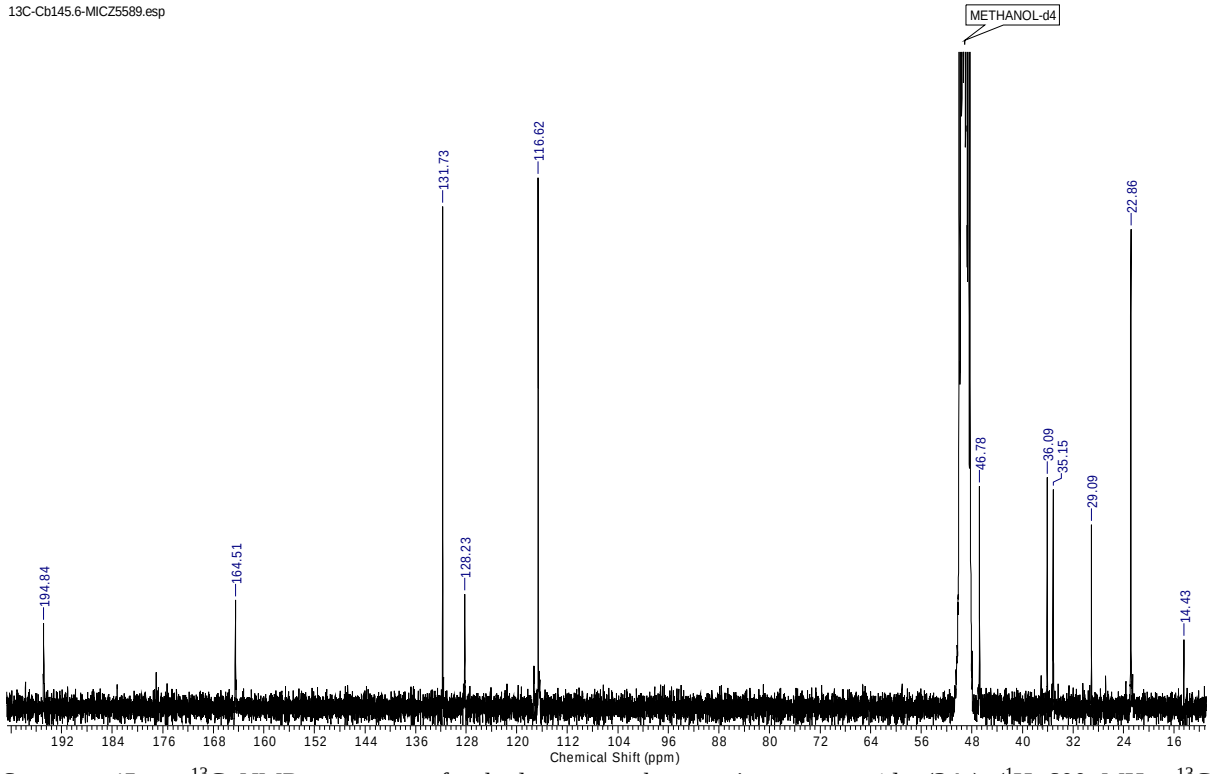

Spectrum 45: ^{13}C NMR spectrum of *p*-hydroxyacetophenone *iso*-pentanamide (**34e**) (^{1}H 600 MHz, ^{13}C 150 MHz, CD_3OD).

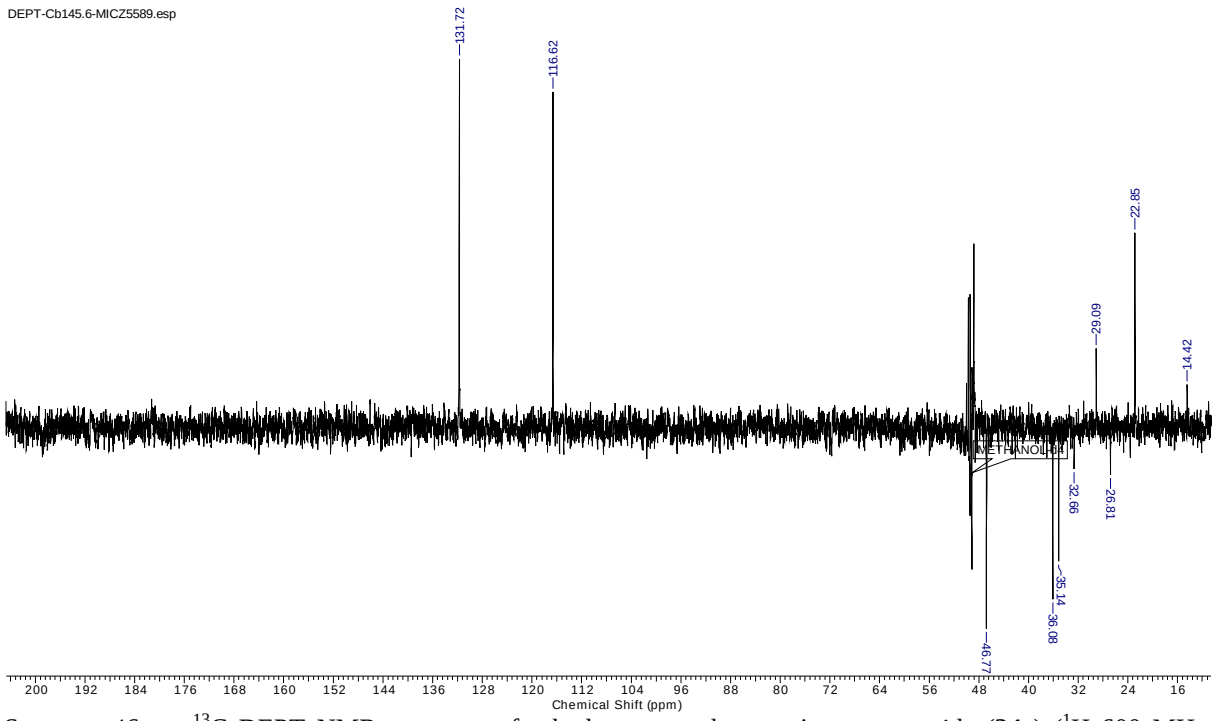

Spectrum 46: ^{13}C DEPT NMR spectrum of *p*-hydroxyacetophenone *iso*-pentanamide (**34e**) (^{1}H 600 MHz, ^{13}C 150 MHz, CD_3OD).

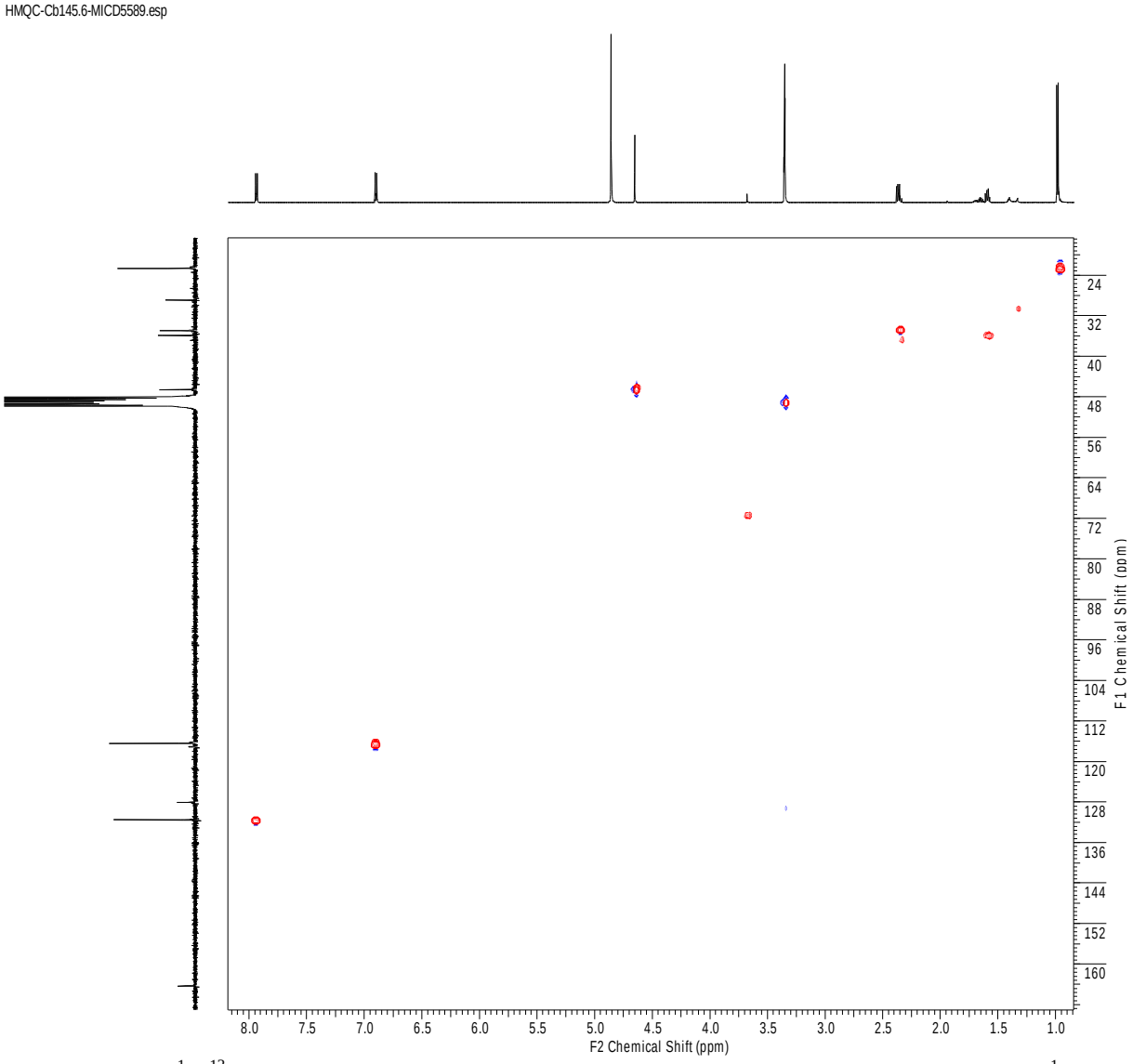

Spectrum 47: $^{1}H,^{13}C$ HMQC NMR spectrum of *p*-hydroxyacetophenone *iso*-pentanamide (**34e**) (^{1}H 600 MHz, ^{13}C 150 MHz, CD_3OD).

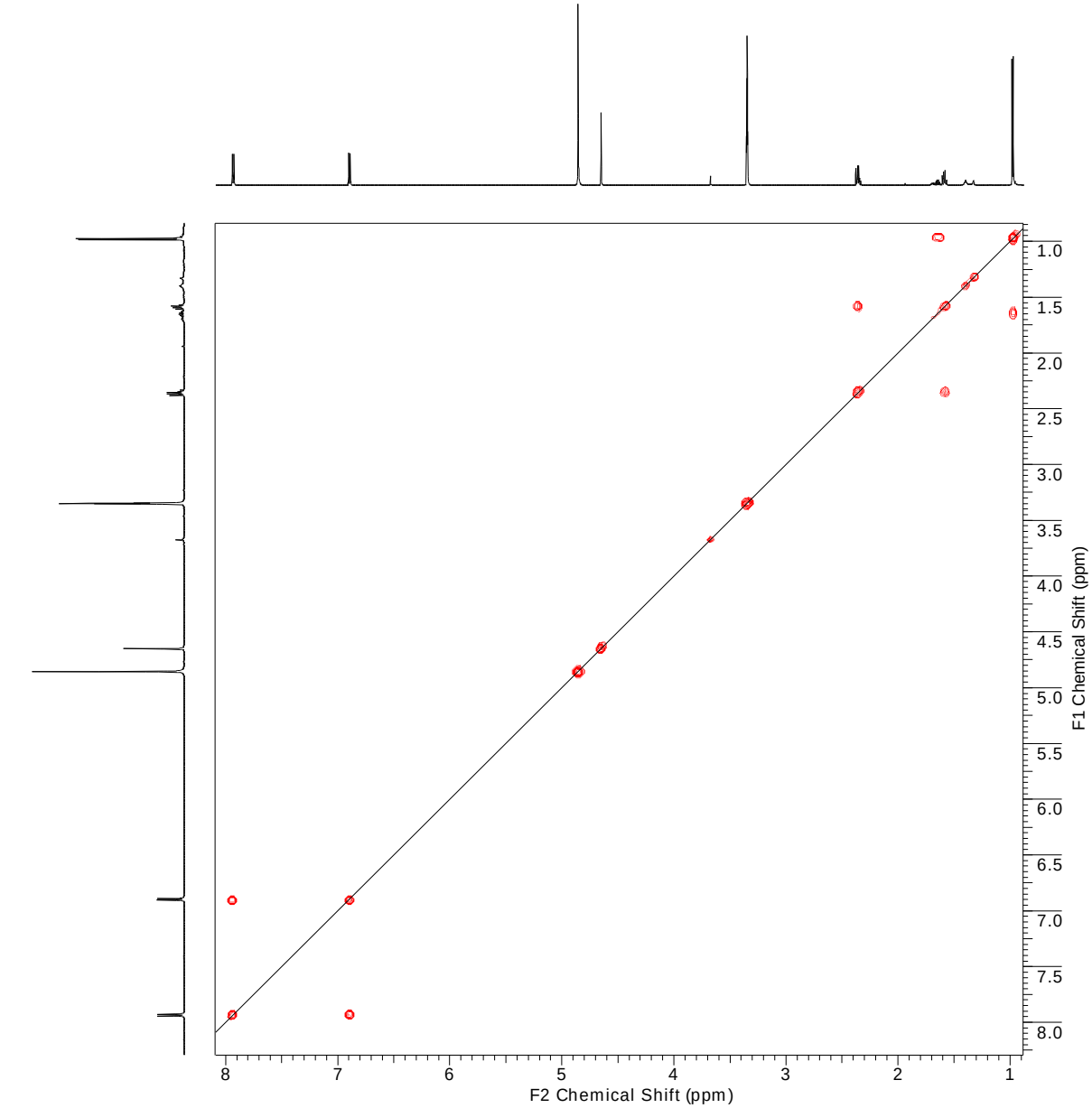

Spectrum 48: $^{1}H,^{1}H$ COSY NMR spectrum of *p*-hydroxyacetophenone *iso*-pentanamide (**34e**) (^{1}H 600 MHz, ^{13}C 150 MHz, CD_3OD).

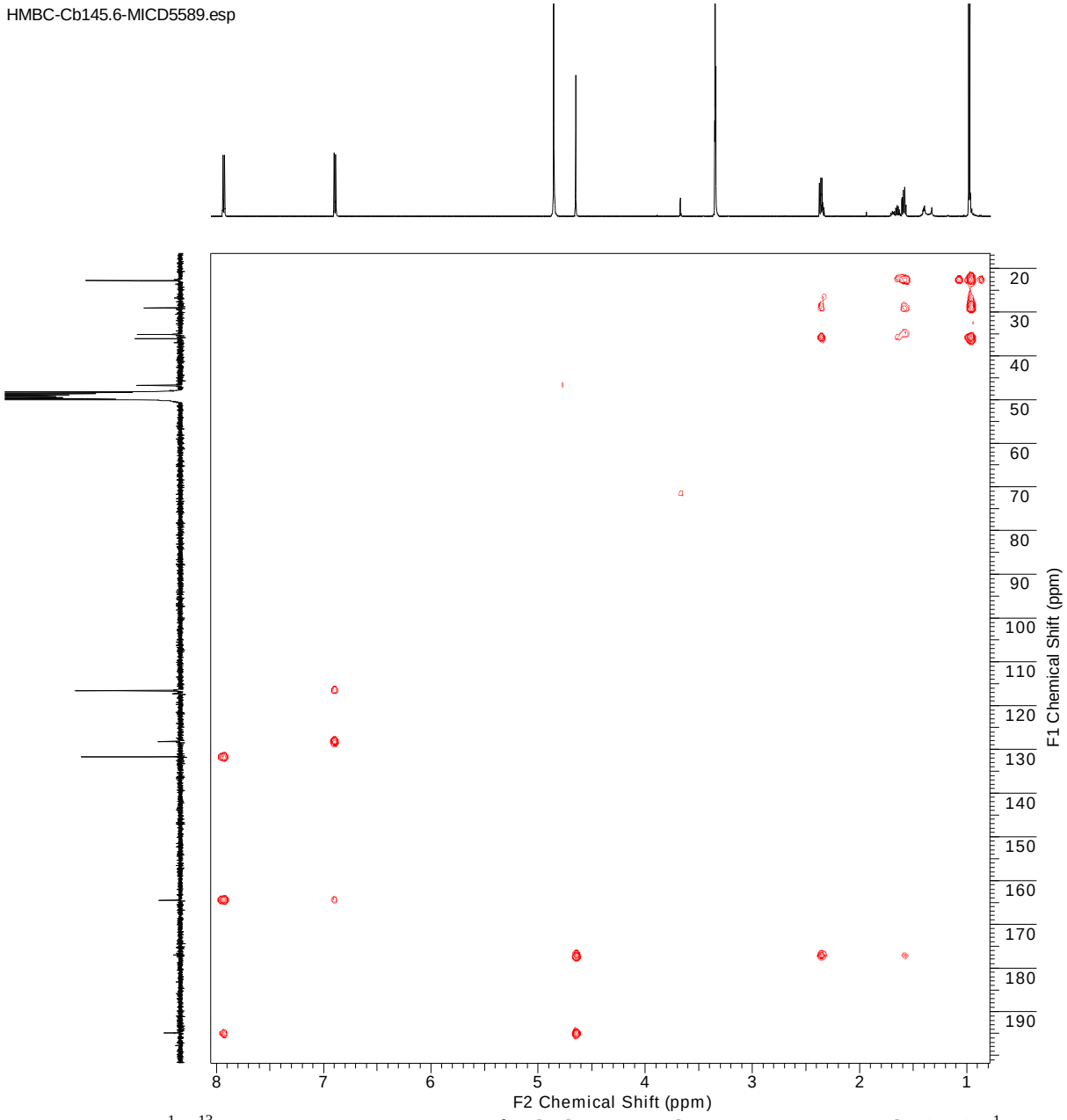

Spectrum 49: $^{1}H,^{13}C$ HMBC NMR spectrum of *p*-hydroxyacetophenone *iso*-pentanamide (**34e**) (^{1}H 600 MHz, ^{13}C 150 MHz, CD_3OD).

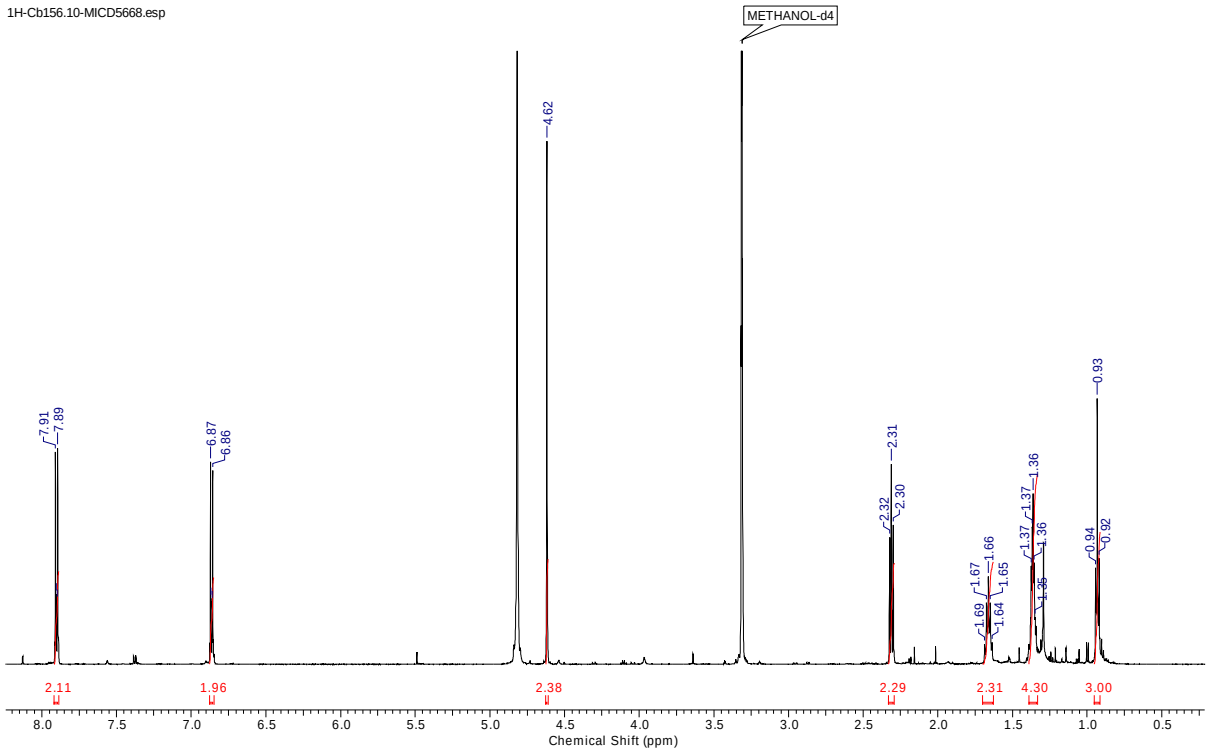

Spectrum 50: ^{1}H NMR spectrum of *p*-hydroxyacetophenone *n*-pentanamide (**34f**) (^{1}H 600 MHz, ^{13}C 150 MHz, CD_3OD).

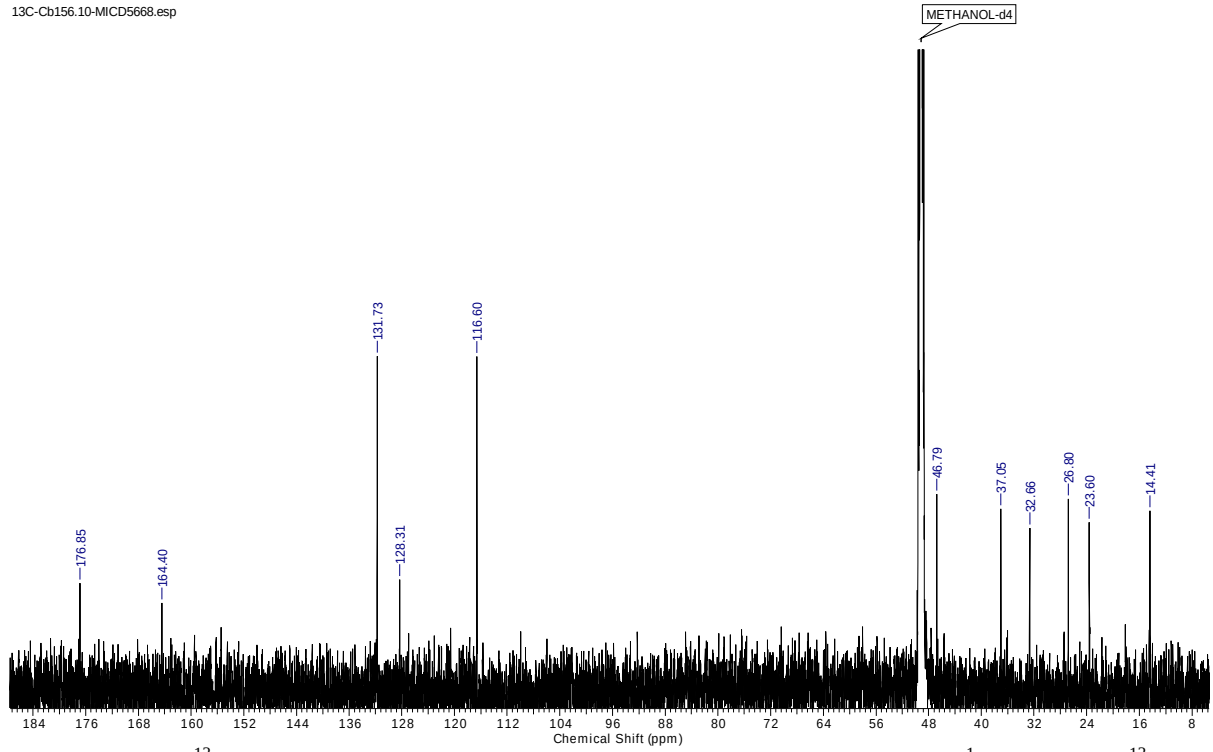

Spectrum 51: ^{13}C NMR spectrum of *p*-hydroxyacetophenone *n*-pentanamide (**34f**) (^{1}H 600 MHz, ^{13}C 150 MHz, CD_3OD).

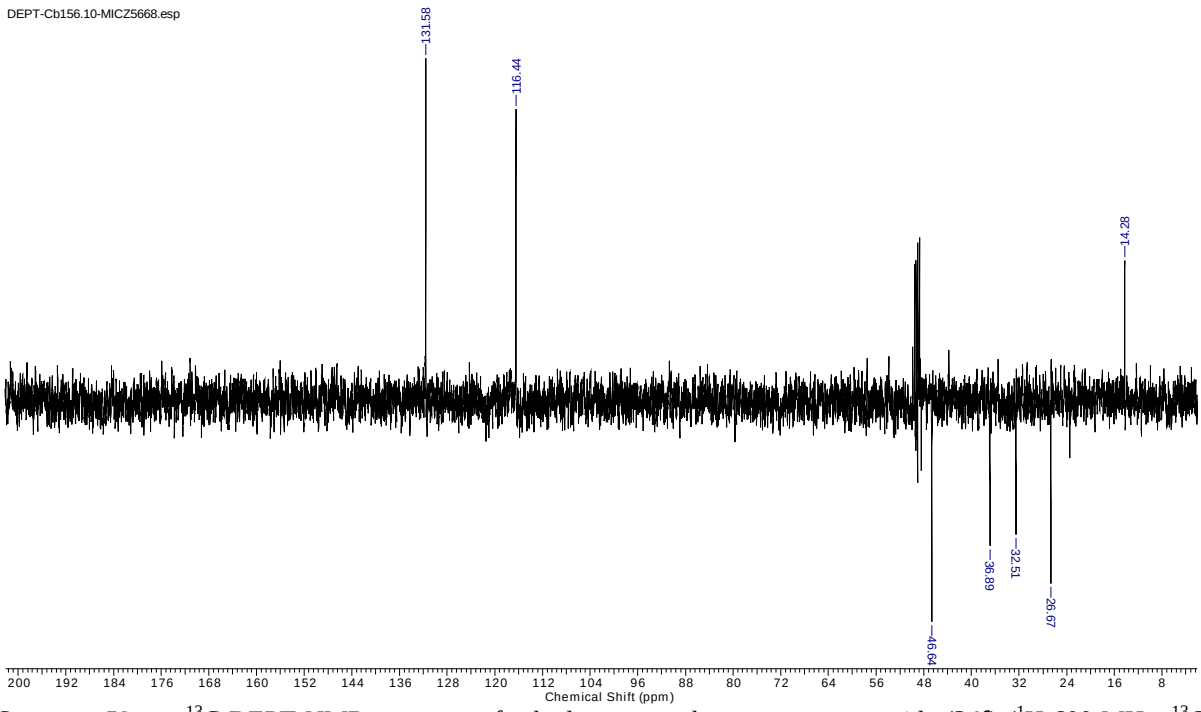

Spectrum 52: ^{13}C DEPT NMR spectrum of *p*-hydroxyacetophenone *n*-pentanamide (**34f**) (^{1}H 600 MHz, ^{13}C 150 MHz, CD_3OD).

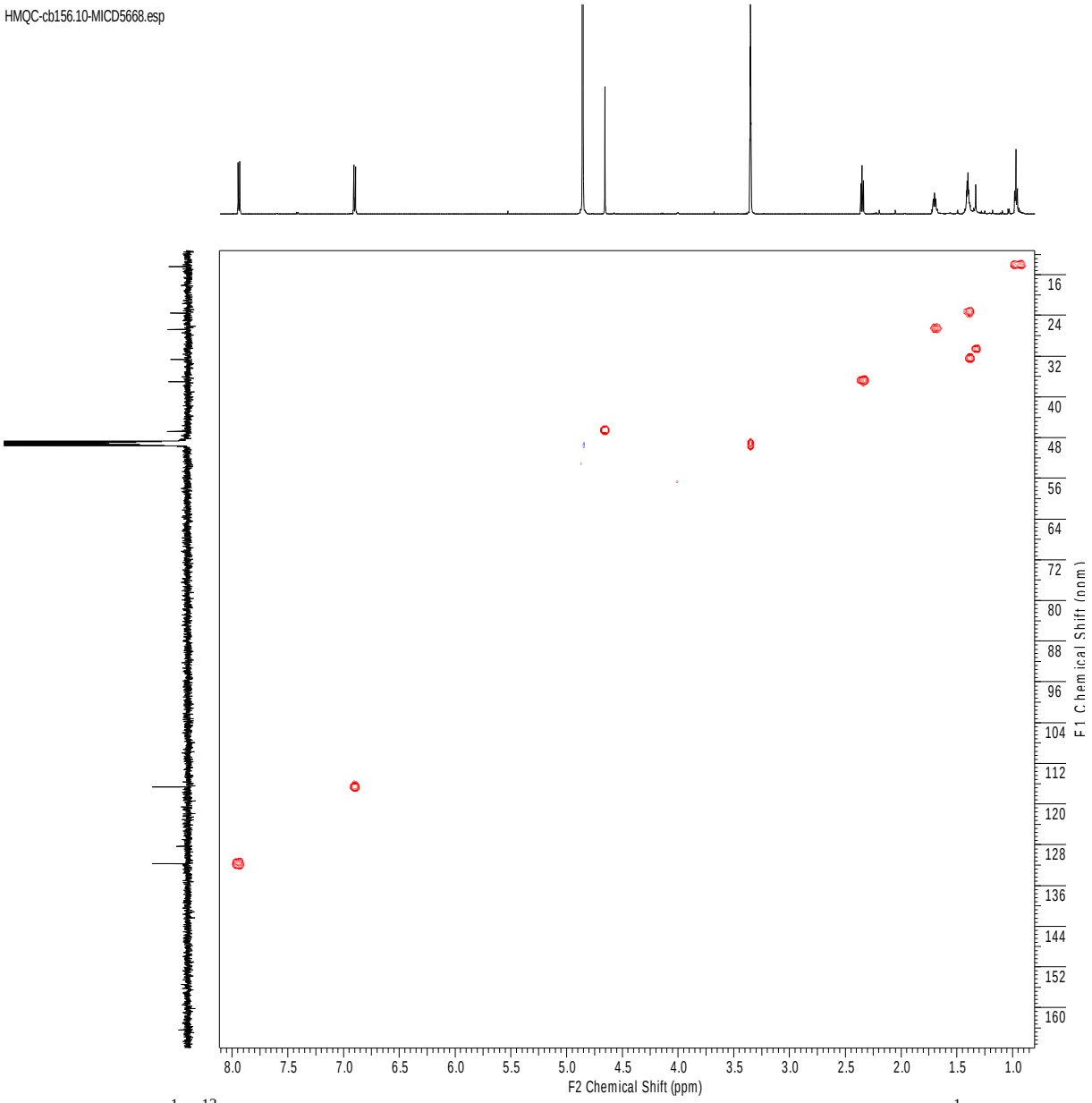

Spectrum 53: $^{1}H,^{13}C$ HMQC NMR spectrum of *p*-hydroxyacetophenone *n*-pentanamide (**34f**) (^{1}H 600 MHz, ^{13}C 150 MHz, CD_3OD).

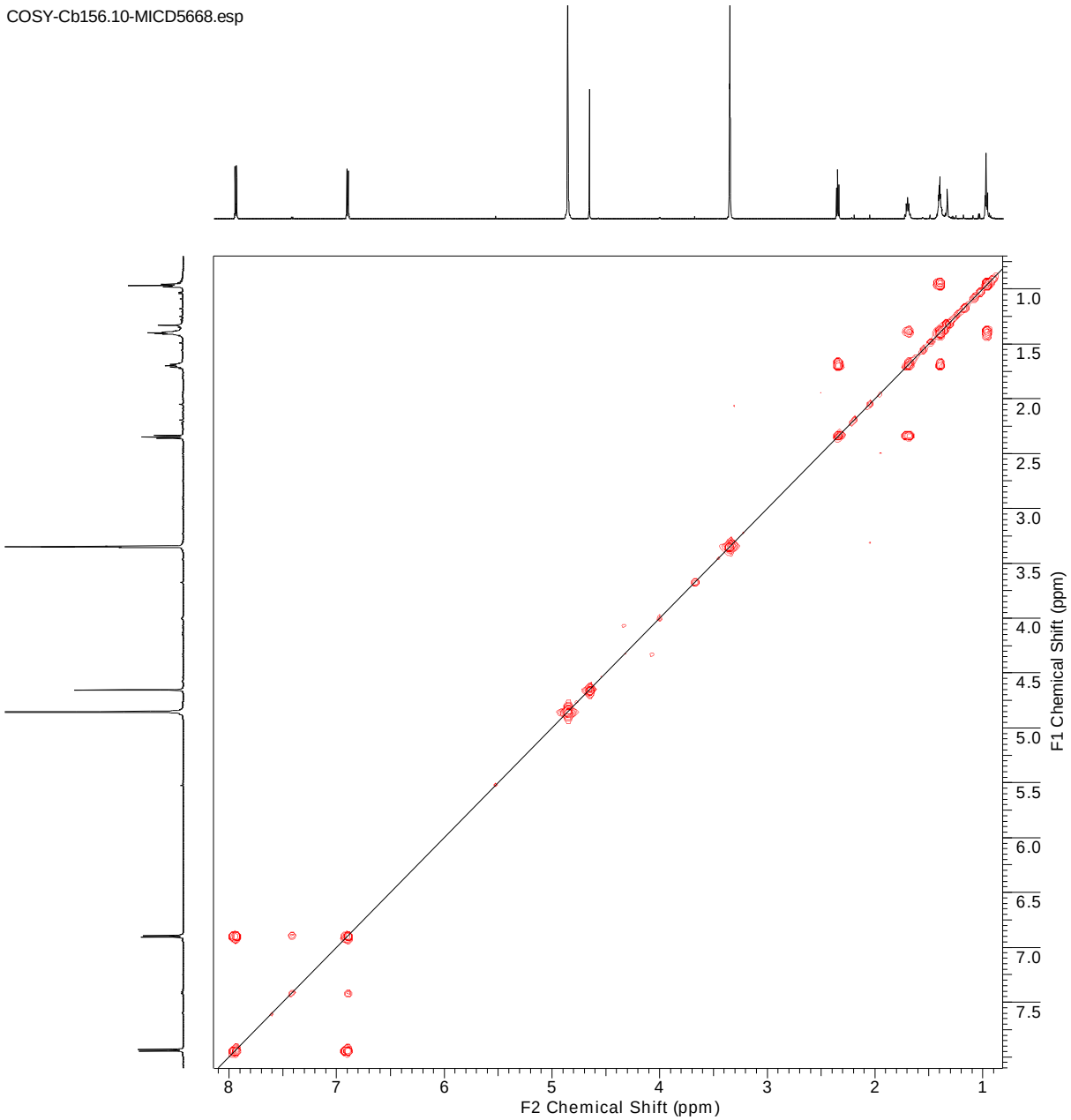

Spectrum 54: $^{1}H,^{1}H$ COSY NMR spectrum of *p*-hydroxyacetophenone *n*-pentanamide (**34f**) (^{1}H 600 MHz, ^{13}C 150 MHz, CD_3OD).

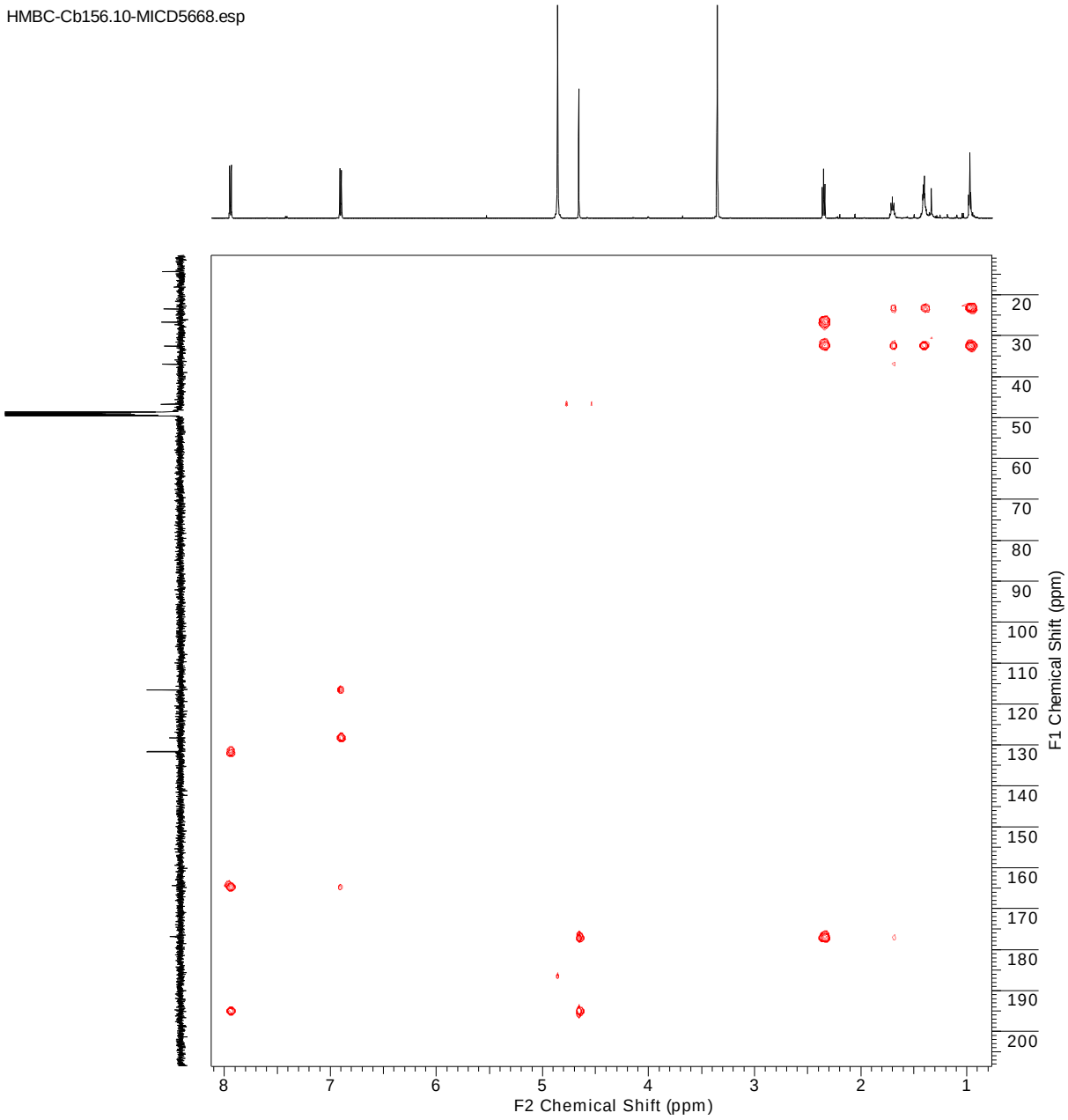

Spectrum 55: $^{1}H,^{13}C$ HMBC NMR spectrum of *p*-hydroxyacetophenone *n*-pentanamide (**34f**) (^{1}H 600 MHz, ^{13}C 150 MHz, CD_3OD).

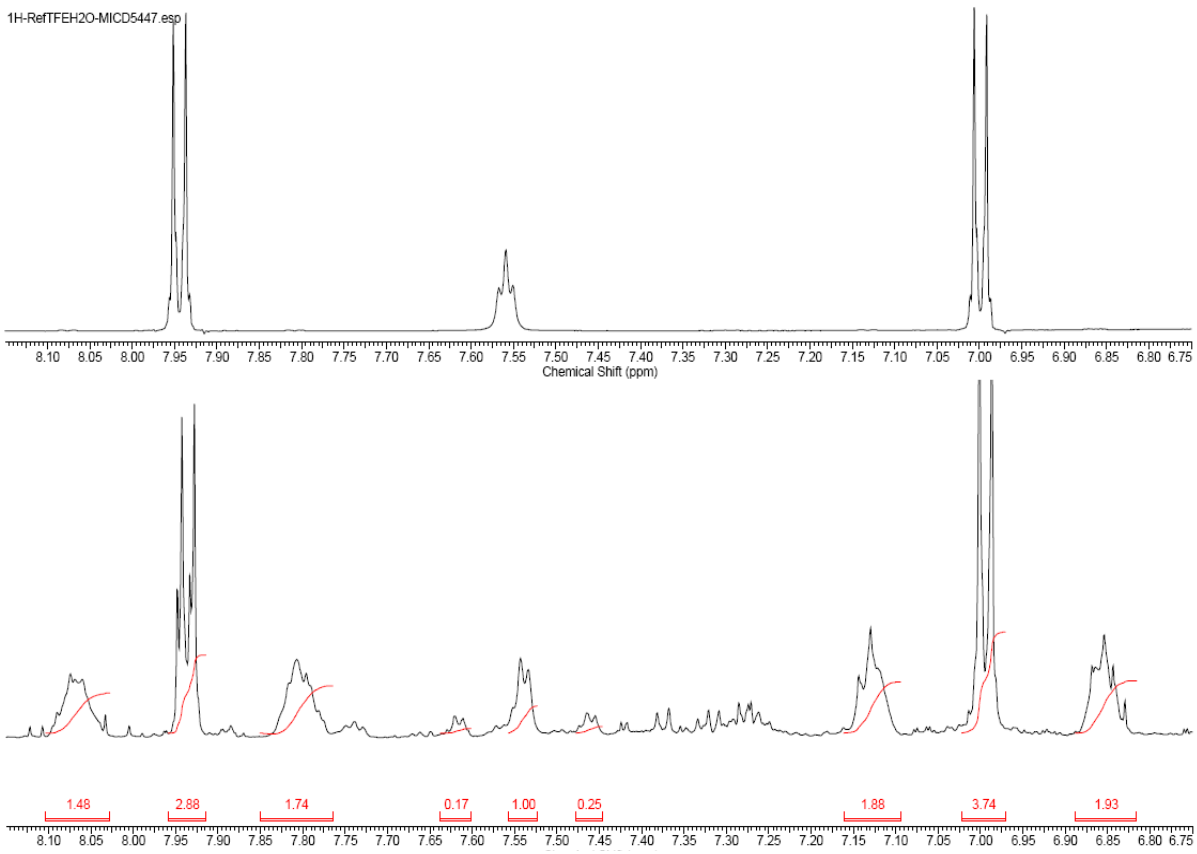

Spectrum 56: Comparison of ^{1}H NMR signals of **34a** unlabeled (above) and [^{13}C,^{15}N]-tyrosine labelled (below) (^{1}H 600 MHz, TFE/H_2O).

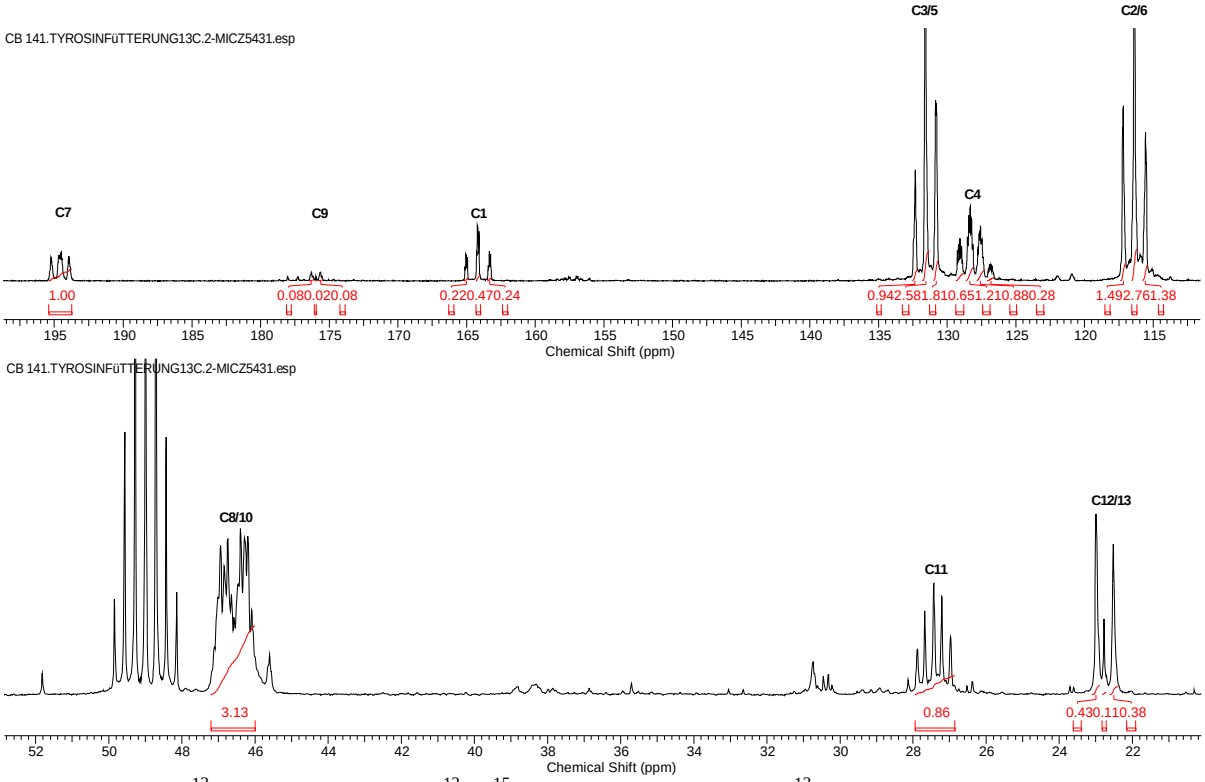

Spectrum 57: ^{13}C NMR spectrum of [$^{13}C_9$,^{15}N]- tyrosine labelled **34a** (^{13}C 75.5 MHz, CD_3OD).

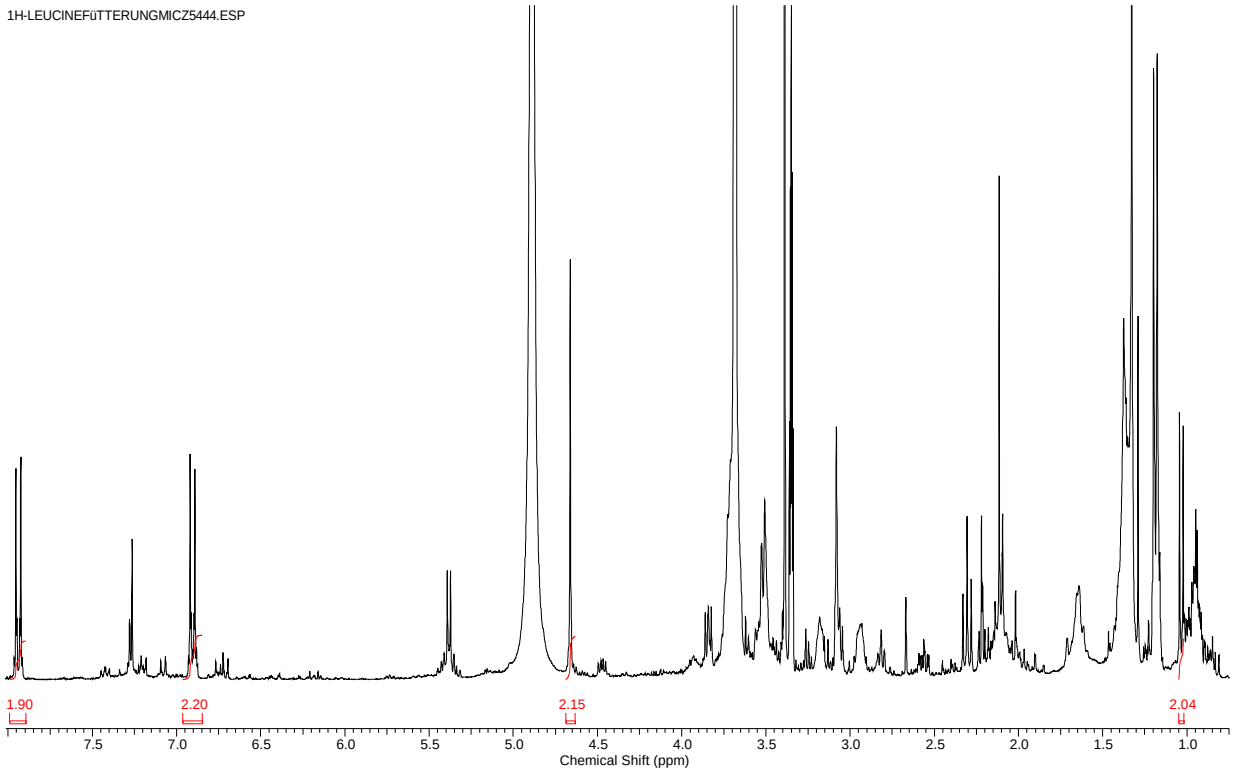

Spectrum 58: ^{1}H NMR spectrum of [D_{10}]-leucine labelled **34a** in the crude extract (^{1}H 300 MHz, CD_3OD).

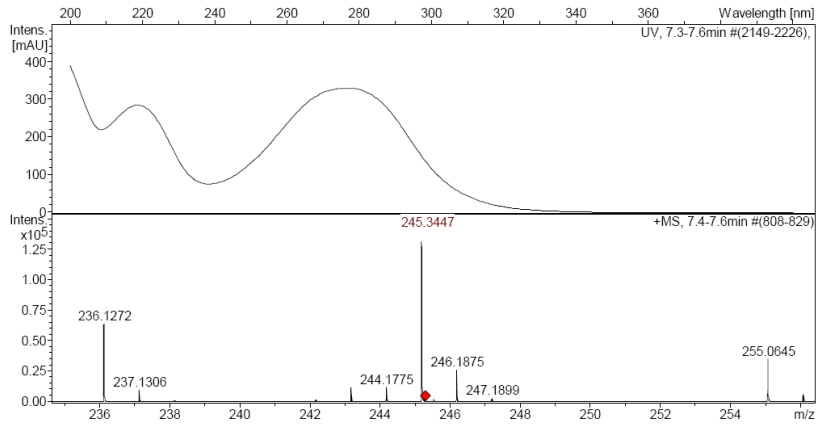

Spectrum 59: UV and HRESIMS spectrum of [D_{10}]-leucine labelled **34a**.

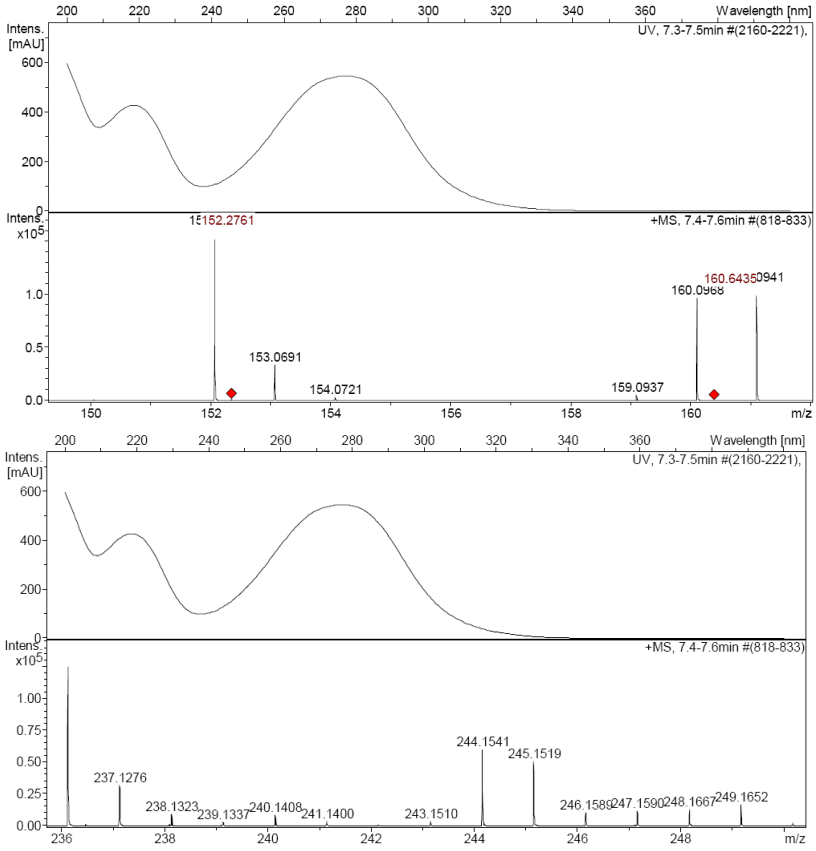

Spectrum 60: UV and HRESIMS spectrum of [$^{13}C_9$, ^{15}N]-tyrosine labelled **34a**.

6.2.3 Spectra of Sulfangolids 25a-d

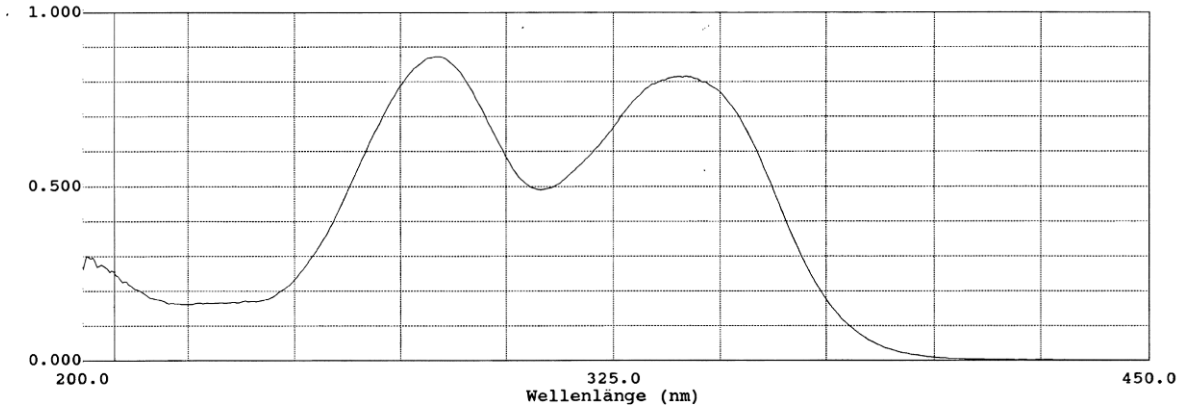

Spectrum 61: UV-spectrum of sulfangolid A (**25a**) in methanol (2 mg/100 mL).

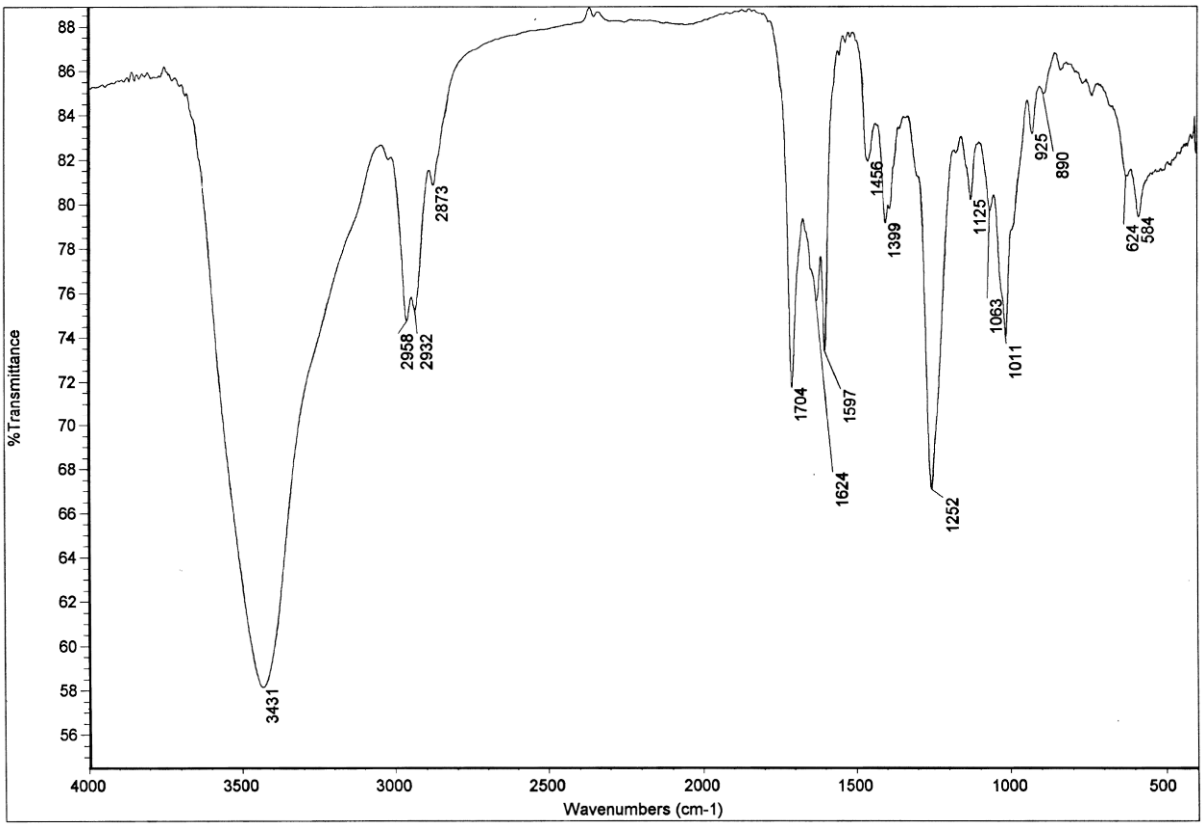

Spectrum 62: IR spectrum of sulfangolid A (**25a**) (KBr).

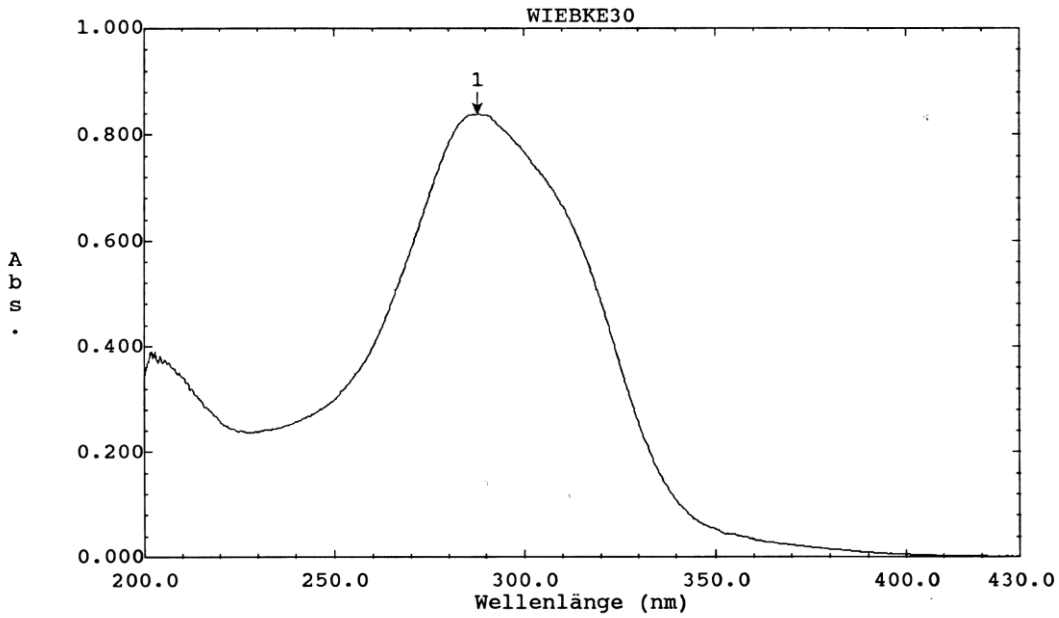

Spectrum 63: UV spectrum of sulfangolid C (**25c**) in methanol (2mg/100 mL).

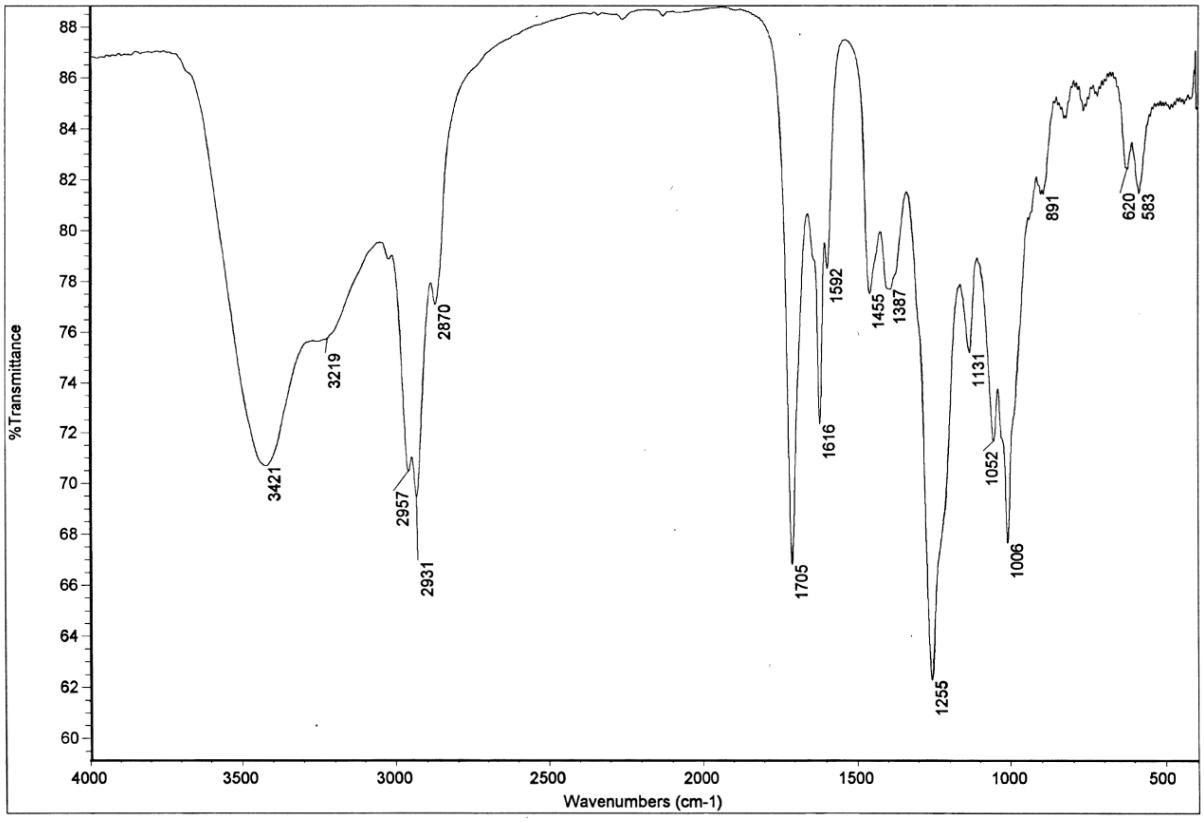

Spectrum 64: IR spectrum of sulfangolid C (**25c**) (KBr).

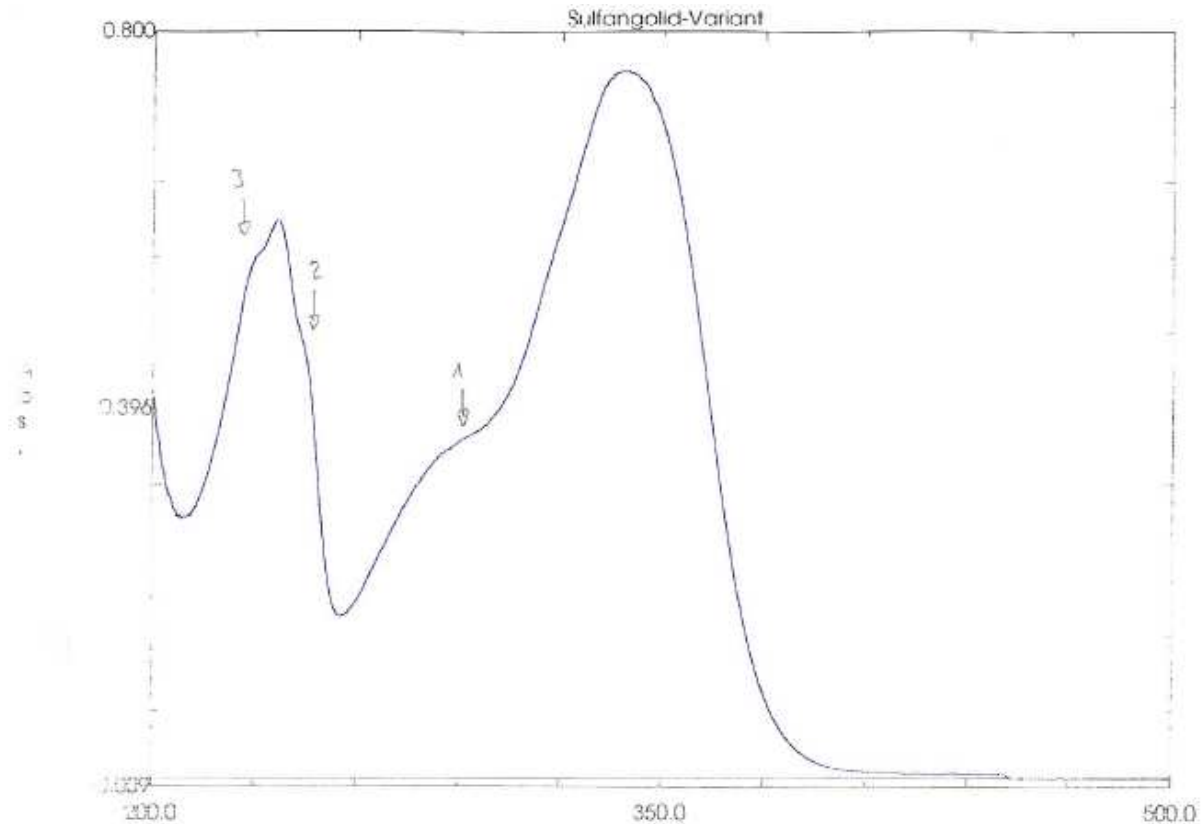

Spectrum 65: UV spectrum from sulfangolid D (**25d**) in methanol.

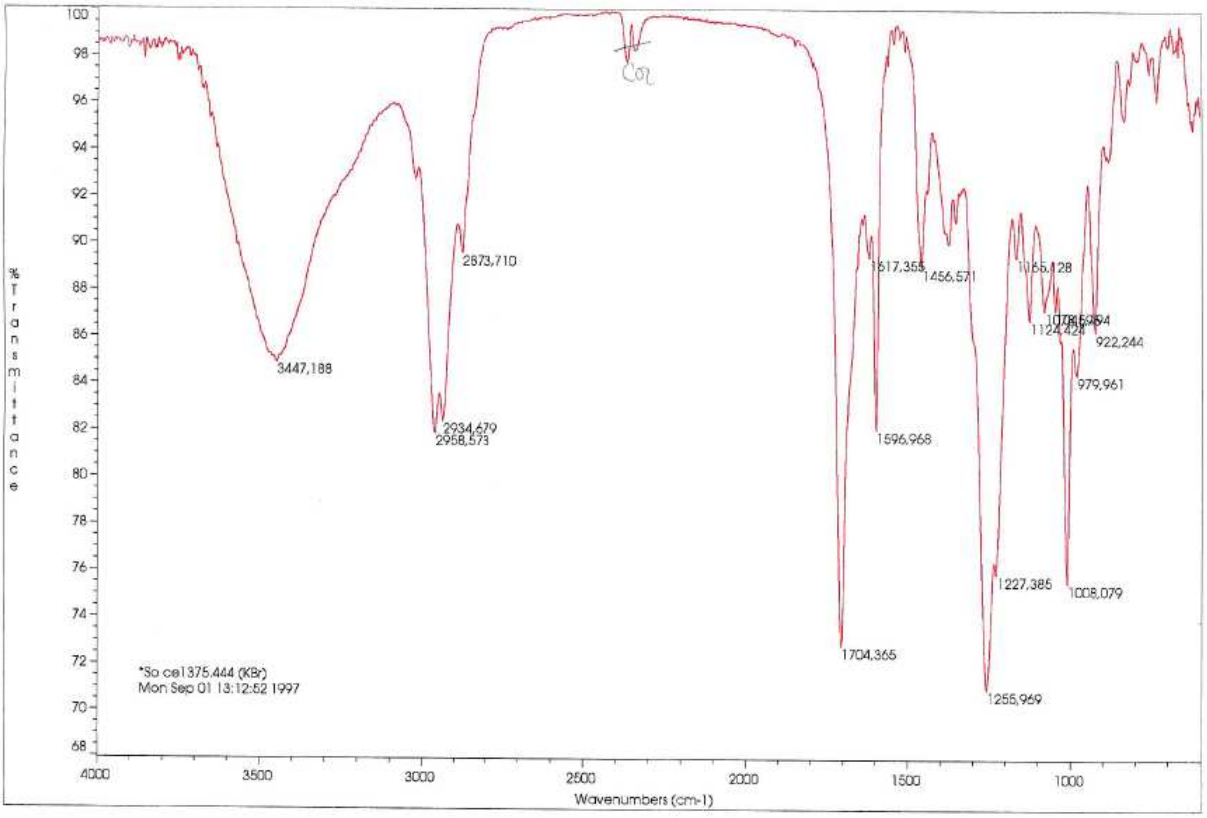

Spectrum 66: IR spectrum from sulfangolid D (**25d**) (KBr).

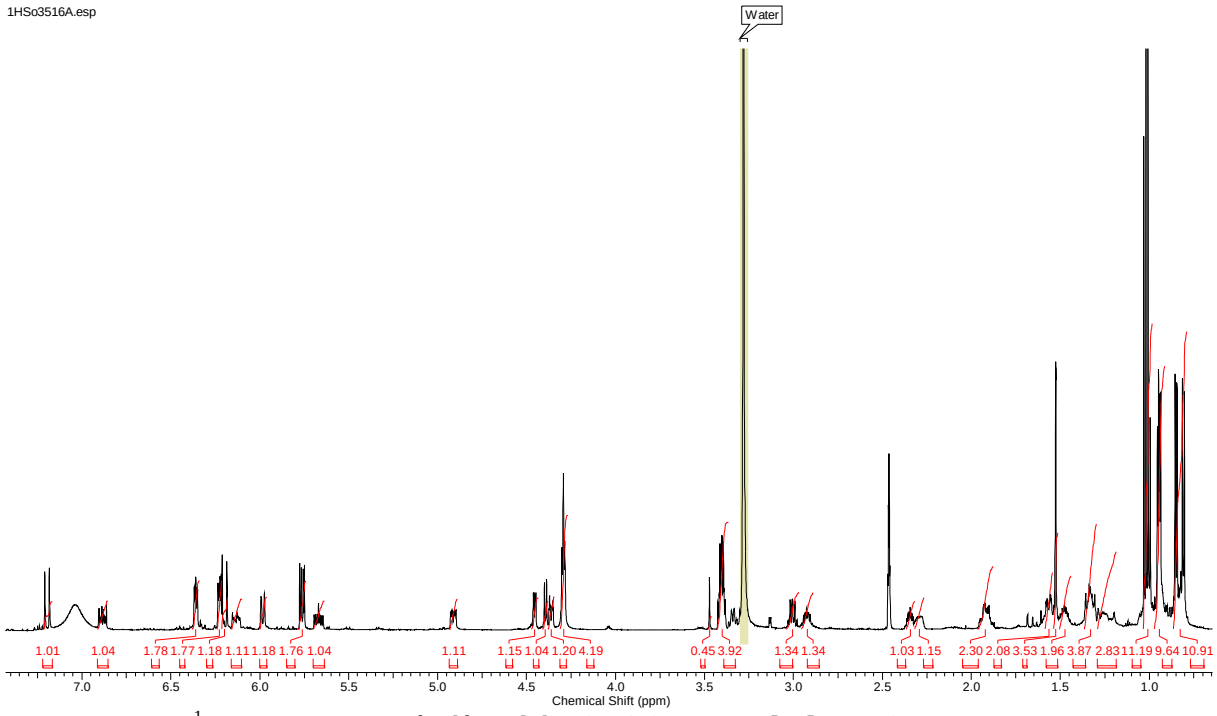

Spectrum 67: ^{1}H NMR spectrum of sulfangolid A (**25a**) (600 MHz, [D_6]DMSO).

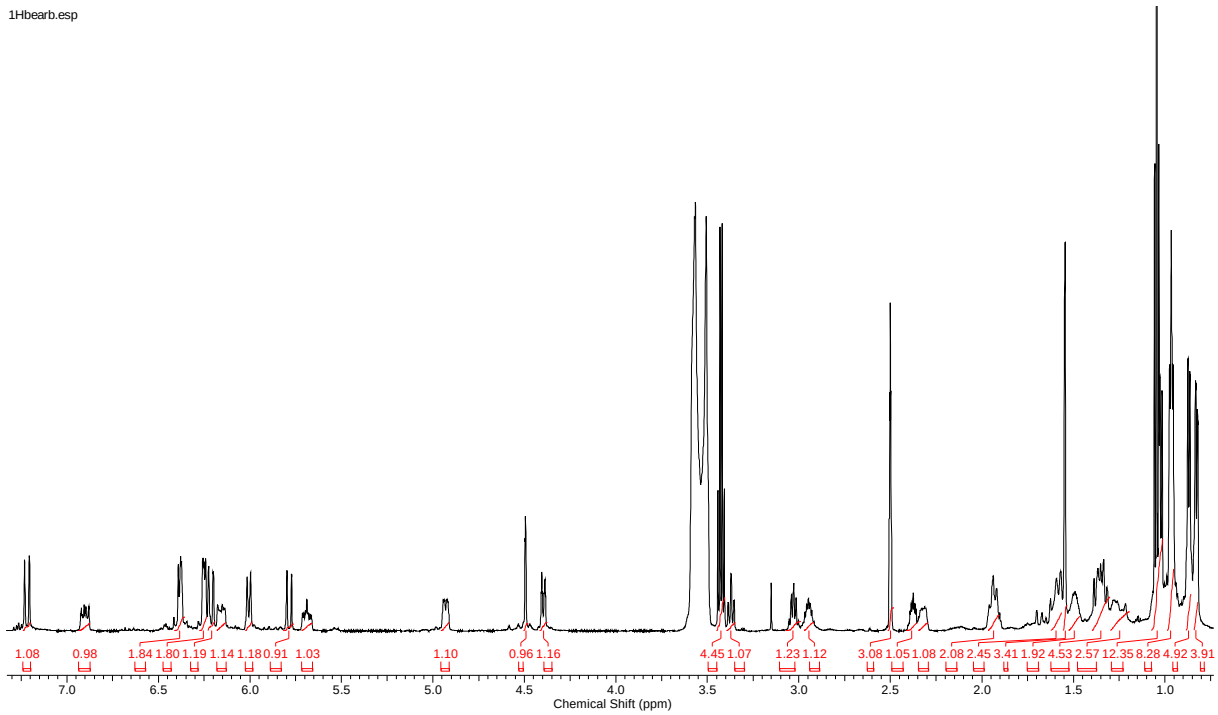

Spectrum 68: ^{1}H NMR spectrum of sulfangolid A (**25a**) (600 MHz, [D_6]DMSO after H/D exchange).

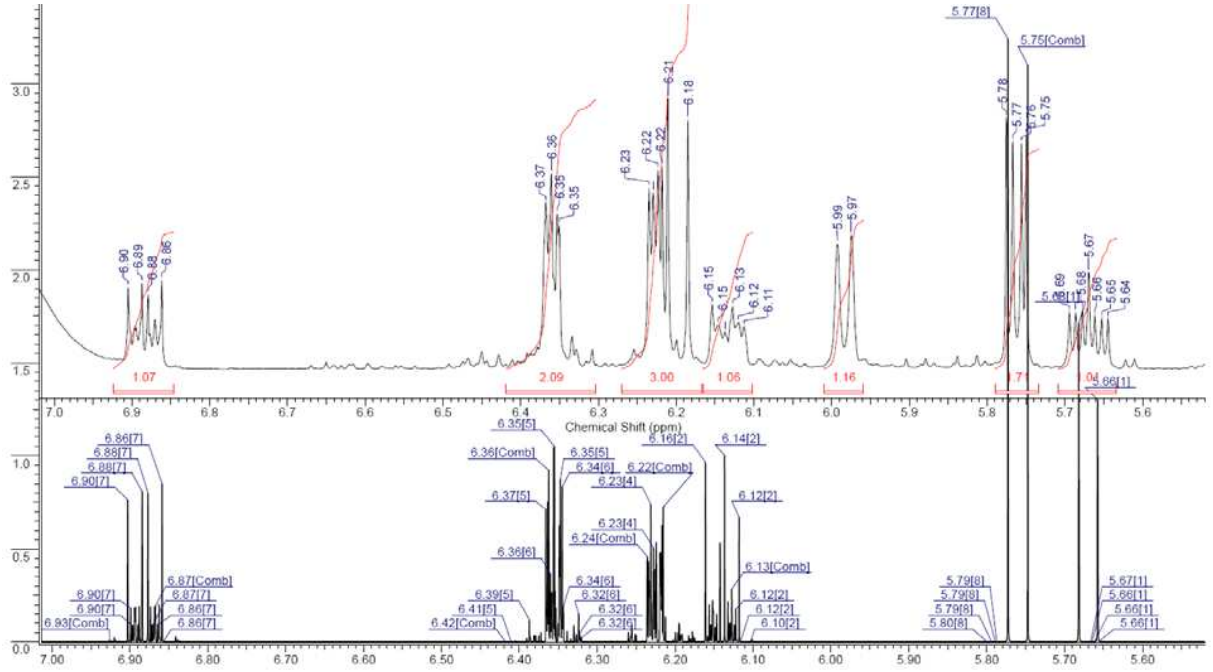

Spectrum 69: simulated ^{1}H NMR spectrum of sulfangolid A (**25a**) with ACD 11.

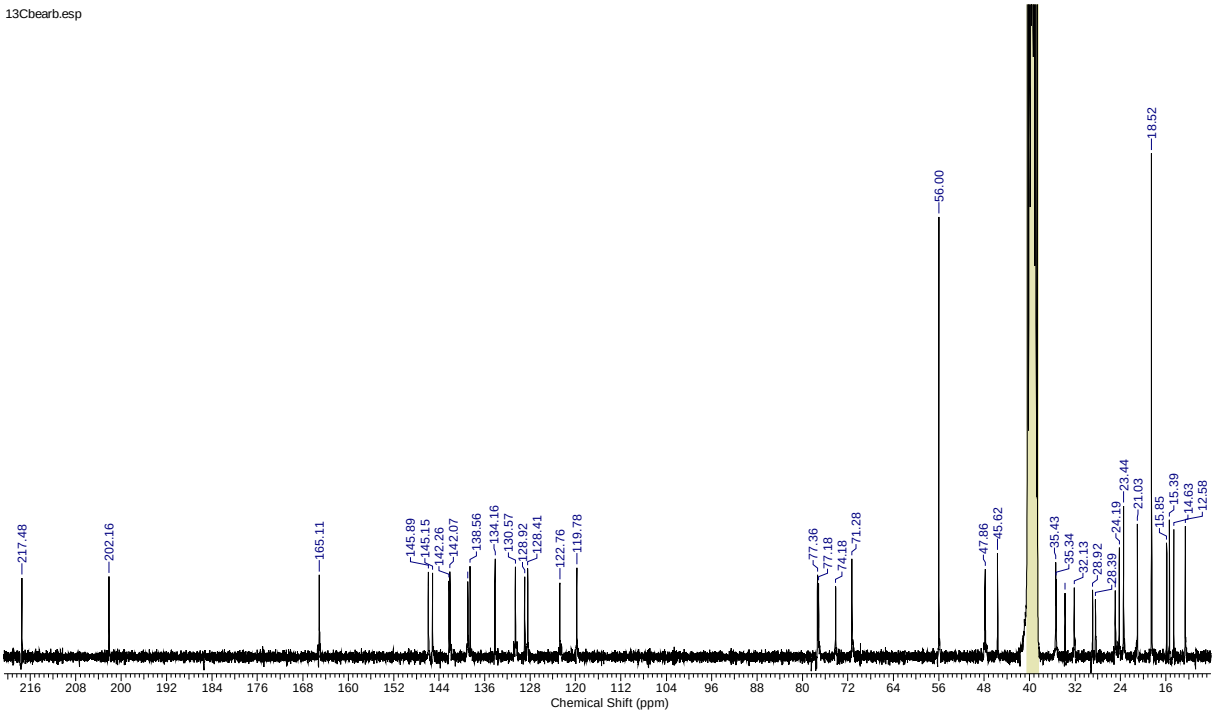

Spectrum 70: ^{13}C NMR spectrum of sulfangolid A (**25a**) (^{13}C 75 MHz, [D_6]DMSO).

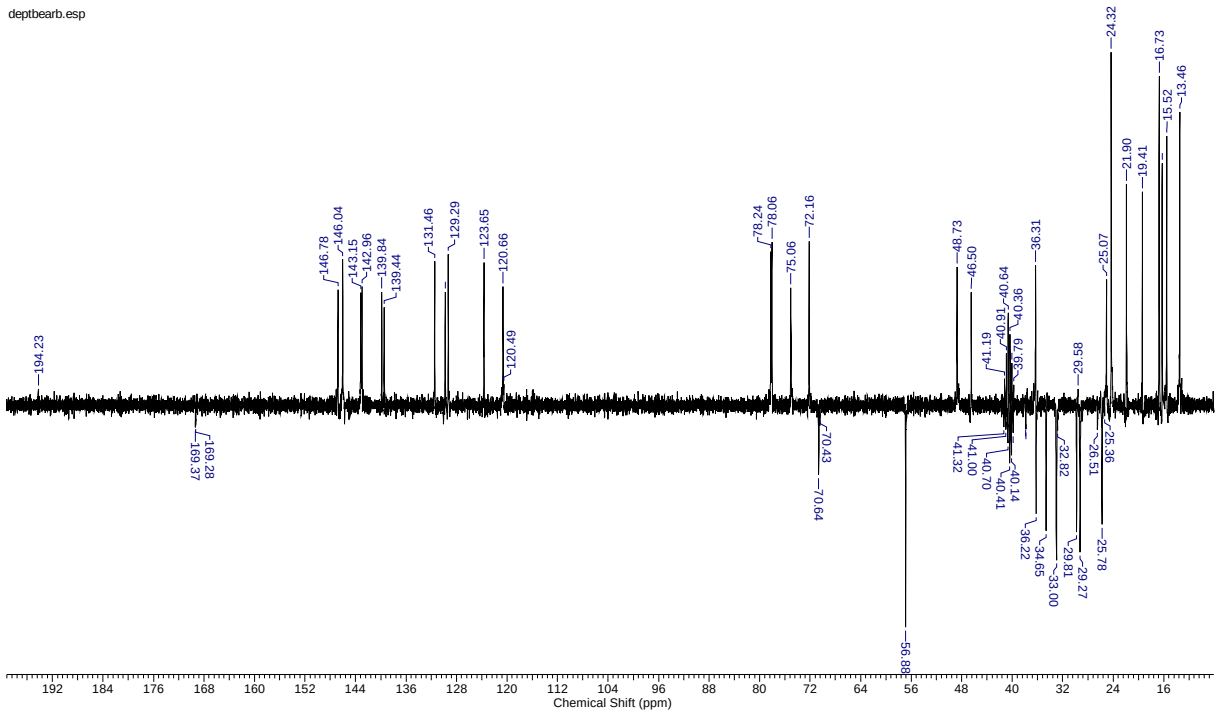

Spectrum 71: ^{13}C DEPT NMR spectrum of sulfangolid A (**25a**) (^{13}C 75 MHz, [D_6]DMSO).

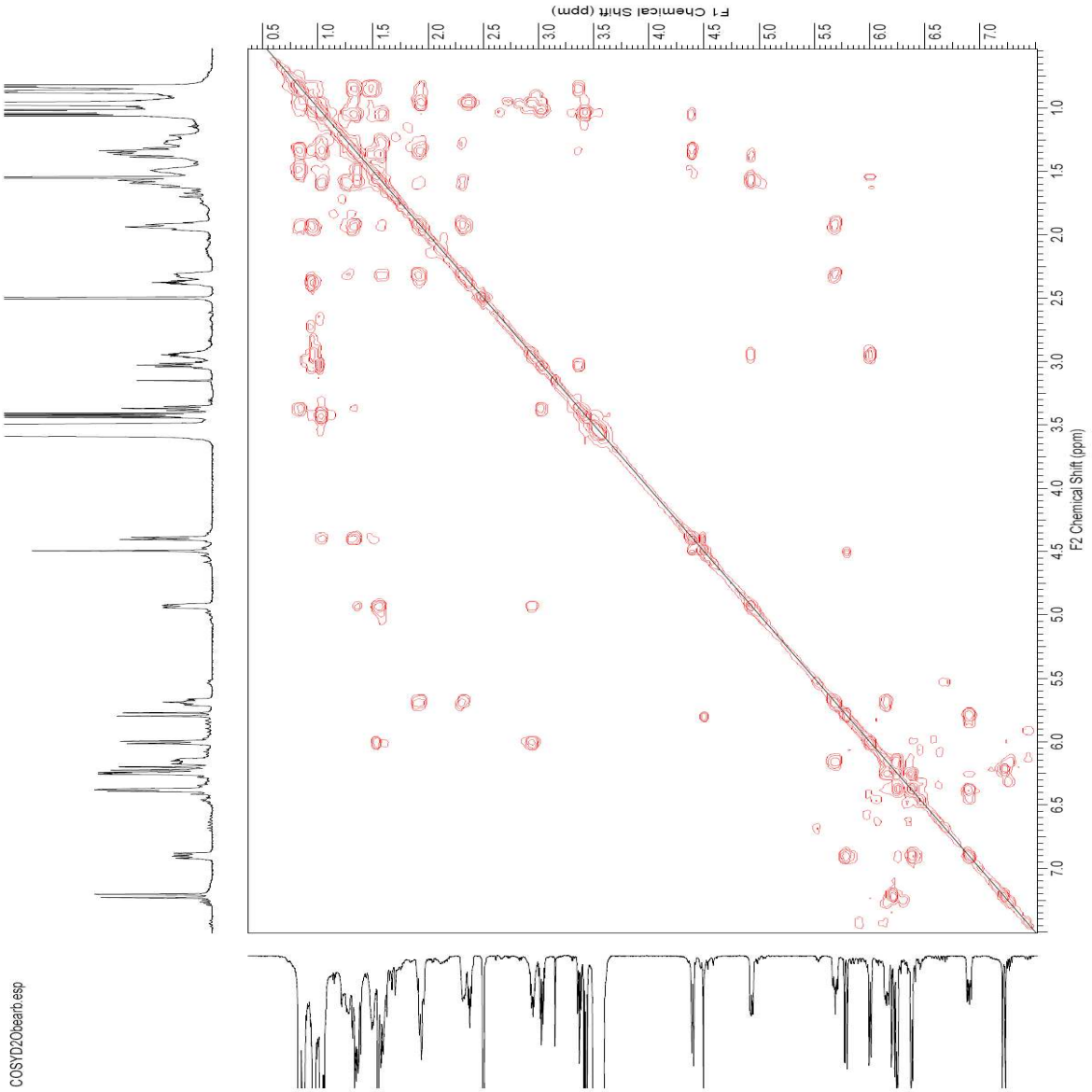

Spectrum 72: $^{1}H,^{1}H$ COSY NMR spectrum of sulfangolid A (**25a**) (^{1}H 600 MHz, [D_6]DMSO).

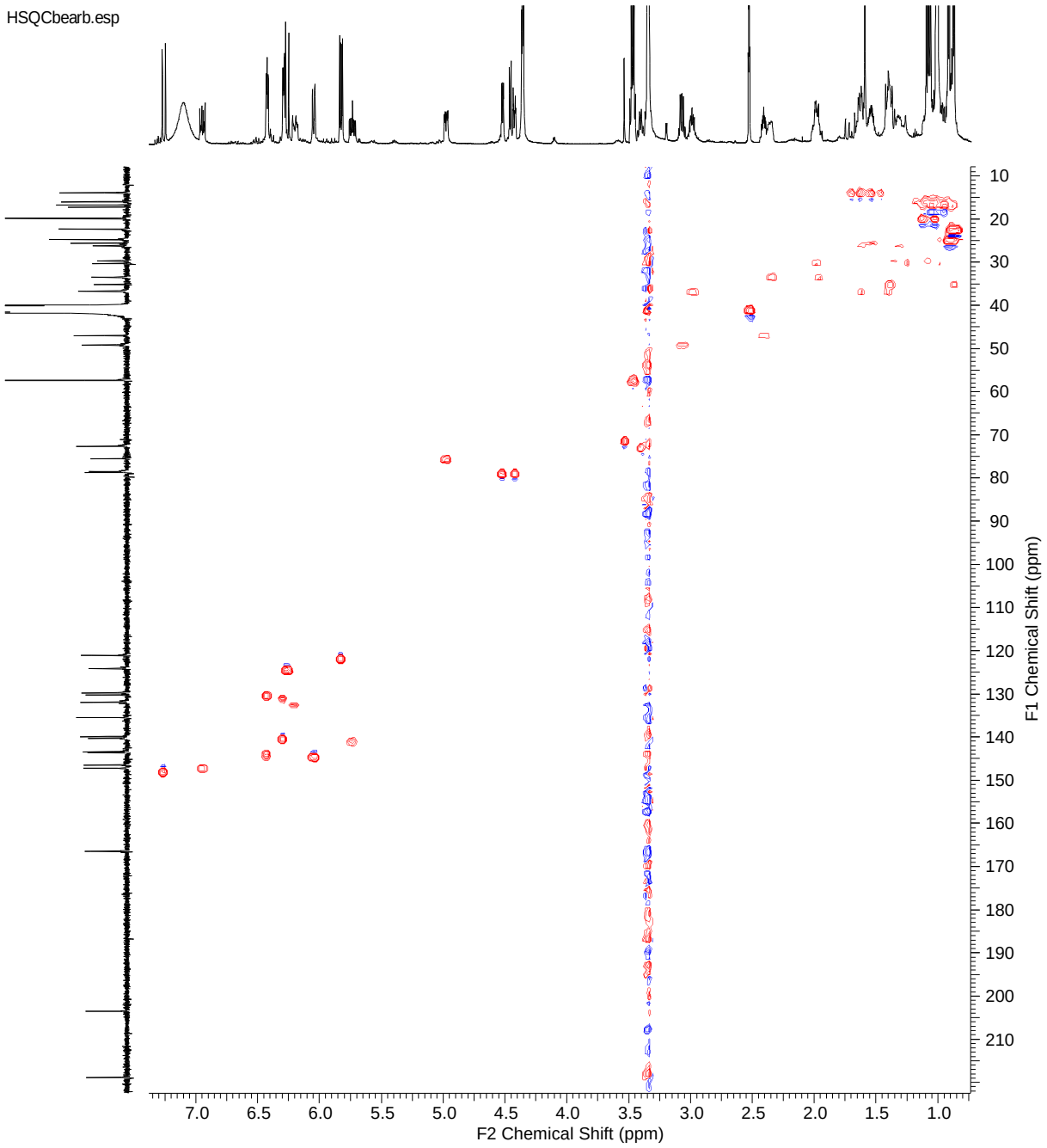

Spectrum 73: $^{1}H,^{13}C$ HSQC NMR spectrum of sulfangolid A (**25a**) (^{1}H 600 MHz, ^{13}C 150 MHz, [D_6]DMSO).

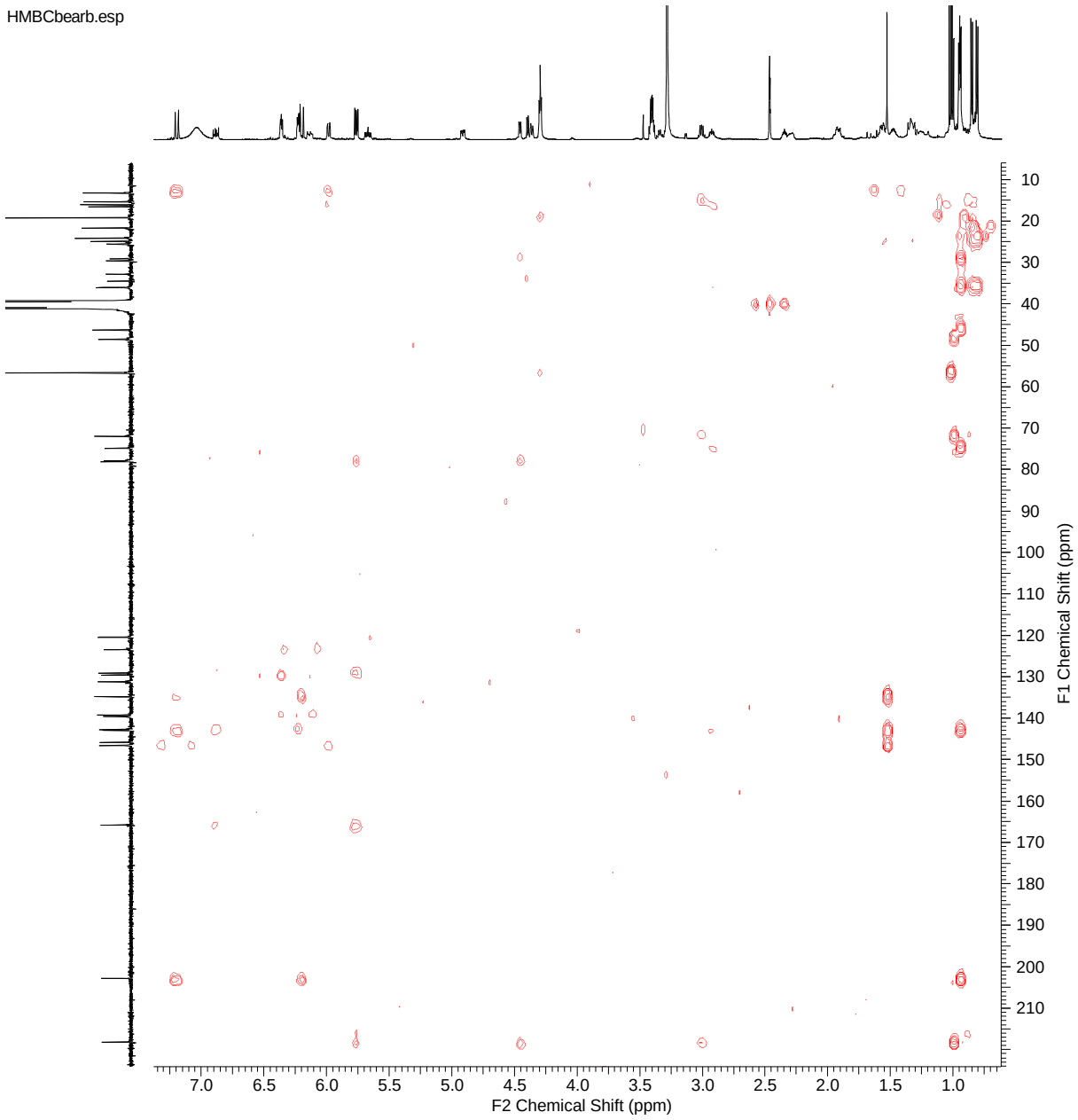

Spectrum 74: $^{1}H,^{13}C$ HMBC NMR spectrum of sulfangolid A (**25a**) (^{1}H 600 MHz, ^{13}C 150 MHz, [D_6]DMSO).

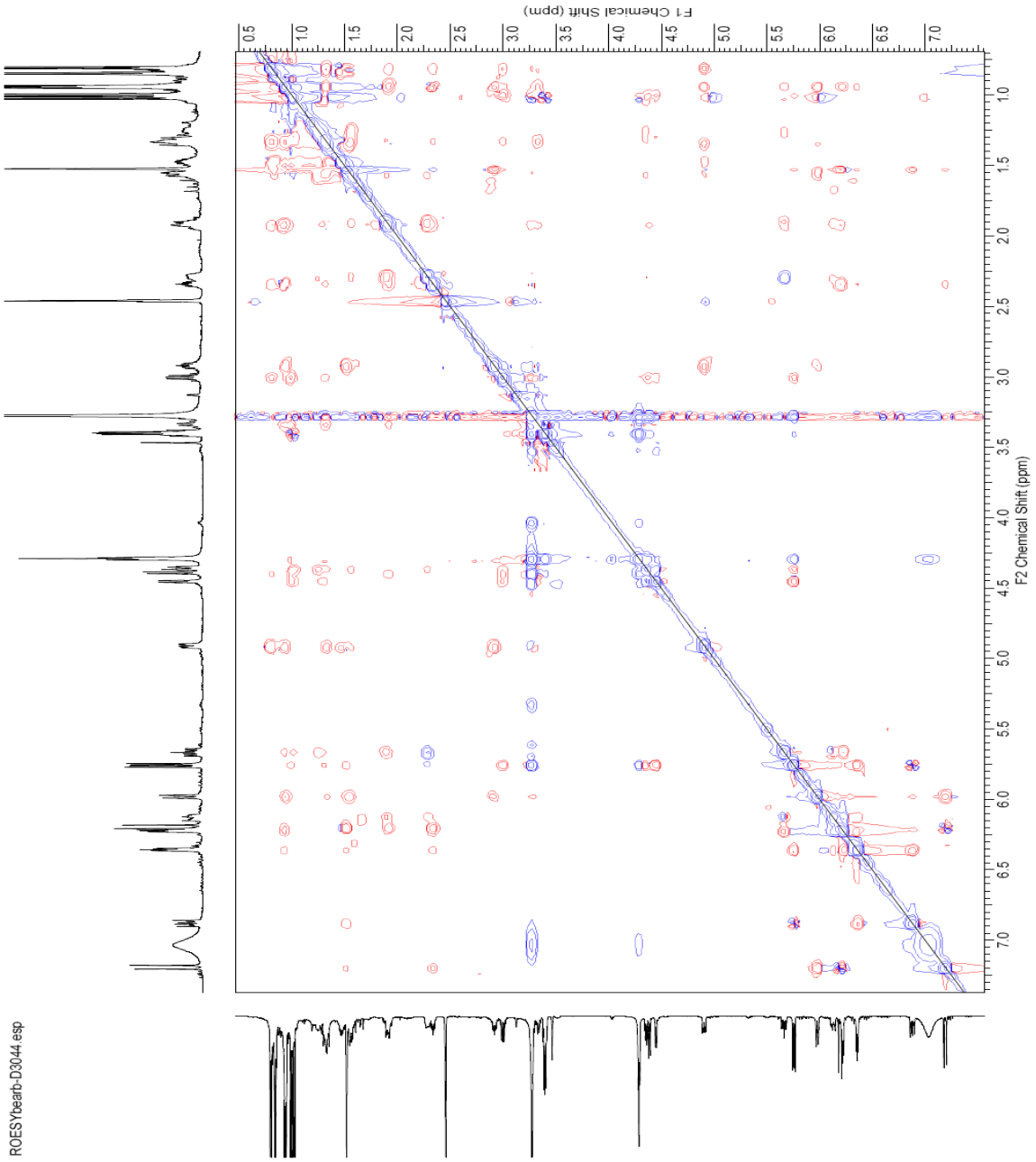

Spectrum 75: $^{1}H,^{1}H$ ROESY NMR spectrum of sulfangolid A (**25a**) (^{1}H 600 MHz, [D_6]DMSO).

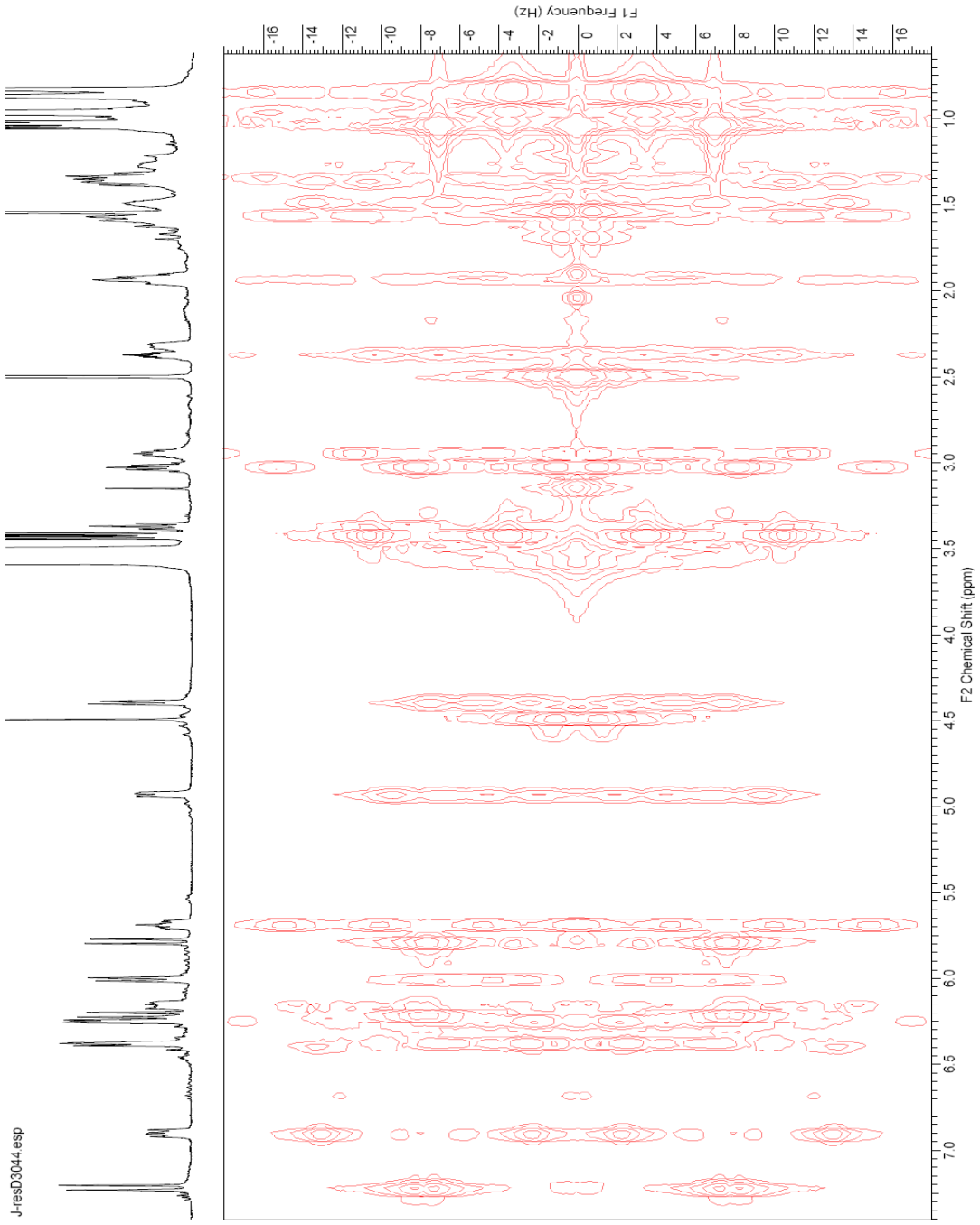

Spectrum 76: *J*-resolved NMR spectrum of sulfangolid A (**25a**) (^{1}H 600 MHz, [D_6]DMSO).

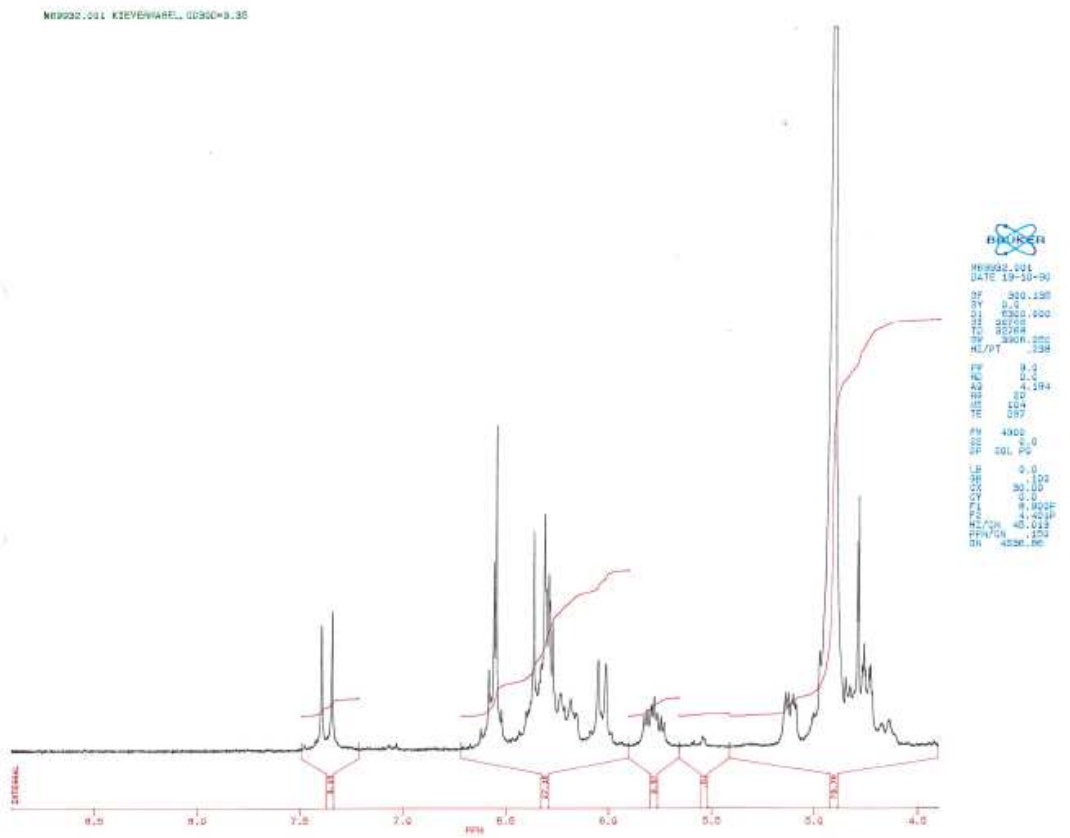

Spectrum 77: ^{1}H NMR spectrum of sulfangolid B (**25b**) from 9.0 to 4.5 ppm (^{1}H 600 MHz, CD_3OD).

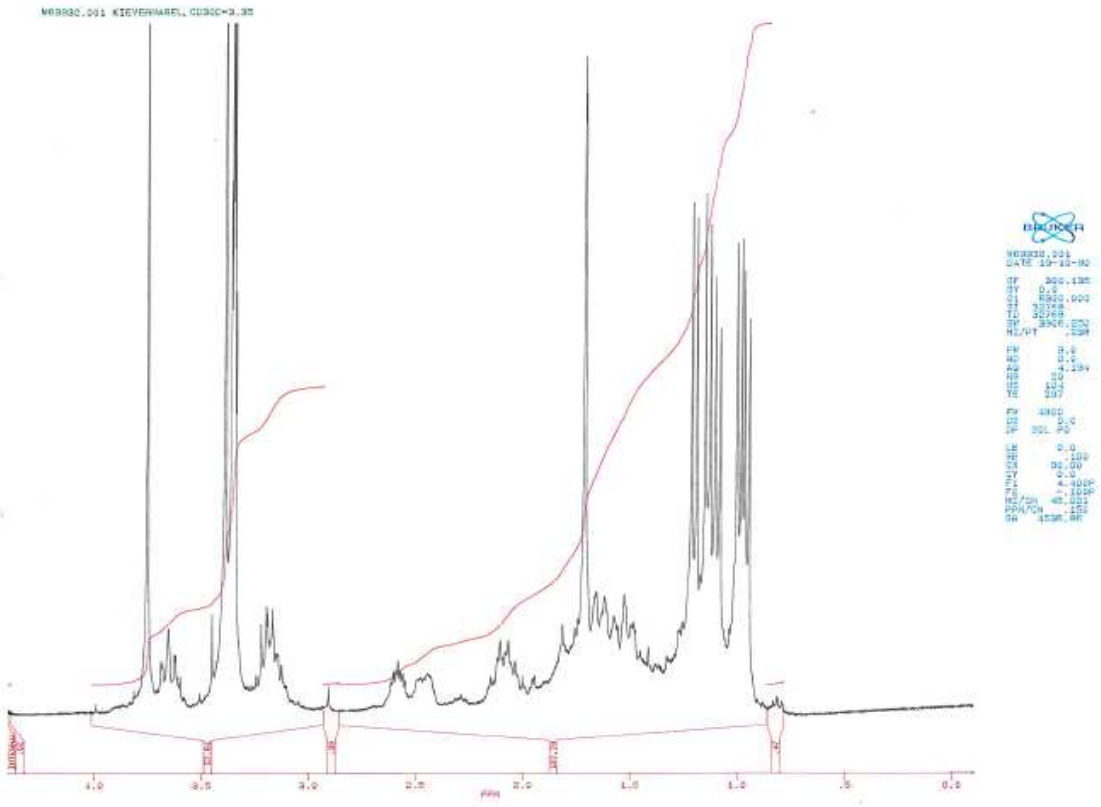

Spectrum 78: ^{1}H NMR spectrum of sulfangolid B (**25b**) 4.0 to 0.0 ppm (^{1}H 600 MHz, CD_3OD).

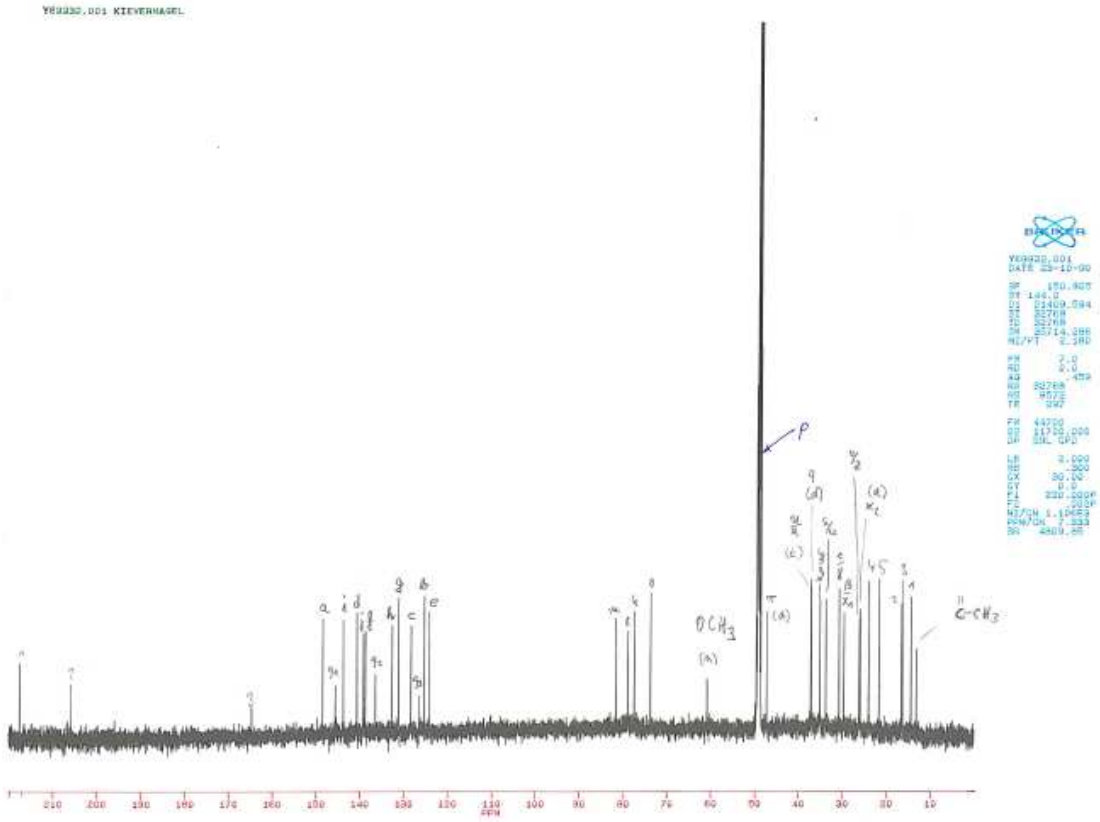

Spectrum 79: ^{13}C NMR spectrum of sulfangolid B (**25b**) (^{13}C 150 MHz, CD_3OD).

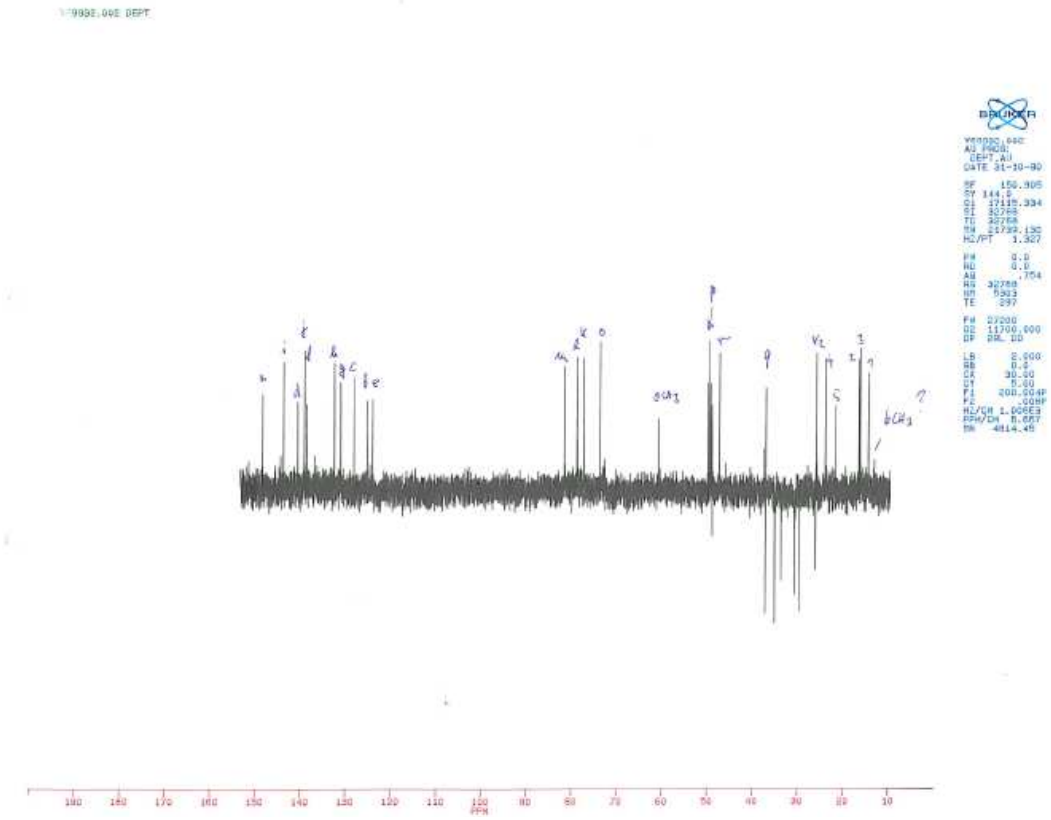

Spectrum 80: ^{13}C- DEPT spectrum of sulfangolid B (**25b**) (150 MHz, CD_3OD).

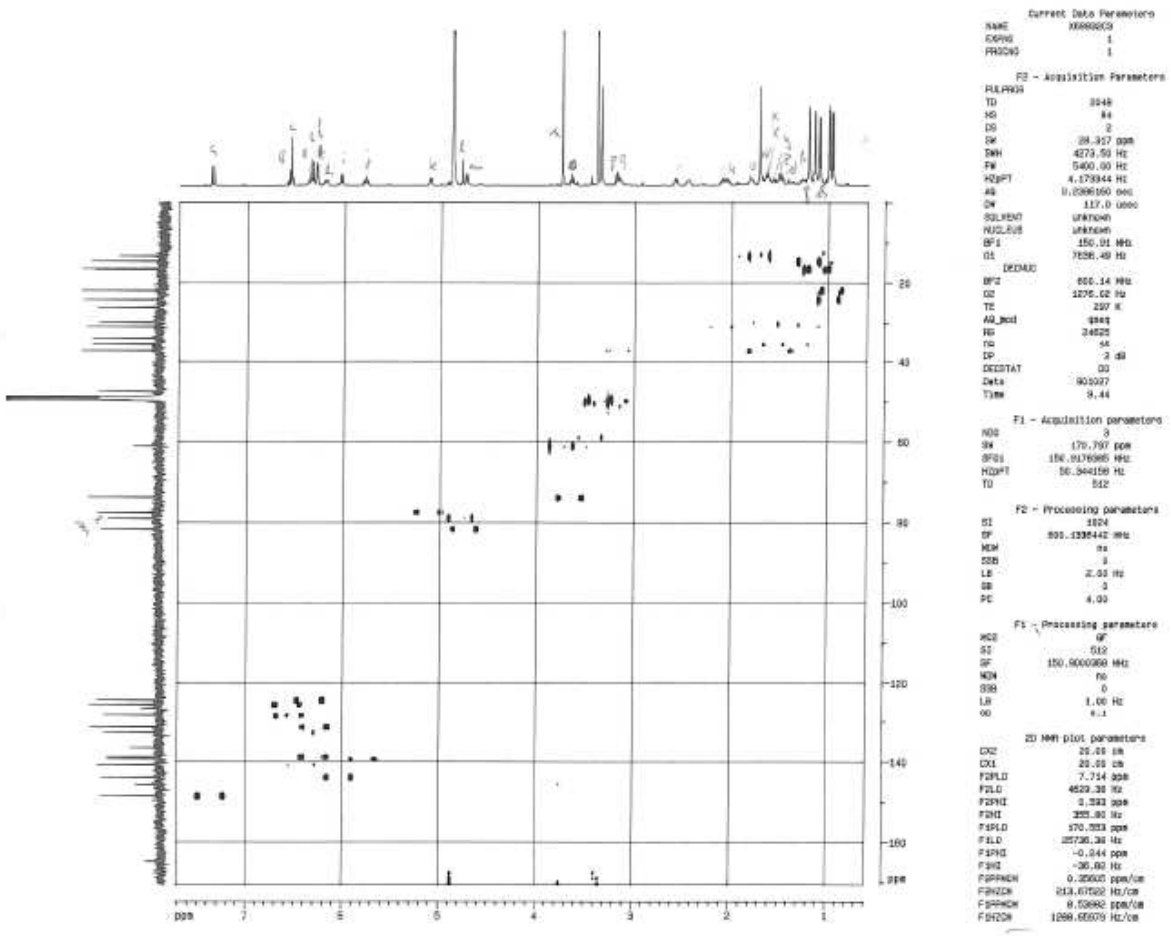

Spectrum 81: Basic-HMQC spectrum of sulfangolid B (**25b**) (^{1}H 600 MHz, ^{13}C 150 MHz, CD_3OD).

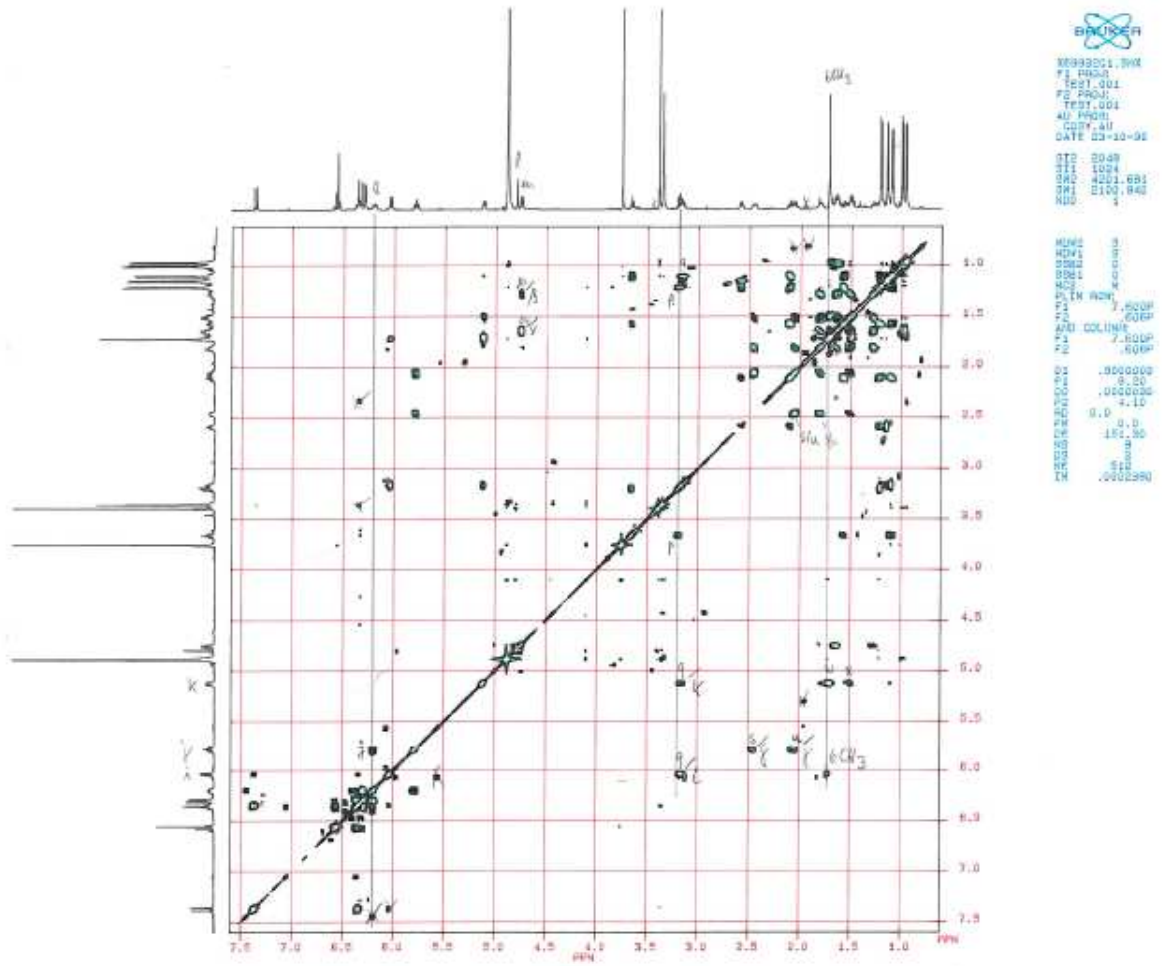

Spectrum 82: $^{1}H,^{1}H$ COSY spectrum of sulfangolid B (**25b**) (^{1}H 600 MHz, CD_3OD).

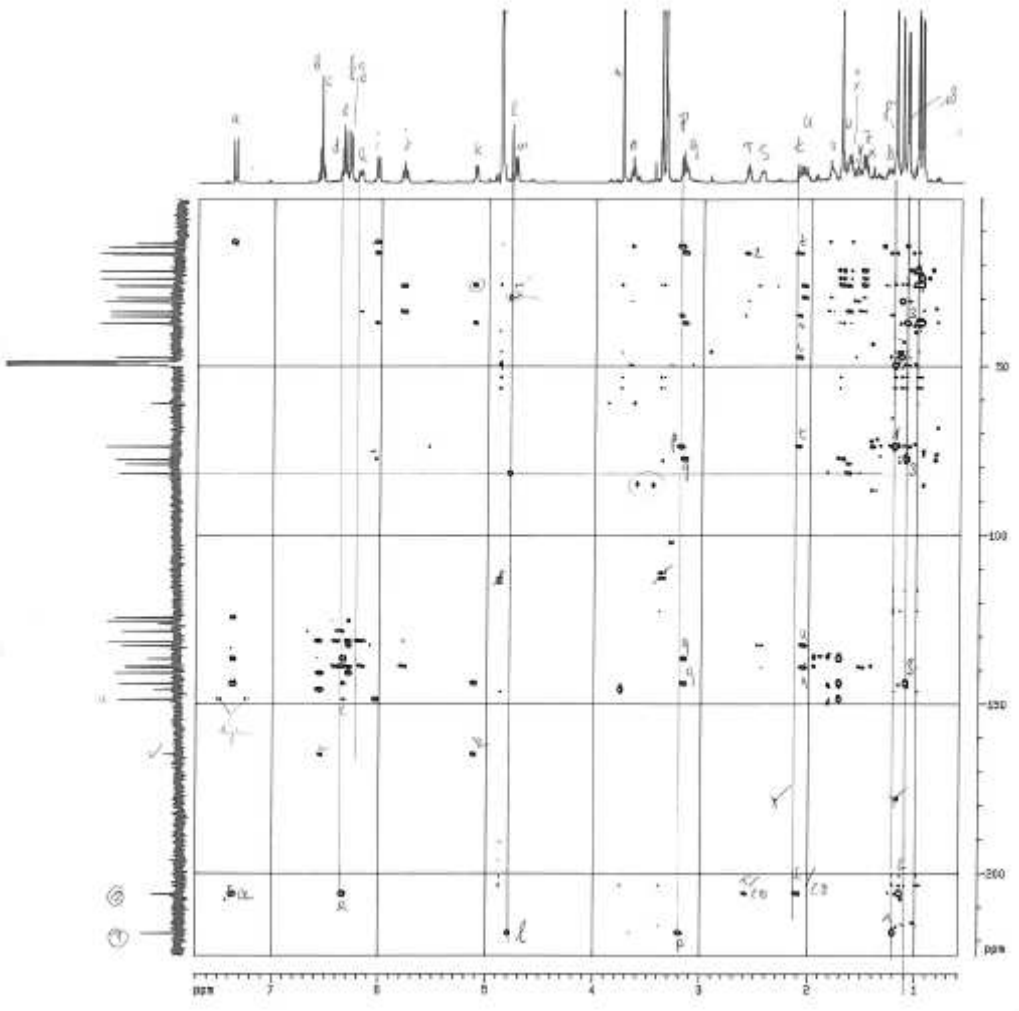

Spectrum 83: $^{1}H,^{13}C$ HMBC of sulfangolid B (**25b**) (^{1}H 600 MHz; ^{13}C 150 MHz, CD_3OD).

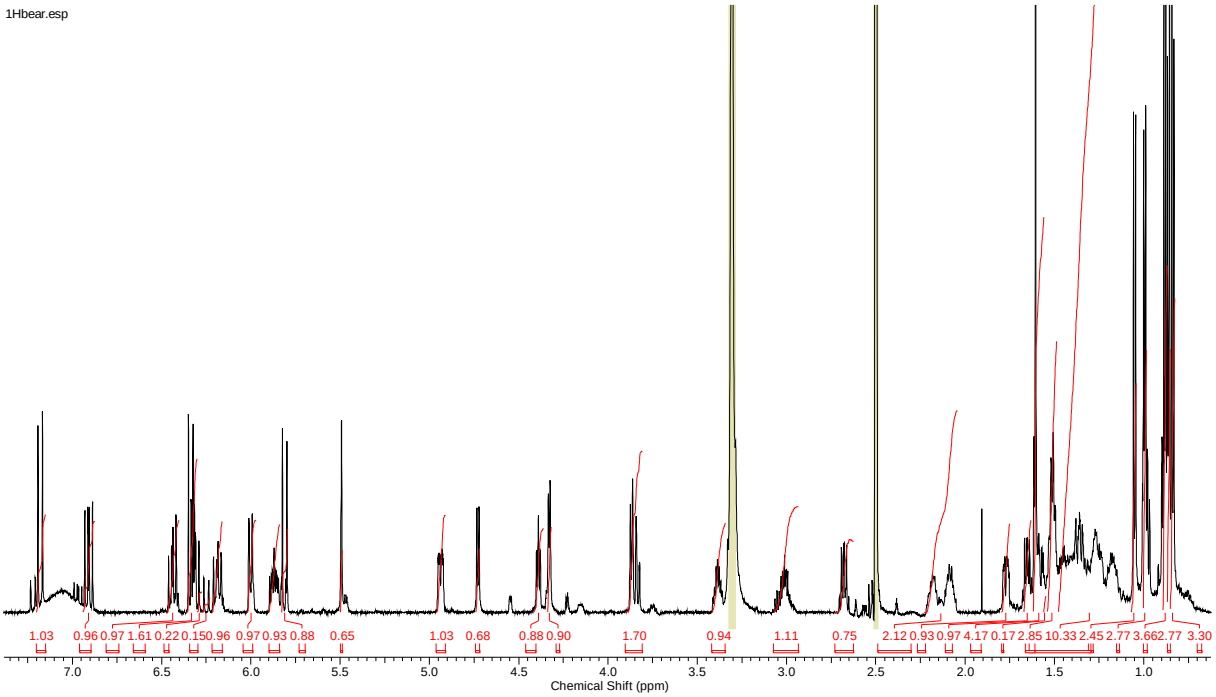

Spectrum 84: ^{1}H NMR spectrum of sulfangolid C (**25c**) (^{1}H 600 MHz, [D_6]DMSO).

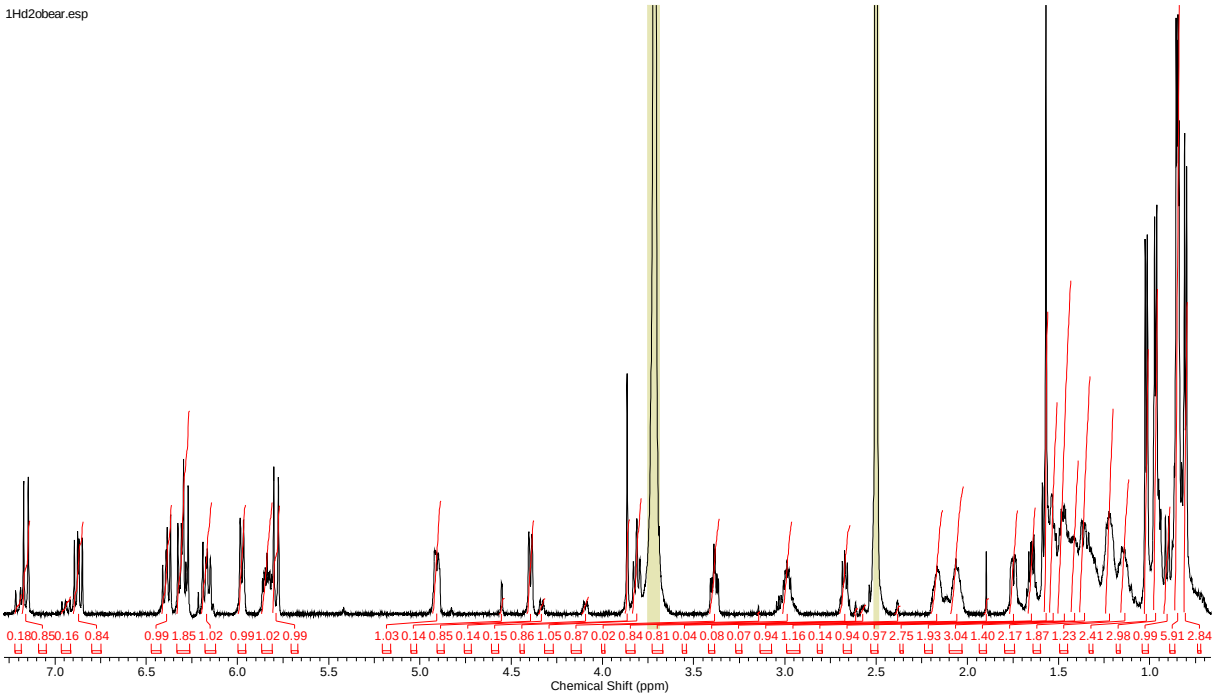

Spectrum 85: ^{1}H NMR spectrum of sulfangolid C (**25c**) (^{1}H 600 MHz, [D_6]DMSO after H/D exchange).

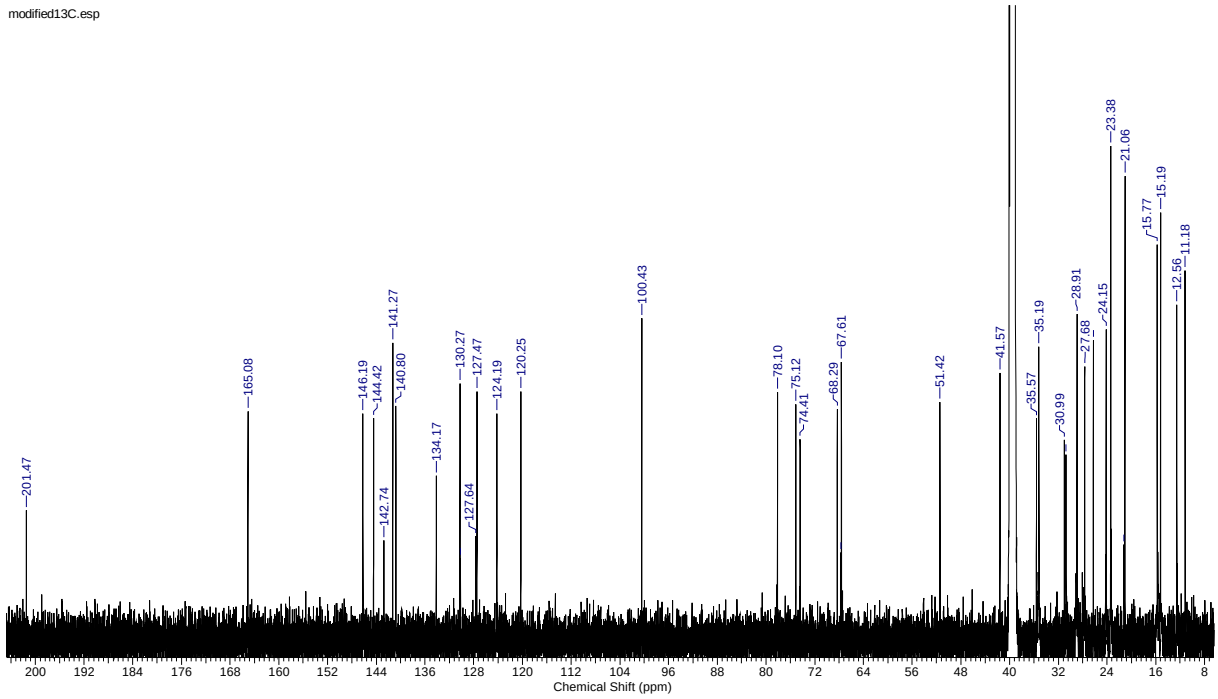

Spectrum 86: ^{13}C NMR spectrum of sulfangolid C (**25c**) (^{13}C 150 MHz, [D_6]DMSO).

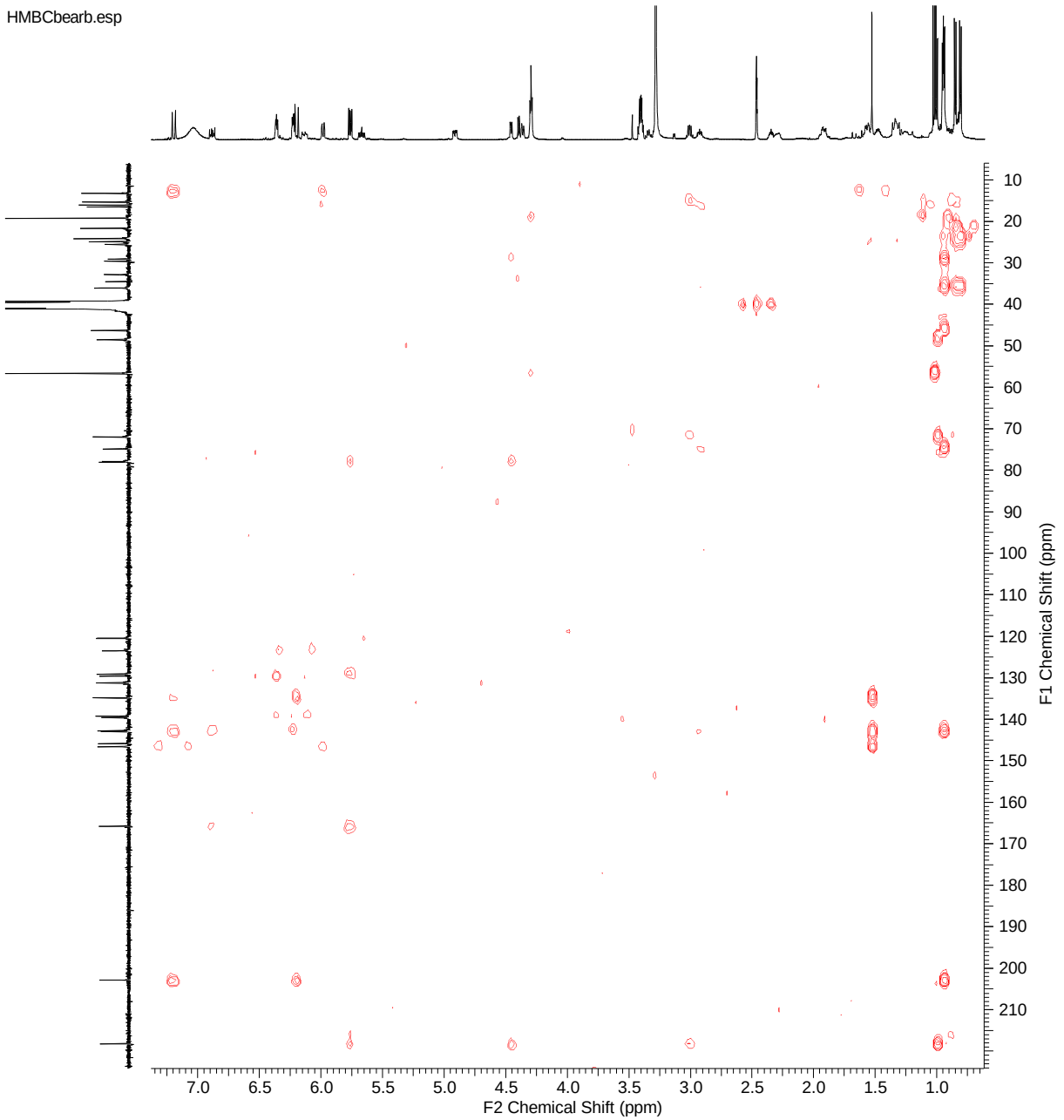

Spectrum 87: $^{1}H,^{13}C$ HSQC NMR spectrum of sulfangolid C (**25c**) (^{1}H 600 MHz, ^{13}C 150 MHz, [D_6]DMSO).

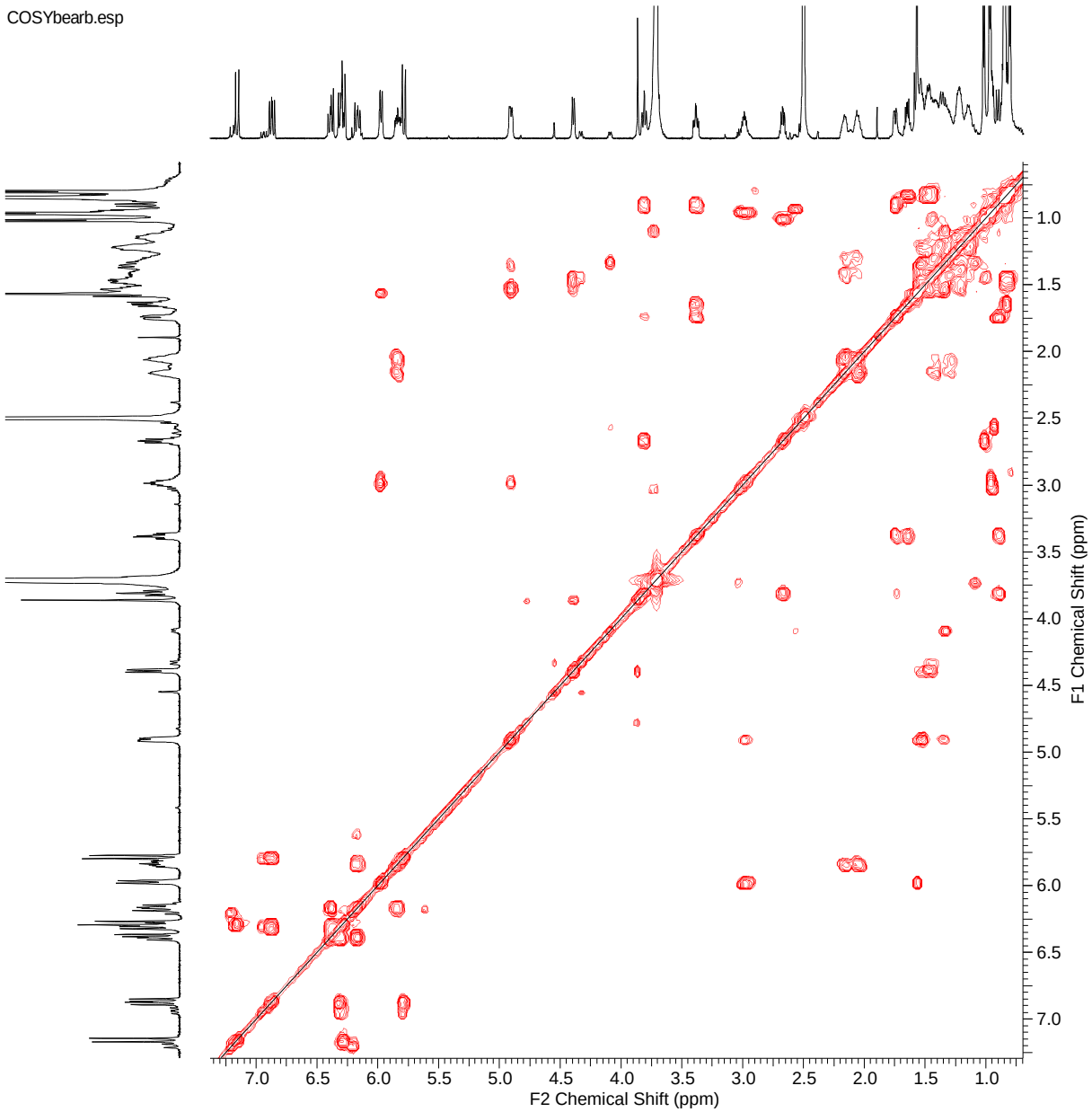

Spectrum 88: $^{1}H,^{1}H$ COSY NMR spectrum of sulfangolid C (25c) (^{1}H 600 MHz, $[D_6]$DMSO after H/D-exchange).

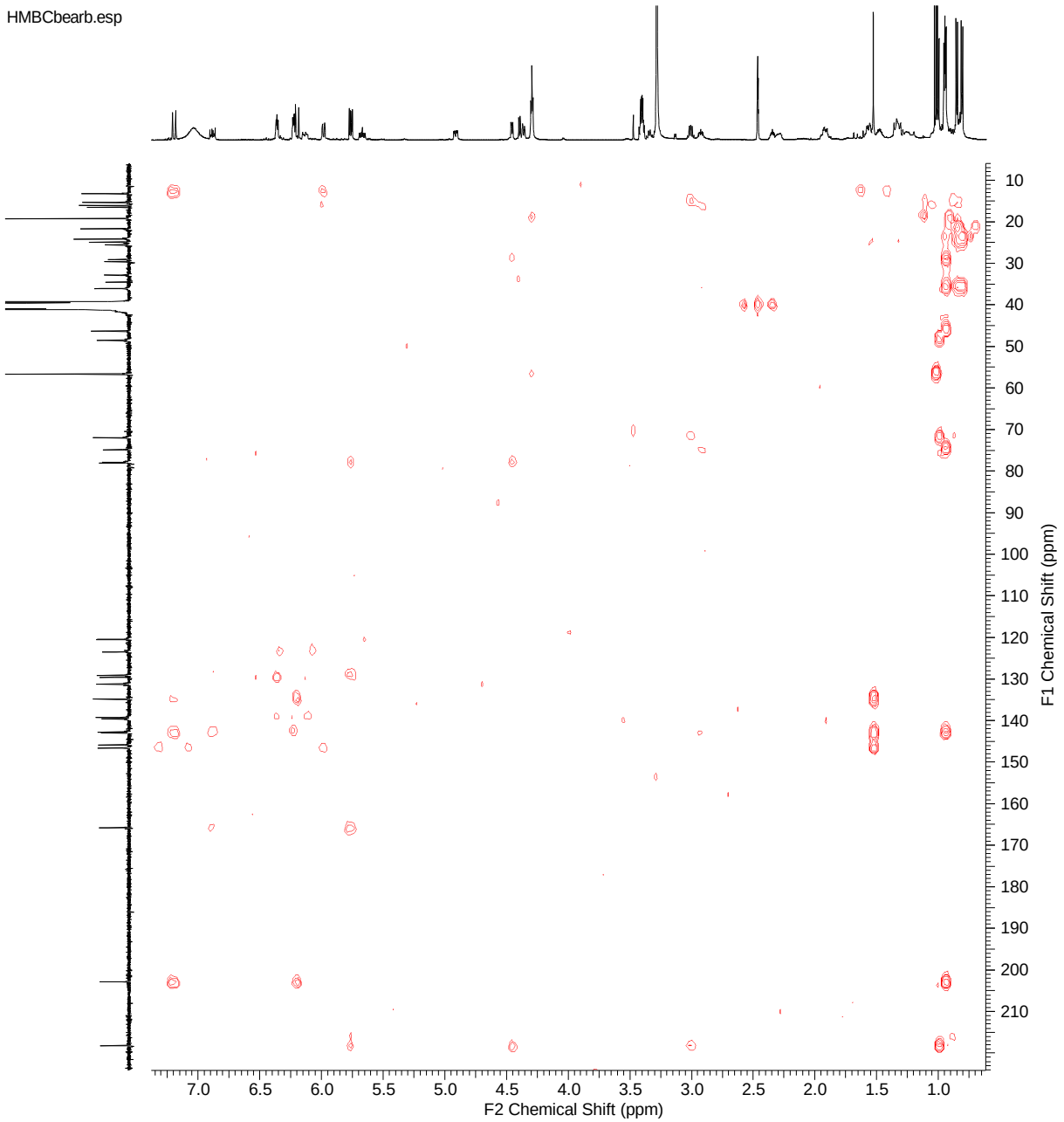

Spectrum 89: $^{1}H,^{13}C$ HMBC NMR spectrum of sulfangolid C (**25c**) (^{1}H 600 MHz, ^{13}C 150 MHz, [D_6]DMSO).

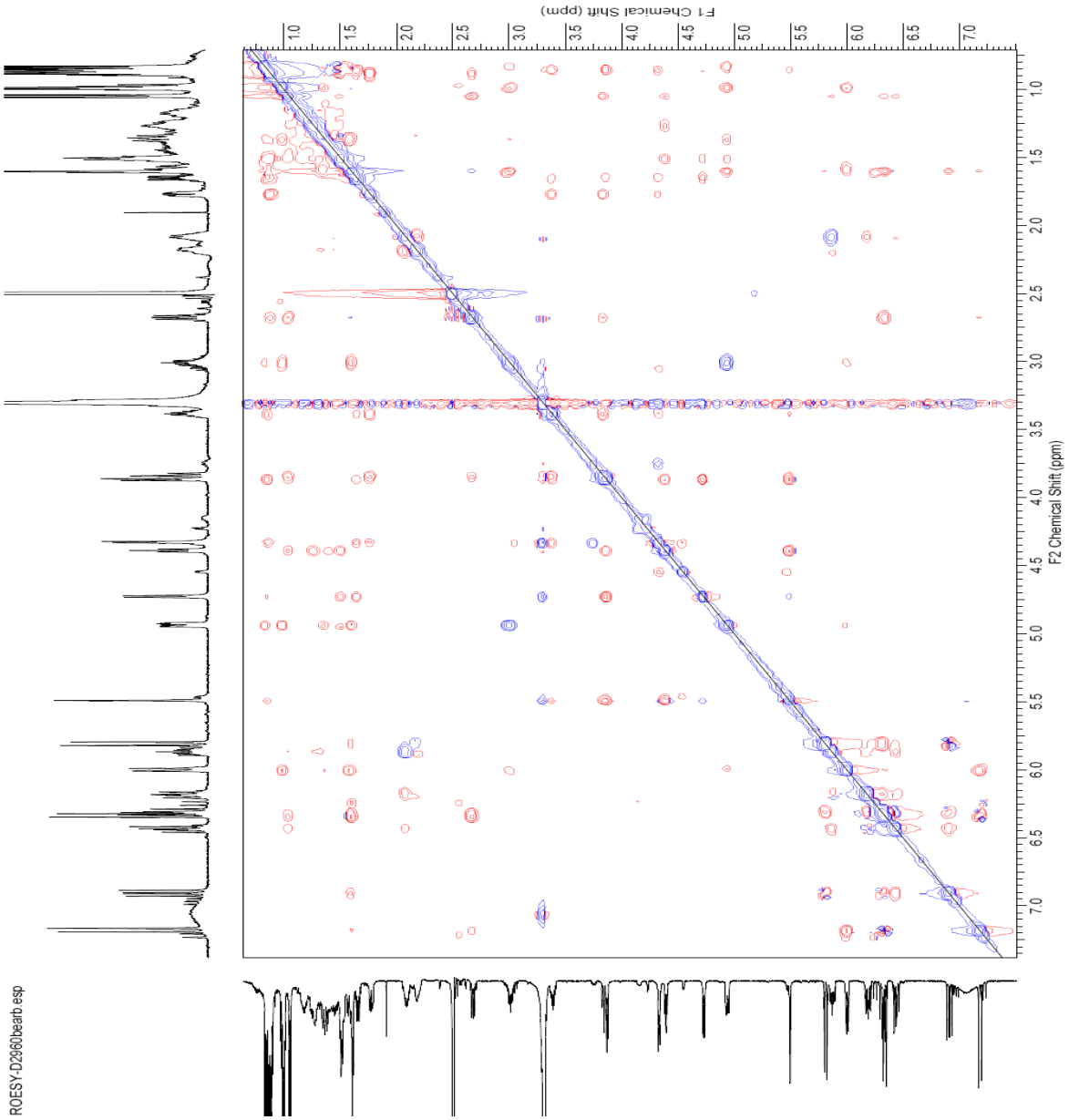

Spectrum 90: $^{1}H,^{1}H$ ROESY NMR spectrum of sulfangolid C (**25c**) (^{1}H 600 MHz, [D_6]DMSO).

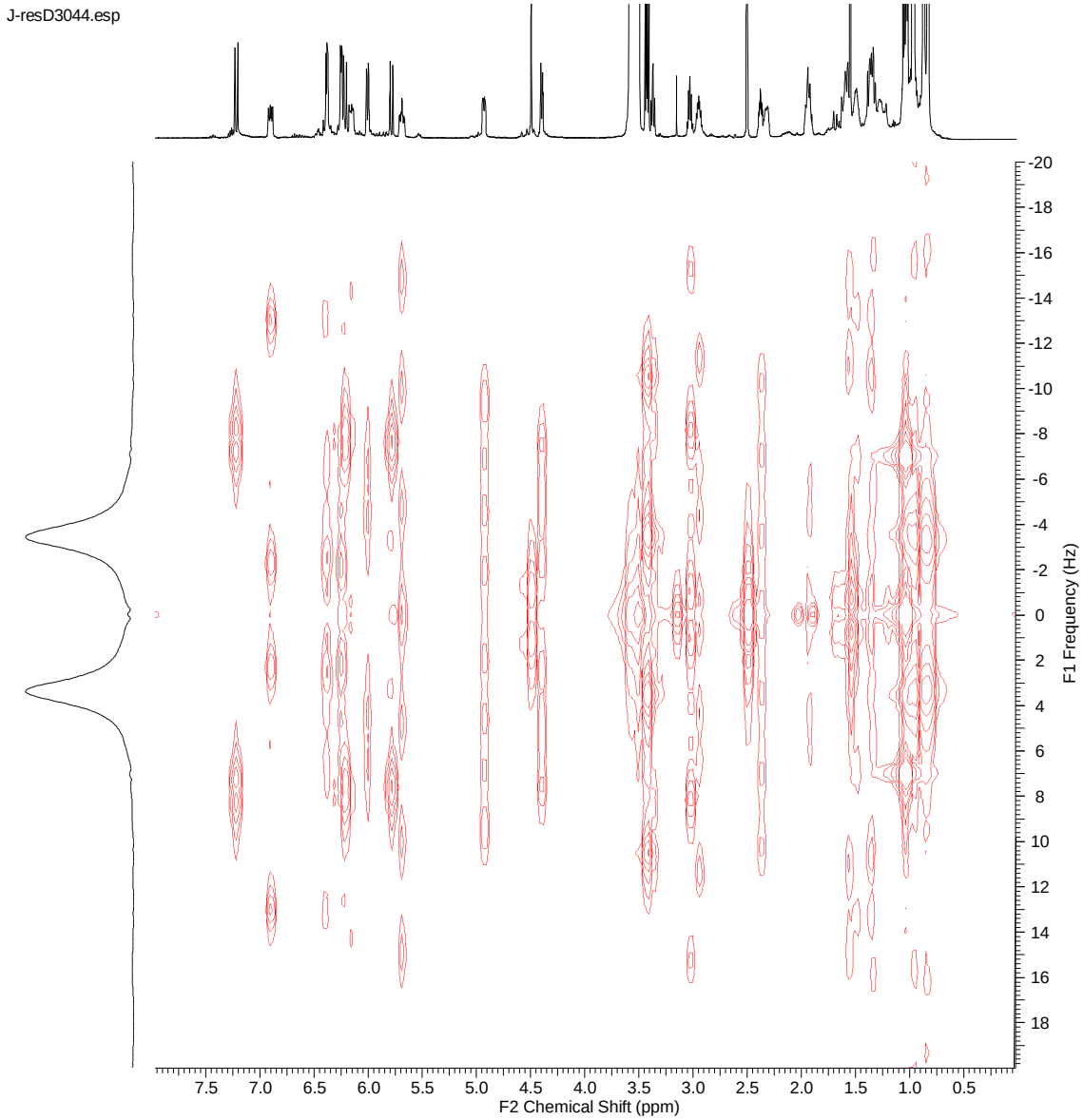

Spectrum 91: *J*-resolved NMR spectrum of sulfangolid C (**25c**) (^{1}H 600 MHz, [D_6]DMSO after H/D exchange).

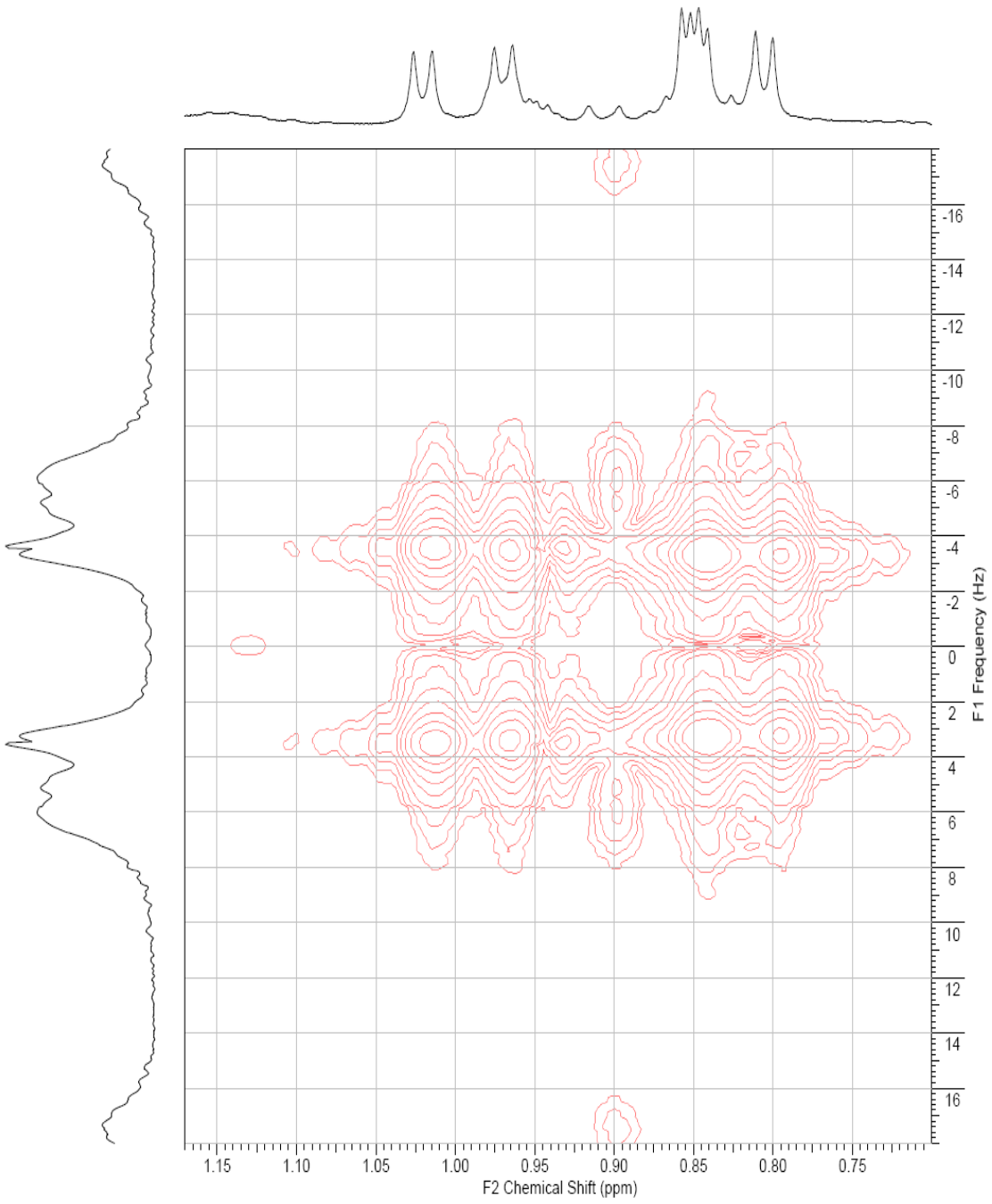

Spectrum 92: Partial view of *J*-resolved spectrum of sulfangolid C (**25c**) (^{1}H 600 MHz, [D_6]DMSO after H/D exchange).

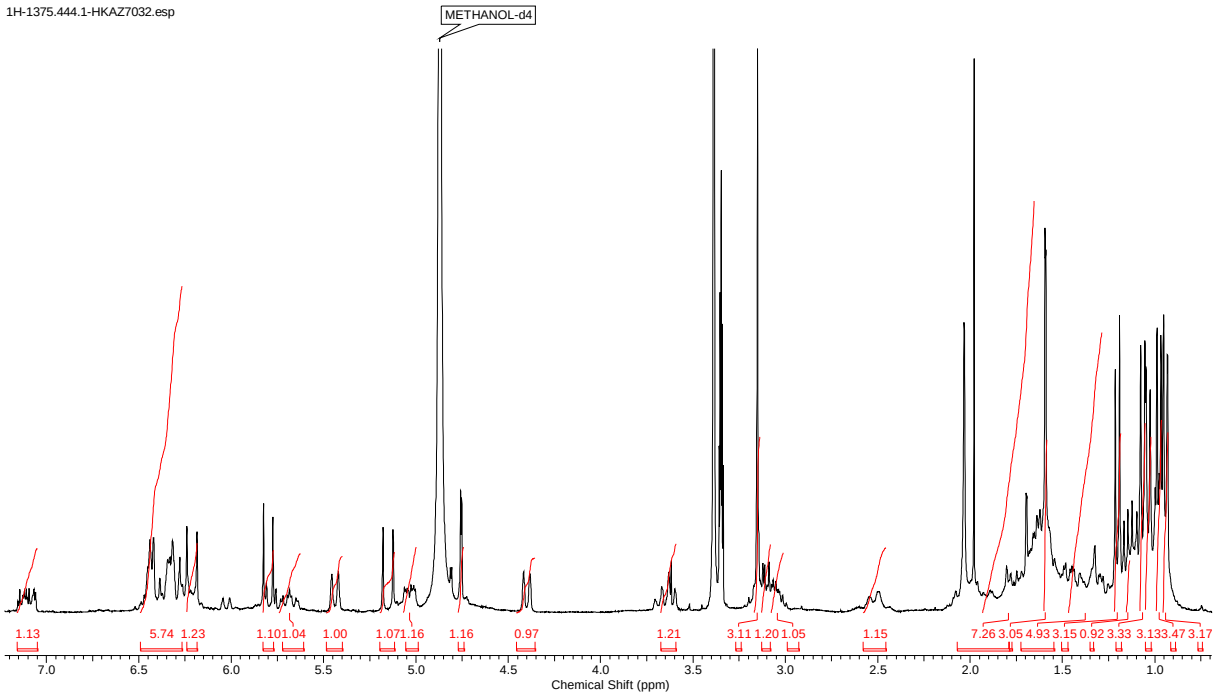

Spectrum 93: ^{1}H NMR spectrum of sulfangolid D (**25d**) (^{1}H 300 MHz, CD_3OD).

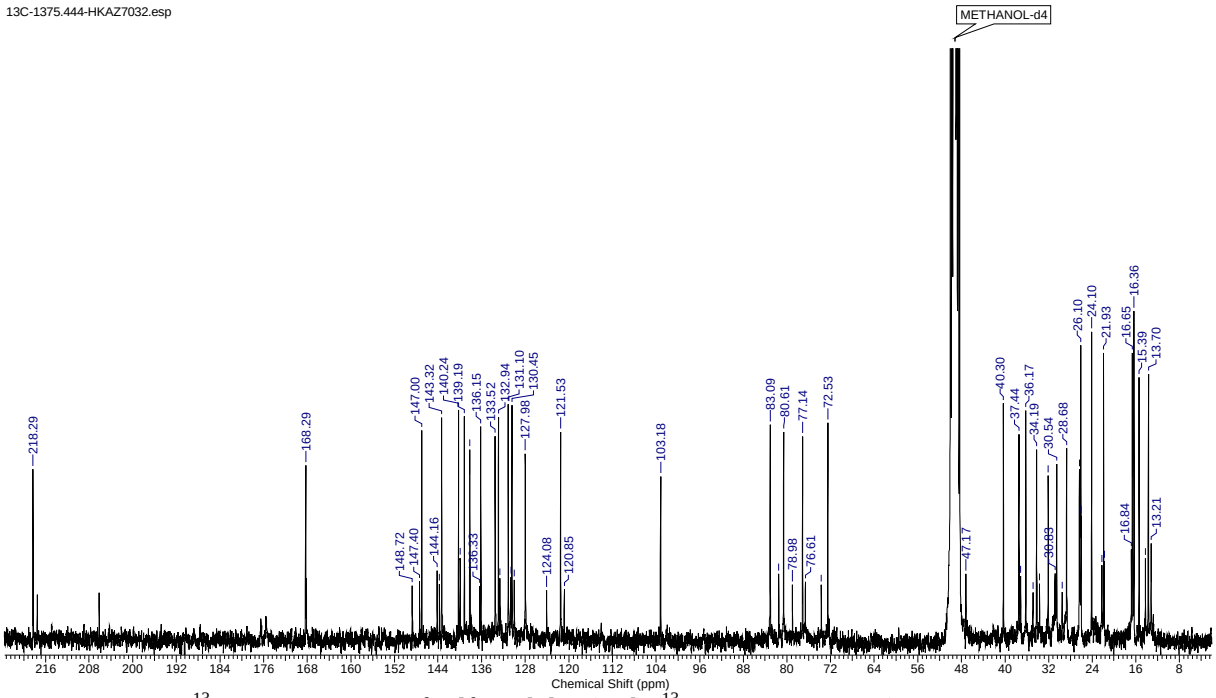

Spectrum 94: ^{13}C NMR spectrum of sulfangolid D (25d) (^{13}C 75 MHz, CD_3OD).

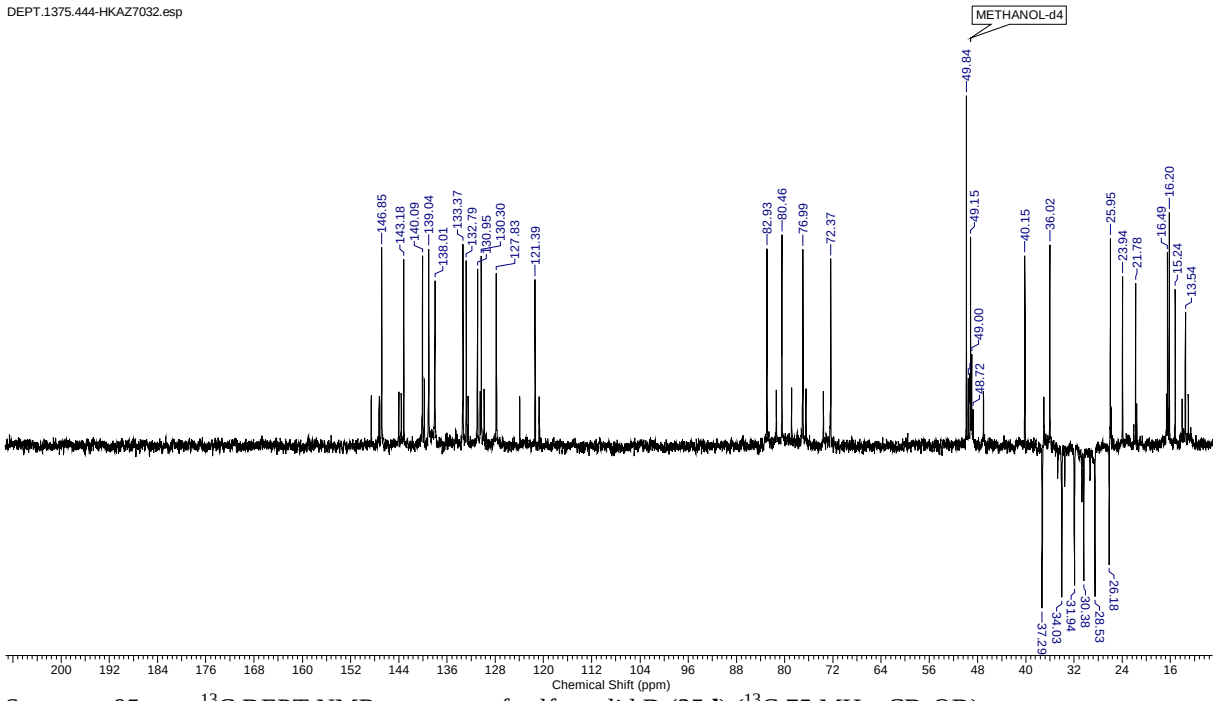

Spectrum 95: ^{13}C DEPT NMR spectrum of sulfangolid D (**25d**) (^{13}C 75 MHz, CD_3OD).

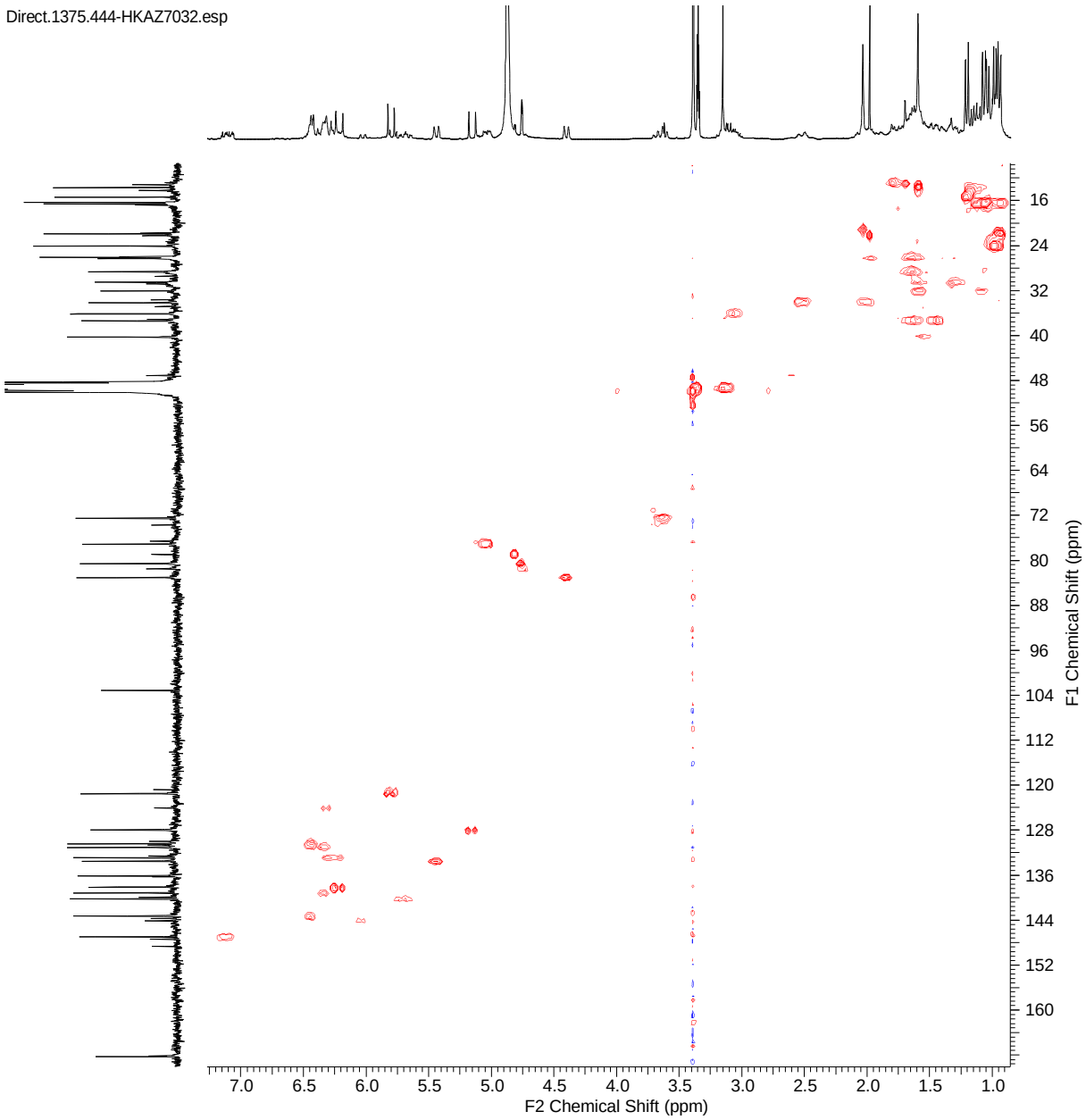

Spectrum 96: $^{1}H,^{13}C$ HSQC spectrum of sulfangolid D (**25d**) (^{1}H 300 MHz, ^{13}C 75 MHz, CD_3OD).

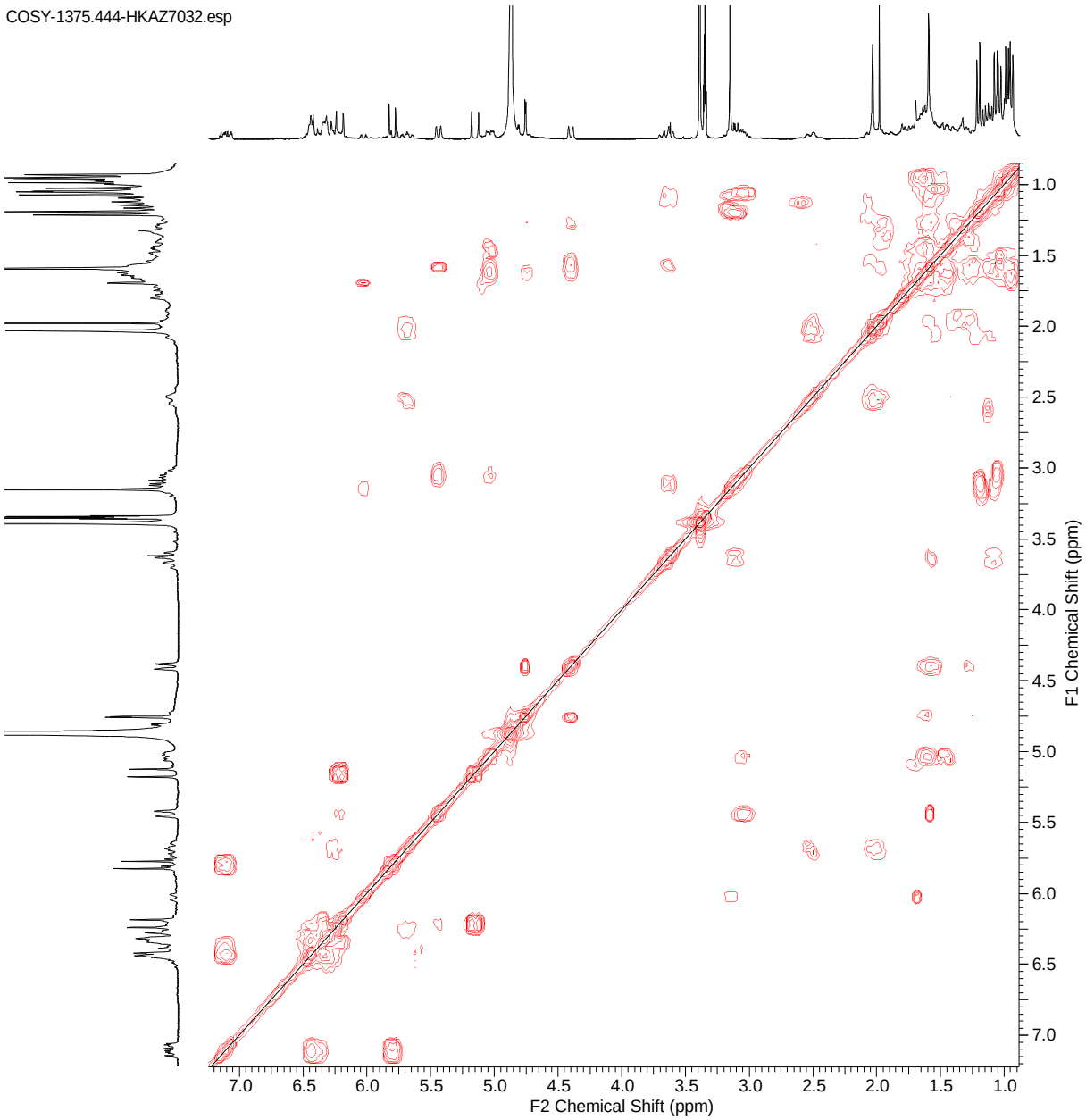

Spectrum 97: $^{1}H,^{1}H$ COSY spectrum of sulfangolid D (**25d**) (^{1}H 300 MHz, CD_3OD).

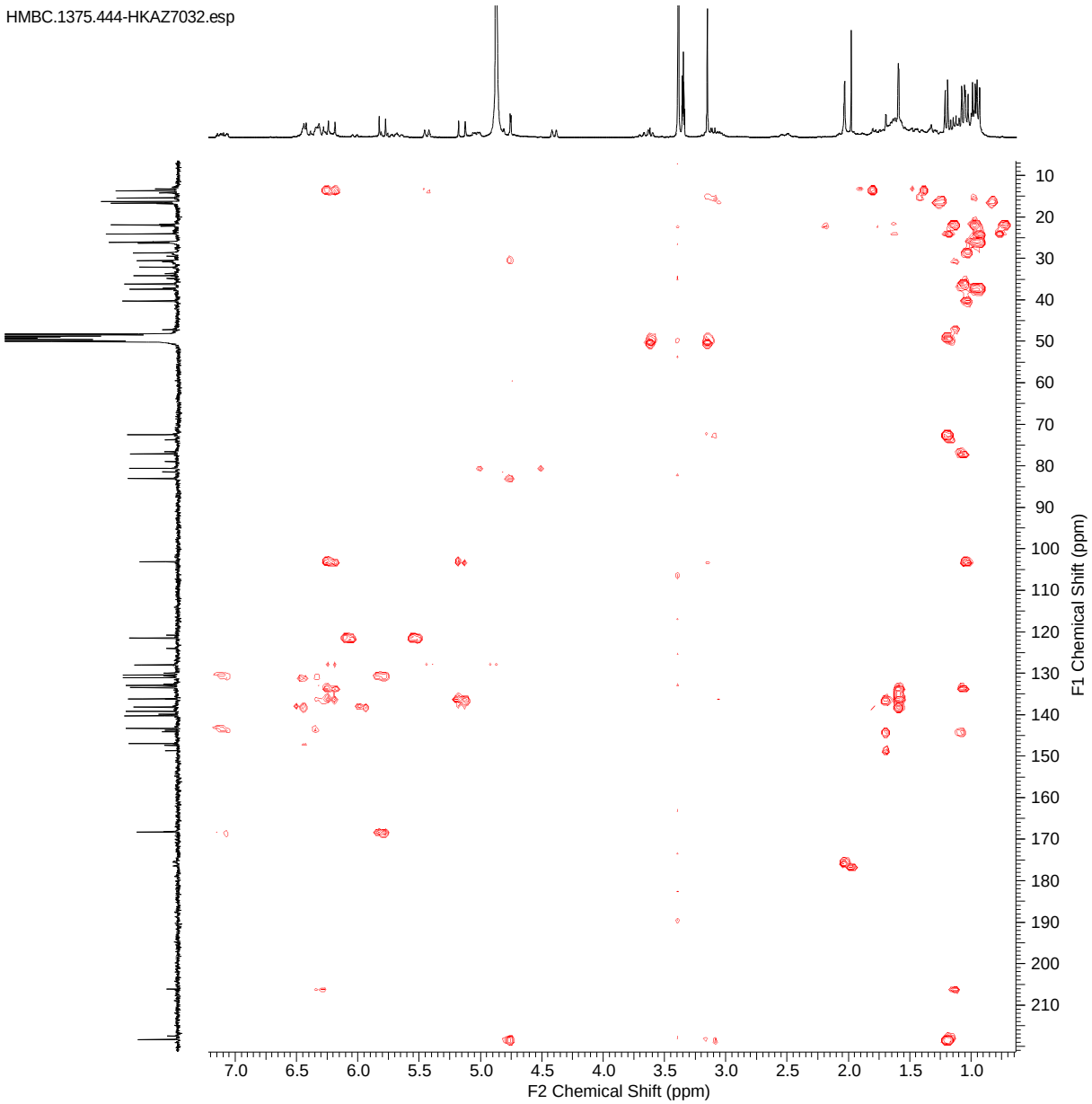

Spectrum 98: $^{1}H,^{13}C$ HMBC spectrum of sulfangolid D (**25d**) (^{1}H 300 MHz, ^{13}C 75 MHz, CD_3OD).